Investigating the innervation and neurogenic activation of lipolysis in white adipose tissue

Kayleigh Elizabeth Goddard

September 2024

A thesis submitted to the University of East Anglia

for the degree of Doctor of Philosophy

School of Biological Sciences

This thesis has been formatted and written using Overleaf, a LaTeX code based platform

All illustrative figures within this thesis have been created using BioRender and Canva

Declaration

I verify that the work presented in this thesis is my own original work and has not been previously submitted for a degree at this or any other university. Where work by other authors has been included, their work has been fully cited and referenced.

In line with the regulations for submission for a degree of Doctor of Philosophy at the University of East Anglia, this thesis has a word count of approximately 88,000 words, which includes the abstract, all footnotes and references, but excludes the title page; table of contents; list of figures and tables; abbreviations; acknowledgments and the appendix.

Portions of the data presented in Chapters 3 & 4 of this thesis are currently pending publication in the British Journal of Pharmacology:

Kayleigh E. Goddard & Samuel J. Fountain, Characterisation of neurogenic lipolytic responses in white adipose tissue ex vivo, *British Journal of Pharmacology*. DOI: 10.1111/bph.17445.

Abstract

Obesity is a growing global concern and research is key to developing understanding and mitigative strategies. Metabolic research often involves *in vitro* culture using cell lines or isolated primary adipocytes, offering limited translatability to *in vivo* physiology, as adipose is heterogeneous, with dense vascularisation and rich nervous innervation. However, nervous innervation of white adipose tissue (WAT) has not been fully resolved, with literature offering contradictory reports on the frequency and type of nerve-adipocyte interactions.

Here, adopting an alternative method of whole-mount immunocytochemistry, I present evidence of nervous innervation of mouse subcutaneous WAT (SAT) in three major modes: in coarse bundles, innervating vasculature, and parenchymal innervation, including direct adipocyte-encapsulating structures. Contrary to other reports, instances of direct nerve-adipocyte interactions were occasional, and were exclusively sympathetic. These casual sympathetic interactions are sufficient for inducing lipolysis, as in a novel neurogenic approach, the use of Na^+-channel opener veratridine to stimulate nerves *ex vivo* in SAT, successfully induced lipolysis to equivalent levels of norepinephrine. Contrary to literature in rodents, the β2-adrenergic receptor (AR), not β3-AR, was found critical to veratridine-driven lipolysis, which presents a novel finding. Pharmacological characterisation indicated norepinephrine as the sole driver of veratridine-evoked lipolysis, with sensory neuropeptides and other sympathetic neurotransmitters neuropeptide Y (NPY) and adenosine triphosphate (ATP), uninfluential in lipolysis. Interrogating the role of purinergic signalling further, there was no role for identified P2X4 and P2Y6 receptors in regulating either stimulated, or basal lipolysis.

These data serve to improve understanding of murine SAT innervation, as well as signalling molecules involved in regulating lipolysis in a model likely more representative of physiology. The investigation into innervation and lipolysis using these approaches could be further developed in rodent, but also human adipose, for study across obese & diabetic states and to investigate other outcomes including lipogenesis, and adipokine secretion. The *ex vivo* platform incorporating veratridine-induced lipolysis could be harnessed for research and development in preclinical trials.

Contents

List of Figures

List of Tables

List of Abbreviations

AC	Adenylyl cyclase
ADP	Adenosine diphosphate
AR	Adrenergic receptor
ATGL	Adipose triglyceride lipase
ATP	Adenosine triphosphate
BAT	Brown adipose tissue
Ca^{2+}	Calcium ions
cAMP	Cyclic adenosine monophosphate
Ca_V	Voltage-gated calcium channel
cDNA	Complementary DNA
cGMP	Cyclic guanosine monophosphate
CGRP	Calcitonin gene-related peptide
CTx	Conotoxin
DAG	Diacylglycerol
DMEM	Dulbecco's modified eagle medium
DMSO	Dimethylsulfoxide
DNA	Deoxyribonucleic acid
DRG	Dorsal root ganglion
EC50	Half-maximal effective concentration
EFS	Electrical field stimulation
ER	Endoplasmic reticulum
FFA	Free fatty acid
G_i	G protein subunit α_i
GPCR	G protein coupled receptor
G_q	G protein subunit α_q
G_s	G protein subunit α_s
HBSS	Hanks' buffered salt solution
HFD	High fat diet
HSL	Hormone sensitive lipase
IB4	Griffonia simplicifolia lectin isolectin B4
IC50	Half-maximal inhibitory concentration

Il	Interleukin
IP3	Inositol-1,4,5-triphosphate
iWAT	Inguinal white adipose tissue
K^+	Potassium
KD	Knockdown
KO	Knockout
MAG	Monoacylglycerol
MGL	Monoacylglycerol lipase
mRNA	Messenger RNA
Na^+	Sodium ions
NAN	Neuro-adipose nexus
Na_V	Voltage-gated sodium channel
NCLX	Mitochondrial sodium/calcium exchanger
NCX	Sodium/calcium exchanger
NE	Norepinephrine
NPY	Neuropeptide Y
P2R	Purinergic receptor
PGP9.5	Protein gene product 9.5
PI3K	Phosphoinositide 3-kinases
PIP2	Phosphatidylinositol 4,5-bisphosphate
PKA	Protein kinase A
PKC	Protein kinase C
RNA	Ribonucleic acid
SAT	Subcutaneous adipose tissue
ScG	Sympathetic chain ganglia
SERCA	Sarcoendoplasmic reticulum calcium ATPase
SMA	Smooth muscle actin
SOCE	Store operated calcium entry
SP	Substance P
SVF	Stromal vascular fraction
TAG	Triacylglycerol
TH	Tyrosine hydroxylase
TTX	Tetrodotoxin

UDP	Uridine diphosphate
UTP	Uridine triphosphate
VAT	Visceral adipose tissue
VGSC	Voltage-gated sodium channel
VTD	Veratridine
WAT	White adipose tissue
WT	Wild type
ZDR	Z-depth reduction

Acknowledgements

I maintain that the acknowledgements section is the first page of any thesis I read. I could honestly fill the word count of the thesis with my acknowledgements alone, but I shall try to exercise restraint. I once read that it takes a village to get a PhD, and I couldn't agree more. I would like to thank my personal 'village' of people that made this final piece of work possible.

Firstly BBSRC for funding all of the work inside this thesis. My supervisors Dr Stephen Robinson & Prof. Samuel Fountain. Sam for inspiring me in lectures to the point of applying for a PhD with you, for pushing me to be a better student and reassuring me when I needed it. Thank you for your support, laughing at my silly jokes, embracing my way with science and being a trusting supervisor.

The Fountain lab and all its inhabitants past and present. With special thanks to Dr Sonia for everything in this last year, Dr Anni (plusminus!) & Dr Dalyan. You have all supported my PhD journey immeasurably. Peripherally, in the BMRC I have been blessed with support from so many lovely people, but over the last year namely; Dr Dan Saffer, Paul Lonsdale, Dr Tim Pearson, Andy Loveday and the technical team Chay and Alex. I am so grateful for all your scientific technical help and camaraderie. Floor 02 lab-life wouldn't be as fun without chats with Becky, Louise, Kelly, Dagne, Sarah, Caitlyn, Molly-Kay, Kasia, Reesha and Finn.

The entire crew of the DMU, thank you for helping me as much as you have. I certainly wouldn't have got here without your kind and generous assistance. Its been a pleasure working with you all and seeing your faces at the hatch each morning.

A huge thanks to all friends and family that have supported me in this long journey.

Thanks doesn't begin to cover this, but to my proofreader, sounding board, logistics consultant and incredible husband, Aston, who I dedicate my undergraduate and now my postgraduate completion to. I will never meet a greater human being or friend.

Thank you for steering my CTV straight for these 10 academic years. You told me I'd "smash it" when I was considering starting a PhD, but no, not without you. We got this PhD together. I love you to the mun.

My biggest cheerleader Sarah, mumma, with our Wednesday voice notes, our "Saturday morning chats" and 'love' pens which all kept me going over the last 4 years. Thank you for your astute advice, lifting me through the lows and losing it with me on the highs. Your exceptional skills as a diabetic specialist nurse inspire me to be as good at my job one day, as you are. It was an honour seeing you work your magic during my placement, Supernurse Sarah.

Prof. Matt Gage who I sadly cannot thank in person, it was an honour to know you and thank you for imparting on me the notion that I should/could do a PhD back in 2019. Without your influence, I absolutely would not be here today.

My doggos who have kept me 'walking out' (pun intended) my science problems in the middle of Norfolk Fields. Thanks Atlas (Lucy) and Taz (Tacobell) for facilitating my steps and my thinking time.

Lastly I want to acknowledge all the mice that were part of this PhD project; I am thankful for the sacrifice they all made, and no work here was completed without this consideration.

"If I have seen further it is by standing *on the shoulders of Giants*"

-Isaac Newton

Chapter 1

Introduction

1.1 Obesity

Obesity is defined as the excessive accumulation of adipose deposits within the body, to the detriment of the individual's health (WHO.org). The current determination of obesity is via the body-mass index (BMI) calculation, which divides body weight (in kg) by the square of height (m^2). The range for a healthy BMI is between 18.5 - 25, where a BMI above this upper range increase the probability there is more mass and therefore adiposity. Although, muscle mass is an unaccounted parameter in the BMI calculation and as such, the BMI calculation serves only as an approximate indicator of obesity.

To echo other reports, obesity is reaching pandemic proportions, with the World Health Organisation (WHO.org) reporting that in 2022, 43% of adults (representing 2.5 billion) were considered 'overweight' and 16% as 'obese' globally.

In fact, if these trends persist, these statistics are predicted to worsen, with current projections of 24% of the world's population set to classify as obese by 2035 (equating to 1.914 billion people) (World Obesity Atlas report, 2023). The outlook for obesity is therefore concerning, as within the World Obesity Atlas report from 2023, no countries have reported declines in obesity prevalence within their population. Further, regions where obesity was less prevalent are now unfortunately seeing increases, such as in Africa and South East Asia, likely due to "Westernisation" of dietary and lifestyle habits (Boutari & Mantzoros 2022).

Obesity, therefore represents a growing global concern and one which cannot be ameliorated instantly. This in part is due to obesity spanning age groups, with more children

than ever with an overweight/obese status (globally 8% in 1990 rising to 20% in 2022) (WHO.org) and are statistically more likely to retain this status as they reach adulthood (Simmonds et al. 2016). Solving obesity through fat loss is a protracted process, requiring individuals' motivation and dedication, which is ultimately difficult to instil and will take time to reflect in longitudinal reports if intervention efforts succeed.

1.1.1 Obesity causes

There are a multitude of hereditary and lifestyle factors that contribute to the onset of obesity, and those with a genetic background or medical conditions predisposing them to obesity are at higher risk (NICE.org). Medical conditions such as hypothyroidism lower the basal metabolic rate, which leads to changes in energy balance (Crowley 2008). Medications such as β-blockers, can also promote obesity as they can simultaneously interfere with β-adrenergic controlled lipolysis (Sharma et al. 2001). Other factors such as age and hormonal changes during menopause can also contribute to the development of obesity (Crowley 2008).

However, lifestyle factors such as excess calorie intake versus expenditure due to overconsumption of food and drink and/or inactivity, are particularly influential (Crowley 2008). Access to intensively processed and calorie-dense food in modern society is likely responsible, at least in part, for the statistics previously described. Additionally, depletion of 'green space' due to growth and expansion of urban and suburban areas is also associated with obesity, which will only exacerbate as global populations continue to rise (Kim et al. 2021). As a corollary, obesity is considered "one of the most important public health problems facing the world today" (World Obesity Federation). Therefore, with the awareness of projected statistics and recognition of the causes of obesity, its vital research is directed to better understand metabolic physiology in order to support increasing demands for mitigative treatments and intervention.

1.1.2 Obesity-associated diseases

Obesity poses a significant risk factor and is a precursor to a suite of serious long-term health conditions. Eventually, as adipose depots continue to expand over time, pathological responses occur as adipocyte secretions becomes dysregulated, described as the "Phenotypic switch" (Kawai et al. 2021). This switch in adipocyte secretions results in

inflammation of adipose tissue, which impairs it's ability to function as an endocrine and storage organ. Resident immune cells, macrophages, become activated by chemoattractant molecules from the altered adipocyte secretions (Kawai et al. 2021). As a response, activated macrophages release a suite of pro-inflammatory cytokines which characterise the inflammatory phenotype and adipocytes lose the ability to respond to their extrinsic regulatory signals (Kawai et al. 2021; Zhang et al. 2020). Increased plasma levels of inflammatory molecules such as interleukins and tumour necrosis factor α (TNFα) are often observed in obese patients, which can affect critical organs such as heart function, indicating the systemic impact adipose inflammation can have (Ouchi et al. 2011; Ashraf et al. 2013). Aberrant expression of growth factors, cytokines and chemokines in obesity are also linked to multiple cancers, such as uterus, gallbladder, colon, thyroid and breast cancer (Pati et al. 2023). As consequence, impairment and unavailability of fat stores leads to ectopic fatty deposits within vasculature and organs (Chusyd et al. 2016), resulting in pathologies such as cardiovascular diseases, non-alcoholic fatty liver disease and liver cirrhosis, a seemingly endless list (Trayhurn 2013; Zhang et al. 2020).

A common pathological association with excessive (particularly visceral and abdominal) adiposity is 'metabolic syndrome' which describes a cluster of individual conditions encompassing; insulin resistance, atherogenic dyslipidemia, hypertension as well as obesity (Straznicky et al. 2009). Obesity-driven metabolic syndrome thereby acts as a risk factor for a constellation of serious long-term health conditions, including type 2 diabetes (T2D). The 'pre-diabetic' state described in metabolic syndrome can quickly tip to a T2D diagnosis due to a pre-existing degree of insulin resistance, which worsens and results in a loss of response to endogenous sources of insulin in peripheral tissues. In turn, a compensatory over production of insulin by pancreatic β cells can ultimately lead to their dysfunction/degradation with a decrease in insulin production and pathologically increased blood glucose levels. Elevated blood glucose levels eventually spiral into a plethora of related health conditions (Barella et al. 2021). Hyperglycemia-induced damage to peripheral vasculature can lead to tissue necrosis, kidney damage and retinopathy (Mota et al. 2020). Metabolic syndrome also lends to development of various cardiovascular diseases including coronary heart disease, where arterial deposits of fat can result in ischemia and myocardial infarction. When these deposits occur peripherally they can

result in strokes (Zhang et al. 2020). Thus, obesity is intrinsically linked to a suite of largely preventable pathologies which can reduce quality of life.

1.1.2.1 Runaway effects

Additional to the diseases and pathologies described above, there are 'runaway' effects of obesity which serve to perpetuate the obese state and increase difficulty in management. As fat stores rapidly expand they experience remodeling in response to adipocyte hypertrophy, which manifests in loss of vascularisation of the tissue due to limited capacity of vascular angiogenesis to match the rate of adipose expansion (Herold & Kalucka 2021). Lack of vascularisation limits the delivery of circulating hormones, oxygenated blood and uptake of free fatty acids (FFA), which promotes adipose hypoxia and FFA-induced lipotoxicity. These ultimately generate unhealthy, inflamed adipose tissue states, which can feed back on to existing microvasculature and induce further damage (Zatterale et al. 2020). Re-vascularisation of adipose does eventually occur, due to adipocyte expression of pro-angiogenic factors in response to inflammation and hypoxia. However the aberrant secretion of growth factors can lead to fibrosis of adipose, as additional matrix components are deposited, such as collagen. Ultimately this changes adipose structure/composition which makes mitigating via simple weight loss efforts challenging (Guardia et al. 2024; Herold & Kalucka 2021; Reggio et al. 2013).

In parallel with obesity-induced remodeling, polyneuropathy from persistently high blood glucose concentrations (Blaszkiewicz et al. 2019b; Blaszkiewicz et al. 2019a), high levels of triglycerides, elevated blood pressure (Callaghan et al. 2020) and inflammatory molecules (such as IL-1β) occurs (Zatterale et al. 2020). These result in disabled communication with, and depletion of, fat stores, limiting sympathetic nerve capacity to reduce hypertrophy and regulate metabolism. This fits somewhat with the paradoxical evidence that shows sympathetic nervous drive is increased in obesity, manifesting in hypertension from increased vascular tone, yet adiposity can persist and progress (Kalil & Haynes 2012). These affects of lost innervation contribute to what is known in obese pathology as 'catecholamine resistance' which can be described as loss of response to endogenous norepinephrine (Duncan et al. 2007). Catecholamine resistance encompasses desensitisation and decreased expression of β-adrenergic receptors (ARs) (β3-AR

in mice and β2-AR in humans) as well as downregulation of lipolysis mechanics (for example lipases involved in lipolysis) (Duncan et al. 2007; Valentine et al. 2022), as well as upregulation of anti-lipolytic mechanisms, such as α2-AR receptor expression in human adipocytes (Arner 2005). Ultimately loss of peripheral sympathetic nerves innervating adipose leads to a loss of control and perpetuation of obesity, as intervention efforts fail to induce lipolysis.

Essentially, islands of isolated adipocytes where vascularisation and neuronal innervation is perturbed lend to loss of control and perpetuation of obesogenic conditions, emphasising the importance of vascularisation and nervous innervation in adipose tissue health.

1.1.3 Impact

Obesity and associated diseases inevitably impose local & global economic costs and strain on healthcare systems, together with millions of premature deaths. Correspondingly, cardiovascular diseases are the leading cause of global deaths, accounting for nearly 17.9 million deaths annually in 2019 (WHO.org) (and an estimated 20.5 million deaths in 2021 [BHF 2024]), with ischemic conditions like stroke and coronary heart disease being responsible for 6.6 & 9.1 million deaths, respectively (BHF 2024, [2019 data]). Diabetes is another global leading cause for premature death and affects around 422 million people globally, accounting for 1.5 million deaths per year (WHO.org). Diabetes costs the NHS around £10 billion per year, with 90% of diabetic cases in UK being type 2, the preventable form (Diabetes UK.org). According to government reports, obesity costs the NHS £6.5 billion per year, which is expected to increase to £9.7 billion each year by 2050 (Gov.uk 2022, 2023). As obesity is predicted to increase in prevalence globally, as discussed in Section 1.1, these economic burdens are unlikely to abate. Therefore, research into physiology surrounding metabolism is crucial to future understanding and strategically tackling obesity with more targeted therapeutics.

1.2 White adipose tissue

1.2.1 Adipocyte subtypes

There are three adipocyte subtypes characterised by their function and described by their mitochondrial-derived appearance (Figure 1.1). Brown adipocytes are implicated in mammalian non-shivering thermogenesis, generating heat opposed to adenosine triphosphate (ATP) in the mitochondrial electron transport chain, possessing greater numbers of mitochondria to facilitate this process. β-adrenergic receptor stimulation induces liberation of FFAs from small lipid droplets which serves to fuel the electron transport chain via β-oxidation, as well as FFAs binding to and activating uncoupling protein-1 (UCP-1) on the mitochondrial inner membrane. The uncoupling allows H^+ protons to rapidly travel across the membrane via UCP-1 independently of ATP synthase dissipating energy as heat, which would otherwise typically harness the gradient to generate ATP (Cannon & Nedergaard 2004). These cells lie in brown adipose tissue depots such as cervical, supraclavicular and perirenal depots, where their main role is the generation of heat in response to cold stress and increased energy intake (Cannon et al. 2004) (Figure 1.1). Brown adipose is most abundant in human infants, however these depots decrease with age and is a concept that researchers are keen to harness in obesity treatments (Evans et al. 2019).

White adipocytes are functionally and visually distinct, with large volumes of lipid stored in their cytoplasm (unilocular), they possess far fewer mitochondria than other types and are non-thermogenic (Braun et al. 2018). Their increased capacity for lipid sequestration facilitates their principle role as storage units for excess caloric intake in the form of triglycerides, which can be released to fulfil increased energy demands. White adipocytes congregate in white adipose depots and are the most abundant subtype in adulthood. While beige adipocytes are also often found in white adipose tissue, white adipocytes constitute the majority and denotes the classic 'white fat' phenotype.

Beige adipocytes are an intermediate subtype that falls between white and brown adipocytes. They possess fewer mitochondria than brown adipocytes and higher vol-

umes of stored lipids (multilocular), but not to the extents of white adipocytes. Beige adipocytes are also capable of thermogenesis when induced by cold stress (termed 'browning'), underpinned by upregulating expression of UCP-1, allowing for an adaptive phenotypic switch in response to demand (Cannon et al. 2004).

The present PhD project is centred around signalling in white adipose tissue, with particular focus on white adipocytes. Therefore, unless otherwise stated white adipocytes are those being referred to and considered in the context of the work undertaken and will remain the core subtype discussed.

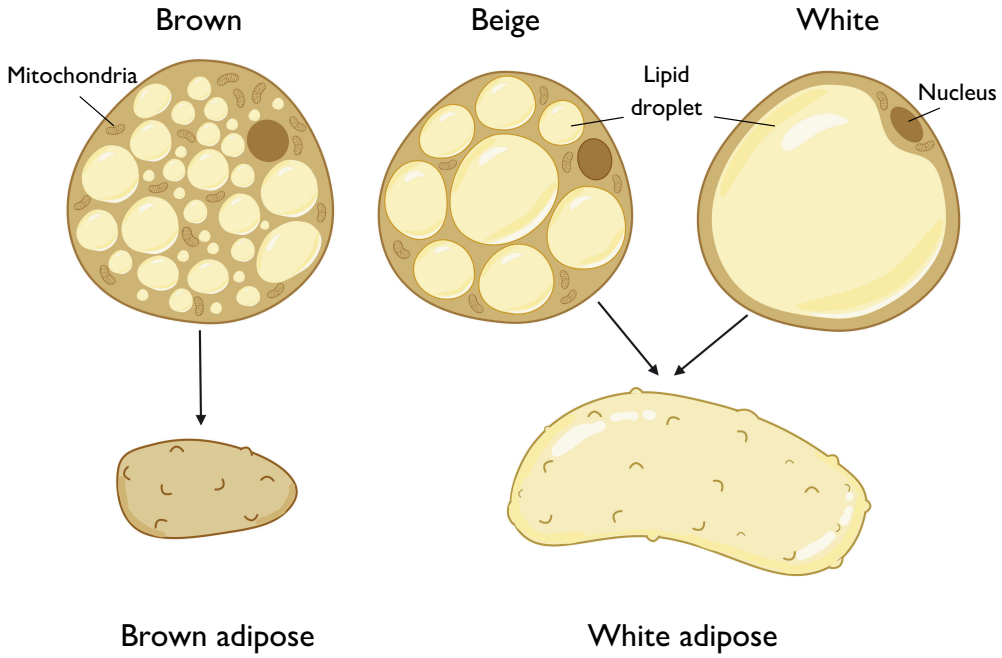

Figure 1.1: Adipocyte subtypes. Illustrative figure of the three key subtypes of adipocyte: brown, beige and white, alongside the depots they reside in. White adipocytes possess the characteristic 'unilocular' appearance, while beige and brown adipocytes share the multilocular appearance.

1.2.2 White adipose tissue organ role and depots

White adipose tissue (WAT) is not only populated by white and beige adipocytes (which approximate to one third of the cells in a given depot), but is enriched by blood and

lymph vasculature, nerves, immune cells, fibroblasts, stromal cells, pre-adipocytes and extracellular matrix components like collagen (chiefly type VI), which collectively comprise the tissue (Cavaliere et al. 2023). The heterogeneous nature of WAT makes it dynamic and responsive to a plethora of signalling cues. Generally, white adipose has two primary storage forms; subcutaneous adipose tissue (SAT), (which accounts for around 80% of total body fat) and visceral adipose tissue (VAT) (accounting for 20%), wherein visceral pertains to those around vital organs, and subcutaneous refers to those 'under the skin' (Cavaliere et al. 2023). The roles of these two forms differ, in that the core purpose of visceral adipose is protection of vital organs, whilst subcutaneous adipose is more implicated in storage and endocrine functions. As such, the depots can differ in presentation and composition (Börgeson et al. 2022).

WAT can expand in volume to accommodate increased incoming energy sources by both hypertrophy (increase in size/volume) and hyperplasia (increase in number) of adipocytes. Hyperplasia of adipose occurs when resident adipocyte precursors differentiate into adipocytes to increase the total adipocyte number in the depot and thus increase the storage capacity. Hypertrophic expansion is associated with harmful and adverse alterations of white adipose tissue remodelling as already mentioned in Section 1.1.2.1 (Choe et al. 2016).

1.2.2.1 Physiological role

Lipid storage as triacylglycerol, also referred to as triglycerides (TAG), in adipocytes within the white adipose depot forms a critical adaptive mechanism that allows for long periods of fasting. The principal role of subcutaneous WAT is therefore to store excess dietary intake as lipids within large chasms in the cytoplasm through the process of lipogenesis (Evans et al. 2019). WAT is dynamic, as fluctuations in dietary caloric intake are mirrored by alterations in metabolism of lipids to balance whole body energy and regulate metabolic homeostasis. WAT offers axillary roles as a protective 'padding' underneath the skin, shielding from mechanical stress (Kwok et al. 2016). The protective padding consequently facilitates thermal regulation as a physical insulating barrier to cold, and WAT stores can also mobilise and redirect lipids under cold stress toward BAT stores, to fuel thermogenesis (Choe et al. 2016). WAT is also the primary site for vitamin

D storage which is crucial for skeletal health, extending the beneficial role of WAT (Park et al. 2021).

1.2.2.1.1 WAT as an endocrine organ

Once regarded as a passive calorific reservoir, metabolic homeostasis is facilitated by the endocrine function of WAT. A substantial portion of appetite control and energy balance is governed by adipocyte-secreted factors known as adipokines. For example, the extensively studied hormone leptin is secreted by adipocytes upon insulin stimulation (Tsai et al. 2012), which acts on neurons AgRP and POMC in the arcuate nucleus within the hypothalamus region of the brain, to reduce appetite and promote satiety (Caron et al. 2018) and increases sympathetic drive to peripheral tissues, including WAT (Zeng et al. 2015). Therefore, leptin acts as an 'adipostat' to control adipose stores via a negative feedback loop. Adiponectin is another key secreted adipokine, which acts both locally in adipose tissue and systemically in skeletal muscle and liver. Adiponectin is considered a health-promoting adipokine due to its numerous beneficial effects and correlates positively to longevity (Zhang et al. 2020). Adiponectin serves to reduce lipolysis, reduce inflammation, increase insulin sensitivity and in the liver lowers hepatic glucose production and promotes hepatocyte survival, all to the benefit of systemic metabolism (Zhang et al. 2020).

Also, adipocytes secrete an array of cytokines, and chemokines; Interleukin (IL)-1, IL6, IL8, IL10, monocyte chemoattractant protein-1 (MCP-1) & TNFα, which can have varying impacts on adipose and systemic health. Of these, IL-6 TNFα and MCP-1 are pro-inflammatory, while IL-1 & IL-10 are anti-inflammatory (Ouchi et al. 2011). Metabolic health/state influences the adipokine profile during the aforementioned "phenotypic switch", wherein obesity-induced adipose dysfunction promotes the release of pro-inflammatory molecules and downregulation of anti-inflammatory molecules, as above (Choe et al. 2016).

1.2.2.1.2 WAT as an energy buffer

A facet of the WAT role is sequestering of lipids away from organs and vasculature in dedicated and specialised organs, to prevent ectopic deposits, lipotoxicity and inflam-

mation, all of which pertain to a suite of high-risk diseases as described in section 1.1.2 (Guilherme et al. 2008). WAT therefore acts as a metabolic 'sink' to decrease the post-prandial loads of circulating glucose and lipids which would otherwise be detrimental to health (Chusyd et al. 2016). As such, certain WAT depots such as gluteal and femoral SAT depots actually incur beneficial protective effects linked with secretion of anti-inflammatory adipokines, while storage in other sites such as abdominal SAT and VAT are maladaptive and associated with the plethora of health concerns as already discussed (Section 1.1.2) (Chusyd et al. 2016).

It is therefore important to note to the reader that adipose tissue is a valuable and crucial part of our physiology. This is demonstrated in diseases such as partial or total lipodystrophy and cachexia where body fat cannot be properly maintained or stored, resulting in complications such as thrombocytosis, hypotriglyceridaemia, cardiovascular disease, liver failure and ultimately premature death (Araújo-Vilar et al. 2019).

1.2.2.2 Mouse and human adipose

Human and other mammalian adipose, such as rodent adipose, differ. These differences likely correspond to evolutionary adaptations in behavioural and physiological roles of each species, which have optimised for their lifestyle habits.

There are key differences in depot anatomical organisation. Mice have two key large SAT depots, the inguinal WAT (iWAT) and axillary WAT (axWAT) which are located anterior and posterior of the animal, respectively (Figure 1.2). Humans have three key large SAT depots; abdominal WAT (abWAT), gluteal and femoral depots, which divide into upper and lower divisions, with upper abWAT localised to the abdomen and lower gluteofemoral WAT around the thighs and gluteal area (Figure 1.2). In humans, abdominal SAT can be further divided into superficial subcutaneous tissue (sSAT) and deep subcutaneous tissue (dSAT), which is congruent with VAT, and are separated by the fascia superficialis (Chusyd et al. 2016). There are no such subdivisions in mouse SAT as described in humans. However, in mice, the SAT and dermal layers of fat are separated with a layer of smooth muscle (panniculus carnosus) which is absent in humans, and is instead congruent with dermal adipose tissue (Figure 1.2) (Luong et al. 2019). Additionally, female mouse SAT is also mammary tissue and presents another key distinction. The inguinal adipose depot in mice is geographically equivalent to the human

gluteofemoral depots and experimental results of mouse iWAT & human abdominal WAT are considered 'comparable' (Chusyd et al. 2016; Börgeson et al. 2022).

VAT depots common to humans and mice are pericardial, perirenal, retroperitoneal, mesenteric and omental (Luong et al. 2019; Chusyd et al. 2016). Although while these are technically shared depots, according to reports, visceral adipose is less comparable between species. Key differences being mice have very reduced mesenteric and omental VAT compared to humans and are likely less implicated in regulating systemic metabolism. Instead mice have large perigonadal/epididymal VAT depots, which are very reduced in humans (Börgeson et al. 2022) (Figure 1.2).

Hypertrophy is the typical route of expansion in human SAT, as studies indicated adipocyte number was constant across obese and lean patients (Spalding et al. 2008). SAT expansion in both humans and mice is generally via hypertrophy, demonstrating important shared physiology allowing for better translation across species models. However, differences in adipocyte size occur across different adipose depots, between species. Mice reportedly have larger adipocytes in VAT depots and smaller more numerous adipocytes in SAT depots, while for human SAT, this is largely the opposite (Börgeson et al. 2022). Human SAT is suggested to have a lower vascular density than mouse SAT owing to the differences in adipocyte size across depots (Song et al. 2016; Ledoux et al. 2008; Börgeson et al. 2022). As adipocyte size is used as a qualitative descriptive of adipose tissue health status, where a larger adipocyte corresponds to a hypertrophic phenotype and thereby dysfunctional tissue, it means that comparisons using these adipocyte parameters may be more challenging to use in isolation. This means, depending on the depots being compared, studies of pathology and effects on adipocyte hypertrophy or hyperplasia aren't directly translatable between species as a marker for adipose health. Adipocyte size cannot be used as an absolute determining factor for dysregulation due to these native differences.

Mice and humans also have a similar order of lipolytic responses to weight loss across depots, with human weight loss efforts preferentially reducing VAT over SAT stores and abdominal SAT opposed to gluteofemoral stores (generally). Similarly, mice undergoing weight loss show greater preference for VAT and over SAT stores in general (Chusyd et al. 2016). For example, the inguinal depot demonstrates plasticity to fasted weight

loss, reducing in weight and dimension after visceral stores have depleted, which can re-expand/recover under normal diet regimes (Tang et al. 2017).

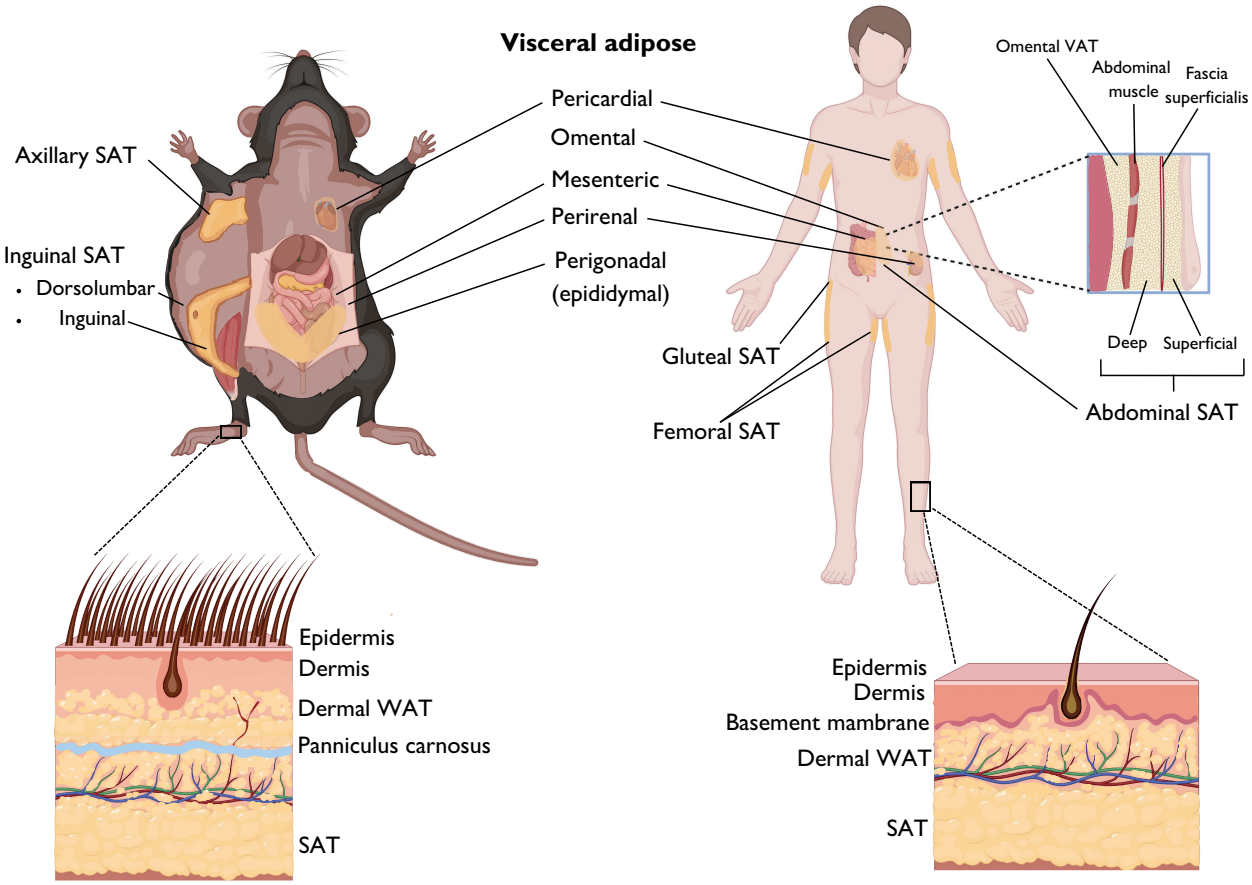

Figure 1.2: Mouse and human adipose depots. Illustrative figure of adipose depots and divisions between species. Mice and humans share pericardial, mesenteric, perirenal and retroperitoneal (not shown) visceral adipose depots (VAT). Mice have large perigonadal (also known as epididymal) VAT, which is reduced in humans, instead possessing large omental depots. Mouse subcutaneous adipose tissue (SAT) presents as two key depots: the inguinal and axillary, whereas humans have gluteofemoral (buttock and thigh) stores and abdominal SAT. Blue box illustrates human abdominal SAT is divided into deep and superficial layers, separated by the fascia superficialis, a division not seen in mice. Mouse skin has clearly defined dermal white adipose tissue (WAT) and SAT due to separation by a sheet of smooth muscle, the panniculus carnosus. In humans this is absent and dermal WAT is congruent with SAT. Figure adapted from Luong et al. 2019; Börgeson et al. 2022; Griffin et al. 2020.

1.2.3 Lipolysis

In addition to their ability to capture and store excess energy, white adipocytes have an opposing mechanism to catabolise and liberate lipids from stores during periods of fasting or increased energy demand (Frühbeck et al. 2014). Lipolysis is the hydrolysis of intracellular stores of TAG during a sequential chain of lipase activity; adipose triglyceride lipase (ATGL), hormone-sensitive lipase (HSL), monoacylglycerol lipase (MGL), to generate one glycerol molecule and 3 fatty acids (one produced at each hydrolysis step). Initially, TAG is hydrolysed into diacylglycerol (DAG) by ATGL, which is then hydrolysed further to monoacylglycerol (MAG) by HSL, and lastly, MGL hydrolyses MAG to glycerol (Grabner et al. 2021) (Figure 1.3).

The resulting products of lipolysis can then be utilised by cells in the body for energetic rebalance. FFAs can be used directly for generation of important cell cycle substrates (acetyl-CoA) via β-oxidation in various tissues like skeletal muscle and the kidney, or converted to ketone bodies in the liver which can then be oxidized by other cells (Bae et al. 2023; Nakagawa et al. 2016). Glycerol fuels production of glucose in hepatic gluconeogenesis to ultimately increase blood glucose concentrations, providing glucose for tissues which cannot utilise FFAs as energy, such as the brain (Malfacini et al. 2023). Some FFAs are reuptaken by WAT and remain within the adipocyte to be re-esterified back into stored TAG (Li et al. 2022). However, WAT has a limited capacity to reuse released glycerol, due to adipocytes having low expression levels of glycerol kinase (Treble & Mayer 1963; Bridge-Comer et al. 2023; Arner 2005).

Ultimately, lipolysis depletes stored triglycerides and buffers the body's energy demand. Increased energy demand from physical activity and/or fasting leading to consistent lipolysis, can result in body fat loss over time. Lipolysis and lipogenesis work in synergy to regulate metabolism and lipolysis occurs at its greatest extent when induced by external stimuli and is termed 'stimulated lipolysis'. Stressors such as aforementioned periods of fasting stimulate a substantial lipolytic response.

1.2.3.1 Stimulated lipolysis

Stimulated lipolysis must be carefully regulated through signalling-dependent mechanisms for precise control of metabolism and represents a highly adapted metabolic response to increased energy demands. The requirement for ligand-governed stimulation of lipolysis is necessary to ensure stored energy is preserved for periods of genuine need.

Stimulated lipolysis is a complex multi-factorial process that comprises pro-lipolytic signalling from hormones, cytokines and catecholamines (norepinephrine, epinephrine), with varying degrees of influence (Grabner et al. 2021; Grant et al. 2015).
The principal means of inducing lipolysis under fasted conditions is via catecholamines commanding TAG hydrolysis through intracellular enzyme activation and is considered the 'canonical' lipolytic pathway (Grabner et al. 2021). Norepinephrine released from sympathetic neurons binds to adrenergic receptors, chiefly G_s-linked G-protein coupled receptors (GPCRs) β1, β2 & β3 adrenergic receptors (ARs), on the adipocyte cell surface. The act of norepinephrine binding causes a conformational change to the intracellular domain of the receptor, which activates the G-protein α subunit causing its dissociation from the β and γ counterparts (Wingler et al. 2020). The α-$_s$ subunit is free to activate adenylyl cyclase (AC) and induce a signalling cascade. AC activity increases cyclic adenosine monophosphate (cAMP) production, whereupon cAMP activates downstream protein kinase A (PKA). After activation, PKA has dual effects, phosphorylating both HSL and perilipin-1. At basal states, perilipin-1 sequesters a protein co-activator, comparative gene identification-58 (CGI-58), which is released post-PKA phosphoactivation and stimulates ATGL activity in the initial stage of lipolysis. Phosphorylation of perilipin-1 also causes disruption of its inhibitive coating on the lipid droplet surface, allowing access of second-stage lipase, HSL (Duncan et al. 2007). PKA-activated HSL translocates to the lipid droplet membrane and is primed to perform the sequential hydrolysis of DAG to MAG (Li et al. 2022). While catecholamines represent dominant route for G_s-mediated lipolysis (Duncan et al. 2007), hormones such as thyroid stimulating hormone (TSH), melanocortins; melanocortin stimulating hormone (MSH) & adrenocorticotropic hormone (ACTH), and secretin, among others, also activate G_s-linked receptors and induce lipolysis as described above (Figure 1.3) (Grabner et al. 2021; Nielsen et al. 2014).

1.2.3.1.1 Additional lipolysis pathways

cGMP-PKG pathway

An alternative to the canonical G_s-coupled activation of lipolytic enzymes is cardiac-derived natriuretic peptide hormone, atrial natriuretic peptide (ANP), which binds to guanylyl cyclase-linked receptors to induce the production of cyclic guanosine monophosphate (cGMP). cGMP is an activator of protein kinase G (PKG) which acts analogously to PKA, phosphorylating HSL and perilipin at the same sites and thus inducing lipolysis (Sengene et al. 2003; Collins 2022). Due to the release of ANP being triggered by distention of muscle fibres in the atria of the heart, stresses such as physical exertion and/or autonomic fight or flight responses result in this route of stimulating lipolysis (Lafontan et al. 2005). This pathway is restricted to primates and there is little evidence of this pathway in rodents (Lafontan et al. 2005).

MEK/ERK pathway

Additional to, and possibly independent of, PKA-mediated lipolysis, other intracellular pathways have been shown to increase lipolysis, such as the mitogen-activated protein kinase kinase and extracellular-signal-regulated kinase pathway of kinases (MEK/ERK). Typically induced via external signals such as growth factors and cytokines (Bost et al. 2005), the MEK/ERK pathway has been shown to increase lipolysis via β-adrenergic receptors β1, β2 and particularly β3-AR and is suggested to account for 20-25% of lipolysis (Collins 2022). Researchers found at low agonist concentrations, inhibition of PKA alone was sufficient to remove lipolysis. However, at higher agonist concentrations, inhibition of PKA removed only 75-80% of lipolysis (in 3T3-L1 adipocytes) as the ERK pathway was recruited to increase lipolysis in collaboration with canonical PKA signalling, which was abolished with antagonism of MEK and kinase Src (Robidoux et al. 2006). The ERK signalling axis has been linked to the negative regulatory AC 'G_i' pathway, as ERK-induced lipolysis was found sensitive to G_i inhibitor pertussis toxin (Soeder et al. 1999). The β3-AR is particularly interesting as it can interchangeably couple to both G_i and G_s proteins and recruit ERK independently of other scaffolding molecules via direct binding of Src SH3 domains to the receptor (Collins 2012). Whereas, the β2-AR recruitment of ERK is thought to only be via post-stimulatory desensitisation of the receptor, whereby the PKA-phosphorylated receptor recruits GPCR kinases (GRKs), then β-arrestins which enable binding of Src which ultimately results in ERK activation.

Researchers have shown the activation of ERK leads to phosphorylation of HSL to induce lipolysis, using a Chinese hamster ovary (CHO) cell line expressing HSL (Greenberg et al. 2001), which is a feasible theory. Other recent research has suggested that phosphorylation of the β3-AR by activated ERK serves to potentiate/activate the cAMP-PKA axis (Hong et al. 2018). However the full downstream effects as to ERK activation of lipolysis, such as targets of ERK that translate to lipolysis, have not been fully resolved and require further research (Collins 2012).

1.2.3.1.2 β-adrenergic receptors in rodents versus humans

Humans and mice are both responsive to sympathetic-derived catecholamine signalling through adrenergic receptors, however, the receptor subtypes dominant in regulating lipolysis is different across species (Lafontan et al. 1995). Research has shown that rodent lipolysis is primarily driven through the β3-AR opposed to β1 and β2-ARs and is the dominantly expressed subtype in rodents, by orders of magnitude (Valentine et al. 2022; Merlin et al. 2018; Schena et al. 2019). Work from early studies inferred a role for the β3-AR in WAT regulation, as genetically obese *ob/ob* mice exhibited a downregulation of the β3-AR in response to obesity (Collins et al. 1994). In this work, obese mice that were shown to have downregulated β3-AR mRNA experienced blunted AC activity compared to controls in response to epinephrine stimulation, indicative of a prominent role in conducting lipolysis (Collins et al. 1994). This notion was further supported in comparisons of lipolytic response to a panel of non-selective adrenergic stimulants alongside a β3-AR specific agonist. The β3-AR agonist (BRL 37344) raised lipolysis to equal levels of catecholamines in mouse, hamster, rat and dog (but not human) adipocytes, suggesting that β3-AR accounted for the entire catecholaminergic response (Carpéné et al. 1998).

The patterns of β3-AR response to selective antagonists further affirms the role for the receptor in rodent lipolysis, with mouse-derived 3T3-L1 adipocyte cell lines demonstrating sensitivity of isoprenaline-stimulated lipolysis to β3-AR-specific antagonists (Jin et al. 2018).

Challenging the importance of β3-AR in the context of the other subtypes, lipolysis in

isolated rat white adipocytes demonstrated the greatest sensitivity to specific antagonism of β3-AR above that of β1 & β2-AR subtypes, at higher concentrations of isoprenaline. Although at lower concentrations, lipolysis was also mediated by β1-AR (Louis et al. 2000). These findings, implicating β3 & β1-AR, were echoed in other studies of rat lipolysis (Germack et al. 1997). In more physiological settings, *in vivo* experiments have shown that systemic doses of β3-AR antagonist SR59230A in mice under calorie restricted 'stimulated' conditions (to theoretically increase sympathetic drive to WAT) had blunted lipolysis compared to controls, as measured by serum glycerol (Sipe et al. 2017).

Genetic knock-out (KO) studies in rodent models have also been used as a tool to explore the role of β3-AR in lipolysis. Deletion of the β3-AR in mice saw a 42% increase in total body fat under a standard chow diet. These metrics were exaggerated under high-fat diet regimes, with a 56% increase in total body fat versus control mice on the same diet, indicating that the β3-AR in mice plays a crucial role in maintaining lipolysis, particularly under obesogenic conditions (Revelli et al. 1997). Comparisons of epinephrine-stimulated lipolysis in isolated white adipocytes from wild type (WT) versus whole-body β3-AR KO mice found that lipolysis was blunted in those lacking the receptor (Preitner et al. 1998). In similar experiments, isolated adipocytes from β3-AR KO mice demonstrated 67% reduced AC activity and 25% reduced glycerol release in response to isoprenaline compared to WT controls, indicating similar trends across experiments using different agonists and measurements of lipolysis (Susulic et al. 1995). More recent evidence from an optogenetic model suggests that β3-AR is involved in leptin-induced sympathetic drive to WAT, as under leptin-stimulated conditions, tissue-specific triple KO (TKO) mice for all three adrenergic receptors had significantly higher body fat percentages than those lacking just β1 and β2-ARs (Zeng et al. 2015).

While there are some studies that support the β3-AR role in human white adipocytes, demonstrating blunted isoprenaline-mediated lipolysis when isolated adipocytes were pre-exposed to β3-AR antagonists (Cero et al. 2021), and lipolyic effects in patients taking β3-AR agonists (Baskin et al. 2018), others fail to see β3-AR sensitivity (Carpéné et al. 1998; Rosenbaum et al. 1993). Instead, human lipolysis is mediated by β1 and possibly β2-ARs and human adipocytes have low to negligible expression of β3-AR (Valentine

et al. 2022; Arch 2008; Evans et al. 2019; Hostrup et al. 2022; Collins 2022). Additionally, human WAT expresses high numbers of α2-ARs which negatively regulate lipolysis via G_i-linked reduction in cAMP. These are considered absent in rodent WAT and therefore represent key physiological differences as to how responses in lipolysis are not fully translatable across species (Chusyd et al. 2016; Evans et al. 2019).

Anti lipolysis mechanisms

The 'brakes' on lipolysis are achieved through a variety of pathways. The chief brake on lipolytic activity is via post-prandial introduction of insulin, which binds to insulin receptors (IR) on the adipocyte surface and drives the activation of phosphodiesterase 3 B (PDE3B) to degrade cAMP, disabling the activity of PKA and thus limiting lipolysis (Grabner et al. 2021). The associated intracellular pathway is via ligand-driven autophosphorylation of the intracellular domains of the insulin receptor activating associated insulin receptor substrate 1 (IRS-1) proteins. In turn, this causes phosphatidylinositol 3-kinase (PI3K) to produce phosphatidylinositol-3,4,5-triphosphate (PIP3), which activates a phosphoinositide-dependent kinase (PDK) to ultimately activate protein kinase B (PKB) which mediates the induction of PDE3B (Figure 1.3) (Petersen et al. 2018). These effects can also be achieved by the meal anticipation and hunger hormone, ghrelin, produced by the stomach (Li et al. 2022).

A second route of reducing lipolysis is via G_i-linked GPCRs on adipocyte membranes, which can be activated by a number of signalling molecules. The activation of G_i linked receptors liberates the α subunit to downregulate the activity of AC to decrease the production of cAMP, in opposition to stimulatory G_s subunits. Examples of activators of the G_i pathway include adenosine binding to A1 or A3 receptors, norepinephrine producing both stimulatory (as above) and also inhibitory effects via the α2-AR (in humans) and neuropeptide Y (NPY) Y1 and Y2 receptors (Figure 1.3) (Li et al. 2022). Other pathways can indirectly reduce lipolysis though curtailing downstream effectors of AC-produced cAMP, such as adiponectin, which suppresses PKA activity through interference of the PKA positive regulatory subunit PKA RIIα (Qiao et al. 2011).

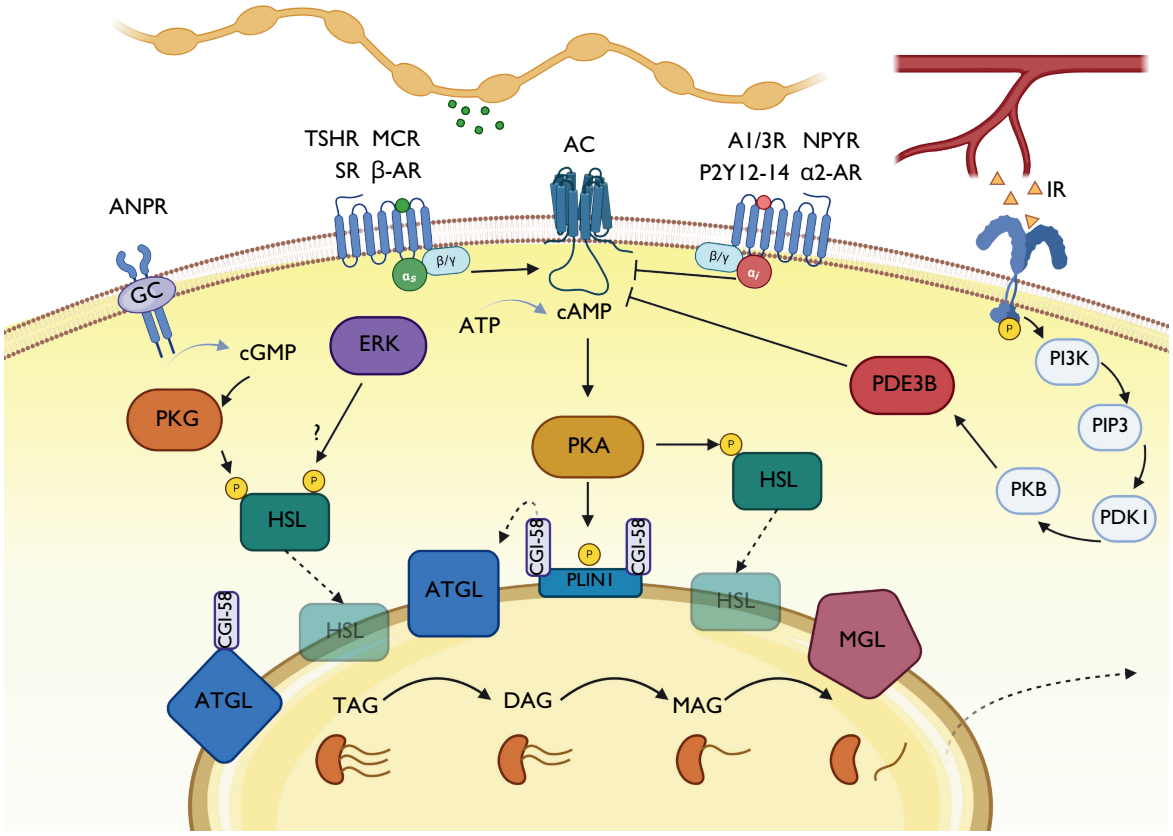

Figure 1.3: Stimulated lipolysis and anti-lipolytic pathways. An illustrative figure describing common routes of stimulated lipolysis, namely G_s-linked receptors such as β-adrenergic receptors (ARs), melanocortin receptors (MCR) binding melanocortin stimulating hormone & adrenocorticotropic hormone, thyroid stimulating hormone receptor (TSHR) and secretin receptors (SR). The G_s receptors culminate on increasing adenylyl cyclase (AC) activity to raise cAMP-activated protein kinase A (PKA) activity. Perilipin-1 (PLIN1) phosphorylation by PKA encourages dissociation from the droplet, as well as release of adipose triglyceride lipase (ATGL) co-activator, comparative gene identification-58 (CGI-58). Phosphorylated hormone sensitive lipase (HSL) relocates to the lipid droplet to hydrolyse ATGL-produced diacylglycerol (DAG) into monoacylglycerol (MAG). The final fatty acid is removed by monoacylglycerol lipase (MGL) to produce glycerol. Other lipolytic routes include atrial natriuretic peptide binding to its receptors (ANPR) and instead inducing activity of guanylyl cyclase (GC) and protein kinase G (PKG) to phosphorylate HSL. ERK-induced lipolysis is yet to be fully resolved. Anti-lipolytic mechanisms include G_i-linked receptors which reduce AC activity, such as adenosine A1 & A3 receptors, NPY 'Y' receptors, purinergic P2Y12,13 & 14 receptors and α2-ARs. A core anti-lipolytic rote is via insulin receptor (IR)-induced phosphodiesterase 3 B (PDE3B) activity, which degrades cAMP, via PI3K pathway activation.

1.2.3.2 Basal lipolysis

Basal lipolysis is the steady turnover of TAG at low levels, independent of external stimuli. In stimulated lipolysis, the key players have been identified as ATGL and HSL acting in harmony to efficiently hydrolyse TAG to DAG, as illustrated by KO studies (Schweiger et al. 2006). However, during basal lipolysis, HSL appears to play less of a role, with overexpression having no upregulatory effect on basal lipolysis in human adipocytes (Bezaire et al. 2009). While research into the signalling mechanism underpinning basal lipolysis is ongoing, it is clear that ATGL is critical to the process. A core aspect preventing uncontrolled lipolysis in the absence of extrinsic stimuli, is lipase localisation (Frühbeck et al. 2014; Bezaire et al. 2009). During basal states, ATGL is dominantly located at the lipid droplet membrane, while HSL is dominantly found in the cytosol, unassociated with the lipid droplet membrane (Figure 1.4) (Granneman et al. 2009; Bezaire et al. 2009). It is only when stimulated that translocation occurs, due to PKA phosphoactivity at both HSL and perilipin-1, dually coordinating both the removal of perilipin-1 from the lipid droplet and promoting HSL translocation toward the lipid droplet, whereupon HSL can more freely access targets via the lipid droplet membrane.

Also, under stimulated conditions, PKA liberates the ATGL co-activator CGI-58 to substantially increase activity of ATGL-induced TAG hydrolysis, which under basal conditions is sequestered by perilipin-1 (Figure 1.4) (Granneman et al. 2009). However, ATGL can still hydrolyse TAG in absence of CGI-58 at reduced rates (Lu et al. 2010; Granneman et al. 2009). Negative ATGL regulation is compounded by the action of an accessory protein trio, which interact with ATGL at the lipid membrane; G0/S2 switch protein 2 (G0S2) (Yang et al. 2011), fat specific protein 27 (FSP27) and hypoxia induced lipid droplet associated protein (HILPDA) (Grahn et al. 2014). The combined effect of these negative influences on ATGL activity therefore maintains a low level of TAG turnover and rate of basal lipolysis. Under stimulated conditions HSL is rate-limiting, as it is the primary conductor of DAG hydrolysis (Schweiger et al. 2006). However under basal conditions, evidence suggests ATGL also has lipase activity at DAG, owing to increased glycerol release observed when ATGL is overexpressed alongside HSL silencing, in basal conditions (Yang et al. 2011) (although ATGL has 10x lower specificity for DAG resulting in reduced efficiency [Frühbeck et al. 2014]). Thus, the working hypothesis is

that low levels of lipid droplet-dwelling ATGL activity in the absence of CGI-58 are driving basal lipolysis (Figure 1.4). Recycling of lipolysis products can occur, with glycerol (although not much in adipocytes, as mentioned in Section 1.2.3) and around 50-70% of FFAs (reports in mice and humans, respectively) released during basal lipolysis are re-esterified back into TAG in lipogenesis (Li & Spalding 2022; Wang et al. 2003; Wolfe et al. 1990).

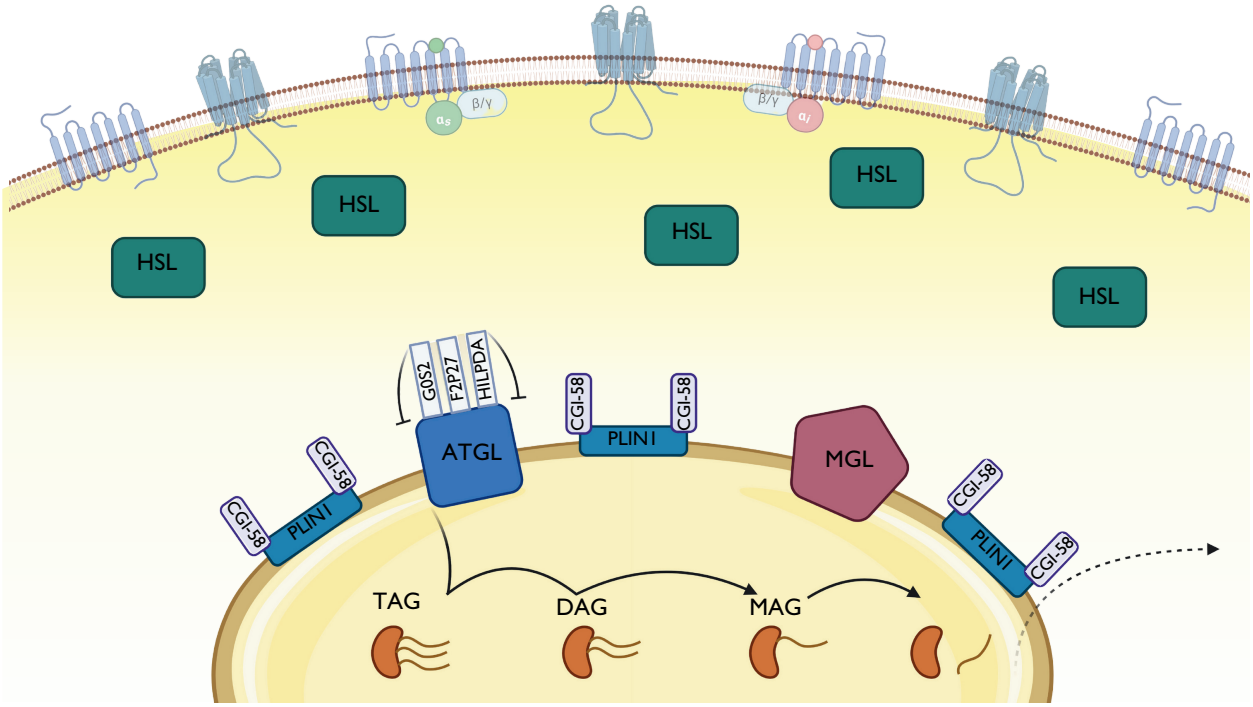

Figure 1.4: Basal lipolysis. An illustrative figure describing basal lipolysis. Under non-stimulated conditions, hormone sensitive lipase (HSL) remains dominantly in the cytosol and the lipid droplet is coated in obstructive perilipin-1 (PLIN1) which also sequesters adipose triglyceride lipase (ATGL) co-activator, comparative gene identification-58 (CGI-58). Further to lacking it's co-activator, ATGL activity is additionally quashed by negative regulators G0/S2 switch protein 2 (G0S2), fat specific protein 27 (FSP27) and hypoxia induced lipid droplet associated protein (HILPDA). ATGL is proposed to turn over triacylglycerol (TAG) and diacylglycerol (DAG) at low rates.

1.2.3.3 Lipogenesis

Lipogenesis in white adipocytes is the counteracting pathway to lipolysis and is key to its primary function as a storage organ. Lipogenesis refers to the synthesis of TAGs from lipids in the circulation, whereupon free fatty acids (FFAs) are esterified to a glycerol backbone and stored in the lipid droplet (Rowland et al. 2023). However not all consumed energy comprise of lipids, therefore synthesis of fatty acids from non-lipid sources, such as carbohydrates and protein, is essential to remove excess from the circulation and economise dietary intake. This latter process is termed *de novo* lipogenesis (DNL). While thought to contribute little to the overall TAG content compared to lipogenesis derived from circulating lipids, it is an important process as it allows for buffering of circulating glucose and amino acids away from other organs, safely converted into a storage component/precursor to prevent vascular or organ damage (Rowland et al. 2023).

During lipogenesis, glucose is converted into glycerol-3-phosphate (G3P) during steps in glycolysis, or from entry of circulating lipids and acts as a backbone for the esterification of fatty acids (FAs), those either derived from circulation, those as products from lipolysis, or synthesised FAs. FFA synthesis pathways generate acetyl-CoA which is then utilised as a precursor to synthesise palmitate, for TAG synthesis (Hsiao & Guertin 2019). Key enzymes facilitating TAG synthesis from DNL-derived FAs are acetyl-CoA carboxylase (ACC), and fatty acid synthase (FASN) (Hsiao & Guertin 2019).

Lipogenesis is more associated with the "fed" state induced by insulin, whereas DNL can occur in either state, although is responsive to high levels of glucose from meals (Luo & Liu 2016). However, adipocytes are also considered to have much lower rates of DNL over standard lipogenesis pathways, owing to their lower numbers of DNL enzymes. Most DNL occurs in the liver which generates circulating FFAs sequestered in lipoprotein carriers for use by adipocytes (Possik et al. 2021).

1.3 Calcium signalling

Although there are key activators to induce the core lipolysis pathways, there are also other signalling elements that act to modulate lipolysis, for example Ca^{2+}.

1.3.1 Calcium signalling

Calcium as a signalling molecule is critical in regulating cell homeostasis, survival, death and gene regulation which transcends across the eukaryotes of the animal kingdom and plants, to prokaryotes such as bacteria (Clapham 2007).

Adipocytes possess a suite of Ca^{2+}-permeable channels and receptors on their surface membranes, including; store-operated calcium entry (SOCE) mechanisms via calcium release activated channels (CRAC), voltage-gated calcium (Ca_V) channels and purinergic channels/receptors, as well as ion exchange mechanisms via (reverse-mode of) the Na^+/Ca^{2+} exchanger (NCX) (Zhai et al. 2020). Activation of these can ultimately influence/regulate the concentrations of cytosolic calcium.

For instance, activation of a G_q-linked GPCR elevates calcium via the activation of phospholipase C (PLC) at the intracellular membrane, which can then hydrolyse phosphatidylinositol 4,5-bisphosphate (PIP2) into two messenger molecules, diacylglycerol (DAG) and inositol-1,4,5-triphosphate (IP3). DAG is free to activate protein kinase C (PKC) and initiate other pathways, while IP3 binds to IP3 receptors on the surface of the endoplasmic reticulum (ER) to release Ca^{2+} into the cytosol (Berridge 2016). The increase in cytosolic Ca^{2+} often induces further release from intracellular stores in the process calcium induced calcium release (CICR), for example through Ca^{2+}-sensitive ryanodine receptors on the ER (Figure 1.5) (Bootman et al. 2002).

SOCE occurs after depletion of intracellular Ca^{2+} stores which refill via CRAC channels at the cell surface membrane. The emptying of the ER stimulates resident protein Stim1 to relocate to the ER surface. This induces relocation of the ER towards the cell membrane, which can then interact with ORAI1 proteins, inducing their reorganisation to form CRAC channels permeable to Ca^{2+} (Hachmane et al. 2018). These sequence of events replenish intracellular calcium stores via smooth endoplasmic reticulum Ca^{2+} ATPase (SERCA) pumps at the ER, which actively facilitate the sequestering of Ca^{2+} back into storage (Figure 1.5). However research suggests the SOCE also acts as a general pathway to increase intracellular calcium in adipocytes (Maus et al. 2017).

Calcium can also enter via the activation of a membrane-bound ligand- or voltage-

gated ion channels, which allows for cation entry directly into the cytosol (Figure 1.5). In the case of voltage-gated calcium channel (VGCC) (Ca_V), changes in the membrane potential, as well as binding of growth hormones, govern gating of the pore (Catterall et al. 2007; Gaur et al. 1996). There are several types of Ca_V channel; N, R, P & Q types (Ca_V 2), 'high-voltage activated' L-type (Ca_V 1) and 'low-voltage activated' T-type channels (Ca_V 3) (Zhai et al. 2020). Members of these subtypes have been identified on white adipocytes, including L & T-type channels (Uebele et al. 2009; Fedorenko et al. 2020).

Ca^{2+} signalling is perceived in terms of frequency and amplitude by various intracellular compartments. Thus, ensuring the Ca^{2+} signal is appropriately terminated is vital to function (Berridge 1997). Unregulated elevated levels of [Ca^{2+}]i can induce cell death pathways, therefore mechanisms are in place to extrude and reduce [Ca^{2+}]i. For instance active ATPases such as SERCA and plasma membrane Ca^{2+} ATPases (PMCA) which use energy from ATP hydrolysis to actively pump Ca^{2+} into the ER or out of the cell, respectively (Clapham 2007). More passive, gradient-driven mechanisms include Na^+/Ca^{2+} exchangers (NCX), however the reverse mode of the NCX also offers a Ca^{2+} entry route following local accumulation of Na^+ (Figure 1.5) (Bentley et al. 2014; Blaustein & Lederer 1999).

1.3.1.0.1 Calcium involvement in Lipolysis

Calcium signalling translates differently depending the function of a cell, underpinned by the physiological 'toolkit' they possess. For example smooth muscle cells will have a different response to intracellular calcium than an adipocyte, based on their role (Berridge 2016). The roles of Ca^{2+} in adipocytes are not restricted to lipolysis, with many other outcomes identified in adipocytes such as differentiation and adipogenesis (Uebele et al. 2009), however roles relating to lipolysis remain the focus here. While Ca^{2+} signalling in some cell types is clear, intuitive and well-characterised, the overall outcomes of Ca^{2+} signalling in adipocyte lipolysis are less clearly defined.

Lipolysis has previously been shown to be negatively regulated by Ca^{2+} increases in human adipocytes, with increased [Ca^{2+}]i reducing cAMP levels and HSL phosphory-

lation, mediated by increased PDE3B activity (Xue et al. 2001). In studies observing effects of dietary calcium and metabolism, elevated intracellular Ca^{2+} via the action of vitamin D3 in human adipocytes reportedly increases lipogenesis and suppresses lipolysis, which can be ameliorated by increased dietary calcium to inhibit vitamin D3 (Zemel 2004). Although, the mechanism underpinning the Ca^{2+}-induced decrease in lipolysis has not been identified in their research.

Similar trends have been observed in mouse and rabbit white adipocyte responses to Ca^{2+}, under isoprenaline-stimulated and unstimulated conditions (Garca-Barrado et al. 2001). Blockade of rabbit adipocyte voltage gated Ca_V channels with elgodipine (T- and L- type Ca_V antagonist) potentiated isoprenaline induced lipolysis, suggesting that Ca^{2+} may be inhibitory to stimulated lipolysis. In mouse adipocytes, increased $[Ca^{2+}]i$ had no effect on lipolysis under stimulated or basal conditions, suggesting no role for Ca^{2+} in lipolysis and inferring potential differences between species (Garcia-Barrado et al. 2001). The evidence in the above studies only seems to offer PDE as the Ca^{2+}-mediated inhibitor of lipolysis, and most literature that refers to $[Ca^{2+}]i$ as inhibitory, reference the research of Xue et al. (2018) in support of their argument/rationale, indicating that evidence in favour of this narrative is sparse.

Conversely, intravenous injection of the calcitonin gene receptor protein (CGRP) stimulated canonical cAMP induction, but also activated the PLC/IP3 pathway, which increased FFA release in rats independently of the cAMP-PKA route (Aveseh et al. 2018). Others have found a link between G_q-linked receptor PKC activation and the ERK/MEK pathway, which results in lipolysis and indicates that activation of G_q-linked and other calcium receptors may increase PKC activity to engage alternate arms of lipolysis (Greenberg et al. 2001).

Other studies show Ca^{2+} is involved in positive regulation of lipolysis, reporting that in mice, increased concentrations of Ca^{2+} via extrinsic sources through L-type Ca_V channels or intrinsic sources though IP3 pathways, reduce lipid stores and downregulate genes associated with lipogenesis e.g. fatty acid synthase, while increasing expression of the rate-limiting HSL (Sun et al. 2012).

In other work, Ca_V channels were found constitutively active and particularly influential to basal lipolysis. Tools to increase Ca^{2+} influx under basal conditions, such

as agonising L-type Ca_V channels, resulted in an increase in basal lipolysis in rat white adipocytes, while antagonists of these channels decreased basal lipolysis. Under isoprenaline-stimulated conditions, removal of extracellular Ca^{2+} or blockade of L-type Ca_V channels reduced lipolytic responses, but induced [Ca^{2+}]i elevation had no increasing lipolytic effect, indicating Ca^{2+} permits but doesn't potentiate stimulated lipolysis (Fedorenko et al. 2020). Similarly, ablation of Ca^{2+} entry through Ca_V channels in adipocytes blunted stimulated lipolysis, which the authors propose is due to [Ca^{2+}]i potentiating the activity of a Ca^{2+}-sensitive AC isoform (Chen et al. 2017; Cooper 2005).
Supportively, Maus et al. (2017) found a signalling axis between starvation-induced SOCE and lipolysis in mice. SOCE-mediated Ca^{2+} entry through plasma membrane CRAC channels & drives lipolysis proposedly via activation of calcium-sensitive ACs, which engages the canonical PKA route, but [Ca^{2+}]i also ultimately resulted in the transcription of pro-lipolytic ATGL and HSL genes.
These latter studies appear to congregate on the idea that increased [Ca^{2+}]i promotes lipolysis via calcium sensitive AC isoforms.

Lastly, in primary white adipocyte cultures from mouse epididymal depots, Ca^{2+}-free conditions were found to reduce basal lipolysis. These lower concentrations of extracellular Ca^{2+} induced activation of hemiconnexins between the adipocytes and generated Ca^{2+} oscillations to coordinate the release of adenosine triphosphate (ATP) vesicles. The release of ATP vesicles ameliorated the lack of extracellular Ca^{2+} by para-autocrine induction of intracellular Ca^{2+} liberation. Removal of the connexin-mediated oscillatory mechanism reduced basal lipolysis, indicating a positive regulatory mechanism of Ca^{2+} on basal lipolysis which can be mediated through purinergic receptors (Turovsky et al. 2021).

Overall, the mechanisms underpinning calcium-induced or inhibited lipolysis are unclear, with no direct or solidified mechanism, and further work is required to fully understand discrete signalling pathways.
This project is focused on a specific subset of Ca^{2+} related receptors, the purinergic receptors. Therefore, understanding the general outcomes of Ca^{2+} signalling from other receptors/channels aids in understanding roles for specific purinergic populations and how they may contribute to lipolysis.

1.3.2 Purinergic Signalling

ATP is a well-known energy 'currency' for cellular activity. It is typically hydrolysed by enzymes to release a phosphate ion, which when attached to appropriate targets, alters their activity. However, purines & pyrimidines such as ATP, adenosine diphosphate (ADP), uridine triphosphate (UTP), uridine diphosphate (UDP) and adenosine are also potent signalling molecules when bound to their corresponding receptors. Many purinergic receptors relate to Ca^{2+} and offer routes of $[Ca^{2+}]$i increases via cation channels and G_q-linked receptors (Figure 1.5).

First proposed by Geoffrey Burnstock in 1970, purinergic signalling faced scientific resistance, however, became recognised and accepted in the proceeding two decades as a legitimate signalling mechanism (Burnstock et al. 1970; Burnstock 2012). Purinergic signalling has since been found to be implicated in a plethora of physiological functions, including inflammation, vascular smooth muscle contraction and nociception (Burnstock 2007). Purinergic signalling can be both physiological and pathological, and advances of research into these signalling mechanisms has generated targeted therapies for thrombosis e.g. clopidogrel (Angiolillo et al. 2017) and chronic cough via gefapixant (Trapero et al. 2020). Therefore, depending on their role in lipolysis, purinergic receptors may provide an attractive target for therapies concerning metabolic disorders.

1.3.3 Purinergic receptor subtypes and signalling mechanisms

Purinergic receptors can be separated into two large groups by their natural ligands: nucleosides (P1 receptors) and nucleotides (P2 receptors).

1.3.3.1 P1 receptors

P1 receptors are metabotropic and consist of GPCRs conjugated to various G-proteins which denote their function. Adenosine acts as the principle ligand and originates from hydrolysed AMP molecules via ecto-5'-nucleotidase enzymes (Robson et al. 2006). P1 receptors are dominantly G_s (A2A and A2B) or G_i-linked (A1 and A3), although there are populations of G_q-linked A3 receptors (Burnstock 2018; Tozzi et al. 2017). Once

adenosine is bound to P1 receptors, the respective intracellular signalling cascade is initiated. Adenosine receptors have been considered as important to the regulation of adipocyte lipolysis, with A1 subtypes commonly found expressed in rodent white adipocytes, with G_i-associated anti-lipolytic activity (Fredholm 1978; Granade et al. 2022). A2B subtypes have also been identified in mice, where it was found upregulated in VAT under high fat diet (HFD) regimes. A2B was suggested to have beneficial roles in systemic metabolism, as KO led to severe metabolic dysfunction (Johnston-Cox et al. 2012). The A3 subtypes are also reported in white adipocytes (Tozzi & Novak 2017). However, the research within the project is focused on P2 purinergic receptors, and therefore P1 receptors will be omitted from further discussion at this stage.

1.3.3.2 P2 receptors

P2 purinergic receptors fall in two categories: ionotropic P2X receptors with 7 subtypes (P2X1 - 7) and metabotropic P2Y receptors with eight subtypes (P2Y1, P2Y2, P2Y4, P2Y6, P2Y11, P2Y12, P2Y13, P2Y14). While the two categories are structurally & functionally different, they both possess the ability to bind and respond to purines and/or pyrimidines to induce intracellular signalling cascades (Table 1.1) (Burnstock 2018).

P2X receptors are ligand-gated ion channels and are commonly expressed in central nervous system (CNS) tissues such as the brain, but also in the peripheral nervous system (PNS) on sympathetic neurons, motor neurons and sensory neurons (Ralevic & Burnstock 1998). Proliferating cells of the skin, gut, heart and smooth muscle also express P2X receptors (Burnstock 2018). As non-selective ion channels, ATP binding to the receptor causes a conformational change, which opens the structure to form a channel which cations such as Ca^{2+}, can pass through.

P2Y receptors are metabotropic GPCRs, with an external ligand binding site and an intracellular domain coupled to a G-protein. P2Y1, P2Y2, P2Y4, P2Y6, P2Y11 are dominantly G_q-linked, inducing rises in [Ca^{2+}]i, although P2Y2 & P2Y4 can also couple to G_i proteins and P2Y11 to G_s proteins (Burnstock 2018). The remaining P2Y12, P2Y13 and P2Y14 receptors couple to G_i proteins (Burnstock 2018). In mice, all but P2Y11 have been identified (Dreisig & Kornum 2016). Uridine-based nucleotides UTP

and UDP are common ligands for P2Y receptors, although some subtypes can bind ATP and ADP (for ligand preferences by P2Y receptor, see Table 1.1).

The chief enzyme responsible for the breakdown of extracellular ATP and UTP to their respective monophosphates are ectonucleotidases (NTPDase) also referred to as CD39 (Robson et al. 2006; Giuliani et al. 2021), which is followed by action of ecto-5'-nucleotidases (CD73). Within WAT, there are multiple possible sources of nucleotides, ATP can be secreted by adipocytes (Sandhu et al. 2021; Tozzi et al. 2020) and nerves are also a potential source of ATP (Burnstock 2009). Resident ectonucleotidases can then generate ADP from these sources. UTP is typically less abundant than ATP (Jain & Jacobson 2022) and cells can synthesise UTP *de novo* and release it into the extracellular space (Anderson et al. 1997).

Table 1.1: P2 receptor agonists and mechanisms. A concise list of agonists and transduction pathways associated with the P2 receptor subtypes, where '*' denotes absent from mouse. Adapted from Weisman et al. (2012) & Burnstock (2018).

	Receptor	Agonists	Transduction Mechanism
P2X	P2X1	ATP	Ion/Cation channel
	P2X2		
	P2X3		
	P2X4		
	P2X5		
	P2X6		
	P2X7		Forms large pore when hyper-activated
P2Y	P2Y1	ADP	G_q
	P2Y2	UTP/ATP	$G_q + G_i$
	P2Y4	UTP/ATP	$G_q + G_i$
	P2Y6	UDP	G_q
	P2Y11*	ATP	$G_q + G_s$
	P2Y12	ADP	G_i
	P2Y13	ADP	G_i
	P2Y14	UDP-glucose	G_i

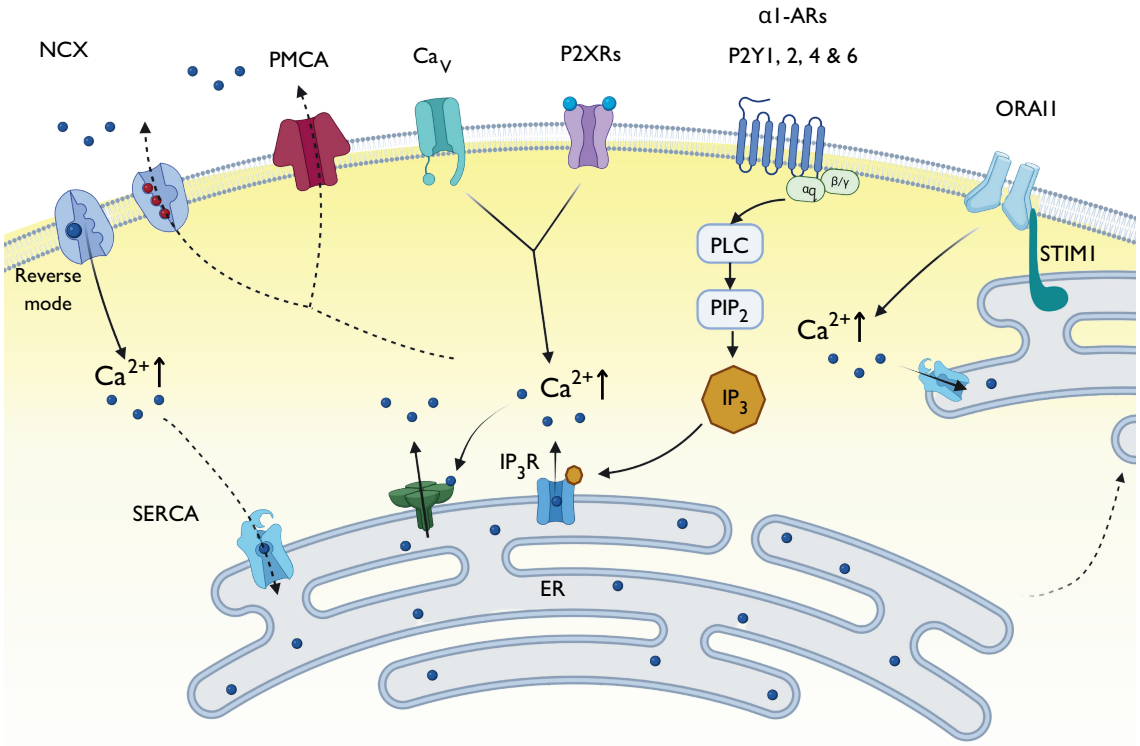

Figure 1.5: Calcium signalling mechanisms. An illustrative figure describing some key Ca^{2+} signalling mechanisms. Intracellular stores of Ca^{2+} can be liberated through activation of G_q-linked receptors to activate phospholipase C (PLC) at the intracellular membrane, which cleaves phosphatidylinositol 4,5-bisphosphate (PIP2) into inositol-1,4,5-triphosphate (IP3) and diacylglycerol (DAG). IP3 binds to IP3 receptors on the endoplasmic reticulum (ER). Localised release of Ca^{2+} can feed back onto calcium-sensitive receptors on the ER to cause further Ca^{2+} release in calcium-induced calcium release (CICR). Extracellular Ca^{2+} entry mechanisms are triggered once the ER is depleted, as it translocates to the cell surface, where stromal interaction molecules (STIM1) protein interacts with ORAI1 proteins and calcium release activated channel (CRAC) channels are formed allowing Ca^{2+} entry. Subsequent increased intracellular Ca^{2+} allows for repletion of the ER stores via smooth endoplasmic reticulum Ca^{2+} ATPase (SERCA) pumps which also serves to rapidly reduce Ca^{2+}. Other extracellular Ca^{2+} entry mechanisms include voltage gated Ca^{2+} channels (Ca_V) and ligand-gated cation channels, such as P2X receptors, which can respond to membrane voltage and external stimuli, respectively, to form Ca^{2+}-permeable channels. The reverse mode of the sodium-calcium exchanger (NCX) also serves as a Ca^{2+} entry mechanism, but also extrudes Ca^{2+} in exchange for Na^{+}. Other Ca^{2+} removal mechanisms include active transport via plasma membrane Ca2+ ATPases (PMCA).

1.3.4 Role of P2 purinergic signalling in adipocyte lipolysis

The contribution of G_i and G_s-linked purinergic receptors in adipocytes is unambiguous, as they regulate AC activity and its downstream effectors such as PKA (just as in β-adrenergic stimulation). However, the outcome of intracellular calcium signalling via P2X receptors and G_q-linked P2Y receptors are less well defined as already discussed in section 1.3.1.

In rats, researchers have found broad exogenous ATP, ADP and AMP application increased lipogenesis in isolated adipocytes, but had no apparent effect on stimulated or basal lipolysis (Schödel et al. 2004). Aligning with the consensus of other routes of calcium signalling, purinergic activation via perfusion of mouse adipocyte cell lines with ATP stimulated a significant increase in glycerol release under basal conditions, and reduction of ATP availability with apyrase significantly blunted isoprenaline-stimulated lipolysis, suggesting broad activation of purinergic receptors promotes lipolysis (Tozzi et al. 2019). Similarly, Lee et al (2005) found that broad activation of purinergic receptors in adipocyte cell lines with ATP and UTP generated glycerol release, which the authors concluded was evidence of G_q-linked P2R activity. However, although these latter studies favour that calcium signalling induced by purinergic receptors may mediate lipolysis, evidence regarding specific P2 receptor roles in lipolysis are more ambiguous and converse to outcomes with other Ca^{2+} entry mechanisms, seem to converge on either neutral or anti-lipolytic roles.

Multiple P2 receptors have been identified on mouse white adipocytes and derived cell lines. For example, P2X4 (Tian et al. 2020), P2X5 (Ussar et al. 2014; Tian et al. 2020) & P2X7 (Li et al. 2022) receptors have all been found expressed in mouse primary white adipocytes from visceral or subcutaneous depots. Additionally, P2Y1 (Laplante et al. 2010), P2Y2 (Musovic et al. 2022; Zhang et al. 2020; Negri et al. 2020), P2Y4 (Lemaire et al. 2017), P2Y6 (Jain & Jacobson 2022; Balasubramanian et al. 2014), P2Y13 (Duparc et al. 2024; Laplante et al. 2010) and P2Y14 (Jain et al. 2021; Xu et al. 2012) receptors have been identified in primary white adipocyte and 3T3-L1 cell lines, as well as in whole adipose tissue (Table 1.2).

Function

The outcomes of purinergic receptor activation on lipolysis are sometimes contradicted, with a lack of consensus in some cases. For instance, purinergic receptors found

implicated in one outcome not being reproduced in the same, or functionally similar, receptor subtypes. For example, daily *in vivo* injections of selective P2X7 receptor agonists in mice increased serum-glycerol levels, suggesting a P2X7 receptor-mediated increase in metabolism and lipolysis (Giacovazzo et al. 2019). However, in other studies, the P2X7 receptor has been found to inhibit lipolysis in favour of lipogenesis, with KO of the P2X7 receptor resulting in decreased lipid droplet formation and reduced expression of lipogenic protein, with increased expression of lipolytic enzymes (Li et al. 2022). Contradictively, Tian et al. (2020) found no significant reduction in body weight of whole body P2X7 KO mice, suggesting a limited influence of the P2X7 receptor on metabolism. Razzoli et al (2016) found P2X5 receptor expression was increased under cold-challenge of brown adipose tissue, which given the association between cold challenge and increased energy demand, may reflect a role for P2X5 receptor in white adipose lipolysis. In other research, P2X receptors were found not to have any meaningful effect on lipolysis upon selective P2X antagonism in 3T3-L1 cells (Kita & Arakaki 2015).

Additionally, G_q-linked calcium contribution to lipolysis has also been contradicted in the context of purinergic receptors (see section 1.3.1.1), as (G_q-linked) P2Y1 receptor activation significantly increased accumulation of TAG in 3T3-L1 adipocytes, and when the receptor was selectively inhibited, the accumulation of TAG decreased by over 33% (Kita & Arakaki 2015). According to Mullins et al. (2014), lipolysis disrupts mammalian target of rapamycin (mTOR) signalling pathways, which in turn inhibits insulin-stimulated glucose uptake. Therefore, increased glucose uptake is considered as an indicator of lipogenesis. As corollary, supporting the evidence above, additional findings that the P2Y6 receptor increased glucose uptake in both primary adipocytes and 3T3-L1 cell lines, support that the receptor may be involved in lipogenesis (Balasubramanian et al. 2014). Similar results have been observed in P2Y2 KO mice, where lack of the receptor provided resistance to HFD (Zhang et al. 2020). In non-rodent examples, KO of the P2Y2 receptor in human differentiated adipocytes increased basal lipolysis, suggesting anti-lipolytic roles (Ali et al. 2018a). The literature implies that G_q-linked purinergic receptors may act in a negative feedback manner to regulate stimulated lipolysis, since they appear to act like 'brakes' on lipolysis.

Unsurprisingly, owing to the G_i-coupling of the receptor, researchers have found KO of P2Y14 receptor in mice increased lipolysis, suggesting P2Y14 suppresses lipolysis (Jain

et al. 2021). Similarly, in KO studies of the P2Y13 receptor in mice, both white adipose tissue explants and adipocytes of KO mice experienced increased basal lipolysis and lipolytic responses to various stimulants, over wild-type (WT) controls (Duparc et al. 2024).

As with other Ca^{2+} signalling mechanisms, activation of purinergic receptors is not restricted to lipolysis and more often results in alterations in gene expression (Zhai et al. 2020). For instance, Ali et al. (2018a) demonstrated human P2Y2 receptor KO acutely increased basal lipolysis, but eventually resulted in alterations to the secretory profile of adipokines and cytokines, becoming more 'anti-lipolytic' as a compensatory mechanism. Intriguingly Jain et al. (2020) found P2Y6 receptor activation inhibited transcription of browning-related genes (*Ppara, ucp1*) in a c-Jun N-terminal kinase (JNK)-dependent mechanism, providing a means of context-dependent white adipocyte phenotype maintenance (Goddard 2021).
In other roles, Laplante et al. (2010) found that P2Y1 receptor had "little effect on adipocyte functions such as lipid storage or lipolysis", instead had roles in leptin secretion. Additionally, release of adiponectin was found to be under the control of P2Y2-mediated ATP and norepinephrine signalling, via a proposed collaborative Ca^{2+} and cAMP-mediated exocytosis event. Authors suggest ATP raises intracellular Ca^{2+} to encourage vesicle docking and cAMP facilitates the release of adiponectin (Musovic et al. 2022).

There appears to be disparity in the outcomes of Ca^{2+} signalling between purinergic receptors and other Ca^{2+} receptors and channels in relation to lipolysis. As most of the studies are *in vitro* or in unconditional KO models, the physiological relevance of these outcomes is less translatable. Therefore, this project seeks to investigate the role of purinergic signalling in lipolysis using a model more representative of physiology.

Table 1.2: P2 purinergic receptors observed in mouse adipose. A literature summary of P2 purinergic receptors found in mouse white adipose tissue and/or adipocytes, including role (if determined) and evidence of screening for contamination of other cell types. iWAT = inguinal WAT, e/gWAT = epididymal/perigonadal WAT, pWAT = pericardial WAT, WB = western blot, ICC = immunocytochemistry, qRT-PCR = real-time quantitative reverse transcription PCR, RT-PCR = reverse transcription PCR, 'cell type' refers to white adipocyte primary cultures, 3T3-L1 cell lines or freshly isolated adipocytes and W.T refers to 'whole tissue'.

Receptor	Cell type	Screened?	Method	Role	Reference
P2X4	Primary (iWAT)	FACS separated	qRT-PCR	Not stated	Tian et al. (2020)
P2X5	Fresh (e/gWAT)	-	qRT-PCR	none claimed	Ussar et al. (2014) Tian et al (2020)
P2X7	Primary (iWAT)	-	WB	Adipogenesis Lipogenesis	Li et al. (2022)
	Primary (iWAT)	FACS separated	qRT-PCR	none stated	Tian et al. (2020)
P2Y1	Fresh (e/gWAT)	-	RT-PCR	Leptin secretion	Laplante et al. (2010)
	3T3-L1	n/a	RT-PCR	Decrease lipolysis	Kita & Arakaki (2015)
P2Y2	Fresh (iWAT)	-	q-PCR	Adiponectin secretion	Musovic et al. (2022)

Continuation of Table 1.2

Receptor	Cell type	Screened?	Method	Role	Reference
	W.T	n/a	RT-PCR	Adipogenesis	Zhang et al. (2020)
P2Y2	W.T (pWAT)	n/a	qRT-PCR	Adipogenesis	Negri et al. (2020)
P2Y4	W.T (pWAT)	n/a	RT-PCR	Decrease adipogenesis	Lemaire et al. (2017)
P2Y6	Fresh (iWAT)	-	RT-PCR	Phenotype maintenance	Jain et al. (2020)
	Primary/3T3-L1	-	-	Glucose uptake	Balasubramanian et al. (2014)
P2Y13	Primary MSCs	n/a	qRT-PCR	Decrease differentiation	Biver et al. (2013)
	Primary (iWAT)	-	RT-PCR	Decrease lipolysis	Duparc et al. (2024)
	Fresh (eWAT)	-	RT-PCR	Not stated	Laplante et al. (2010)

Continuation of Table 1.2

Receptor	Cell type	Screened?	Method	Role	Reference
P2Y14	W.T (eWAT)	n/a	qRT-PCR	Pro-inflammation	Xu et al. (2020)
	Fresh (iWAT/eWAT)	-	RT-PCR	Decrease lipolysis	Jain et al. (2021)

1.4 Nervous system

1.4.1 Structure of the nervous system

The CNS is comprised of the brain, brain stem, spinal column and all nerves within it. The CNS is therefore the core operating system, critical to all function including all voluntary and involuntary movement and processes. The hypothalamus within the brain is considered the "master regulator" for appetite control and for conducting lipolytic events to regulate metabolism, instructing adipose stores to liberate stored triglycerides (Bartness et al. 2005). The nerves that conduct information to and from the CNS in the form of action potentials, constitute the peripheral nervous system, which consists of two branches. The afferent division, including somatic, visceral and special sensory nerves, which deliver information from target organs toward the CNS. The efferent division deliver information away from the CNS to induce effects at target tissues. Efferent nerves include somatic motor and autonomic nerves, which further divide into sympathetic, enteric and para-sympathetic nerves (Hammond 2015). Innervation of WAT is suggested to be sympathetic and sensory with no reported parasympathetic contribution (Bartness et al. 2014; Mishra & Townsend 2024). The sensory nerves deliver information on the state of adipose stores to the hypothalamus, which can appropriately modify the sympathetic outflow to adipose in response (Ryu et al. 2017). The adipokine leptin is a key modulator operating within this axis, potentiating sympathetic outflow in periods of adipose repletion.

While the sensory arm of the axis is not fully resolved, with research ongoing to determine the signalling elements perceived within WAT to stimulate CNS cross-talk, the focus of this PhD project is on sympathetic nerves and their associated signalling components in the regulation of lipolysis.

1.4.2 Autonomic sympathetic nerves

Sympathetic nerves are synonymous with "fight or flight" responses, but also have key roles in the delivery of CNS-derived stimulation for the regulation of involuntary processes, including lipolysis. It was previously thought that blood vessels within WAT were responsible for delivering catecholamines (epinephrine) to induce lipolysis (Bart-

ness et al. 2007; Bartness et al. 2014). However, over the last few decades, researchers have illustrated the irrefutable presence and role of sympathetic neurons within white adipose tissue. In studies of WAT sympathetic denervation, tissues repeatedly display hyperplastic growth, accompanied by increased depot mass, decreased lipolysis and are rendered unable to respond appropriately to applied stresses, such as starvation and cold-challenge (Youngstrom & Bartness 1998; Bartness et al. 2007; Bowers et al. 2004; Shi et al. 2005). Literature has therefore cemented the key role of sympathetic neurons in metabolic homeostasis.

1.4.2.0.1 Sympathetic nerve origins and organisation

Pre-ganglionic sympathetic nerves leave the spinal column via ventral roots, which joins with sensory fibres from the dorsal root to form the spinal nerve, where they travel along together. The sympathetic nerves leave the spinal nerve and branch off to the connecting white rami (white owing to myelination, although in rodents they are unmyelinated and clear) wherein the nerves enter the sympathetic chain ganglia (ScG) (paravertebral ganglia) (Figure 1.6). The ScG is a chain of nervous tissue that flanks either side of the spine from the neck (cervical) to the base of the spine (sacral) with a ganglion 'bulb' associated with nearly every spinal vertebrae (Hammond 2015). Sympathetic nerves can leave the ScG in three main ways: nerves can synapse within the ScG either at the corresponding level of the spine, or can travel along (up or down) the chain to synapse at other levels, and leave as post-ganglionic fibres to innervate tissues (Saladin 2021). Secondly, post-ganglionic sympathetic nerves can integrate with sensory nerves by exiting the ScG via the grey ramus and travel together via the spinal nerve route, which splits into dorsal and ventral ramus. The ventral further splintering into multiple other branches of mixed-identity neurons. Lastly, sympathetic nerves can also travel out of the ScG as pre-ganglionic neurons and congregate together to synapse in collateral ganglia (also termed prevertebral ganglia) away from the ScG, for example the coeliac ganglion. Post-ganglionic projections can then travel toward target organs (Figure 1.6) (Saladin 2021). The individual ganglia comprising the ScG are named and numbered according to their location, which corresponds to the spinal regions; cervical, thoracic, lumbar and sacral regions.

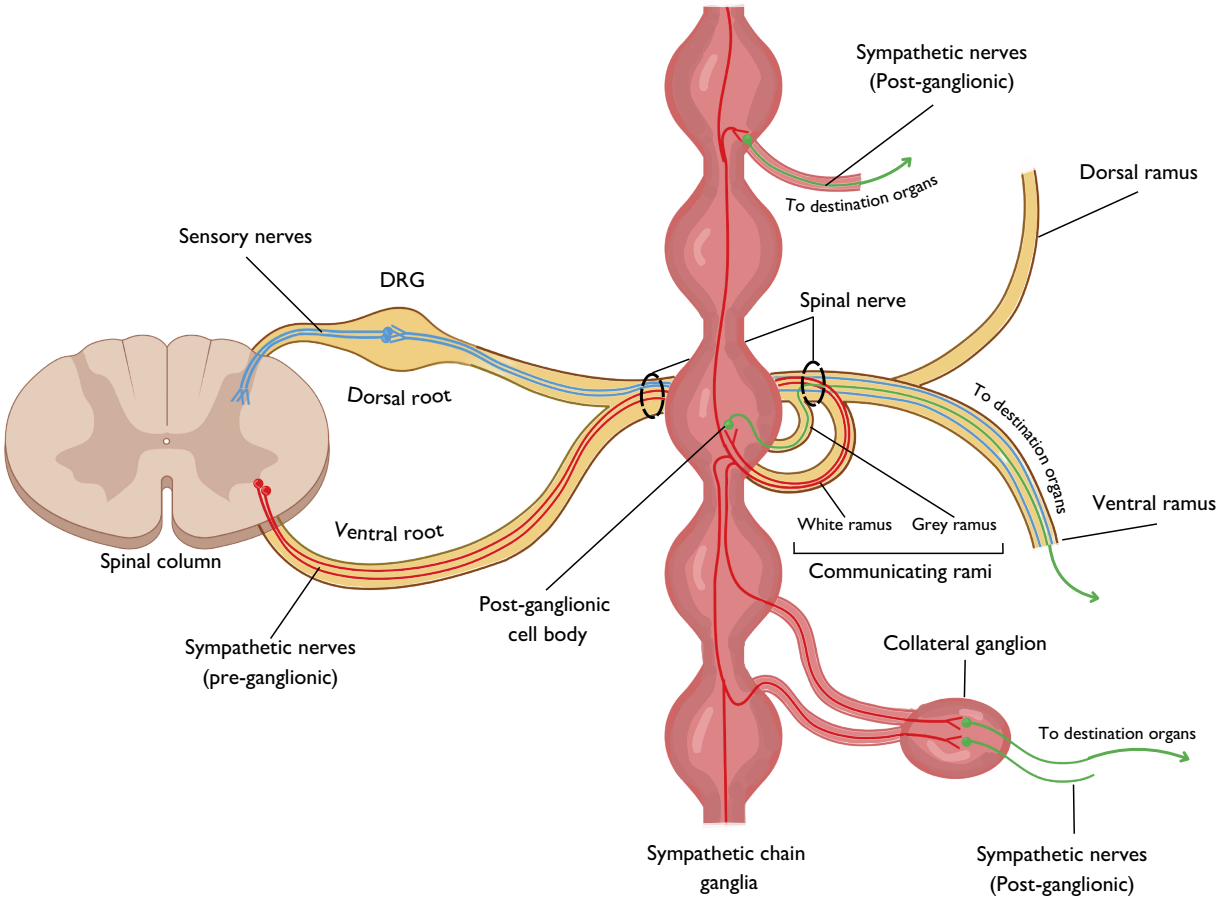

Figure 1.6: Pre- and post-ganglionic sympathetic nerve organisation and travel from the sympathetic chain ganglia. An illustration of pre-ganglionic sympathetic nerve origins and organisation. The sympathetic (red) cell bodies reside in the spinal cord and travel via the ventral root which merges with sensory nerves (blue) from the dorsal root, in the spinal nerve. Branching from the spinal nerve are the white and grey communicating rami, with sympathetic nerves entering the sympathetic chain ganglia (ScG) via the latter. From here, sympathetic nerves can synapse to form post-ganglionic efferents (green) which can leave the ScG at the point of entry, or move to higher or lower ganglia to synapse and leave toward destination organs. Post-ganglionic sympathetic nerves can also leave the ScG via the white ramus to congregate with sensory fibres back in spinal nerves to form the ventral ramus and travel to innervate destination tissues together in mixed-identity bundles. Alternatively, sympathetic nerves can leave the ScG as pre-ganglionic fibres and instead synapse in distal collateral ganglia. 'DRG' refers to dorsal root ganglion. Figure adapted from Saladin 2021.

1.4.2.0.2 Neurotransmitters

Norepinephrine

Once at their destination, sympathetic nerves release neurotransmitters, principally norepinephrine, to target postjunctional receptors. Norepinephrine is a catecholamine derived from precursor tyrosine in a multi-step process. Tyrosine is converted to dihydroxyphenylalanine (DOPA) by tyrosine hydroxylase, which is then converted to dopamine by DOPA decarboxylase and finally dopamine-B-hydroxylase generates norepinephrine (Daubner et al. 2011). The rate-limiting tyrosine hydroxylase enzyme can be synthesised both within the axon and at synaptic terminals of neurons (Gervasi et al. 2016). As already alluded in section 1.2.3, norepinephrine binds to a suite of GPCR adrenergic receptors; α1 (G_q-linked) & α2 (G_i-linked) ARs as well as β1- β2- & β3-ARs (chiefly G_s-linked). The outcome of norepinephrine signalling depends on the palette of adrenergic receptors the target cell expresses and as already established, in adipocytes these link to lipolysis machinery.

Clearance of norepinephrine is critical to termination of signalling and prevention of unregulated over-stimulation. One route of clearance is via extra-neuronal degradation via catechol-o-methyl transferase (COMT), although it is suggested that 90% of norepinephrine is reuptaken by the nerve into the presynapse (Ryuid & Buettner 2019). Uptake is facilitated via active transporter solute carrier family 6 member 2 (SLC6A2) expressed on the presynapse, wherein norepinephrine can be degraded by mitochondrial monoamine oxidase (MAO), or recycled back into vesicles ready for re-release (Ryuid & Buettner 2019). Macrophages are also known to express the SLC6A2 transporter as well as MAO in adipose tissue, with important roles in norepinephrine clearance (Pirzgalska et al. 2017). Adipocytes also express another subtype of active transporter, organic cation transporter 3 (Oct3) along with degradation enzymes, which are now thought to have important roles in norepinephrine uptake (Song et al. 2019). Vasculature can also scavenge and uptake norepinephrine (Horvath et al. 2003), offering a plethora of clearance routes for norepinephrine in WAT.

NPY

Neuropeptide Y (NPY) is a well-established co-transmitter alongside norepinephrine in sympathetic nerves in the CNS and PNS (Beck 2006; Lundberg et al. 1989). NPY acts via principally G_i-linked GPCR Y receptors (Y1-Y5 & y6 in mouse) (Pedragosa-Badia et al. 2013), although Y2 and Y4 receptors may couple to G_q in some cases. The release of NPY from synapses is dependent on stimulation characteristics such as high intensity and frequency, which is less important for the release of norepinephrine or ATP (Hill et al. 2001; Labelle et al. 1997).

The impact of executive-level NPY activity reportedly has profound orexigenic effects on appetite, feeding and thereby weight (Stanley et al. 1986; Long et al. 2015; Chao et al. 2011). NPY is upregulated during periods of energy deficiency to increase caloric consumption and restore energy balance, while also reducing sympathetic outflow to adipose (Zhang et al. 2014). NPY has also been positively correlated with obese phenotypes such as hyperplasia (Zhang et al. 2014), with increases in NPY expression in adipose tissue observed during obesity (Yang et al. 2008). Several cell-based and *in vivo* models have investigated the relationship between NPY and adipose accumulation at a peripheral level. NPY receptors Y1, Y2 and Y5R have been identified peripherally in adipose tissue & adipocytes (Kuo et al. 2007; Gericke et al. 2009; Long et al. 2015). When challenged, Y1 & Y2R were found to have roles in adipogenesis and had anti-lipolytic effects (Kuo et al. 2007; Turtzo et al. 2001; Gericke et al. 2009) potentially serving as a negative regulator of norepinephrine-stimulated lipolysis. There is very little direct evidence that illustrates sympathetic nerves innervating peripheral WAT release NPY to regulate lipolysis in this manner. The closest evidence comes from *in vivo* studies, where conditional (adipose specific) knock down (KD) of the Y2 receptor prevented accumulation of fat in response to HFD, suggesting it is typically present and responding to local release of NPY (Shi et al. 2012). Additionally, adipocytes isolated from rat iWAT showed a 25% decrease in lipolytic response after exposure to NPY, which was attributed to the Y1 receptor (Labelle et al. 1997).

ATP

ATP is now a well-established co-transmitter in sensory, parasympathetic and sym-

pathetic nerves, (Burnstock 2006). ATP has been found as an important pre- and postjunctional modulator of vascular tone, acting both on neighbouring sympathetic neurons and on vascular smooth muscle cells (Burnstock 2009b). At the time of writing, there is no direct evidence published which demonstrates that ATP is being co-released alongside norepinephrine in WAT or more specifically, the inguinal fat depot, and of the references found, the evidence appears based on inference or conjecture (Pfeifer et al. 2024).

Section 1.3.4 has already outlined the possible postjunctional effects of ATP and other nucleotides in WAT. Prejunctional neuromodulatory roles of ATP specifically in WAT are less well studied. Neuromodulation refers to the alteration of neuronal activity by some means of perturbation or potentiation of its output, via prejunctionally expressed receptors. A variety of purinergic receptors have been identified prejunctionally in many species for example P2X1 (Queiroz et al. 2003), P2Y1 (Filippov et al. 2006), P2Y2 (Liu et al. 2000), P2Y12 (Lechner et al. 2004). However, P2X2 and P2X3 subunits are suggested to be the most common and abundant subunits expressed on sympathetic and sensory nerves (Cockayne et al. 2005).

Owing to their [Ca^{2+}]i increasing effects, P2X receptors are often implicated in positive neuromodulation. The P2X2 receptor was found expressed in primary cultured neurons of the rat superior cervical ganglion and P2X2 was proposed a positive modulator of nervous activity, increasing neurotransmitter release in response to ATP (Boehm 1999). Expression of the P2X2 receptor on these nerves was mirrored in other studies, where the proposed physiological role was confirmed by impaired urinary bladder reflexes in P2X2 and P2X2/P2X3 DKO mice (Cockayne et al. 2005). Guinea pig sympathetic nerves also reportedly express P2X2 and P2X2/3 heterotrimeric receptors (Zhong et al. 2000) and in Guinea pig atria, activation of either P2X3 or P2X2/3 has been associated with stimulating norepinephrine outflow (Sperlágh et al. 2000). Similarly, P2X3 and P2X2/3 were suggested to be involved in facilitatory modulation of norepinephrine outflow in rat sympathetic nerves of the vas deferens (Queiroz et al. 2003).

1.4.3 Somatic sensory nerves

Alongside sympathetic innervation within adipose tissue, over the last few decades research has illuminated the presence of sensory neurons and provided evidence of their

function (Ryu et al. 2017). Sensory neurons are afferent fibres that transmit signals from peripheral tissues, towards the CNS/brain for processing (Liu et al. 2019). In the context of WAT, these nerves are thought to communicate information regarding adipose energy store status, in response to local stimuli (Bartness et al. 2005).

Advancements in 3D imaging techniques have illustrated sensory neuron innervation in WAT in several research papers in the last decade. Some reports suggest moderate abundance compared to sympathetic innervation (Willows et al. 2021; Giordano et al. 2006), while others suggest sensory innervation is abundant (Wang et al. 2022). Secondly, the importance of sensory innervation of WAT has been demonstrated in sensory denervation studies. Deafferentation of the inguinal fat depot in Siberian hamsters led to hypertrophic adipocytes and an overall increase in fat depot mass, which the authors proposed was due to a break in communication circuit between the brain and adipose (Shi & Bartness 2005; Bartness et al. 2005). Evidence such as this indicates sensory neurons are important in limiting lipogenesis and adipocyte size. In recent studies, sensory nerves are suggested to act as regulatory brakes on apparent lipogenic signals derived from sympathetic nerves. Genetic ablation of somatosensory nerves from mouse iWAT, led to enlarged depots, in spite of sympathetic nerve presence, and was suggested to be due to local regulatory signalling mechanisms that counter sympathetic signalling (Wang et al. 2022).

1.4.3.0.1 Antidromic/reflex arc signalling

As above, alongside afferent signalling, sensory innervation in WAT also presents an efferent means of communication that may influence metabolism. In what is termed antidromic signalling, receipt of stimulatory signals by sensory nerves innervating the peripheral tissue can induce a reflex arc, where vesicles of neurotransmitter are released back onto the tissue to signal locally (Burnstock & Ralevic 1994). This type of signalling has been described in vascular control (Burnstock & Ralevic 1994; Burnstock 2009). Therefore, sensory neuropeptides calcitonin gene related peptide (CGRP) and substance P (SP) are candidates for local reflex signalling in WAT. CGRP receptors are predominantly linked to G_s mechanics to raise intracellular cAMP (Walker et al. 2010), while SP NK receptors are predominantly G_q-linked (Mishra & Lal 2021). Receptors for both sensory neurotransmitters, are found expressed on white adipocytes (Miegueu

et al. 2013; Liu et al. 2017; Halloran et al. 2020) and are reported to have roles in lipogenesis and lipolysis (Walker et al. 2014). However, there is conflicting evidence regarding CGRP roles in lipolysis, with some suggesting a lipolytic role (Walker et al. 2014), and others an anti-lipolytic role (Liu et al. 2017). The role of these neuropeptides in WAT-level regulation is under debate, with mixed evidence pertaining to their role. There is also limited evidence that demonstrates adipose-specific release and response of these neuropeptides, thus the roles in adipose remain unclear (Mishra & Townsend 2023; Mishra & Townsend 2024).

1.4.4 Mechanics of nervous conduction

1.4.4.1 Action potentials

Nerves are excitable as they can generate action potentials, which are an ionic propagation along the length of an axon toward the synaptic terminals, and are governed by electrochemical gradients (Hammond 2015). An axon membrane is embellished with ion channels and active ion transporters to generate an imbalance of electrical and chemical charge across the membrane, rendering the intracellular axonal compartment more negative than the extracellular environment. At rest, the axon membrane potential is around -60mV and is maintained by greater permeability to K^+ than Na^+ ions, which creates a electrochemical disequilibrium to which the Na^+ gradient is harnessed to conduct a signal (Barnett & Larkman 2007). At the inception of stimulation at the cell body, activation of ligand-gated ion channels allow Na^+ entry into the axon, which upon generating enough charge to reach the threshold potential of -50mV, activates a dense population of voltage-gated sodium (VGSCs) (or Na_V) channels. These channels perceive increased charge via intracellular voltage-sensing domains, which causes a conformational change and induces rapid opening and subsequent local Na^+ entry into the axon (Armstrong & Hille 1998). This in turn triggers opening of neighbouring Na_V channels, which rapidly decreases the membrane potential (depolarises), as Na^+ moves to equalise the gradient, rising to near +40mV. In response to these rises, the Na_V channels shut and enter an 'inactive' state whereupon they are unresponsive to any changes in membrane potential for a period of time (Ulbricht 2005). Concurrently, the decreased membrane potential causes K^+ ions to leave though K^+-permeable channels, while also triggering

slow-activating voltage gated K^+ (K_V) channel opening (after a slight delay), allowing more K^+ to leave the axon to initiate repolarisation. The resulting fall of membrane potential continues beyond the point of restoring the rest membrane potential, and proceeds to around -70mV which constitutes a refractory period. During this period it is not possible for another depolarising event to occur in the localised region of the axon, preventing 'backward' propagation of the Na^+ signal (Barnett & Larkman 2007). Instead, the Na^+ ions propel forward to trigger Na_V channel opening in a sequential chain of local regions toward the synapse, away from the site of activation, thus generating and conducting an action potential (Hammond 2015).

1.4.4.1.1 Toxins in nerve conduction

There are tools to study nervous activity derived from plants and animals, for example veratridine is a plant-derived steroidal alkaloid from the Veratrum genus of Lilies and is a recognised neurotoxin. It acts upon Na_V channels located on excitable cell types, such as neurons (IC50 18.39 μM) (Hemmings 2009). Veratridine binds to receptor site 2 on the transmembrane 6 segment of domain I and IV of the α-subunit of the Na_V channel (Ruiz et al. 2015; Suppiramaniam et al. 2010; Zhang et al. 2018; Cestèle et al. 2000) on the inner vestibule of the pore domain (central cavity) (Figure 1.7). Veratridine binding occurs in a state-dependent manner, having preference for the open "activated" state (Hemmings 2009), although has been suggested as capable of binding to closed, but not inactive, states (Ruiz et al. 2015). Binding in this manner slows down inactivation and closure of the channel, allowing Na^+ to enter the axon and conduct the action potential (Hemmings 2009). Wada and colleagues found that exposure of excitable cells to veratridine increased Na^+ influx and subsequent catecholamine efflux (Wada et al. 1992).

There are ten known Na_V channels, ranging from Na_V 1.1-9 & NaX, which are grouped in terms of sensitivity to the Na_V channel blocker, tetrodotoxin (TTX). Na_V 1.1, 1.2, 1.3, 1.4, 1.6, 1.7 & NaX being TTX-sensitive, and Na_V 1.5, Na_V 1.8, & Na_V 1.9 as TTX-insensitive (Zhang et al. 2018). The Na_V channel subtypes are localised to different tissues/cells, in particular Na_V 1.7 being found on peripheral sympathetic and sensory neurons (Wang et al. 2017).

TTX is an animal-derived toxin, originating from the family of Tetraodontidae pufferfish. As above, TTX also acts on Na_V channels with high affinity (Kd 1-10 nM) by binding to, and blocking, the entrance to the pore at site 1 on the TM6 of the αD1-4 units of the channel, preventing Na^+ influx (Park et al. 2023) (see Figure 1.7). TTX-resistant subtypes (Na_V 1.5, Na_V 1.8 & Na_V 1.9) have mutations at critical binding sites, which prevent effective binding of TTX (Jost et al. 2008; Chen et al. 2014).

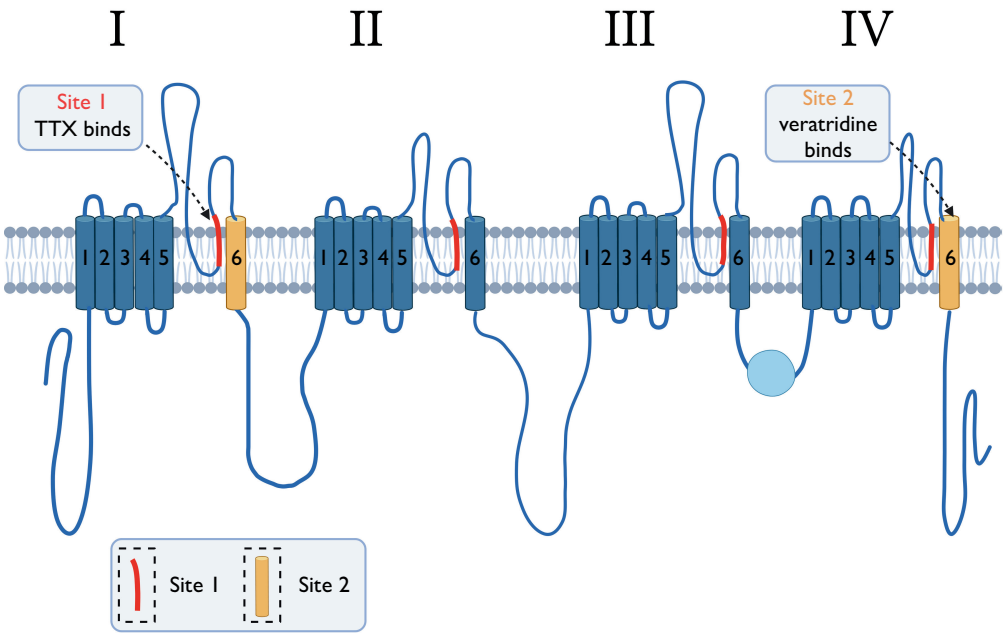

Figure 1.7: Binding sites for neurotoxins tetrodotoxin and veratridine on voltage-gated sodium channels. 2D illustration of the α-subunit of a voltage gated sodium channel, including each domain I-IV and binding sites 1 & 2. Site 1 where tetrodotoxin (TTX) binds is indicated in red, and Site 2 where veratridine binds in yellow. Figure adapted from Ruiz et al. (2015).

1.4.4.2 Exocytosis

The dependence on extracellular Ca^{2+} to induce synaptic vesicular fusion was first described in the late 1960s (Katz et al. 1967), which has been characterised and established as the canonical route of exocytosis in decades since (Südhof 2012). In the canonical

route of Ca^{2+}-dependent exocytosis, once the action potential has reached a synapse, the Na^{+}-induced membrane depolarisation culminates to evoke activation of Ca_V channels (predominantly N-type). Ca_V channel voltage sensors perceiving the depolarisation induce a conformational change, which allows Ca^{2+} entry down the concentration gradient into the synapse via the pore of the channel (Catterall 2011). Within the synapse, vesicles containing neurotransmitter have proteins embedded within the vesicle wall, synaptotagamin and synaptobrevin, which are soluble NSF attachment receptors (v-SNAREs). Synaptotagamin (Syt1) is a Ca^{2+} sensor, and when bound to Ca^{2+} has a high affinity for phospholipids, and rapidly translocates towards the inner membrane of the terminal (Chapman 2018; Brose et al. 1992). At the membrane, v-SNARE synaptobrevin coils with t-SNAREs (syntaxin and SNAP-25) to form SNARE complexes, which allows the vesicle to dock the membrane to release its contents (Südhof 2012; Chapman 2018; He et al. 2018). The Ca^{2+} dependency of the exocytosis event is demonstrated by removal of rapid exocytosis when Syt1 is genetically deleted (Geppert et al. 1994), or when active Ca^{2+} binding sites of Syt1 are blocked (Pang et al. 2010).

Chemical synaptic terminals, those that deliver information via a chemical stimulus as described above, can form a terminal 'bouton' structure, commonly found within the CNS (Burns & Augustine 1995). Synapses can also present as axonal varicosities, with multiple terminal 'beads' along the length of the axon as it innervates the target tissue. These are frequently observed in the autonomic PNS, for example in smooth muscle of vascular systems and the urinary bladder (Burnstock et al. 2009). Terminal bouton synapses offer direct communication to specific recipients, while axonal varicosities allow for diffuse delivery of catecholamines for broader, efficient communications to multiple cells in synchrony (Bennett et al. 1998).

1.5 Anatomy of inguinal adipose

Investigation into SAT using mouse models commonly feature iWAT owing to its size, innervation and vascularisation, enabling it to respond to dietary challenge. For example, the inguinal depot is prone to flux in volume in response to caloric restriction and abundance (Tang et al. 2017), and capable of induced stimulated lipolysis under *ex*

vivo conditions (Bridge-Comer et al. 2023; Roy et al. 2022). Over years of study, researchers have worked to characterise the inguinal adipose depot vascularisation and innervation. The mouse inguinal fat depot is generally compartmentalised into regions, with anterior portions proximal to the spine, termed dorsolumbar regions and posterior portions, proximal to the leg, as inguinal regions (Figure 1.8).

The dorsolumbar region is the principal site of venous entry, via major branches of thoracoepigastric vein. Within the dorsolumbar portion are the inguinal lymph nodes (LN), which is a key site of arterial entry from the superficial caudal epigastric artery (a branch of the femoral artery) (Blaszkiewicz et al. 2019a). From the LN, lymphatic vessels traverse the depot and extend downward toward the hind leg, where lymph is drained (Harrell et al. 2008). The inguinal region contains smaller vasculature, including minor branches of the common iliac vein. Spanning these regions are large, heterogeneous bundles of nerve fibres (Blaszkiewicz et al. 2019a). Further to the large bundles of neurons are networks of individual nerve fibres, which innervate the entire depot.

Research over the last few decades has illuminated the spinal origin of sympathetic innervation in white adipose tissue. Bartness and colleagues led the investigation into the origin of sympathetic neurons innervating WAT using pseudorabies virus (PRV) and Fluorogold retrograde tracing techniques (Youngstrom et al. 1995; Bartness et al. 2007). PRV techniques can be misleading and non-specific as they can 'leak' to stain other nerves in neighbouring ganglia (Martinez-Sanchez et al. 2022). There are mixed reports of innervation origins published, and the evidence has recently advanced due to thorough policing of signal in retrograde tracing techniques. In recent work, authors use a transgenic sympathetic TH-tomato reporter mouse to identify the sympathetic neurons, before injecting GFP labelled PRV into the iWAT. Then, using whole mount clearing techniques to clear entire torsos, trace the origins of sympathetic innervation (Huesing et al. 2021).

Spinal inputs toward the inguinal fat depot are from T7 - T11, which feed into the sympathetic chain ganglia (ScG). From there, dorsolumbar regions are innervated from ScG T12 - L1 by lateral cutaneous rami, which coarse through the fat depot through to dermal layers, with some branching within adipose to potentially form origins of innervation (Figure 1.8) (Huesing et al. 2021).

The inguinal portion is largely innervated from lumbar regions of the ScG L1 - L2,

which form the anterior cutaneous femoral nerve and lateral cutaneous femoral nerves. These innervations, as well as other minor nerve inputs, derive from the lumbar plexus (Figure 1.8) (Huesing et al. 2021). Other studies have suggested innervation arises from the collateral coeliac ganglia, using similar techniques (Jiang et al. 2017), but in more recent work, all of the innervations within the inguinal fat depot are suggested to be post-ganglionic, with none arising from collateral ganglia (Huesing et al. 2021).

Others have confirmed these findings, while demonstrating sensory input also occurs via T11 - L3 dorsal root ganglia (DRG) (Wang et al. 2022).

There are mixed reports as to the extents of sympathetic innervation in iWAT, particularly in regard to parenchymal and adipocyte innervation, with some reports declaring greater density of innervation (Jiang et al. 2017; Giordano et al. 2006), than others (Zeng et al. 2015; Willows et al. 2021). The mode of synaptic terminal is also not fully resolved in iWAT and termed "elusive" in literature, as adipocyte-neuron synapses are not well defined (Willows et al. 2021). Literature has offered both terminal synaptic bouton structures (Zeng et al. 2015) and axonal varicosities (Willows et al. 2021; Huesing et al. 2021) as the terminals present in iWAT, indicating the synaptic mode in iWAT is unresolved.

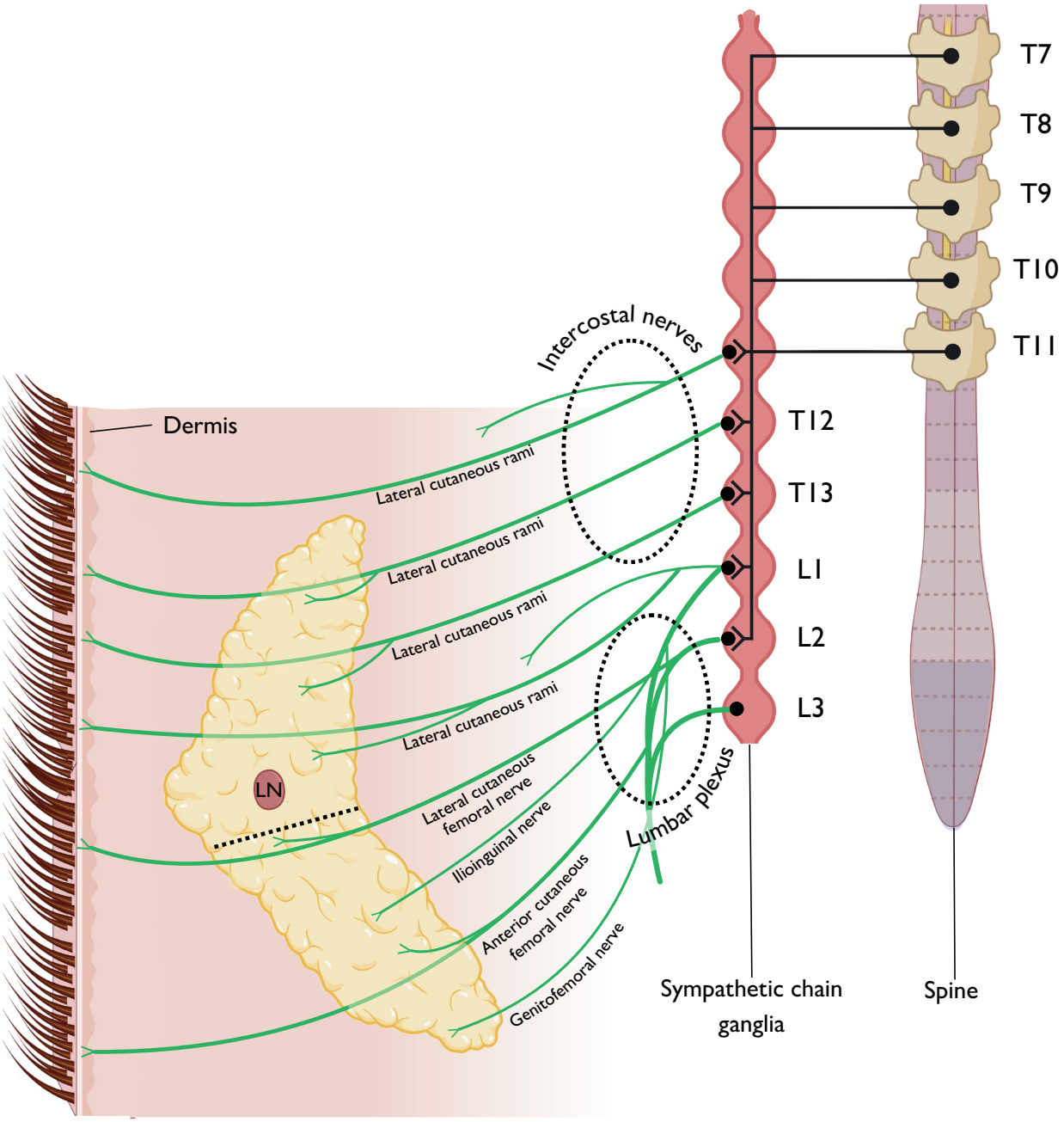

Figure 1.8: Anatomy of sympathetic innervation of the inguinal adipose depot. Illustrative diagram of the spinal and sympathetic chain ganglion (ScG) anatomy of sympathetic nerves that innervate the inguinal adipose depot. Spinal inputs into the ScG from T7 - T11 which then leave as post-ganglionic sympathetic nerves from T12 - L1 to innervate the inguinal depot dorsolumbar regions in the form of lateral cutaneous rami. Inputs to the inguinal regions of the depot derive from the lumbar plexus with main innervations branches of the femoral nerves. Nerves travel through the depot to innervate dermal layers. 'LN' refers to lymph node. 'T' refers to thoracic and 'L' to lumbar. Dotted black line across the inguinal depot shows division of upper dorsolumbar and lower inguinal regions. Figure adapted from Huesing et al. 2021 and Martinez-Sanchez et al. 2022.

1.6 Aims and objectives

Obesity is a key concern, and research is rightfully occupied in understanding the mechanics of metabolic physiology to provide therapeutic insights for potential future treatment and mitigative strategies. As hopefully ascertained though the thread of the present chapter, understanding the innervation of white adipose tissue is important to proper function. Vasculature and nerves have been illustrated to become dysfunctional or lost during obesity, which perpetuates the obese state. Vascularisation and nervous innervation therefore plays an important role in physiological maintenance, health and control of white adipose.

The research that investigates lipolysis frequently stems from models that are not fully representative of physiology *in vivo*, often using cell lines and 2D culture methods. There are limited models available to study lipolysis, incorporating all cells of the tissue and include endogenous nerve activation. Nervous innervation is integral to providing sources of key metabolic regulators such as norepinephrine, alongside others. Genetic-based KO and *in vivo* models to study lipolysis are better, but there are limited examples where all components of signalling such as NPY and ATP are investigated in more physiologically representative systems, additional to β-adrenergic roles.

The main aim of the project is to supplement published works and investigate the innervation of the inguinal fat depot, with emphasis on sympathetic nerve innervation of adipocytes, to inform functional inquiry. Then, harnessing this data, to re-investigate lipolysis mechanics using a more representative model, via inducing endogenous sources of nerve-derived norepinephrine. I also aim to interrogate involvement of other nerve-derived neurotransmitters in lipolysis, including sympathetic NPY and ATP and sensory SP and CGRP, with pharmacological challenge of their respective receptors in an effort to resolve their role. More specifically, I seek to establish whether purinergic signalling has any contribution to nerve output in white adipose tissue, or lipolysis (either basally or stimulated).

Chapter 2

Methods

2.1 Drugs and reagents

Details of the concentrations of given drugs, alongside supportive references, can be found in-text of relevant chapters. All drugs and kits used throughout this work are stored at -20°C and thawed to room temperature or kept on ice while in use. The glycerol assay kit described in Section 2.4 was split into aliquots to prevent degradation. Drugs were dissolved in dimethyl sulfoxide (DMSO), Hanks balanced salt solution (HBSS), phosphate buffered saline (PBS) or dH_2O according to manufacturers instructions. HBSS containing sodium chloride (136.9 mM), potassium chloride (5.3 mM), calcium chloride (1.26 mM), magnesium sulphate heptahydrate (0.4 mM), magnesium chloride (1.05 mM), sodium phosphate (0.42 mM), potassium phosphate (0.44 mM), D-glucose (5.5 mM) and sodium bicarbonate (4.16 mM) (adjusted to pH 7), was freshly prepared in-house on a weekly basis and refrigerated at 4°C or frozen at -20°C for long-term use.

Main suppliers of drugs and reagents were; Abcam (Cambridge, UK), Thermo Fisher Scientific (Loughborough, UK), Sigma-Aldrich (Gillingham, UK), Tocris Bioscience (Bristol, UK), Alomone (Jerusalem, Israel), Cayman Chemicals (Michigan, USA).

Table 2.1: List of pharmacological agents used in this thesis. A list of all pharmacological agents used within this thesis, including supplier, purpose of use and vehicle for each, in order of appearance. 'CTx' refers to conotoxin, *broad-spectrum.

Drug	Purpose	Supplier	Vehicle
Heparin sodium	Anticoagulant	Sigma	PBS
Norepinephrine	Lipolysis stimulant	Sigma	PBS
Isoprenaline	Lipolysis stimulant	Abcam	dH_2O
Veratridine	VGSC opener	Abcam	DMSO
Tetrodotoxin	VGSC blocker	Abcam	HBSS
Propranolol	β-AR antagonist	Sigma	EtOH
Sotalol	β-AR antagonist	Cayman	DMSO
CGP 20712	β1-AR antagonist	Tocris	dH_2O
ICI 118551	β2-AR antagonist	Tocris	dH_2O
L-748337	β3-AR antagonist	Tocris	DMSO
SR59230A	β3-AR antagonist	Tocris	DMSO
CTx GVIA	N-type Ca_V antagonist	Tocris	dH_2O
CTx MVIIC	P/Q/N-type Ca_V antagonist	Tocris	HBSS
Cilnidipine	N/L-type Ca_V antagonist	Sigma	DMSO
Nifedipine	L-type Ca_V antagonist	Sigma	DMSO
CGP 37157	mNCLX antagonist	Tocris	DMSO
KB-R7943	NCX antagonist	Tocris	DMSO
Yohimbine	a2-AR antagonist	Sigma	dH_2O
A-317941	P2X2 & P2X3 antagonist	Tocris	DMSO
BIBN 4096	CGRPR antagonist	Tocris	DMSO
CP-96345	SPR antagonist	Tocris	DMSO
BIBO 3304	NPY Y1R antagonist	Tocris	DMSO
BIIE 0246	NPY Y2R antagonist	Tocris	DMSO
L-152804	NPY Y5R antagonist	Tocris	DMSO
Suramin	*P2R antagonist	Sigma	dH_2O
PPADS	*P2R antagonist	Sigma	dH_2O
PSB-12062	P2X4R antagonist	Sigma	DMSO

Continuation of Table 2.1

Drug	Purpose	Supplier	Vehicle
MRS-2578	P2Y6R antagonist	Tocris	DMSO
ATP	Purinergic agonist	Abcam	dH_2O
ADP	Purinergic agonist	Sigma	dH_2O
UTP	Purinergic agonist	Sigma	dH_2O
UDP	Purinergic agonist	Sigma	dH_2O
ARL-67156	Ecto-enzyme inhibitor	Sigma	dH_2O
Apyrase	Nucleotide hydrolysis enzyme	Sigma	dH_2O

2.2 Mice and tissue

Male C57BL/6J mice were used in all experimental work due to their stable hormonal pattern and the lack of ductal structures in adipose depots (Chusyd et al. 2016). The C57BL/6J mouse strain is also receptive to diet-induced obesity (DIO), enabling future work to incorporate obesity states (Surwit et al. 1998). Mice were all adults of ages spanning 8-10 weeks old and were housed in the University of East Anglia's (UEA) Disease Modelling Unit (DMU). Within the DMU, the animals are maintained under stable conditions, with a set 12-hour light/dark cycle at a constant temperature of 21°C ($\pm$ 2°C) and humidity of 55% ($\pm$10%), with each cage ventilated and housing a maximum of 8 mice (typically 5). Water and standard chow food was available to mice *ad libitum*. The mice were sacrificed by primary CO_2 asphyxiation and secondary cervical dislocation by members of the DMU staff, in accordance with the Animals (Scientific Procedures) Act 1986.

To recapitulate, the murine inguinal fat depot is a subcutaneous white adipose depot and is located toward the mouse posterior, spanning the dorsolumbar, to inguinal region. As such, the inguinal depot is considered geographically comparable to human gluteofemoral (buttock) depots (Chusyd et al. 2016). The inguinal depot was selected due to its ability to expand via hypertrophy (Fryklund et al. 2022; Börgeson et al. 2022) and respond to metabolic flux (Tang et al. 2017; Frykland et al. 2022) and being one of the

largest SAT depots available in mice. The inguinal adipose depot is established within the research community and therefore is attractive to use as basis for investigation.

2.2.1 Dissection

Sacrificed mice were dissected as swiftly as possible post-mortem, typically within 5-10 minutes of sacrifice. To access the inguinal depot, incisions were made into the skin from approximately centre of the diaphragm and cut downwards to the genitals. The animal was essentially degloved from arm to leg in a lateral manner, away from the body, where the resulting pinned skin presented the subcutaneous depots. The inguinal depot was dissected out whole with fresh, sharp scalpels and carefully transported to HBSS to wash away residue hair and blood. From this point, tissues entered into one of three core techniques, immediately sub-dissected for glycerol assay experiments, fixed in 4% paraformaldehyde (PFA) for immunocytochemistry experiments, or the depots were enzymatically digested for adipocyte experiments.

2.3 Adipocyte isolation

For suitable yields of adipocytes, two full inguinal fat pads were required in each adipocyte isolation attempt, typically weighing 170 - 190 mg (wet weight) combined. Inguinal depots were minced in 15 mL Falcon tubes (Thermo Scientific) with 5 mL filtered digestion solution containing 1 mg (0.2 mg/mL) collagenase type IA from *Clostridium histolyticum* (Sigma) and 0.2 mg (40 μg/mL) bovine pancreatic DNase I (Biomatik) using clean and sterilised small embroidery scissors. Post maceration, the tissues were quickly transferred to an incubator at 37°C for 30 minutes, with gentle inversions every 10 minutes to encourage cell-matrix dissociation. Digested tissue was then passed through a 100 μm cell strainer (Corning®) into a 50 μL Falcon tube to remove larger undigested portions of tissue, then gently washed over with 50 mL HBSS. Suspended cells were centrifuged at approximately 50 xg (550 rpm) for 4 minutes at room temperature (RT) to gently separate adipocyte and stromal vascular fractions (SVF). In theory, the floating fraction should contain only adipocytes, while the pelleted SVF fraction contains all remaining cell types found in the fat pad, including lymph and blood vasculature, neurons, and immune cells. The floating layer of adipocytes were carefully removed into a fresh 15 mL

Falcon tube, washed with HBSS (or low-glucose DMEM for glycerol assay experiments) and re-centrifuged for a further four minutes at 50 xg to remove any adherent SVF cells. Two washes were found to be optimal purity/yield balance, as loss of adipocytes occurs during each transfer. Harvested adipocytes were then treated immediately with TRI reagent for RNA extraction, or taken into the glycerol assay protocol. See Figure 2.1 for illustrative representation.

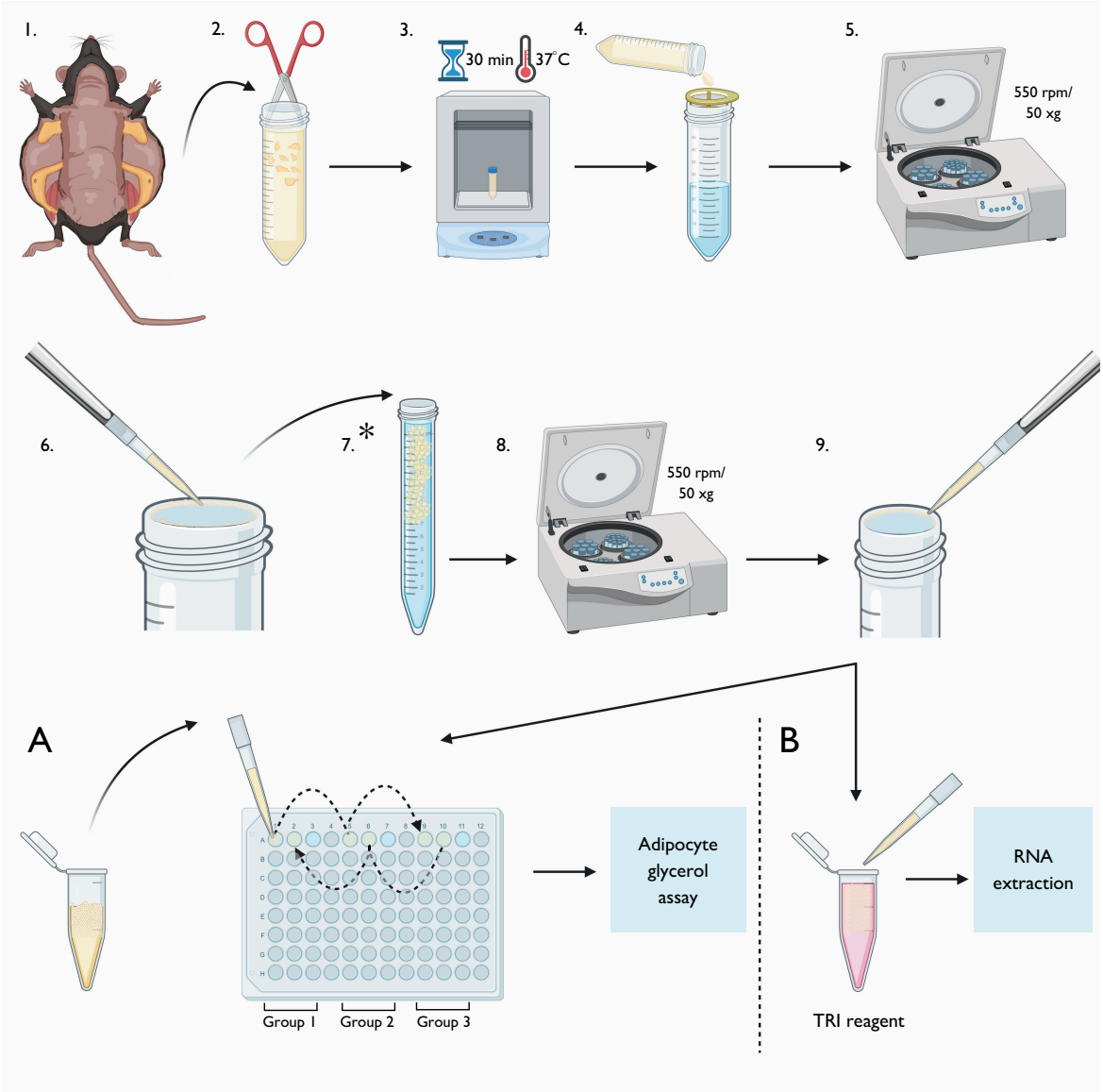

Figure 2.1: Adipocyte isolation. Illustration of the method used to isolate adipocytes from inguinal adipose depots. **1.** Inguinal depots are dissected and **2.** minced in digestion solution before **3.** incubation at 37°C for 30 minutes with gentle inversion. **4.** Digested tissues are passed through 100 μm strainer and washed with HBSS before **5.** centrifugation at 50 xg for 4 minutes. **6.** The 'halo' of adipocytes are gently removed and **7.** transferred to a Falcon tube containing experimental DMEM or HBSS (*depending on destined protocol) and **8.** re-spun at 50 xg for 4 minutes. **9.** Adipocytes carefully removed and taken forward into **A** adipocyte glycerol assay protocol or **B** RNA extraction for non-quantitative RT-PCR.

2.4 Glycerol release in adipose tissue *ex vivo*

2.4.1 Glycerol assay

Measurement of glycerol release from *ex vivo* sections of inguinal adipose tissue from mice was conducted using the following protocol. Harvested inguinal adipose depots were placed into an in-house made silicone-based (Sylgard™) petridish containing HBSS. The fat pads were carefully sub-dissected horizontally along the short edge into even sections (approximately 10-20 mg) with a single cut using a fresh scalpel (as to reduce mechanical disturbance). Tissue sections were blotted to remove any excess HBSS, then weighed to the nearest 0.1 mg. Next, tissues were placed into 1.5 mL Eppendorf tubes containing 150 μL 'experimental media', consisting of phenol red-free, low glucose (5 mM) Dulbecco's Modified Eagle Medium (DMEM) (Sigma) supplemented with 2% FFA-free BSA (Sigma) and 25 mM HEPES (Fisher) with pharmacological agents or vehicle controls. When using agents that require time to access and modulate their target, tissues were pre-incubated in this format for 30 minutes at RT, before moving to fresh tubes containing both agonists (veratridine, norepinephrine or isoprenaline) and modulatory agents. Tissues were then transported to an incubator and left un-lidded at 37°C and 5% CO_2 for 1 - 4 hours depending on the experimental design (most experiments lasted 3 hours). At the appropriate experimental time point, samples were removed from the incubator. Tissues were quickly removed and the remaining supernatant was sampled for glycerol content via colorimetric assay. All surplus sample media was frozen at -20°C. See Figure 2.2 for diagrammatic illustration.

It is important to note that this *ex vivo* process was time-critical during the initial stages. The dissection and tissue weighing was performed as rapidly as possible as to introduce tissues to DMEM in the least amount of time post-sacrifice. Delays in dissection of over 10 plus minutes after sacrifice would reduce lipolytic responsiveness of tissues to stimulants and thus cause experimental failure.

2.4.2 Adipocyte glycerol assay

To isolate the adipocytes, enzymatic digestion was performed as previously described, see section 2.3. Post digestion, adipocytes were washed in HBSS as above and centrifuged at 50 xg for 4 minutes. The floating 'halo' of adipocytes were carefully removed and placed into a 15 mL falcon containing a small volume of experimental DMEM, and slowly suffused with further DMEM until maximum volume of 15 mL was reached. The cell suspension was centrifuged for a second time at 50 xg for 4 minutes in experimental DMEM. The halo of cells was carefully removed again and placed into a 1.5 mL Eppendorf. To use the cells, gentle trituration of the cell solution was performed to ensure the cells were as evenly distributed as possible. A 50 μL aliquot of cell suspension was carefully added into wells of a 96-well plate containing 50 μL experimental DMEM including vehicles or pharmacological agents. To try and eliminate uneven adipocyte distribution across wells, the addition of cell suspension was stratified so that each test group received n = 1 cells in turn, one at a time, working from left of the plate to the right, and then right to left, with gentle cell trituration before each deposition, until each test group had n = 3 (see Figure 2.1 A for illustration). Where antagonists were used, all cells were incubated in experimental DMEM with antagonists at appropriate concentrations (or vehicle) for 30 minutes in a reduced volume of experimental DMEM at RT, prior to the addition of agonist (including antagonist to allow for dilution) in experimental DMEM, up to final volume of 100 μL. The plate of cells was then incubated at 37°C for 3 hours as above. Post-incubation, samples of infranatant were taken for colorimetric assessment of glycerol content.

2.4.3 Colorimetry

The colorimetric analysis was performed using Eppendorf 6131 spectrophotometer. Samples were prepared by vortexing (or triturating) and 10 μL of each sample alongside an experimental DMEM blank were loaded into Eppendorf cuvettes (Fisher). Using a glycerol assay kit (Sigma-Aldrich), an enzyme mixture was prepared per manufacturers instructions using provided ATP (1 μL), dye (1 μL), buffer (100 μL) and enzyme (2 μL) for each of the samples. 100 μL of the enzyme mixture was carefully added to each of the samples as to not introduce light-refractive bubbles. Any bubbles that did

occur were popped using a fine gauge needle. Samples were incubated for 20 minutes protected from light as per manufacturer instructions, then samples were processed in the spectrophotometer following the experimental DMEM 'blank', using absorbance of 550 nm. The assay works via a coupled enzyme reaction, with glycerol kinase converting glycerol to glycerol-3-phosphate (G3P), and glycerol phosphate oxidase generating hydrogen peroxide (H_2O_2) from G3P. Lastly, peroxidase enzymes catalyse the coupling of dye compounds with H_2O_2 to produce a colour change. The colour change, and thus absorbance, is proportional to the amount of glycerol substrate and therefore concentration can be determined with the use of a standard curve.

Herein, absorbance readings were recorded and used to calculate the μM concentration of glycerol using a standard curve generated with serial dilutions of manufacturer supplied 100 mM glycerol from concentrations of 500 μM to 3.9 μM. Using the equation gained from the standard curve, glycerol concentration of a given sample was calculated based on absorbance values, for the concentration of released glycerol in total 150 μL (100 μL adipocytes) media.

Glycerol concentration (μM) = (Sample - Blank) / Slope of standard curve

The calculated glycerol concentration was divided by the wet weight of the tissue to gain a μM glycerol/mg value corrected to tissue weight. These values were averaged within each condition to produce a mean μM glycerol/mg tissue value. For adipocytes, the control concentration values were averaged and treated as blank which were subtracted from "test group" values, for a response corrected to controls.

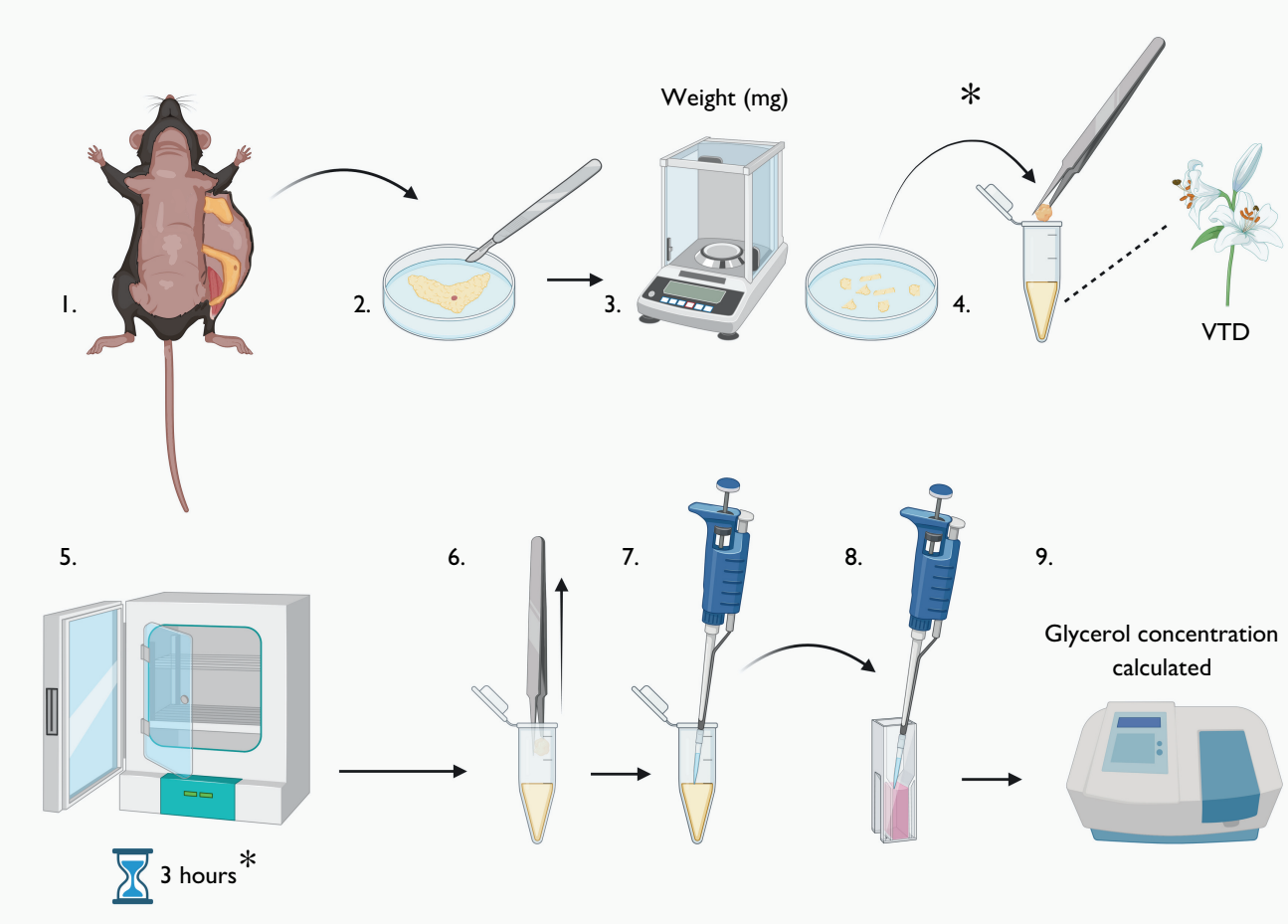

Figure 2.2: Glycerol assay protocol. Illustration of the methods used to conduct the glycerol assay. **1.** Inguinal depots dissected and **2.** sub-dissected into 10-20 mg sections and **3.** weighed then **4.** added to 1.5 mL Eppendorfs containing 150 μL experimental DMEM with stimulants such as norepinephrine or veratridine (***** preincubated with antagonists for 30 minutes before transferring into tubes containing stimulants). **5.** Samples transferred to culture incubators for 3 hours (*****depending on experiment, between 1 - 4 hours). Post-incubation **6.** tissues are removed from media and **7.** samples of supernatant transferred into **8.** cuvettes where glycerol determination enzyme solution is added and samples are incubated for 20 minutes and **9.** samples are loaded into spectrophotometer for colorimetric analysis and calculation of glycerol content based on absorbance values.

2.5 Non-quantitative reverse transcription (RT) PCR

Reverse transcription (RT) polymerase chain reaction (PCR) was conducted to firstly demonstrate isolated adipocyte populations were free from contamination of other cells, using candidate markers of the stromal vascular fraction (SVF). Secondly, to probe the expression of P2 receptors in the inguinal fat pad and adipocytes.

2.5.1 Total RNA extraction

For RNA extraction of the whole inguinal fat pad, a single fat pad was minced in 2 mL of TRI reagent (Sigma-Aldrich) using sharp sterile embroidery scissors, while the adipocytes having been isolated were split between two Eppendorf's and treated with 1 mL TRI reagent each. Samples were incubated in TRI reagent for 5 minutes at RT. Samples were then spun at 12 x 10^3 xg for 10 minutes and the lipid layer coating the surface was removed. Lysed cell contents were then perfused and vortexed with 100 μl 1-bromo-3-chloropropane (Fisher) to separate DNA from RNA in discrete 'phases' and left for 10 - 15 minutes at RT before undergoing a 4°C centrifugation at 12 x 10^3 xg for 15 minutes. The clear RNA-containing aqueous phase was transferred to a new 1.5 mL Eppendorf, where 500 μL of 100% isopropanol alcohol was added and the samples mixed and left at RT for 10 minutes, before centrifugation at 12 x 10^3 xg RT for a further 15 minutes. Following precipitation, pelleted samples were washed with 75% (v/v) ice-cold ethanol in nuclease-free water, centrifuged at 12 x 10^3 at 4°C for 10 minutes, then supernatant removed, and the RNA pellet allowed to air-dry for 10 minutes. The resulting pellet of RNA was subsequently re-suspended in an appropriate quantity of nuclease-free water and heated to 65°C for 5 minutes for complete RNA dissolution. Removal of any potential genomic DNA contamination was achieved using a DNA-*free* kit (Fisher), wherein the sample was incubated with 1 μL recombinant DNAse I (rDNAse I) and 3 μL associated buffer (DNAse I buffer) for 30 minutes at 37°C. Post incubation, 3 μL DNAse inactivation reagent was added to the sample and incubated for 2 minutes at RT before centrifuging at 10 x 10^3 xg for 2 minutes. The RNA-containing supernatant was carefully removed, and quality of RNA yield assessed using the Nanodrop 2000 (Thermo Fisher Scientific) and associated software. Yields of RNA varied, with typical adipocyte values ranging from 20 - 150 ng/μL and 260/280

nm absorbance ratios of 1.5 - 1.9. Full fat pad RNA quality and yield was generally improved, ranging from 150 - 380 ng/μL and 260/280 nm absorbance ratios between 1.7 and 2.0.

Generally, yield and quality was improved through optimising the protocol after consulting literature. After the addition of TRI reagent, there was a thick lipid raft on the surface, which others have noted affected the purity of RNA obtained (Sinitsky et al. 2018; Cirera 2013). Therefore, this lipid raft was removed by centrifuging with TRI reagent for 10 minutes at 12 x 10^3 xg and carefully siphoning of the lipid layer to improve quality. Also, steps were adjusted to reduce the amount of potential organic solvents or salts contaminating the RNA, where samples were spun at RT opposed to 4°C with isopropanol and the samples were gently inverted with ethanol opposed to vortexed (Sinitsky et al. 2018; Cirera 2013).

2.5.2 cDNA synthesis

To perform experimental processes such as PCR, the extracted RNA must be converted to complementary DNA (cDNA). Using reverse transcription, RNA template sequences are used to synthesise a cDNA strand via the action of reverse transcriptase enzymes. Therefore, 500 - 1000 ng (whole tissue) or 1000 - 2000 ng (adipocytes) of isolated total RNA was primed with 100 ng of random hexamer primers (Promega) in a solution up to 11 μL with nuclease free water, via a 10-minute 70°C heat induction then left on ice. Following heat treatment, each sample was then incubated at 42°C for 1 hour with a series of reagents and buffers essential for cDNA generation, including: 250 μM dNTPs (0.5 μL) (Bioline), 30 U RNasin®ribonuclease inhibitor (0.75 μL) (Promega), 10 mM DTT (2 μL), First-Strand Buffer (4 μL) (Invitrogen) and 200 U SuperScript™III reverse transcriptase (1 μL) (Invitrogen). Post incubation, the reaction was terminated with a 10 minute 70°C incubation to denature the reverse transcriptase enzymes, then synthesised cDNA samples were stored at -20°C. With each separate production of cDNA, a duplicate control was created without reverse transcriptase, to act as control for genomic DNA contamination. Further to this, per batch of cDNA produced, an additional water control was generated including all reagents without sample, to ensure any bands observed in gel electrophoresis were not attributable to contaminated PCR products, reagents or nuclease-free water.

2.5.3 Primer design

To investigate the purity of isolated adipocytes from the inguinal fat depot, a number of markers of the SVF were established. Literature was assessed as to components of the SVF and suitable antigen targets for identification (Bora & Majumdar 2017; Guo et al. 2016). These included **vasculature**: platelet-derived growth factor receptor (PDGFRβ), α-smooth muscle actin (α-SMA), lymphatic vessel endothelial hyaluronan receptor 1 (Lyve-1), platelet endothelial cell adhesion (Pecam-1), cluster of differentiation 146 (CD146); **immune cells:** lymphocyte common antigen (CD45), cluster of differentiation 8 (CD8), cluster of differentiation 14 (CD14); **neurons:** β3-tubulin. Perilipin-1 was used as a positive identification marker for adipocytes (Table 2.2). For each identified target, primer sequences were sourced directly from published literature, or generated using the Primer Blast tool (NCBI.gov) (Table 2.2). Where possible, primers selected had optimum melting temperature (Tm) values (55 - 60°C) and product sizes (500 - 700 base pairs), spanned exon-exon junctions (to reduce amplification of any present genomic DNA), had high gene of interest (GOI) specificity and where multiple options for gene variants, those targeting all or most common variants were chosen. For example readers will note CD146 has two reverse primers, 'a' and 'b', which authors designed to amplify two isoforms of the gene (Despoix et al. 2008).
For investigations into P2 receptor expression in murine adipocytes, primers were designed and sourced by former PhD student Dr Dalyan Eldaly and were tested for performance in mouse brain as a positive control prior to use.

All oligonucleotide primers were sourced from Thermo Fisher Scientific and are provided in a standard lyophilized powder form, which was then reconstituted to 100 μM master stocks with nuclease-free water. From these 100 μM stocks, working concentrations were made to 10 μM. All primers were stored at -20°C. For all RT-PCR work, the housekeeping gene glyceraldehyde 3-phosphate dehydrogenase (GAPDH), ubiquitously expressed in cells, was used with the following sequence: forward (5'-3'): ACAGTCCATGCCATCACTGCC Reverse (5'-3'): GCCTGCTTCACCACCTTCTTG and an expected band size of 266 base pairs (bp).

Table 2.2: SVF marker primers. A summation of markers and related primer sequences for various components of the stromal-vascular fraction of adipose, used to confirm purity of isolated adipocytes. Expected band size provided in base pairs (bp). References pertain to where primer sequences were sourced.

Marker	Gene	Sequence (5'-3')	Product size (bp)	Reference
Vasculature				
Endothelial cells, SMCs	PDGFR-β	F: AGCTACATGGCCCCTTATGA R: GGATCCCAAAAGACCAGACA	367	Basciani et al. (2020)
SMCs	αSMA	F: GACGTACAACTGGTATTGTG R: TCAGGATCTTCATGAGGTAG	144	Zhao et al. (2018)
Lymph	Lyve-1	F: TGGTGTTACTCCTCGCCTCT R: TTCTGCGCTGACTCTACCTG	214	Lim et al. (2018)
Endothelial cells	Pecam-1	F: AGGCTTGCATAGAGCTCCAG R: TTCTTGGTTTCCAGCTATGG	273	Srivastava et al. (2021) Li et al. (2009)
Pericytes & SMCs	CD146	F: TCACAGTCAGTCCTCACACCAG		Despoix et al. (2008)

Continuation of Table 2.2

Marker	Gene	Sequence (5'-3')	Product size (bp)	Reference
		R**a**: CCATCTCTTCTGGGAGCTTATCTG	**a**:261	Despoix et al. (2008)
		R**b**: CAGATCGATGTATTTCTCTCCATCTC	**b**:211	
Immune cells				
Haematopoietic stem cells & macrophages	CD45	F: GAACATGCTGCCAATGGTTCT R: TGTCCCACATGACTCCTTTCC	71	Manczak et al. (2009)
T-cells	CD8	F: CCGTTGACCCGCTTTCTGT R: CGGCGTCCATTTTCTTTGGAA	121	Molloy et al. (2017)
Macrophages	CD14	F: AAGGGTACAGCTGCAAGGAC R: GGAGCAAAGCCAGAGTTCCT	350	
Neurons				
Pan neuronal marker	β3-tubulin	F: ATGTCGTGCGGAAAGAGTGT R: CATCGAACATCTGCTGCGTG	534	
Adipocytes	Perilipin-1	F:TGGGCTGTCTGAGACTGAGG R: CTCACAAGGCTTGGTTTGGC	705	

Table 2.3: P2 receptor primers. A list of P2 purinergic receptor primer sequences used within this PhD project and expected band sizes in base pairs (bp).

P2R	Primer sequence (5'-3')	Band size (bp)
P2X1	F: CTGGGGAGGGTGAACGTGA R: GCAGTCACAGGCCAAAAGTG	505
P2X2	F: CGGGGTGGGCTCCTTTCTGT R: GGACATGGTTACTGAAGAGCG	499
P2X3	F: AGCTGGTGAGCTGGGATAGA R: AACCCACCCCACAAAGTAGG	533
P2X4	F: TCACCCTCTTGGTAAAGAACAAC R: CACGGTCGCCACCCCTA	500
P2X5	F: CCTGAAGGGCGGTGTGATAG R: ATCTGTTCCCTGCCAAGAGC	647
P2X6	F: CAGGCCAAGAACTTCACACTC R: GGGGCTCTTGCCTCTTCATATT	566
P2X7	F: GCTCCTAGGTGAGGGTTTGC R: GGCAAGATGTTTCTCGTGGT	712
P2Y1	F: TTATGTCAGCGTGCTGGTGT R: AGGGATGTCTTGTGACCATGT	668
P2Y2	F: TCTAGAGCGTGATCTCGGAGT R: TAAATGGCCAGTGGTCACCC	516
P2Y4	F: AGCCCAAGTTCTGGAGATGGTG R: GGTGGTTCCATTGGCATTGG	492

Continuation of Table 2.3

P2R	Primer sequence (5'-3')	Band size (bp)
P2Y6	F: TTGCATGAGACAGACTCTCCG R: CACGACTCCACACACTACCC	500
P2Y12	F: ACCCTACAGAAACACTCAAGGC R: CAGGGTGTAGGGAATCCGTG	978
P2Y13	F: AAACAAAGCTGATGCTCGGGA R: TGTGACTGACCACCTGATGC	591
P2Y14	F: GCTGACTTTCTCATGGGCCT R: AGGGGATTCTGGCAATGTGG	571

2.5.4 PCR

PCR was performed using prepared sample cDNA, the corresponding no-reverse transcriptase control and water controls (without sample). 2 μL of samples and controls were added to 25 μl of PCR Taq polymerase Master Mix (Promega), 1 μL (0.2 μM) each of forward and reverse primers, and nuclease free water made up to the final volume of 50 μL. This was conducted for each of the primers listed in Table 2.2 and 2.3. Thermocycling settings were largely kept consistent, with denaturation and extension temperatures remaining the same throughout all PCR experiments. Denaturation at 94°C for 1 minute, then cycles of 94°C for 30 seconds, extension temperature of 72°C for 40 - 45 seconds (approximately 1 minute per kb) during cycling, with a 6 minute and 30-second final extension time. However, annealing temperature (See Table 2.4) and number of cycles were optimised for each gene of interest (GOI) as required, to enhance product amplification. All P2 receptor primers underwent 40 cycles with the exception of P2X2, P2X6 and P2Y4 with 38 cycles. All SVF makers underwent 35 cycles, with the exception of β3-tubulin which underwent 40 cycles. All thermocycling was conducted using Veriti™96-Well Fast Thermal Cycler (Applied Biosystems®) (See Figure 2.3 for

illustrative diagram). PCR products were either stored short-term at 4°C or long-term at -20°C until required.

Table 2.4: Annealing temperatures for primers used within this PhD project. A list of primers used within research, grouped by optimal annealing temperature.

Annealing temperature	Primer
48°C	Pecam-1, α-SMA
51°C	CD146b
52°C	PDGFRβ, P2Y1
53°C	CD45, CD8, P2Y12, P2X2
54°C	Lyve-1, CD146a, P2X1, P2X4, P2X7, P2X3, P2X5, P2Y13, P2Y14
55°C	Perilipin-1, CD14, P2Y6, P2Y4
56°C	P2X6, P2Y2

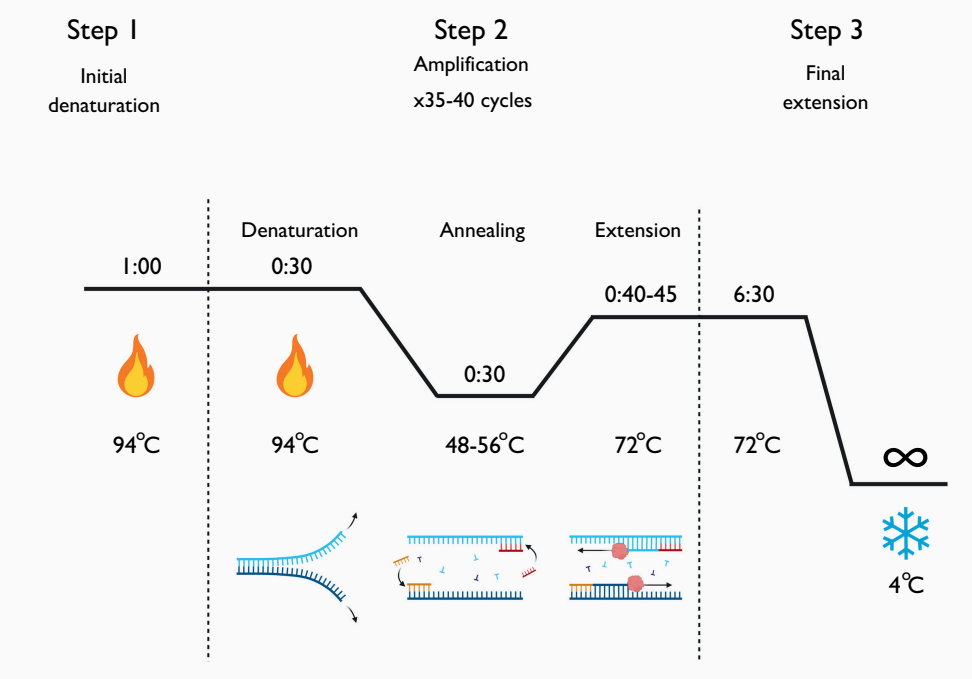

Figure 2.3: PCR schematic. Visual illustration of each step of the PCR process including time (minutes) and temperature (°C) settings used. Step 1 - initial denaturation; Step 2 - amplification cycling; Step 3 - final extension. Accompanying cartoons further illustrate the process occurring in denaturation, annealing and extension steps.

2.5.4.1 Agarose gel electrophoresis

Using a 1.8% (w/v) agarose gel, each PCR product generated was separated according to size. To prepare the gel, 8.1 g of agarose (Fisher) was dissolved via heating in 450 mL of water with 9 mL of 50x Tris-acetate-EDTA (TAE) buffer (Thermo Scientific). For the visualisation of amplified cDNA, 22.5 μL ethidium bromide (EtBr) was added (Final concentration of 0.5 μg/ml). The liquid gel was poured into moulds with well-combs in place and left to set at RT for 45 - 60 minutes, or until solid. Before loading into the pre-set gel wells, 25 μL of each PCR product was combined with 7 μL of 6x gel loading dye (New England Biolabs) to achieve a total volume of 32 μL. The set gel was submerged in an electrophoresis tank containing 1x TAE buffer where each sample, including a 100 bp reference ladder (New England Biolabs), were loaded into each well. Electrophoresis was run typically at 110 V for 50 minutes, whereupon the electric current moves downwards from the cathode, towards the positive anode, carrying negatively charged DNA fragments with it. The larger the fragment, the slower the migration, and

thus the DNA fragments become separated by size. Completed electrophoresis gels were then visualised using the UV setting of the GelDoc-It®^{e} imager.

2.6 Cell culture

Cell culture was performed using the 1321N1 human astrocytoma cell lines, derived from human glioma cancer cells. These lines are fast-growing and low-maintenance, adherent cell lines. For the purpose of the project, 1321N1 lines stably expressing the human P2X2 or P2X3 receptor were used. Parental 1321N1 cell lines do not naturally express P2X or P2Y receptors, therefore the parental cells can be transfected to stably express either P2X2 or P2X3 receptors (in-house stocks).

2.6.0.1 Maintenance

All cell culture took place in the Biomedical Research Centre (BMRC) tissue culture facilities at the UEA. All cells were cultured in incubators at 37°C and 5% CO_2 temperature and humidity conditions. Cells were grown in standard filtered T75-size culture flasks (Thermo Scientific). Cells were bathed in high-glucose (4.5 g/L) DMEM supplemented with L-glutamine, then further supplemented in-house with 10% (v/v) fetal bovine serum (FBS) (Sigma) and 1% (v/v) penicillin-streptomycin combined solution, wherein the final concentration was 50 U/mL and 50 μg/mL respectively (Sigma) (referred to as 'culture DMEM' from this point).

2.6.0.2 Passage

All cells were handled in a Class II Microbiology Safety Cabinet and all media and reagents were pre-warmed to 37°C prior to use. When cells reached approximately 80% confluence, they were gently washed with 5 mL 1x PBS (in-house) before treatment with 2 mL trypsin-EDTA (Sigma) dissociation solution for 5 minutes. Once cells had detached, 3.5 mL culture DMEM was added and cells gently swirled to mix. The cells were removed and centrifuged at (RT) 450 xg for 5 minutes to achieve a pellet, whereupon old media was removed and the pellet re-suspended in fresh media. To estimate the cell number for seeding, the pellet was resuspended in 5 mL culture DMEM and a hemocytometer was used to count number of cells per mL. The appropriate quantity of cell suspension was

seeded into fresh T75 flasks, or seeded into Nunc™Lab-Tek™II chamber slides (Thermo Scientific) for use in immunocytochemistry.

2.6.0.3 Freezing and thawing

After use, cells were spun at 450 xg for 5 minutes and cryopreserved by suspending in a mixture of DMEM, 30% FBS (v/v) and 10% (v/v) DMSO. Cells were transferred into cryovials at an approximate density of 1 x 10^6 per vial and to steadily cool and freeze the cells at a rate of 1°C/min, these vials were transferred to a Mr Frosty box (isopropanol-filled) and kept at -80°C for 12 hours before transferring to liquid nitrogen storage at -196°C. For thawing of cells in liquid nitrogen storage, cells were taken from liquid nitrogen storage and placed on dry ice, before thawing in a 37°C water bath for 2 minutes. Next, 1 mL culture DMEM was added to cryovials and cells were spun down at 450 xg for 5 minutes to remove the cryopreservation mixture, then cells were transferred to a T25 flask containing pre-warmed culture DMEM.

2.7 Immunocytochemistry

To qualitatively establish the presence and pattern of neurons within the inguinal fat pad, whole-mount immunocytochemistry was used. To perform immunocytochemistry, antibodies and stains were mainly sourced from Abcam and Thermo Fisher Scientific (see Table 2.5). Where possible, antibodies sourced were knockout validated and/or verified with western blot analysis by the manufacturer and had been published in peer-reviewed literature. Generally, antibody concentrations were used under the suggestion of the manufacturer. For vasculature, Griffonia simplicifolia lectin isolectin B4 (IB4) was used as a stain, which is a common and widely used stain for microvasculature in many models (Corliss et al. 2019).

Table 2.5: List of antibodies and stains used for immunocytochemistry. A full list of all antibodies and stains used to perform immunocytochemistry in this PhD project, plus their manufacturer and product code. 'Alexa' refers to Alexa Fluor®conjugated secondary antibodies.

Antibody/stain	Concentration	Host species	Manufacturer/code
Anti-β3-tubulin	1:500	Chicken	Abcam/Ab41489
Anti-Tyrosine Hydroxylase	1:250	Rabbit	Millipore/AB152
"	1:250	Chicken	Abcam/Ab76442
Anti-PGP9.5	1:250	Guinea pig	Abcam/Ab10410
Anti-P2X2	1:200	Rabbit	Alomone/APR-003
Anti-P2X3	1:200	Rabbit	Invitrogen/P15-115707
Anti-chicken Alexa 405	1:500	Goat	Abcam/Ab175674
Anti-chicken Alexa 488	1:500	Goat	Abcam/Ab150173
Anti-chicken Alexa 647	1:500	Goat	Abcam/Ab150171
Anti-rabbit Alexa 647	1:500	Goat	Fisher/A-21245
Anti-Guinea pig Alexa 647	1:500	Goat	Abcam/Ab150187
Isolectin B4	1 μg/mL	-	Invitrogen/132450
BODIPY 493/503	20 μg/mL	-	Invitrogen/D3922
Sudan Black B	0.1%	-	Sigma/199664
DAPI mounting medium	-	-	Abcam/104139

2.7.1 Whole mount immunocytochemistry of the inguinal fat depot

2.7.1.1 Tissue preparation

Whole mount tissue preparation methods were adopted from Willows et al. (2021). The inguinal fat depot pair were isolated and washed in HBSS. Where required, tissues were cleaned of adherent hair. Occasionally the depot was dissected further into half sections to enable more experimental potential per depot pair.
Tissues were fixed in 4% PFA for 2 - 3 hours at 4°C (depending on depot size), then washed in 1x PBS at RT for 10 minutes, twice at 4°C. 1x PBS containing heparin at 10 U/mL was typically used during early PBS-washing stages to reduce vascular autofluorescence. However, heparin was excluded when exploring the neuro-vascular relationship to exploit naturally occurring autofluorescence from erythrocytes.

Post-fixation, tissues were placed in 3 mL blocking buffer consisting of 1X PBS + 1% Triton X-100 + 5% bovine serum albumin (BSA) + 5% normal goat serum (NGS), for a period of 2 - 4 days gently agitating at 4°C. At the end of the blocking period, tissues were flattened between two large microscope slides (using bulldog clips) for 90 minutes at 4°C to reduce the tissue Z-plane (thickness). Tissues were rinsed in 1x PBS before being stained with 0.1% w/v Sudan Black B in 75% v/v EtOH rotating for 20 minutes at RT to reduce lipid autofluorescence. This step was implemented as an alternative measure to tissue clearing. Tissues were then washed with 1x PBS for up to 8 hours at 4°C to remove excess stain. Next, tissues were placed in blocking buffer containing appropriate concentrations of primary antibodies and left for 48 hours gently agitating at 4°C. After this incubation period, a series of hour-long 1x PBS washes ($\pm$ heparin) occurred, with the PBS being replaced each hour for 7 - 8 hours. Tissues were then incubated with secondary antibodies, rotating at 4°C overnight. IB4, if being used, was added at this stage. Again, post removal of the secondary antibodies, the tissues received a series of hour-long 1x PBS washes spanning up to 8 hours, with PBS being replaced every hour. If BODIPY was being used, after 4 hours of washing, samples were placed into blocking buffer containing 20 μg/mL BODIPY for 30 minutes at RT gently agitating, before recommencing the wash steps up to 8 hours.

Each fully-stained sample was mounted onto a microscope slide using 100% glycerol as mounting media and further flattened using lead weights for 3 - 5 days at 4°C before imaging. Secondary antibody-only control tissues were treated in exactly the same manner, minus the introduction of primary antibodies. See Figure 2.4 for illustrative description.

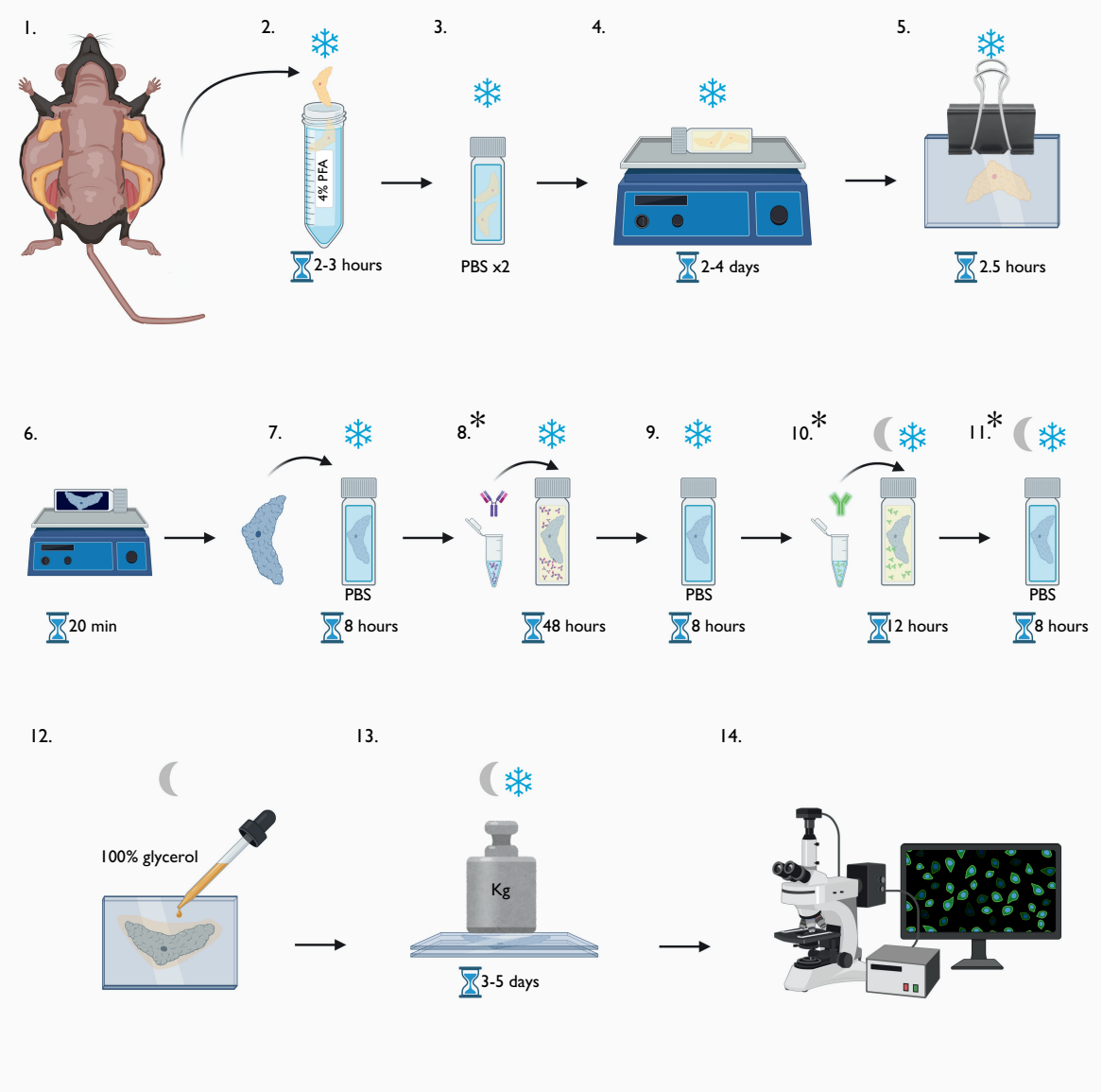

Figure 2.4: Methodology for whole mount immunocytochemistry of the inguinal fat depot. Illustration of methods applied for whole mount immunocytochemistry of the inguinal fat depot. **1.** Inguinal depots dissected and **2.** fixed in 4% PFA for 2-3 hours before undergoing **3.** 2x 10-minute PBS washes. **4.** Samples are incubated in blocking buffer for 3-4 days then **5.** flattened between microscope slides for 2.5 hours. **6.** tissues incubated with Sudan Black B for 20 minutes and **7.** washed with PBS for 8 hours before adding to **8.** blocking buffer containing primary antibodies (*except secondary antibody-only controls) for 48 hours. **9.** Samples are then washed with PBS for 8 hours before **10.** incubating with secondary antibody in blocking buffer overnight (*IB4 if being used was added at this stage) then **11.** washing with PBS for 8 hours (*BODIPY added half way through at this stage if being used) prior to **12.** mounting with 100% glycerol and **13.** re-flattening with weights for 3-5 days before **14.** using confocal microscopy to visualise fluorescent structures.

2.7.1.2 Cell preparation

Cultured P2X2- and P2X3-expressing astrocytoma 1321N1 cells were cultured and maintained as per Section 2.6 and seeded into chamber slides at approximately 1 x 10^5 per chamber, then were incubated for several hours or overnight in culture DMEM. To stain the cells, culture DMEM was removed and cells were washed twice with 1x PBS before fixation with 4% PFA for 10 minutes at RT. Post-fixation, cells were rewashed with 1x PBS then permeabilised with 1x PBS + 0.25% Triton-X for 10 minutes at RT. Cells were then blocked using 1 x PBS + 3% (w/v) BSA blocking buffer for 1 hour at RT. Primary antibodies were diluted in the same blocking buffer at the desired concentration and added to test samples for 1 hour at 4°C. After primary antibody incubation, cells were washed 3 times with 1x PBS for 10 minutes each before secondary antibodies diluted in blocking buffer were added and left for 45 minutes at RT. The secondary antibodies were washed off with 3x 10-minute 1x PBS washes in darkness. The chamber slide was dismantled and cells were then mounted using mounting media containing DAPI and imaged immediately, or left covered at 4°C until ready to image.

2.7.2 Image acquisition and processing

All images were taken using the Zeiss LSM 980 Airyscan 2 confocal microscope. Generally, settings were kept consistent, with laser intensity maintained between 1 - 2%, with the pinhole set to 1 airy unit (AU) and captured at a resolution of 8192 x 8192 pixels with bidirectional scanning, where each pixel was exposed for 2.05 μs and 16 bit image depth. Master gain was optimised on a frame-by frame basis, typically within a range values of 700 - 900 V. The main lasers used were 488 and 639 and on occasion 405 nm. Control images were acquired with the same settings as the test samples.

To obtain 'whole' depot images, the 'AI sample finder' option in the Zeiss Zen 3.6 acquisition software was used to produce an overview image using multiple individual tiles with the 2.5x objective, which were then automatically stitched together within the software to produce a complete image. Number of tiles varied depending on the size of the tissue.

To generate z-stack projections for a composite 3D image, a region of interest (ROI) was identified and the 'z-stack' option was used, whereupon number of images within

a defined depth were selected. These were dependent on thickness of each sample and ranged between 14 and 104 slices. To generate the composite images, Zeiss Zen 3.6 (blue edition) was used to process the z-stacks, where the software provided '3D' visualisation tools which included scale measurements and merging of multiple channels. This was used to generate all projections within this thesis.

For 2D images, post-image acquisition, merging of colour channels (for composite images), zoom and cropping, image colour adjustments (brightness and contrast) and scale bars were all managed in Fiji (Image J based) software. When appropriate, images were processed with noise removal functions, such as 'despeckle' to remove graininess and where images experienced severe instances of non-specific spotting of antibody which distracted or negatively impacted the overall focal point of the image, outliers were removed with an area of 5 - 10 pixels. Secondary antibody-only control images were processed in the same manner as test images.

2.7.2.1 Assessments of colocalisation by area

For approximate assessment of colocalisation between two channels, using FIJI, the colour channels of the two markers were merged. Then colour thresholding was assessed by selecting appropriate colour ranges for green, red and yellow as to best represent each of the secondary fluorophore channels and the colocalised areas. These were based on arbitrary values on a colour wavelength scale from 0 - 255 wherein selections between 0 - 27 were considered 'red', 28 - 54 as 'yellow' and 55 - 99 as 'green' and these were kept consistent throughout each analysis. These respective regions of colour were measured as area coverage within the image, which was divided by the total colour threshold of the whole image to give a percentage of total area 'cover' for each of the individual channels (See Figure 2.5 for visual representation). Where possible, particularly where structures were 3D such as nerve bundles, multiple Z-planes were assessed, calculated and combined to produce a mean coverage of a particular channel across multiple planes of view within a single ROI for a more comprehensive assessment.

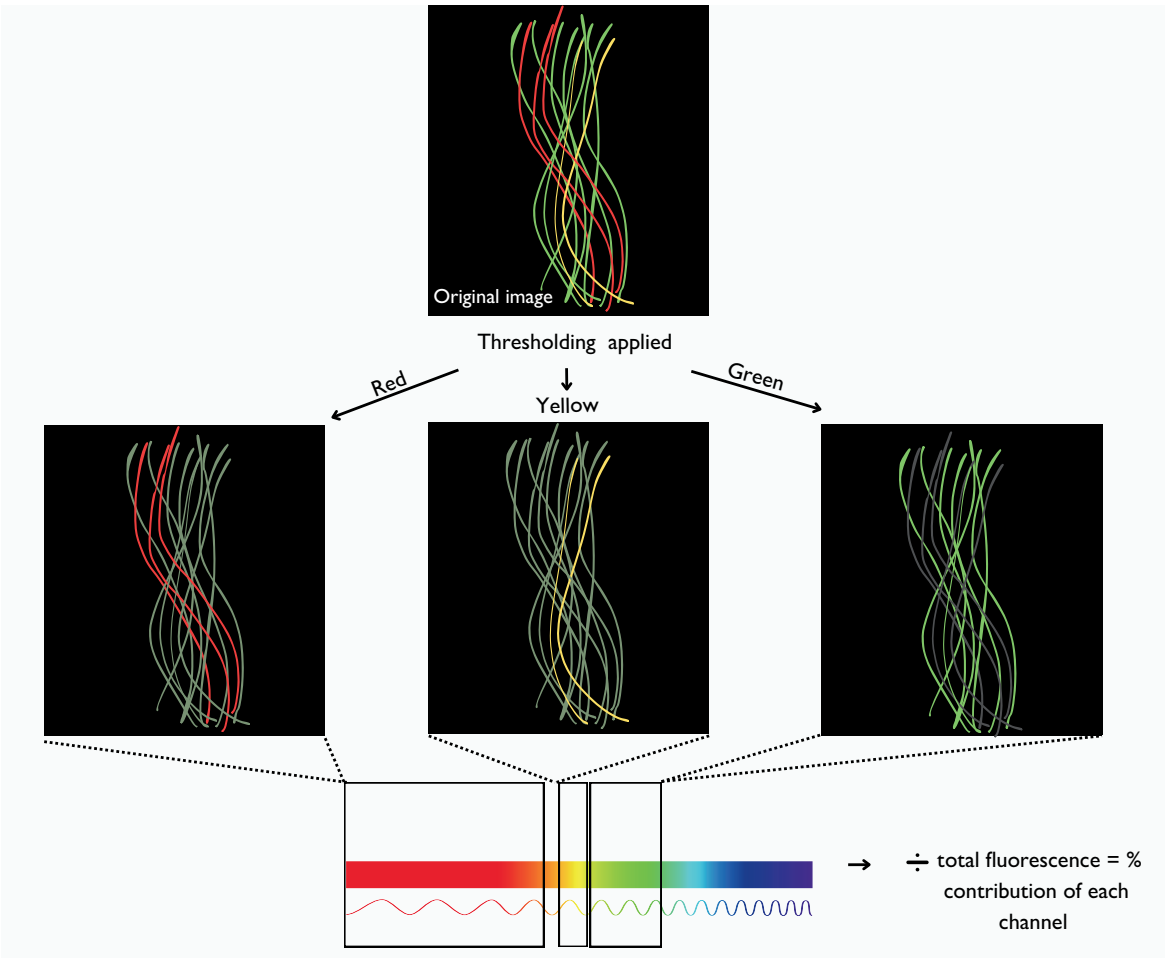

Figure 2.5: Visual description of the assessment of colocalisation. An illustration describing the assessment of colocalisation performed on images. Thresholding was applied to a given image (cropped to remove any background noise) whereby red, yellow and green channels were separated and their area within the image measured. Each channel area was divided by the total threshold (fluorescence) with all channels combined to provide an approximate % proportion of fluorescence of a given channel. Yellow is used to describe colocalisation of two channels (red and green). These analyses were performed using FIJI software.

2.8 Statistical Analysis

All data analysis within this thesis were performed using Origin(pro) software, student version 2021(b) (OriginLab Corporation, Northampton, USA). Unless otherwise indicated, data written in text and expressed in figures represent mean $\pm$ standard error of the mean (SEM). Standard deviation (SD) has not been reported in the main text and figures within this thesis, however tabulated values are presented for reference in the Appendix (Table 7.1). References to 'N' denote biological repeats (animals) and 'n' refers to technical repeats. In cell immunocytochemistry experiments 'N' refers to chamber and 'n' refers to within-chamber sampling. All glycerol assay experiments were conducted to a minimum N of 3, with at least two replicates in each condition ($n \geq 2$). Wherever possible, data is presented as raw, non-normalised values. However adipocyte experimental data has been corrected to control values and presented as 'response subtract control' values and is clearly indicated as such.

Dose-response calculations for the estimation of the half-maximal effective concentration (EC50) for norepinephrine were made by applying the Hill1 equation (below) to data in OriginPro software.

$$y = START + (END - START) * x^n \ / \ (k^n \ + \ x^n)$$

Where y = is the effect/response, k = the EC50, n = number of cooperative sites, x = concentration, START = baseline and END = maximal/plateau.

Prior to statistical analysis, data are assessed for normality using the Shapiro-Wilk test and for equal variance using the Levene's test. Post checks, normal data proceeded to parametric analysis, such as one-way ANOVA with *post-hoc* Tukey test, or one- and two-sample t-tests. Whereas datasets in violation of parametric assumptions were analysed via Mann-Whitney U tests, Kruskal Wallis ANOVA with *post-hoc* Dunn's test, or Welch's ANOVA with *post hoc* Games-Howell Pairwise Comparisons. Details on statistical tests used for each figure can be found in corresponding figure legends, or in-text where no figure is present. Throughout this work, the threshold for statistical significance was $P<0.05$ (* $P<0.05$, ** $P<0.01$, *** $P<0.001$) and symbols used in graphs to represent significance are described in figure legends.

Chapter 3

Investigating innervation of the inguinal fat depot

3.1 Introduction

The vascularisation and nervous innervation of tissues is critical to function, health and homeostasis. In cases where these innervations are missing or damaged, pathologies ensue and tissues cannot perform their primary functions. For example, damage to the skin barrier in diabetic vasculopathy and neuropathy leads to necrosis and ulcerations, or loss of appropriate vascularisation in the eye retina can result in impaired, or even loss, of vision i.e. retinopathy (Mota et al. 2020). In the case of obesity, runaway effects can occur where hypertrophy of adipose tissue can result in hypoxia and pro-inflammatory pathological conditions. As vasculature becomes dysfunctional due to inflammation, or cannot expand to facilitate the growth of the tissue, the primary storage functions of adipose become impaired (Trayhurn 2013). Polyneuropathy and subsequent loss of nervous innervation to peripheral tissues, including adipose, can also occur as a result of obesity and may contribute to catecholamine resistance (Blaszkiewicz et al. 2019a; Duncan et al. 2007). Understanding the vascularisation and nervous innervation of adipose is therefore fundamental to full comprehension of lipolysis; capacity, span and ultimately, also dysregulaton.

Firstly, how nerves innervate the resident network of vasculature is important as to interpret the control of incoming oxygen, metabolites, hormones and nutrients for metabolic health and homeostatic regulation, which both directly and indirectly influence lipolysis

(Bartness et al. 2014). These patterns of innervation are often altered in disease states, such as obesity, where nervous innervation of vasculature and parenchyma is perturbed (Willows et al. 2023). Secondly, the extent of nervous parenchymal and adipocyte innervation is key to understanding how lipolysis is regulated.

It was previously thought that vascular networks presented the primary route of lipolysis regulation via the delivery of circulating catecholamine, epinephrine, to adipose tissue. The influence of circulating catecholamines in lipolysis regulation is now considered inconsequential compared to those derived from sympathetic nerves innervating adipose (Bartness et al. 2014). Evidence suggests sensory, but not parasympathetic nerves, are also present, and are thought to have roles in afferent delivery of information to the CNS, but also a potential antidromic signalling axis if and when stimulated (Mishra & Townsend 2024). There are mixed reports as to the extent or density of nerve-adipocyte interactions in the inguinal fat depot (Zeng et al. 2015; Jiang et al. 2017; Huesing et al. 2021), which means understanding how lipolysis may be influenced by nerves is not completely resolved. The purpose of this chapter is to use immunocytochemistry techniques to investigate nervous innervation of white adipose tissue, while hopefully elucidating extents of neuro-adipose interactions to form a basis in which functional enquiry can be applied. In order to understand the response, we must first understand the innervation.

3.2 Aims

1. Establish a sound method for visualising nerves in the inguinal fat depot using a 'whole mount' approach.

2. Define the structures and innervation modes present within the inguinal fat depot.

3. Qualitatively assess the frequency of innervation observed.

4. Investigate sympathetic nerve innervation and perceive and describe the extents of sympathetic versus non-sympathetic innervation, with particular emphasis on parenchymal innervation modes.

3.3 Results

3.3.1 Optimisation and development of a suitable whole mount method

3.3.1.1 Establishing a suitable whole mount method

Initially, to tackle the first aim of the investigation, I approached whole mount microscopy techniques by applying passive clearing methods that allow intact full-volume imaging of tissues (2-3 mm deep) by exposing tissues to high refractive index solutions in order to correct the refractive index of the tissue. One method encompassed a fructose clearing approach, whereby paraformaldehyde (PFA) fixed tissues were serially exposed to increasing concentrations of fructose (20 - 100 % w/v in dH_20) for a minimum of 8 hours each, before mounting and imaging (Figure 3.2 A). The second approach was a trial of a glycerol clearing method which required PFA-fixed tissues to clear in a 90% v/v glycerol solution (in dH_20) for 72 hours, before mounting and imaging (Figure 3.2 B). While these approaches did work, clearing the tissue and allowing for visualisation, the antibodies had a high propensity to become tissue-bound, stuck between adipocytes and at times making it difficult to discern signal (neurons) from noise. The Townsend research group developed a non-conventional method, whereby tissue depth is reduced, termed Z-depth reduction (ZDR), and combined with application of a neutral lipid stain Sudan Black B, it negates the need for clearing and reduces much of the background (Willows et al. 2021) (referred to in the chapter as the 'Townsend method'). In casual/anecdotal observations, using the methods described in Chapter 2 Section 2.5, the depth of the inguinal tissue was reduced from original circa 2-3 mm (undulating in depth over the span of the tissue) to values ranging between 150 - 300 μm when observed scanning through the whole Z-plane of the tissue during confocal image acquisition (unimaged), matching observations in Willows et al. (2021). These anecdotal observations were largely confirmed when using BODIPY to fluorescently stain for adipocytes, where Z-stack projections of adipocytes assimilated into composite three-dimensional images illustrated adipocytes spanned between approximately 115-175 μm deep (Figure 3.3), with a mean of 134 μm (N = 3, n = 5). Although, some error in depth estimation may occur from inadequate Z-stack projection 'slices' to cover the entire depth, therefore

these equate to approximate measurements of depth only.

The use of either a clearing technique, or lipid stain, was necessary to correct the refractive index of the lipid-laden adipocytes. Adipose tissue appears naturally fluorescent due to the presence of lipids, as they refract light in multiple directions as it penetrates through the tissue. Figure 3.1 (A) illustrates this, as a section of inguinal tissue with no preparation, other than Z-depth reduction, can appear as if it had exposure to a fluorescent antibody. Figure 3.1 (C) demonstrates the effectiveness of Sudan Black B at attenuating the autofluorescence compared to Figure 3.1 (B), where neither received post-image contrast and brightness adjustment or processing.

Figure 3.2 indicates the performance of the three methods, fructose & glycerol clearing methods and the Townsend method applied alongside pan-neuronal marker β3-tubulin (1:500), where no post-imaging adjustments in brightness, contrast or noise-reducing processing have been made. Application of the novel tissue Z-depth reduction approach in conjunction with Sudan Black B appeared to successfully reduce the noise in comparison to the other methods (Figure 3.2 C). Additionally, the 2' antibody-only controls indicate to some degree the improvement in antibody freely washing out of the tissue when using the Townsend method, compared to whole-depth tissue clearing methods. As such, from the point of discovery of the Townsend method, any further optimisation and data collection was based on this core protocol (Willows et al. 2021).

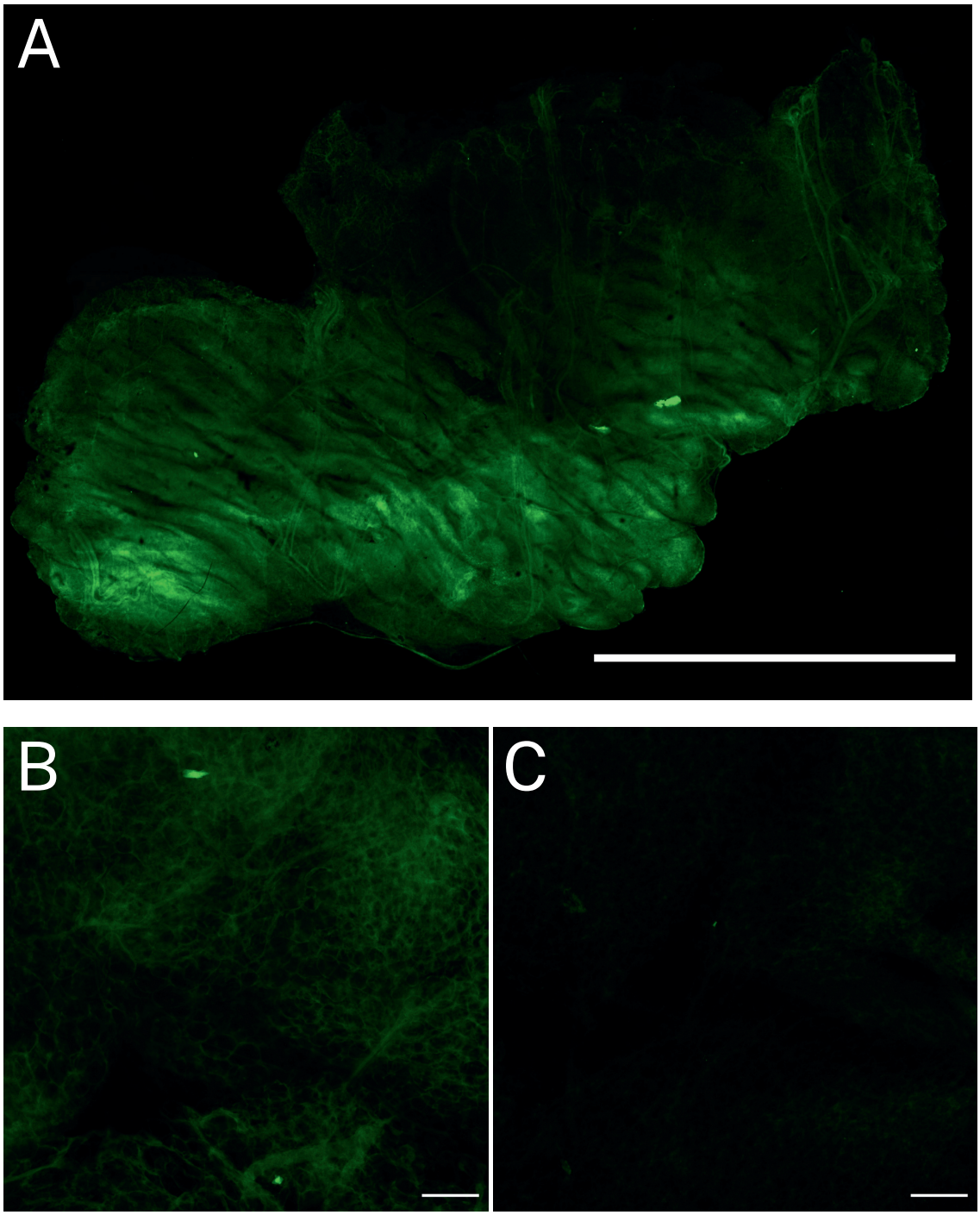

Figure 3.1: Autofluorescence of inguinal adipose tissue. An example of the challenges of autofluorescence faced when imaging adipose via confocal microscopy (A) Overview image of approximately half of an unstained inguinal adipose depot using ZDR, without Sudan Black B or antibody application, image taken using the green channel to showcase autofluorescence (N=1). Autofluoresence of inguinal tissue prepared excluding (B) and including (C) the addition of Sudan Black B, both with the addition of 2'antibody only (Alexa 488). Images taken with (A) a 2.5x objective with 35 stitched tiles and (B & C) a 10x objective. Scale bars represent 2 mm (A) and 100 μm (B & C).

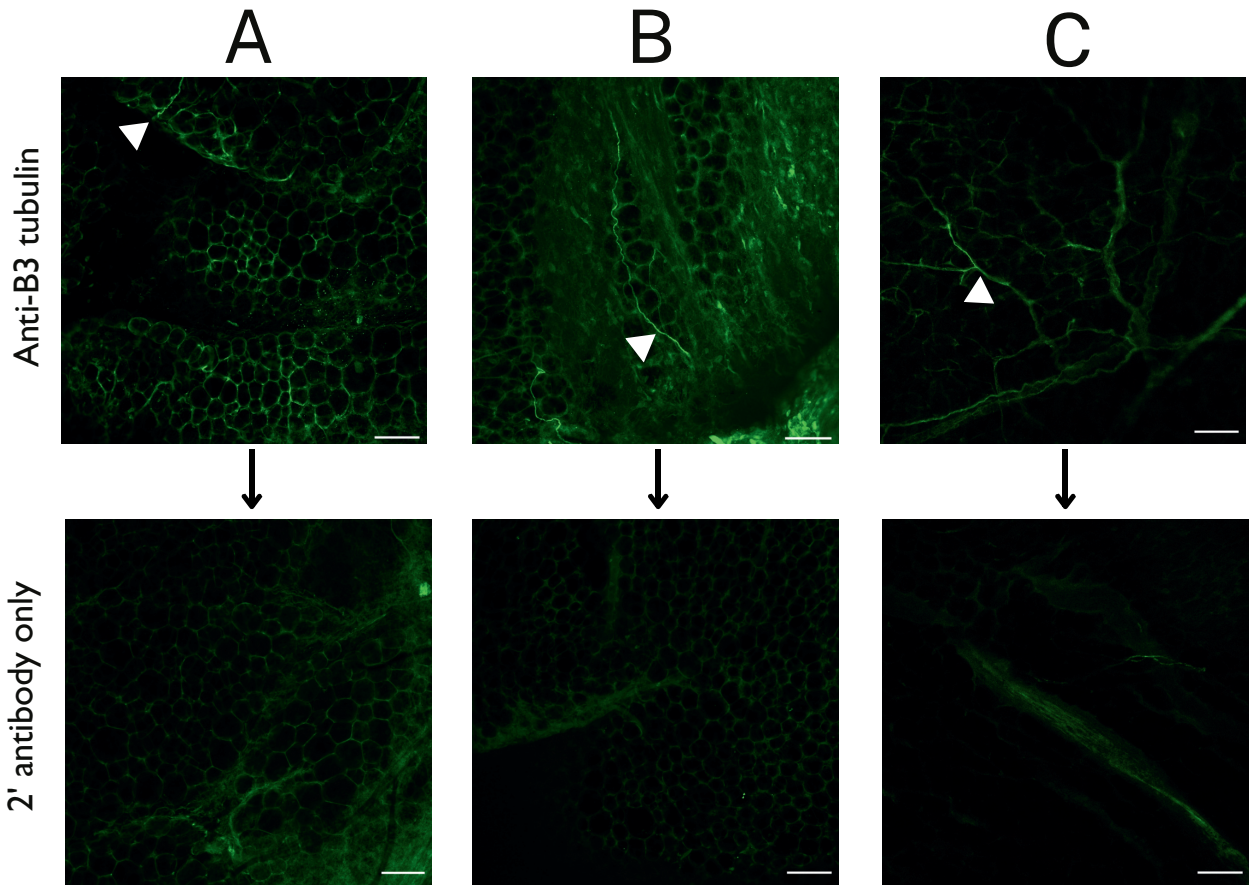

Figure 3.2: Comparison of clearing versus alternate methods for whole mount immunocytochemistry. Representative confocal images of an initial exploration into (A) a fructose clearing method using a series of fructose steps to clear the tissue (N = 4) (B) a glycerol clearing method (N = 1) and (C) the alternate non-clearing method from the Townsend lab (N = 13). Top Panels for (A) (B) and (C) show anti- β3-tubulin staining for presence of nerves (green, Alexa 488) with white arrowheads indicating examples of nerves, while bottom panels reflect respective and representative 2' antibody-only controls. None of the images have been adjusted for brightness and/or contrast and appear exactly as captured. Images taken with 10x objective and scale bars represent 100 μm

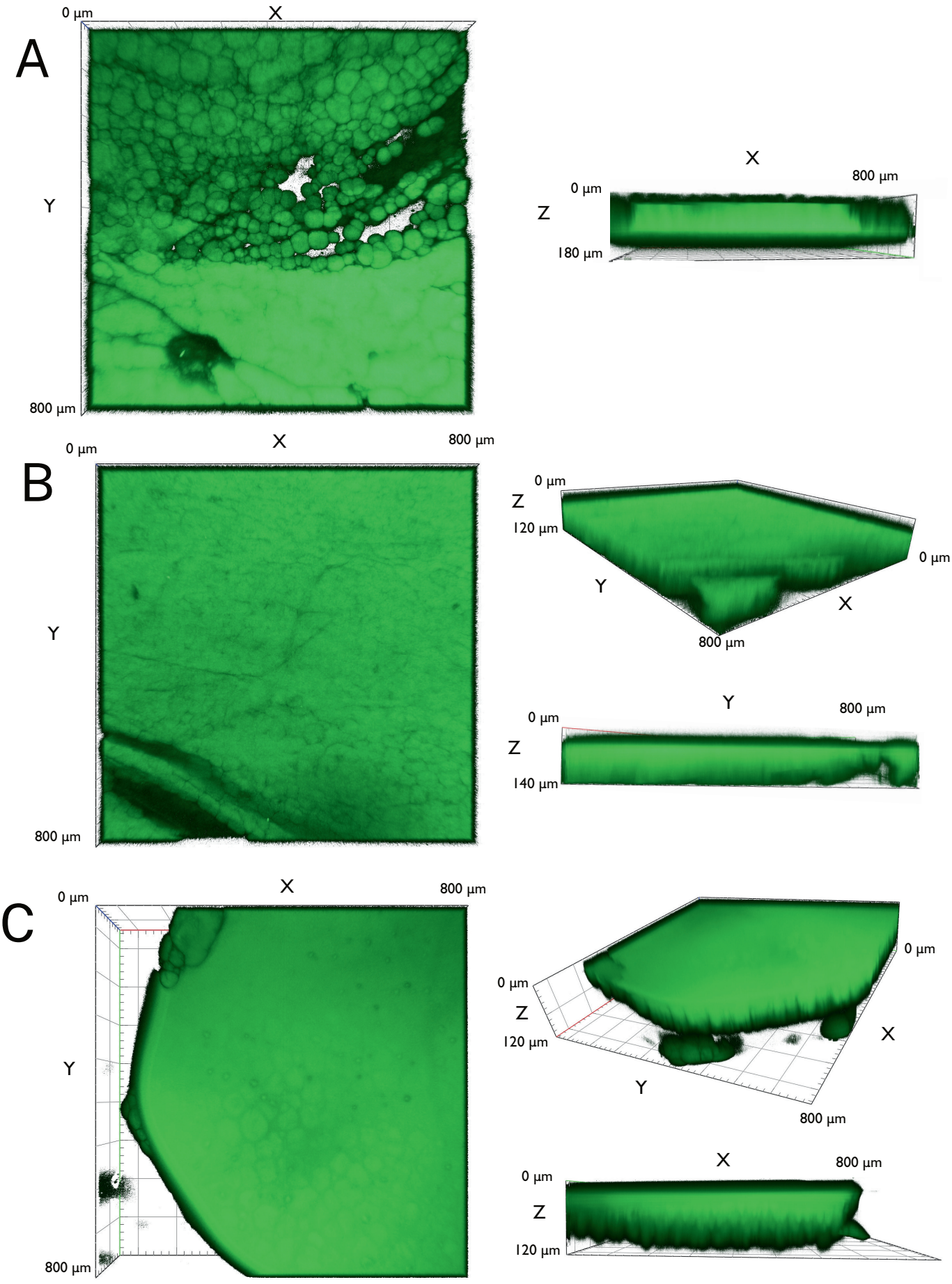

(Figure legend on next page.)

Figure 3.3: Approximate thickness of Z-depth reduced inguinal fat Representative confocal Z-stack projection views of BODIPY-stained adipocytes in the green channel (N = 3, n = 5). The approximate thickness in μm of the inguinal fat depot post- Z-depth reduction steps, using Z-stack confocal images in 'slices' in multiple consecutive Z-planes, merged to form a composite '3D' construction, where (A) (B) and (C) refer to different examples and next to them are respective face-view and/or perspective xy plane axis. Projections had thresholding applied to remove unstained areas and increase visualisation of positively stained adipocyte structures. Scale presented on X Y and/or Z axis in μm. Images taken using 10x objective.

3.3.1.2 Selection of an appropriate pan-neuronal marker

To ensure I obtained sufficient immunoreactivity along the axon for full visualisation, antibodies targeting cytoplasmic proteins found in neuron projections were sought. Therefore, in the interest of comprehensive assessment, I conducted a comparison of antibodies against two well-cited cytoplasmic-targeting pan-neuronal markers; β3-tubulin and protein gene product 9.5 (PGP9.5), to ensure I was able to visualise neurons to their fullest extent.

In a similar comparison of antibodies against pan neuronal markers β3-tubulin and PGP9.5, Blaszkiewicz and colleagues found there was near complete overlap of staining between the two markers, stating PGP9.5 may be slightly better for visualising singular neuronal innervation (Blaszkiewicz et al. 2019a). Therefore, with respect to these claims, to ensure thorough investigation of parenchymal innervation of the inguinal fat depot, PGP9.5 was compared against β3-tubulin, with the main objective to compare singular neuron innervation.

In order to provide semi-quantitative values for how the markers compared, I categorically assessed each image for three staining patterns; 1. β3-tubulin marking nerves where PGP9.5 is clearly absent, 2. evidence of defined overlap of the two markers, and 3. evidence where PGP9.5 detected structures which were not detected by β3-tubulin. Visually comparing the staining pattern of β3-tubulin (1:500) and PGP9.5 (1:500) in the images taken, there were rare occurrences of overlap between the two markers, with only 9% of total images showing instances of visible overlap (Figure 3.4 C) (N = 1, n = 13). With the antibody used here, PGP9.5 appeared to be a poor marker for nerves, with PGP9.5 negativity noted in 75% of images where structures were positively stained by β3-tubulin (Figure 3.4 B). There were also only 19% of images assessed where PGP9.5-positive neurons were observed that lacked β3-tubulin staining, indicating that PGP9.5 had no greatly improved single neuron visualisation over β3-tubulin (Figure 3.4 A). Therefore, under the conditions and using the tools employed here, the selection of pan-neuronal antibody against β3-tubulin was justified and used henceforth for the visualisation of nerves.

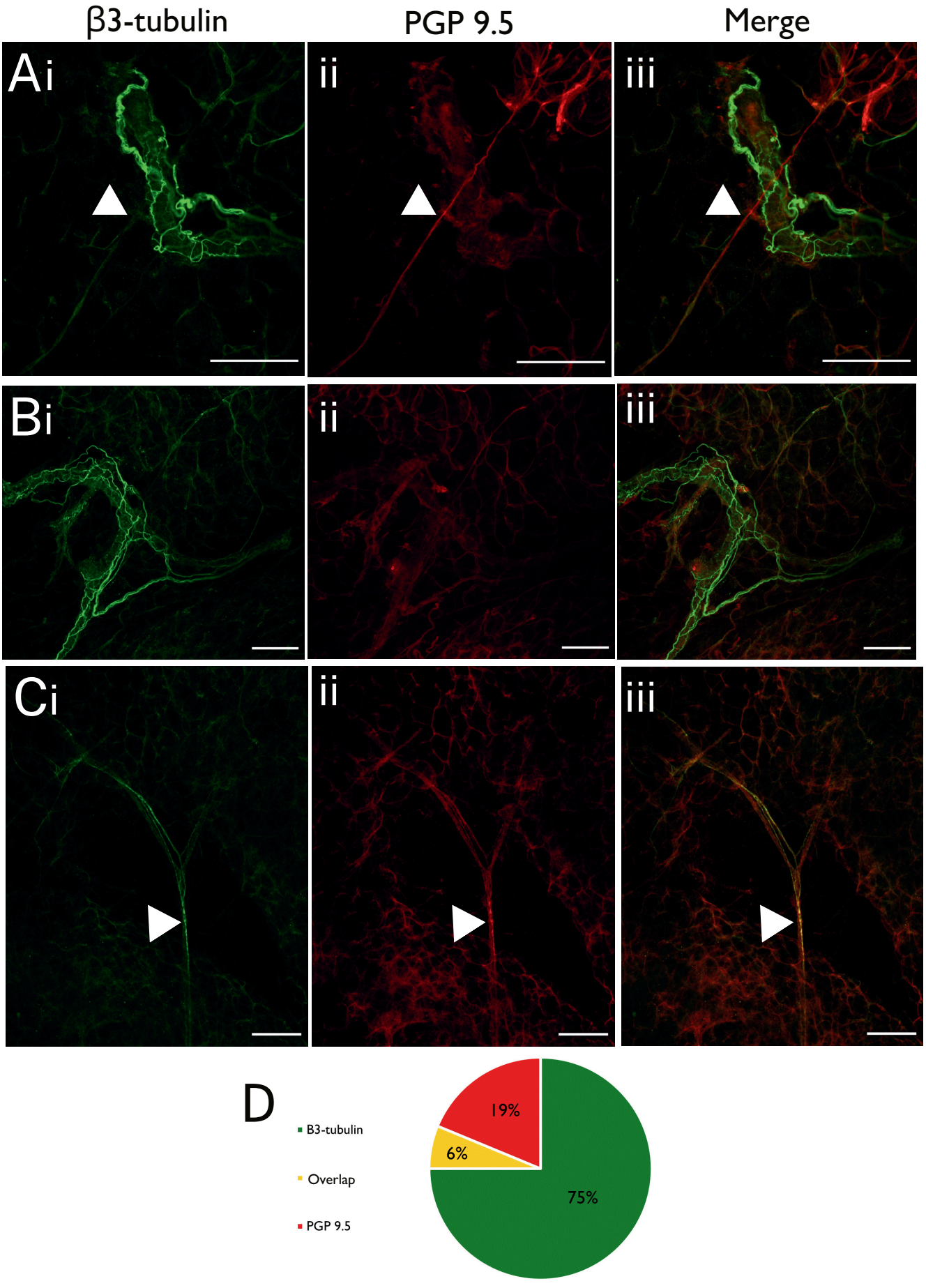

(Figure legend on next page.)

Figure 3.4: Comparison of pan-neuronal markers PGP9.5 and β3-tubulin for detection of nerves. Representative confocal images of a comparison between two different pan neuronal markers PGP9.5 (red Alexa 647) and β3-tubulin (green Alexa 488) ability to detect nerves in the inguinal fat depot. Images indicating (A) where PGP9.5 was able to detect nerves that β3-tubulin was not, (B) β3-tubulin stained nerves that were absent of PGP9.5 positivity and (C) overlap where β3-tubulin and PGP9.5 appeared to detect the same nerve. (D) Diagrammatic representation of instances of overlap and independent staining for each marker by visual assessment in images, as percentage of total number of images observed (N = 1, n = 13). Scale bars represent 100 μm. Images taken with 10x objective. 2.1x digital zoom applied in (A).

3.3.1.3 Confirmation of the presence of nerves

The combined application of the tools and methods described in sections above culminated to produce evidence that nerves are detected with β3-tubulin (Figure 3.5) and are found spanning across the entire fat depot (Figure 3.7). Initial impressions on the appearance of the β3-tubulin-positive structures was supportive of neuron identity due to their morphology; singular neurons demonstrated a distinct wavy/crinkled and thread-like appearance, with a distinct nodule often observed at multiple points along the axon (Figure 3.6), and axons measured approximately 1.8 μm in width (N $=$ 3, n $=$ 130) , in accordance with previous reports in literature (Willows et al. 2021; Cao et al. 2018). The distinctive morphology of nerves was a key element in positive identification additional to nerve marker positivity, particularly when there were high degrees of background, distinguishing nerves from similar sized vasculature. The nerves did not appear to undergo bifurcation which also served to distinguish them from vasculature. These structures can be seen innervating across the entire length and width of the tissue in various forms. Implementation of the optimised methodology serves as a means to investigate how nerves and other structures innervate the inguinal fat depot, in the proceeding sections of this chapter.

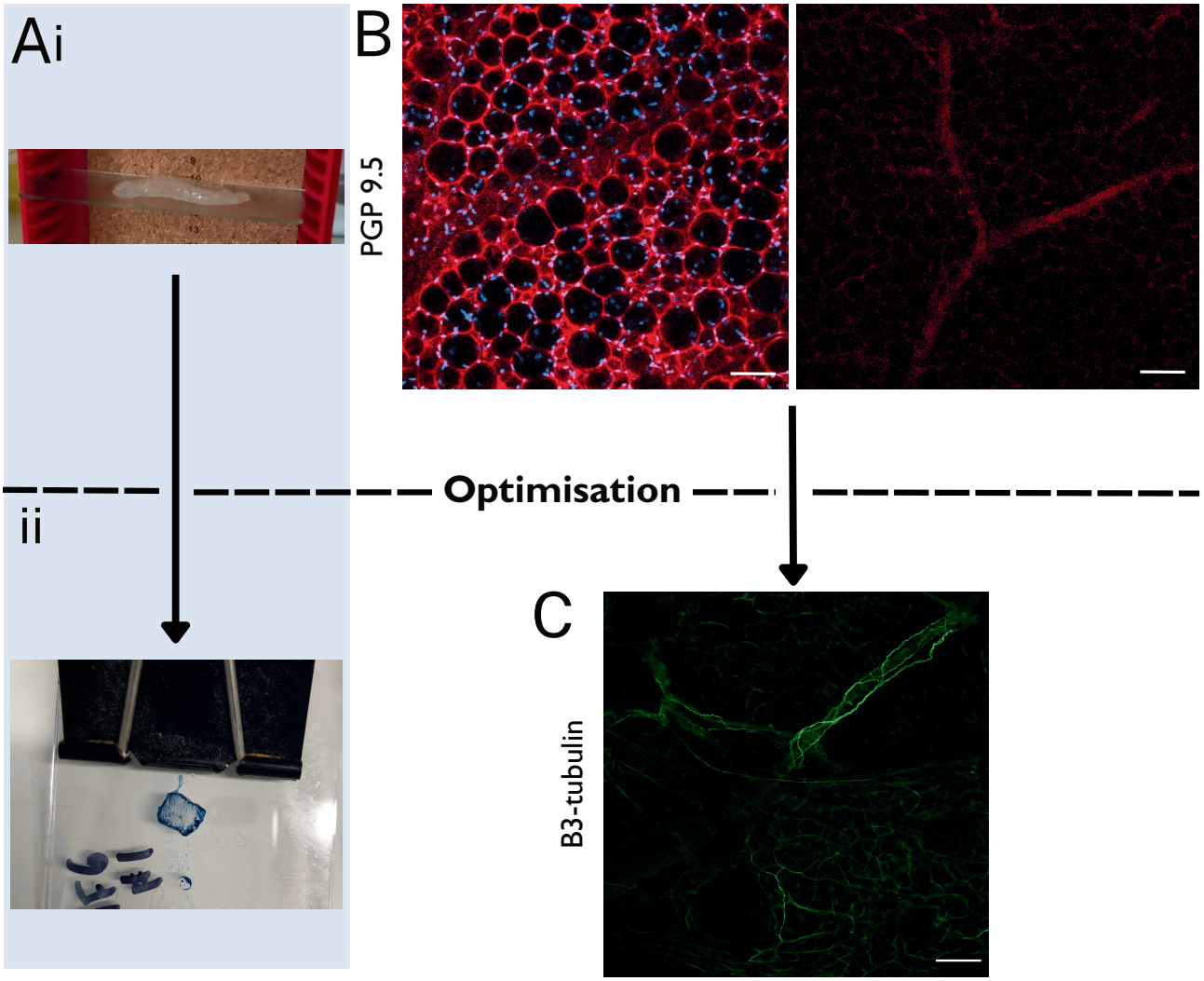

Figure 3.5: Optimisation journey of the inguinal fat depot using whole mount immunocytochemistry. (A) Photographs illustrating the difference in thickness of tissue (i) pre- and (ii) post- optimisation once ZDR has been applied, with the latter picture showing ZDR taking place, with an inguinal tissue section in between slides secured with binder clips, (i) demonstrates the thickness of tissues using clearing techniques. Confocal images in (B) represent initial attempts at whole mount microscopy using PGP9.5 (red, Alexa 647) (DAPI in blue) using the glycerol clearing method while, (C) illustrates the product of optimisation of the whole-mount method using β3-tubulin (green, Alexa 488) as pan-neuronal marker and the Townsend method. Scale bars represent 100 μm and images taken with 10x objective.

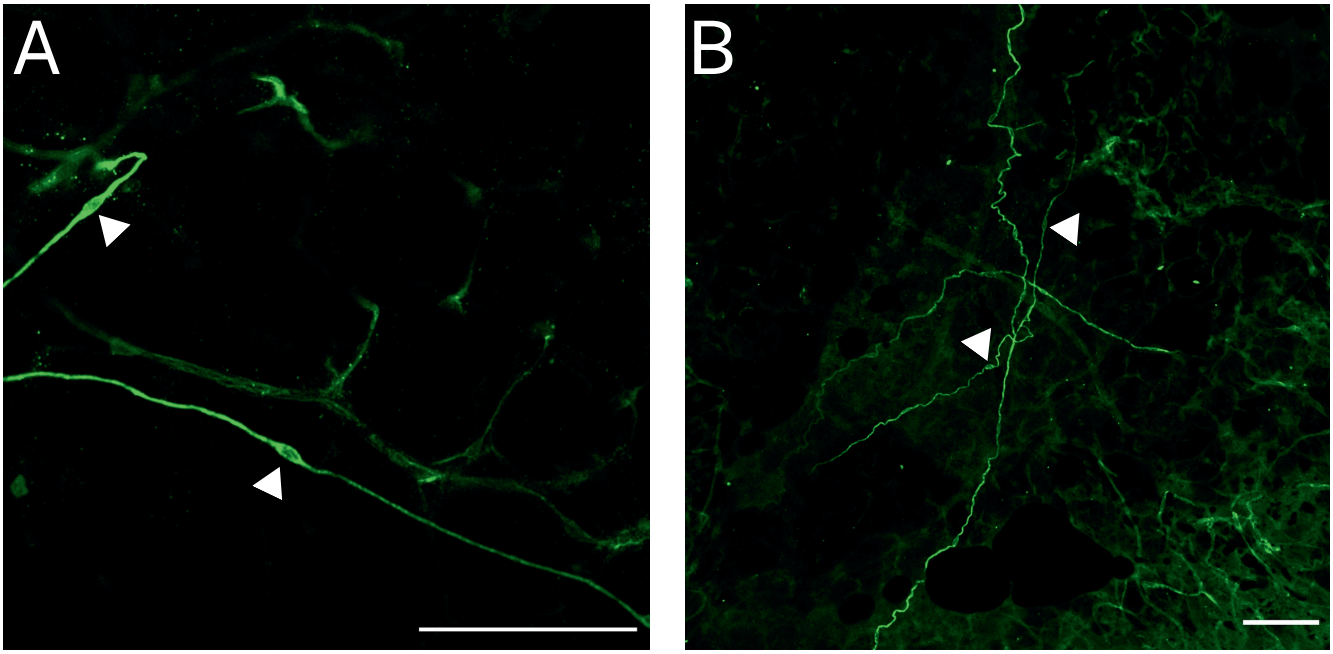

Figure 3.6: Nerve morphology in the inguinal fat depot. Representative confocal images of nerves stained with β3-tubulin (green, Alexa 488) in the inguinal fat depot where (A) demonstrates characteristic nodules along the axon which aided identification and (B) illustrates the 'wavy' innervation pattern of nerves as they travel through the tissue. White arrowheads point to the nodule-like structures. Images taken with 10x objective and scale bars represent 100 μm. 3x zoom applied in (A). (N = 3).

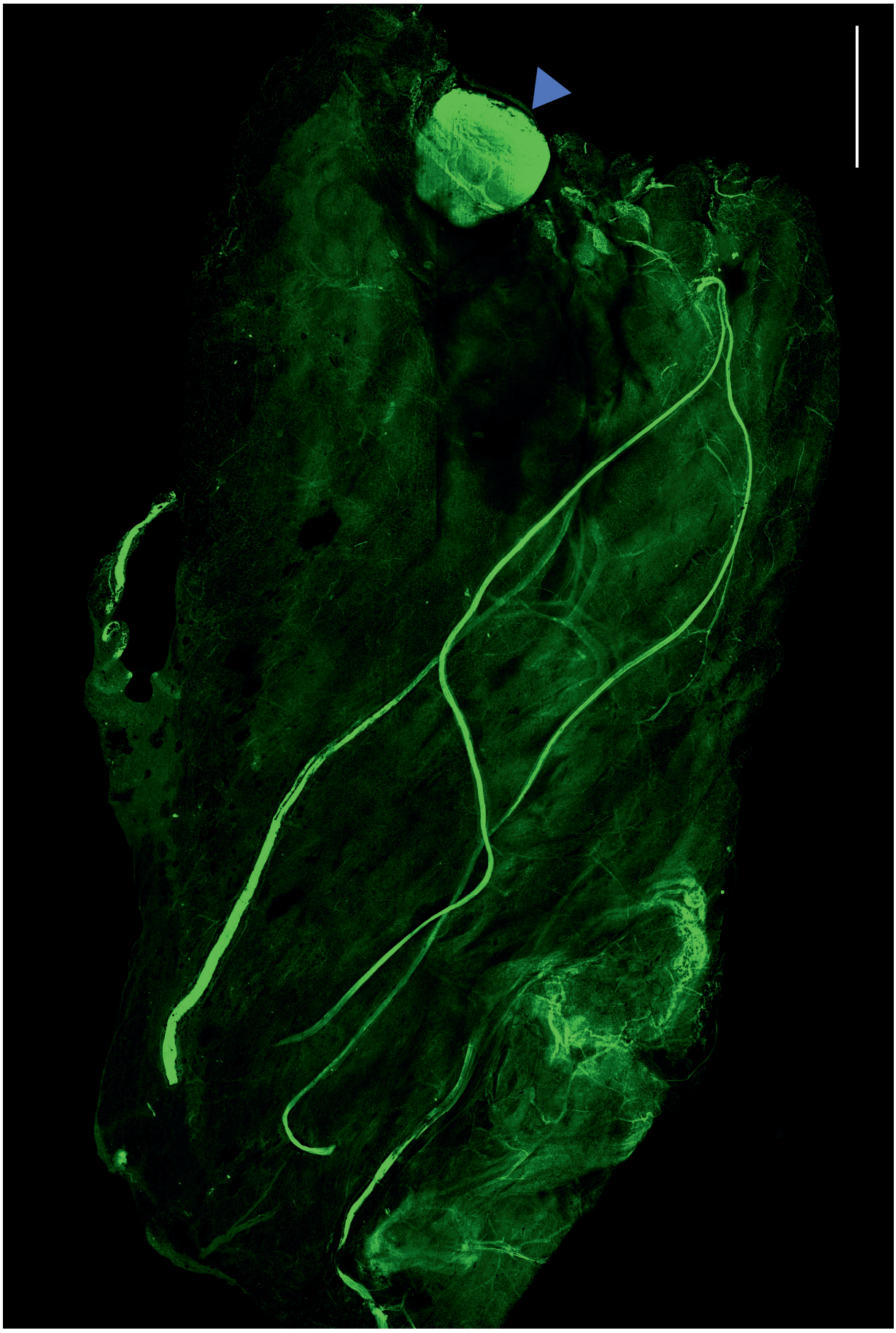

(Figure legend on next page.)

Figure 3.7: Overview of nervous innervation in the inguinal fat depot. Whole-mount confocal overview image of approximately half of the inguinal fat depot (dorsolumbar region), transversely dissected at the lymph node (blue arrowhead). Nerves stained with β3-tubulin (green, Alexa 488) over the entire length of the tissue portion dissected. Tissue prepared using the Townsend method. Scale bar represents 1 mm. Image taken with 2.5x objective and 24 stitched tiles.

3.3.2 Investigation into the innervation of the inguinal fat depot

Representative images within the following sections were all drawn from a complete set of 13 main experiments in total (out of 36 attempts and optimisation experiments), which were successful in experimental aim (optimised to produce a clear image), and all utilised neuronal marker β3-tubulin in addition to whichever other markers were appropriate for the scientific enquiry at hand, either for nerve subtype or vasculature. These 13 experiments can be subdivided into discrete experiment sets including each additional other marker, to at least an N of 3 for each set. Observational qualitative data regarding the approximate frequencies of innervation incidence were all therefore based on these experiment sets, excluding the experiments primarily conducted for optimisation. Provided is a table (Table 3.14) to define and clarify use of descriptive terms of frequency referred to throughout these sections.

Table 3.1: Frequency scale and definitions for describing qualitative observations. Frequency scale terminology and associated descriptions used to describe occurrences of innervation of the inguinal fat depot used in this chapter. Where "experiments" refers to observations during confocal imaging sessions.

Term of frequency	Definition/Description
Always	Observed consistently and constantly when appropriately stained for, unavoidable.
Very Frequent / Very common	Observed on multiple occasions within each experiment and observed consistently across every experiment. Very easy to locate and capture.
Frequent / Common	Observed within experiments, with more than a few examples found, easy to locate and capture and observed consistently across every experiment.
Occasional / Uncommon	Oberved during experiments, but not abundantly within each, only a couple of times or less per experiment and not easy to locate and capture. Less consistent observations between experiments, but present in most.
Rare	Observed inconsistently between experiments, and limited examples found within each experiment, with difficultly locating and capturing examples.

3.3.2.1 Nerves of the inguinal fat depot exhibit three modes of innervation

After successfully adopting and optimising a method to visualise the nerves, experiments began in earnest to discover the types of innervation that exist within the mouse inguinal fat depot, under normal health and weight physiology. Having a visual comprehension of the various structures within the inguinal fat depot was critical for qualitative analysis of innervation modes observed.

3.3.2.1.1 Nerves innervate coarsely in bundles

Individual neurons were observed clustered into bundle-like structures (Figure 3.8). These bundles measured approximately 63 μm in width (mean, N = 4, n = 15) and could be seen in half-depot overview images tracking the entire length and width of the tissue sections imaged, circa 2 - 3 cm with a slight lateral bias. (Figures 3.8 & 3.9 A). The bundles, overall, were very frequently observed, present in every experiment conducted into visualisation of nerves (N = 13). There were differing types of bundle innervation pattern; one form commonly seen tracking through the tissue coarsely, independently of vasculature and through the parenchyma of the tissue (Figure 3.8 B & C). However, the bundles also appeared to track with large vasculature for long distances, innervating in tandem, which was a frequent observation. Lastly bundles also experienced innervation and tracking by medium sized blood vessels, which was overall an occasional to fairly frequent observation (Figure 3.8 D & E). Bundles were always apparently independent of small blood vessels. On rare occasions, bundles were observed appearing to branch, with finer neurites disseminating from the main trunk of the bundle (Figure 3.9 C & D), and appearing to innervate independently of visible blood vessels (Figure 3.9 A).

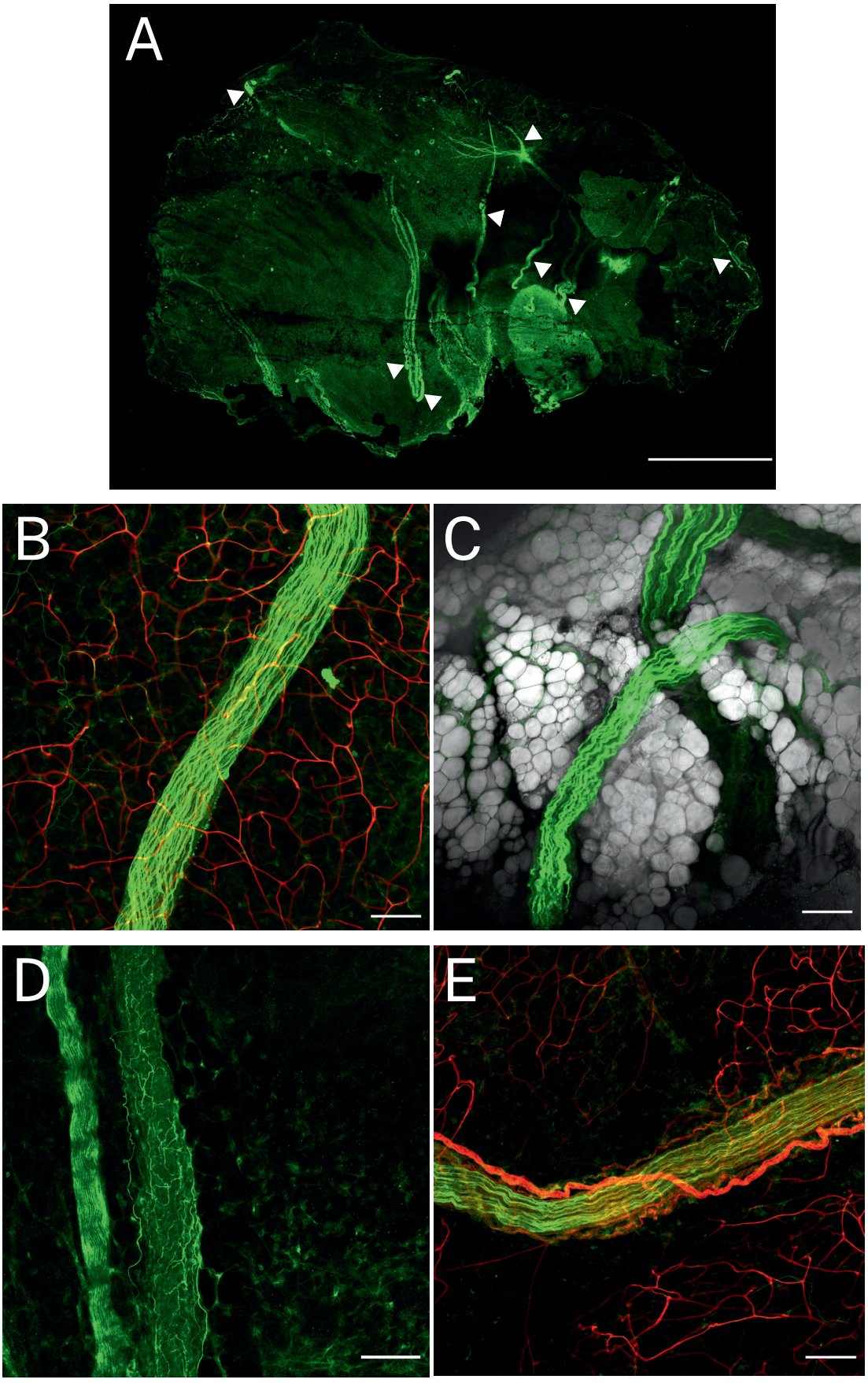

(Figure legend on next page.)

Figure 3.8: Nerve bundle innervation types in the inguinal fat depot. Representative confocal images of β3-tubulin stained nerves (green, Alexa 488) in bundles innervating the inguinal fat depot in differing formats. A section of inguinal fat imaged in (A) depicting nerve bundles (white arrowheads) innervating across the span of tissue. (B) & (C) illustrate coarse bundle innervation, (B) independent of IB4 stained capillaries (red, Alexa 647) and (C) coarsely through BODIPY-stained adipocytes (artificially coloured grey). (D) Illustrates a bundle running alongside large vasculature with limited direct interaction, while (E) medium-sized vasculature can be seen appearing to innervate and track a nerve bundle. Images taken with (A) 2.5x objective with 35 stitched tiles and (B) - (E) a 10x objective. Scale bars represent 1 mm in (A) and 100 μm in (B) - (E). (For IB4 + β3-tubulin N = 4, for β3-tubulin + BODIPY N=3)

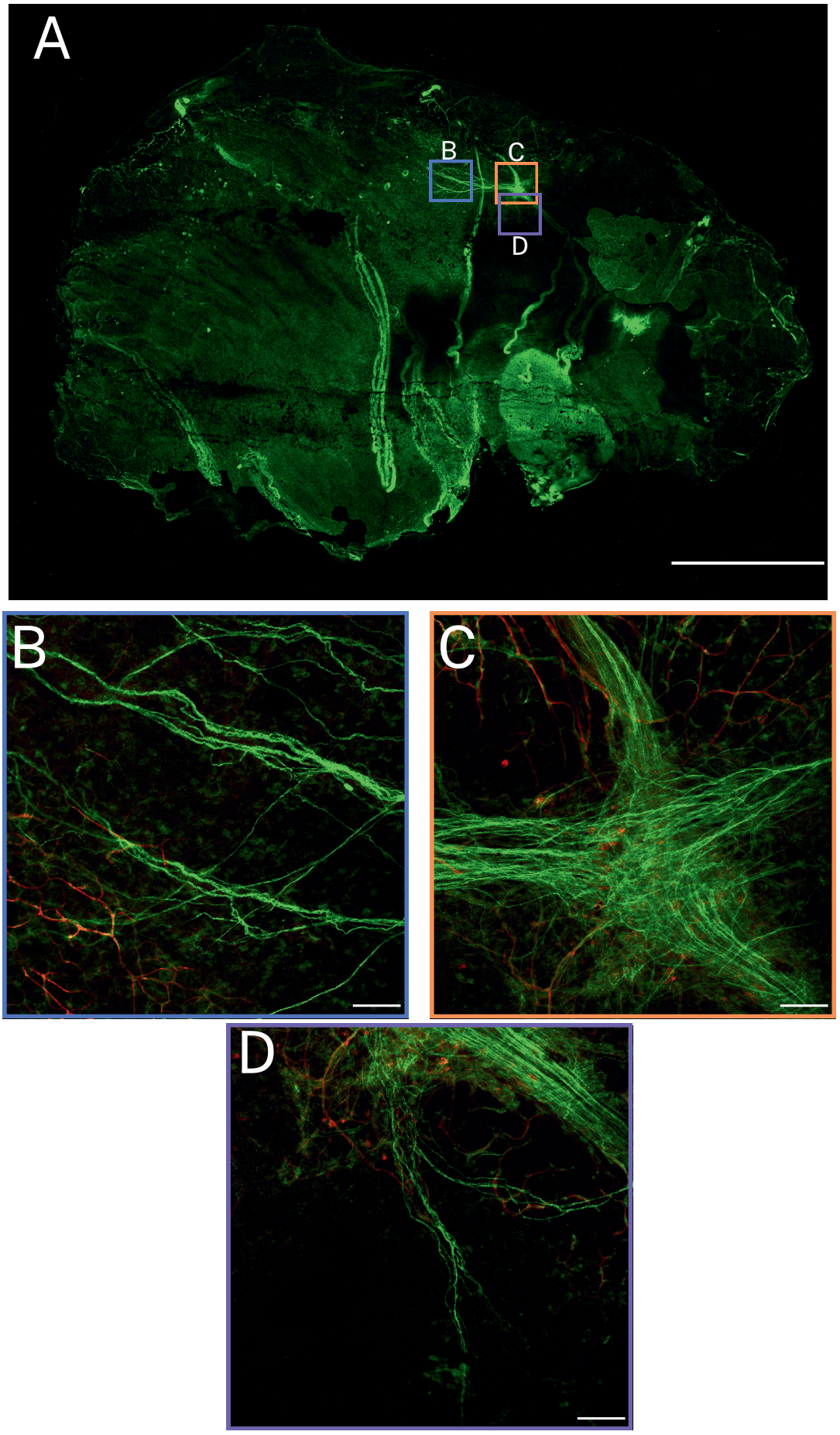

(Figure legend on next page.)

Figure 3.9: Potential evidence of nerve bundle branching into the inguinal fat depot. Confocal images of a nerve bundle appearing to branch into the inguinal fat depot. (A) Overview image of approximately half-depot section of inguinal adipose taken at 2.5x magnification with 35 stitched tiles, stained with β3-tubulin (green, Alexa 488) indicating coloured boxes, blue for (B), orange for (C) and purple for (D), around a potential branching bundle structure. (B) - (D) referenced in the larger annotated overview depict the nerves branching into the tissue as single neurons, or small bundles (B) & (D) and (C) directly over the branching point of the bundle. Images (B - D) taken at 10x magnification. IB4 staining vasculature (red, Alexa 647). Scale bars represent 1 mm (A) and 100 μm (B - D).

3.3.2.1.2 Nerves innervate vasculature

Vascular structures were determined via a combination of Griffonia simplicifolia lectin isolectin B4 (IB4) stain positivity, autofluorescence, size, morphology and innervation pattern. Due to the nature of the IB4, whereupon it agglutinates group B erythrocytes and binds to α-d-galactosyl residues upon endothelial cells, vasculature are readily stained (Laitinen 1987; Corliss et al. 2019). Consequently, microvasculature is stained with intensity, as both erythrocytes that persist through washing steps as well as endothelial cells, are stained. Vessels with larger lumens such as arteries and veins stain less intensely likely due to more effective removal of erythrocytes in washing steps, but experienced higher degrees of autofluorescence. The exposure to 70% v/v EtOH during Sudan Black B staining may also have promoted dehydration and degradation of the glycocalyx within the larger vessels, potentially reducing the binding capacity for IB4 (Li et al 2023). As such, differing IB4 positivity and autofluorescence aided in the classification of vascular structures.

Smaller vessels, classified as capillaries, measured on average 4.2 μm with a range of 2.3 – 8.5 μm in width (N = 4, n = 118) (Figure 3.10 E i) (corroborated by Steinman et al. 2017), with the variance in width likely reflective of their order, ranging 1st - 4th order, largest to smallest (respectively) (Grubb et al. 2020). Capillaries were identified through substantial IB4 positivity, due to their high affinity for the ligand, their charac-

teristic morphology; tube-like and highly-aborised structures in a mesh/net-like pattern, which allowed for their constant and extensive innervation of the tissue. These structures generally lacked innervation by β3-tubulin-positive neurons, with only rare occurrences of nervous innervation of vessels toward the wider ends of the spectrum, which further aided characterisation, as evidence elsewhere supports (Huang et al. 2021) (Figure 3.10 A).

Medium-sized vessels measuring on average, 19.3 μm with a range of 9 - 37.6 μm in width (N = 4, n = 53) (Figure 3.10 E ii) were identified via their fair IB4 positivity and were mostly very frequently and thoroughly innervated by β3-tubulin-positive neurons, although not always, with some receiving fewer nervous innervations than others (Figure 3.11). These mid sized vessels were long, straight and were very commonly observed structures. Bifurcation of these vessels was also very frequently observed, although not to the extreme extents of smaller vessels, and often presented in a distinctive 'Y' shape (Figures 3.10 B & 3.11). These vessels are likely arterioles/venules given their size and morphology.

Larger vessels were IB4-negative or very weakly stained and were largely identified via the exploitation of natural vascular autofluorescence (Figure 3.10 C). The average width observed for larger vessels was 86.4 μm, with a range from 39.5 - 141 μm wide (N = 9, n = 14) (Figure 3.10 E iii). Their long, straight and rare instances of bifurcation further served to differentiate and identify larger vessels (Figure 3.10 C). Large vessels were always innervated by nerves to some degree, which both flanked and shrouded the vessel in a distinctive 'plexus'-like manner (Figure 3.10 C), and oftentimes served to increase ease of identification. Given their size and morphology, these vessels are likely veins and arteries. These vessels could present with longitudinally striped autofluorescence, or more diffuse with a patchy autofluorescence. These structures were frequently to very frequently observed innervating the inguinal fat depot, but I obtained fewer clear examples of larger vasculature within the experiments compared to medium-sized vessels, likely due to reliance on autofluorescence which could limit definition of large vasculature in some cases.

Lymph vessels were occasionally observed and were identified though their characteristic heterogeneous autofluorescence pattern, which presents as distinctive horizontal stripes (Bachmann et al. 2019), especially distinguishable in combination of different channels, for example where both autofluorescence and IB4 staining can be exploited (Figure 3.10 D). Their large width averaging 155 μm, with a range between 123 - 246 μm (N = 3, n = 7), alongside moderate to frequent instances of bifurcation allowed for further recognition of lymph vessels when occasions did arise where they were observed. Their range in size is likely reflective of smaller lymph capillary vessels and larger collecting vessels. Lymph structures were not found to be readily or clearly innervated by nerves using the tools applied here. Occasions where lymph was clearly defined and able to be identified and imaged were uncommon across the suite of experiments (N = 13).

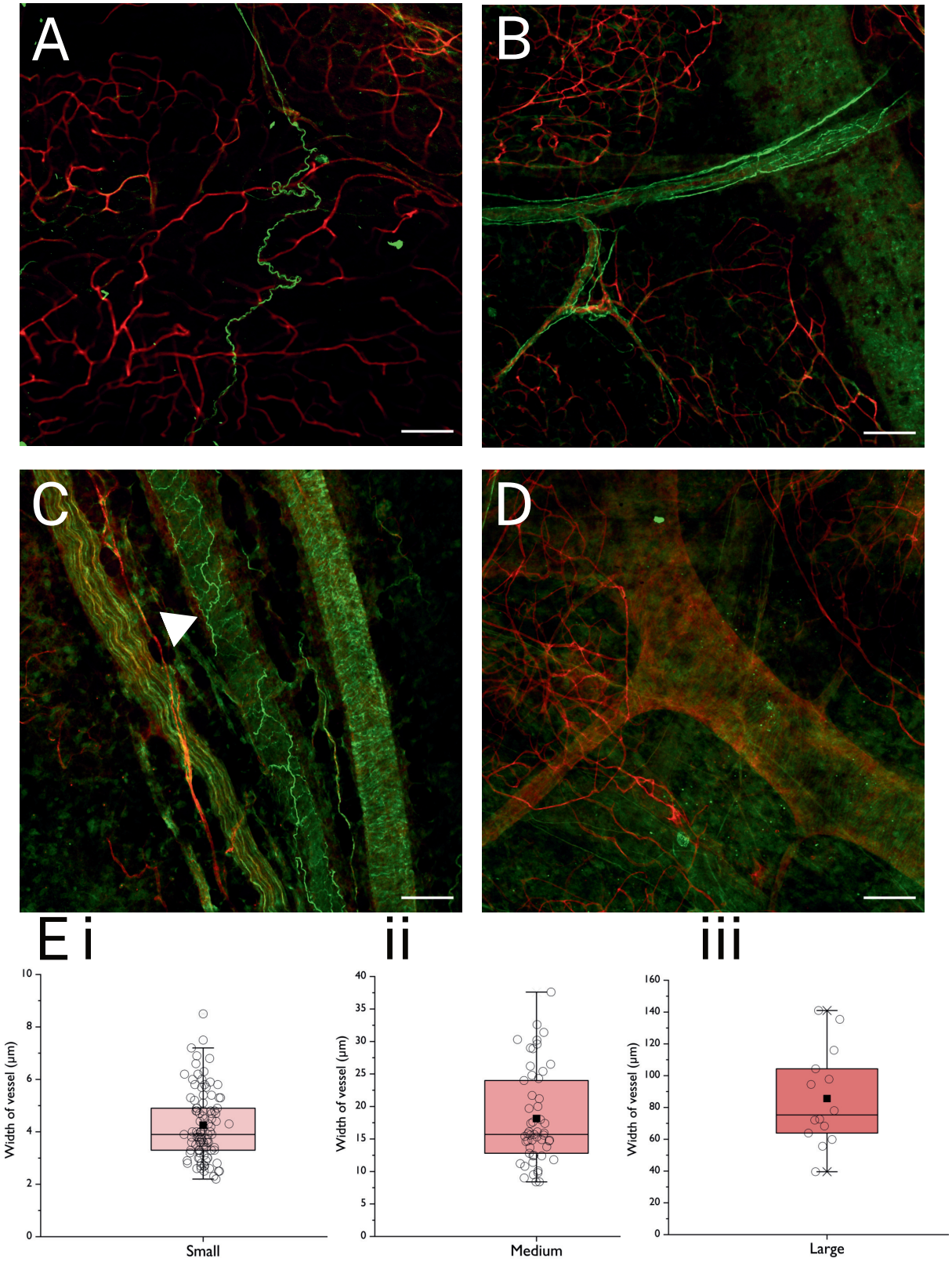

(Figure legend on next page.)

Figure 3.10: Modes of neurovascular interaction in the inguinal fat depot. Nervous innervation of various vascular structures within the fat depot, where vasculature is marked by IB4 (red, Alexa 647) or by autofluorescence and nerves detected by β3-tubulin (green, Alexa 488). Representative confocal images illustrating (A) nerves are found independent of small-calibre vessels deemed capillaries (B), medium-calibre vessels richly innervated with nerves (C), large vasculature wrapped by nerves (white arrowhead) (D) lymph vasculature did not show obvious signs of nervous innervation. Scale bars all represent 100 μm and images taken with a 10x objective. (β3-tubulin + IB4 N = 4) (E) Box plots for (i) small (N = 4, n = 118), (ii) medium (N = 4, n = 53) and (iii) large (N = 9, n = 14) vessel widths in μm, with jitters (open circles) representing each data point, illustrating the range within each. The box indicates the interquartile range (IQR), where 50% of the data lie, while the whiskers represent 1.5x IQR (minimum and maximum extremities of data) where outliers extend beyond. Black line represents the median, while solid squares indicate the mean for each group.

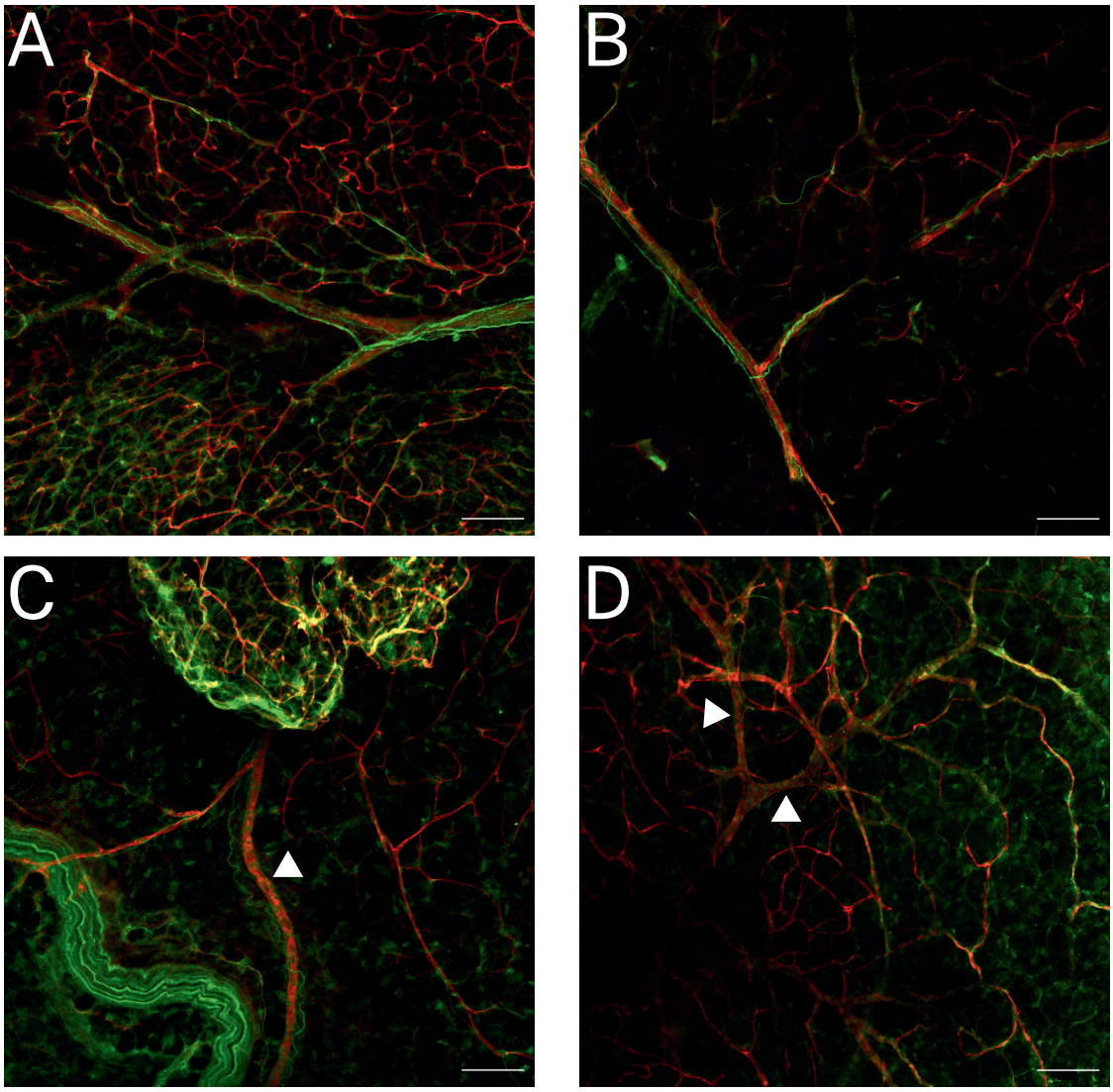

Figure 3.11: Differences in nervous innervation of medium-sized vessels of the inguinal fat depot. Representative confocal images of nerves differentially innervating medium sized vasculature. Nerves stained with β3-tubulin (green, Alexa 488) and vasculature stained with IB4 (red, Alexa 647) in the inguinal fat depot, where (A) demonstrates a extensively innervated vessel (B) a moderately well-innervated vessel, while (C) and (D) illustrate vessels with little to no nervous innervation. White arrowheads indicate where medium sized vasculature lacks innervation. Images taken with 10x objective and scale bars represent 100 μm. (β3-tubulin + IB4 N = 4).

3.3.2.1.3 Nerves innervate parenchyma and adipocytes

Lastly, neurons are observed singularly extending through the parenchyma of the depot, independent of vasculature, interweaving between adipocytes (Figure 3.12).
To examine the adipocyte-neuron relationship more clearly, lipids within the tissue were stained with BODIPY. Using BODIPY fluorescent lipid dye combined with neuronal marker β3-tubulin and vascular stain IB4 (incorporated in 2 of 3 BODIPY experiments), evidence of neurons that innervate independently of vasculature was gained, to ensure any parenchymal innervation observed was not explainable by vascular association by neurons. Neurons were observed consistently innervating independently of nearby IB4-positive capillaries (N = 2) and weaving around defined BODIPY-stained adipocyte boundaries (N = 3) (Figure 3.12 A & B). Instances of parenchymal innervation were observed consistently across experiments, the overall regularity of observations within each experiment was considered fairly frequent, not found to be very frequent and was at times inconsistent.

Supplementary to evidence of parenchymal innervation, in images taken using β3-tubulin both with and without BODIPY, I found evidence of neurons gathering in a complex apparently three-dimensional web-like cluster, termed by the Townsend group as the 'neuro-adipose nexus' (NAN) (Willows et al. 2021). Nerves, compared to general parenchymal observations, appeared to more finely innervate around in a spherical structure, which was unconfirmed here, but likely to be an adipocyte. These net-like structures measured around 80 μm wide and 100 μm in length, which represent adequate dimensions for the encapsulation of a single or multiple adipocytes, as previously shown (Willows et al. 2021). Observations of these structures were rare when using β3-tubulin as sole marker for nerves, over N = 10 confocal experiments (comprising of different 'sets'), they were observed just twice (Figure 3.12). Other than these nexus structures, I did not observe any clear evidence of singular synaptic bouton terminations onto adipocytes, where the nerve appeared to end abruptly.

Lastly, when producing simple exploratory Z-stack projections to produce a composite 3D image during confocal imaging, I noted that singular nerves appeared to innervate somewhat superficially compared to vasculature, only innervating a plane of tissue circa 10 - 20 μm from one surface of the tissue within the Z-axis (Figure 3.13). Whereas

vasculature, with reference to IB4 stained microvessels, apparently innervated greater depths of tissue, overlapping with the plane in which singular nerves innervate, and beyond to fuller extents of the tissue volume (Figure 3.13). Singular neurons repeatedly illustrated this restricted depth of innervation in Z-stack projections performed here. In observations during data collection, nerves that did innervate deeper into the tissue were associated with vasculature, or within bundles.

Therefore, acquiring a clear image of a close neuro-adipocyte interaction was challenging due to clear/discrete adipocyte structures residing deeper within the tissue and neuronal innervation being largely superficial, as described (Figure 3.13). Surface-level adipocytes rarely stained with clear cell boundaries, which may be due to sample handling and tissue processing steps (ZDR) potentially causing lysis of adipocytes on the outer surface of the fat depot.

Summary To conclude, using the tools and methodology outlined, I found non-selectively stained nerves innervate in three main modes; very frequently seen in large bundles, very frequently but inconsistently associating with medium and always large vasculature, with rare innervation of microvessels and no clear innervation of lymph vessels. Innervation consisting of individual neurons extending into the parenchyma was observed fairly frequently, and rare cases of what appeared to be direct adipocyte innervation, in the form of fine web-like neuro-adipose 'nexus' structures. Parenchymal innervation appeared somewhat superficial under these conditions. These data provide clear evidence of the vascular, neuronal and neurovascular innervation of the inguinal fat depot.

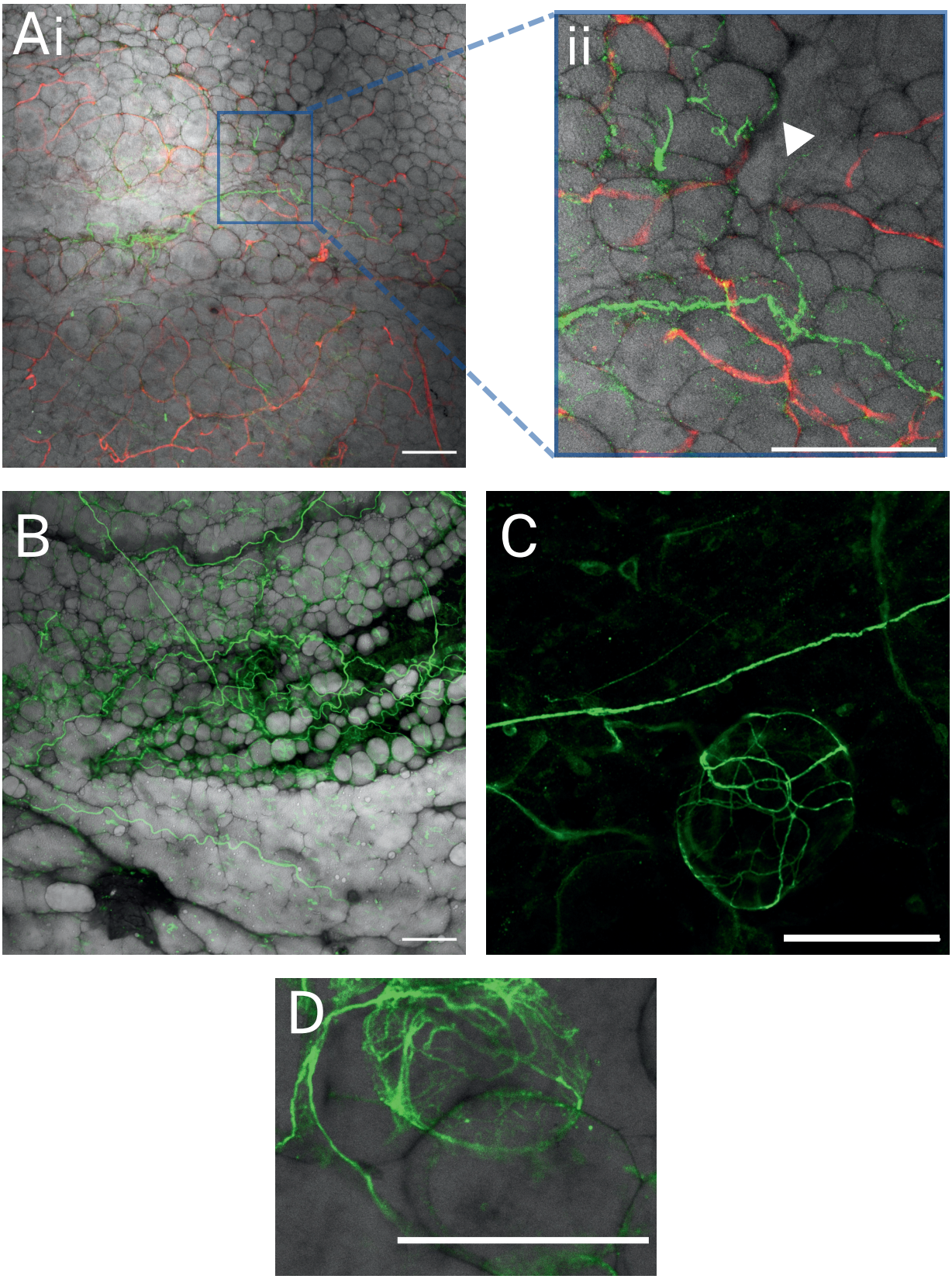

(Figure legend on next page.)

Figure 3.12: Nervous innervation of parenchyma and adipocytes within the inguinal fad depot. Representative confocal images of parenchymal and adipocyte level interactions of nerves identified with β3-tubulin (green, Alexa 488). In (A) (i) nerves are seen innervating independently of small-calibre vessels marked with IB4 (red, Alexa 647) and around the boundaries of adipocytes (ii) (white arrowhead) stained with BODIPY (artificially coloured grey), the blue box around structures in (i) is presented in (ii) as 3x digitally zoomed image. (B) Nerves innervating between well-defined adipocytes. (C) and (D) are zoomed images (2.9 and 4.2x respectively) of nerves finely innervating in the web-like pattern of the neuro-adipose nexus structure. Images taken with a 10x objective. Scale bars represent 100 μm. (N = 3 for BODIPY + β3 tubulin, N = 2 for BODIPY + IB4 + β3-tubulin).

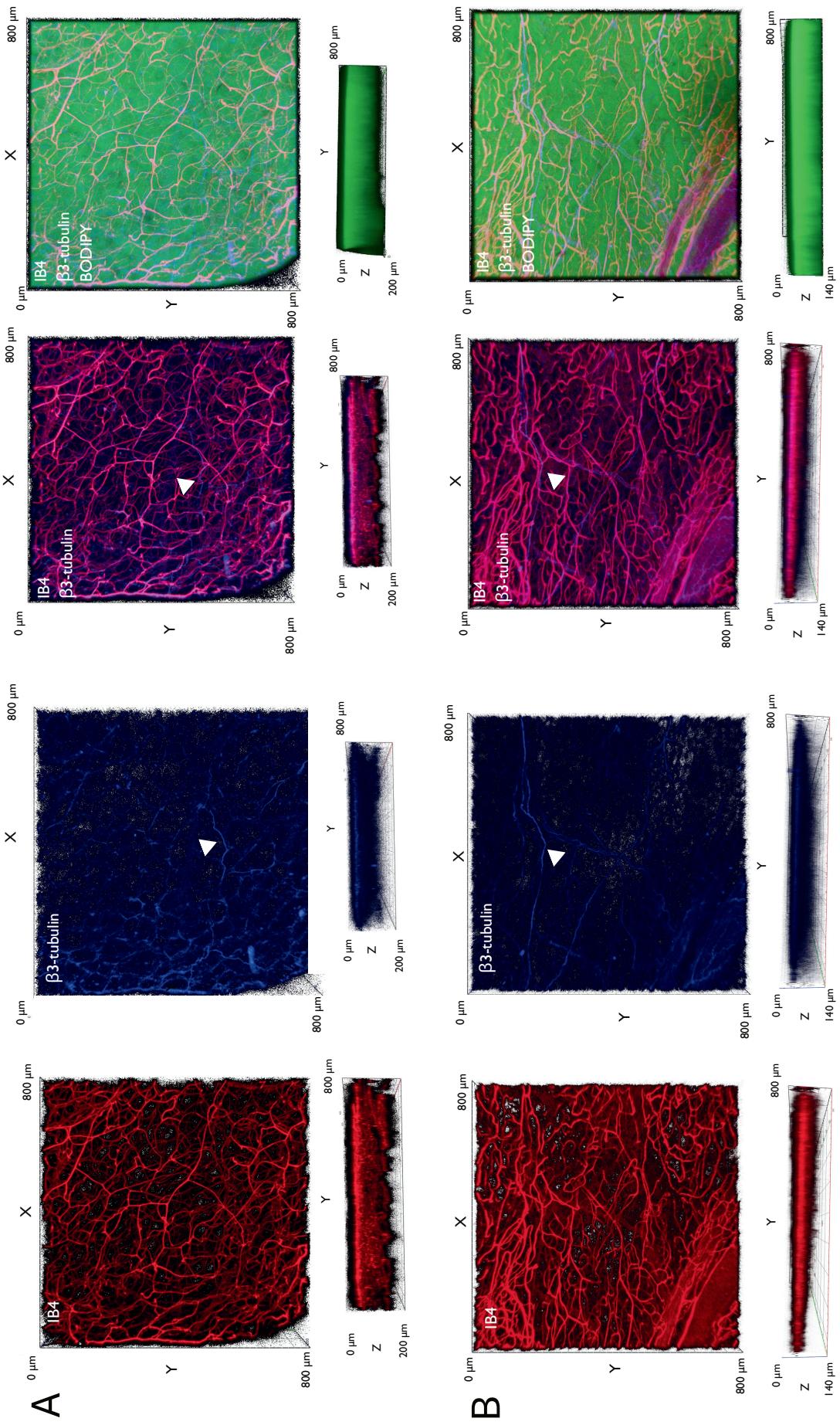

(Figure legend on next page.)

Figure 3.13: Approximate depth of innervation observed of nerves and small-calibre vasculature in the inguinal fat depot. Representative examples of Z-stack projection views taken during confocal imaging, illustrating the approximate depths of innervation of various components of inguinal adipose tissue, where nerves are marked with β3-tubulin (blue, Alexa 405), small vessels marked with IB4 (red, Alexa 647) and adipocytes are fluorescently dyed with BODIPY (green). (A) and (B) refer to two examples from different animals. Each component image accompanied below by a Z-plane face view indicating approximate depth of innervation. X Y and Z axis are labelled with dimensions as appropriate. White arrowheads depict examples of nerves. Projections are thresholded to reduce unstained areas (black) for improved structure visualisation. All images are captured using a 10x objective.

3.3.3 Exploring sympathetic innervation of the inguinal fat depot

After the initial data obtained indicating general nervous innervation, further experiments were necessary for the detection of sympathetic nerves, to infer the potential scope of norepinephrine signalling in adipose tissue, informing future functional experiments. Therefore next, in order to determine the overall abundance of sympathetic innervation as part of total nerves marked by β3-tubulin, antibodies against selective marker for sympathetic nerves, tyrosine hydroxylase (TH) (1:250), were chosen. The absence of TH and positivity for β3-tubulin would thereby also serve as an indicator of the presence of another non-sympathetic nerve subtype; putative sensory nerves.

3.3.3.1 Sympathetic nerves innervate in all three modes

Putative sympathetic neurons (TH-positive) were observed innervating inguinal adipose tissue in all three modes (as previously described in section 3.3.2); in bundles, innervating both medium and large vasculature and independent innervation of parenchyma, extending to (apparently) individual adipocytes in the encapsulating neuro-adipose nexus structure (Figure 3.14). These findings were in alignment with findings in literature (Willows et al 2021).

Adding further detail, fluorescently-labelled nerves stained with antibodies against both β3-tubulin & TH demonstrated both convergence and divergence in staining across

the three innervation modes.

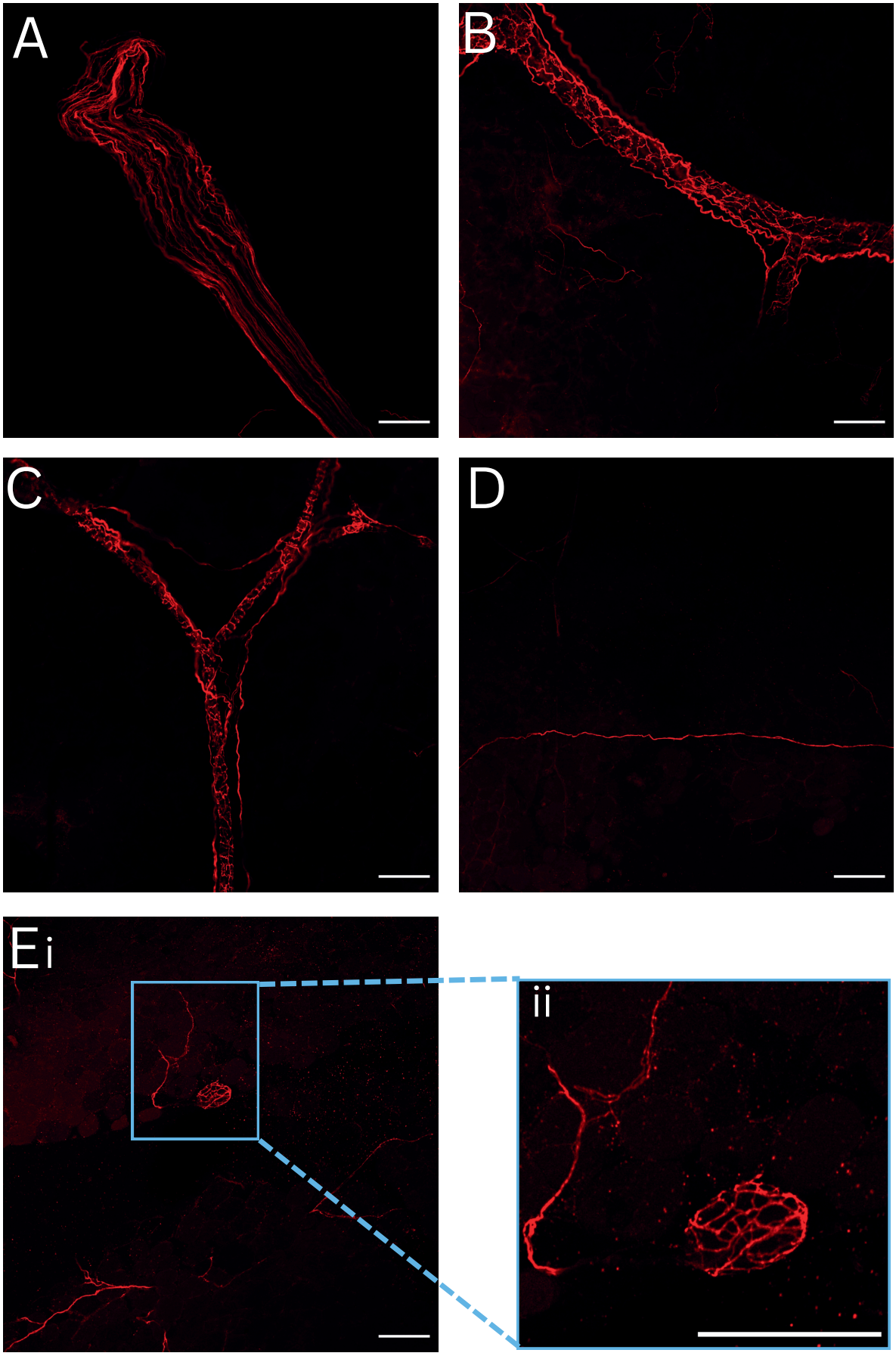

(Figure legend on next page.)

Figure 3.14: Sympathetic nerves innervate the inguinal fat depot in all three modes.

Representative confocal images of sympathetic nerves identified with tyrosine hydroxylase (TH) (red, Alexa 647) displaying the 3 modes of innervation; (A) in bundle structures and extensive innervation of both (B) large and (C) medium sized vasculature, also observed (D) innervating independently through the tissue and (E) finely in the neuro-adipose nexus structure (i) indicated by the blue box, where (ii) is a (3.1x) digitally zoomed representation of boxed area in (i). Images all taken with a 10x objective and scale bars represent 100 μm. (N = 3).

3.3.3.1.1 Sympathetic innervation within nerve bundles

Nerve bundles appeared to consist of a heterogeneous population of nerves (Figure 3.15 A). The morphology of these differentially stained nerves was identical, the only difference pertaining to their emission wavelength through the use of two different fluorophore- conjugated secondary antibodies against the respective primary antibodies. When moving through the Z-plane during image acquisition, I noted the subtypes within the bundle did not cluster by type or form discrete patterns, instead integrated without particularly defined organisation. Though, the perceived proportion or ratio of each subtype present within a bundle differed depending on the Z-plane observed (owing to the three-dimensional structure of the bundle), with some planes of view displaying more sympathetic presence than others, making it challenging to capture representatively. This issue was considered when handling example images during estimations of staining proportion, where multiple planes were assessed and an average proportion over all available planes calculated.

In these approximate measures of staining proportion by area coverage in the bundles assessed, TH positivity equated to 28% of total fluorescence, where β3-tubulin positivity in the green channel constituted an average of 72% of the overall proportion of staining (N = 2). This may indicate that 28% of nerves in a given bundle are sympathetic, while 72% are non-sympathetic. As these structures are 3D in situ, I noted when taking images that relative proportions of staining did change depending on the plane observed. There were only two valid examples captured of the same bundle in multiple planes which could be used for a semi-quantitative measurement of colocalisation. Therefore, while

comments can be made on the proportion of wavelength-based neuron identity, solid conclusions cannot be drawn

It was noted during data handling, there also appeared to be a population of nerves that solely stained with TH with an absence of β3-tubulin. This phenomenon was consistent across innervation of other structures and across experiments. Collectively, the approximate proportions of TH-positive staining alone in the red channel made up 44% of the total TH-positive staining, with the remaining 56% of the total stained positively for both β3-tubulin and TH in yellow i.e. colocalised (Figure 3.15 B).
Lastly, almost every bundle during data collection was captured without evidence of branching. However, as previously described in β3-tubulin experiments in section 3.3.2, during optimisation and trial experiments a subsection of TH-stained sympathetic nerves within the bundle have been observed branching away from the trunk and into the parenchyma (Appendix Figure 7.3). Although, this was not observed during the core experiments, therefore is deemed rare.

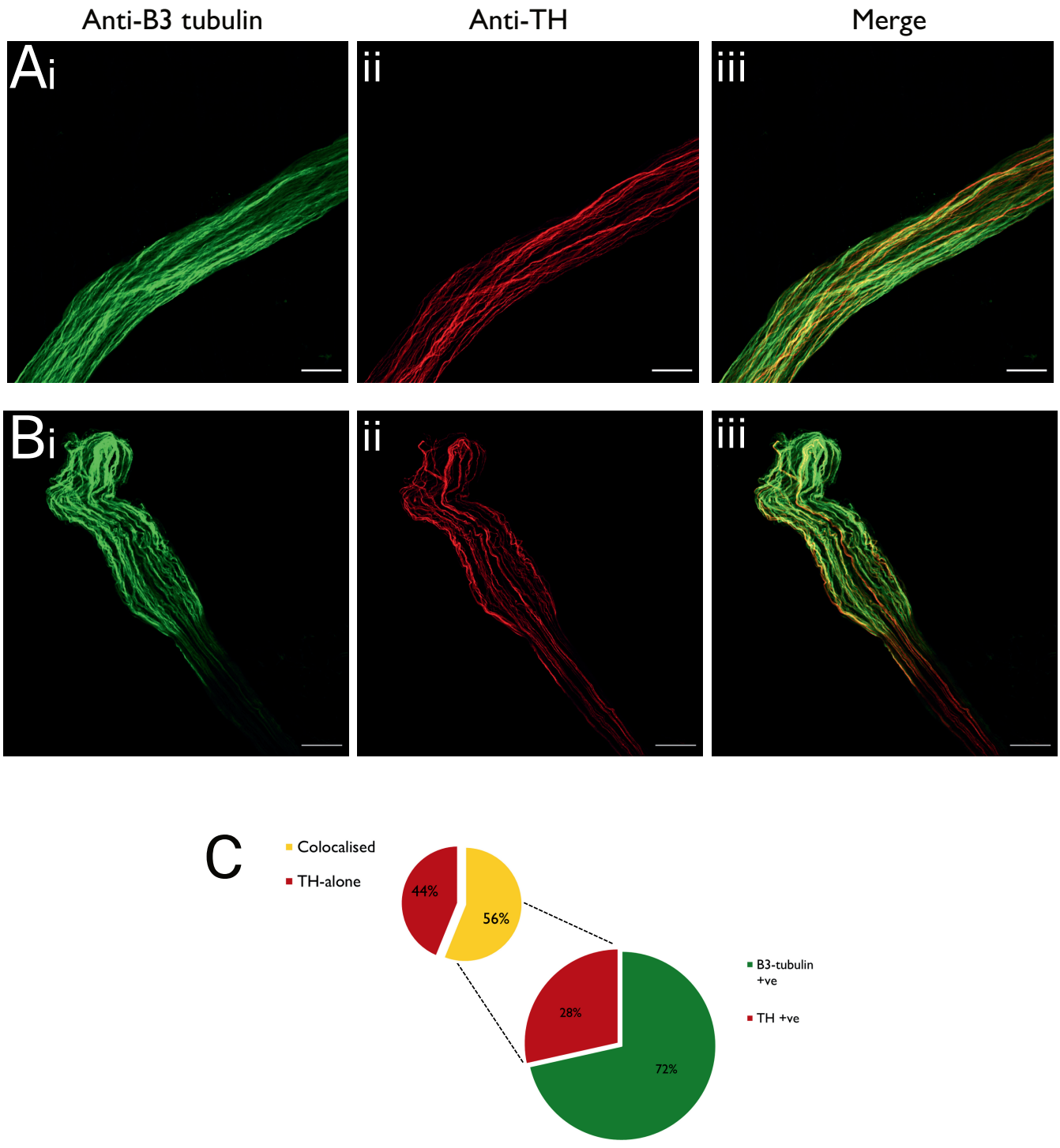

(Figure legend on next page.)

Figure 3.15: Sympathetic subtypes represent a portion of nerves within bundles. (A) & (B) Representative confocal images of nerves stained with (i) β3-tubulin (green, Alexa 488), (ii) tyrosine hydroxylase (TH) (red, Alexa 647) and merged (iii) to illustrate the heterogeneous population of nerves in a nerve bundle. Images taken using a 10x objective and scale bars represent 100 μm. (C) Approximate proportions of nerve population in bundles, based on assessments of area coverage for red, green and colocalised yellow channels as percentage of the total fluorescence in each example. The main pie chart refers to overall TH negative and β3-tubulin positive versus TH positive staining, while the smaller pie illustrates the portion of the TH-positive structures that had colocalised with β3-tubulin versus those that stained negatively for β3-tubulin (N $= 2$).

3.3.3.1.2 Sympathetic innervation of vasculature

In line with other research, sympathetic innervation is closely associated with vasculature (Huesing et al. 2021), with a large proportion of nerves innervating vasculature being sympathetic. The examples in Figure 3.16 demonstrate the tight association between sympathetic nerves and medium-sized vessels, where the nerves (stained with TH in red) appear to flank and wrap around the vessel along the entire length captured.

Estimations of staining proportion by area coverage suggest that 38% of total fluorescence staining measured was β3-tubulin-positive in the green channel, with 62% classified as TH positive, wherein 63% of this staining was solely in the red channel, while 37% of TH-positive staining indicated colocalisation with β3-tubulin in yellow (N $= 2$, n $= 3$) (Figure 3.16 B). This staining assessment suggests, that in an average medium vessel showcasing nervous innervation, 62% may be of sympathetic identity, with 38% of non-sympathetic identity. Collectively these data suggest that medium sized vessels, putative venules and arterioles, are dominantly innervated by sympathetic but also non-sympathetic nerves.

Nervous innervation of large vasculature also appeared dominantly sympathetic in nature, with images illustrating a high proportion of TH-positive sympathetic nerves

(Figure 3.17).

Examples assessed for staining by channel indicated an average of 59% of total fluorescence staining as TH-positive, wherein 68% was TH alone in the red channel, with the remaining 32% as colocalised TH plus β3-tubulin-positive staining in the yellow channel. The remaining 41% of total staining showing β3-tubulin positivity in green channel (N = 2, n = 3) (Figure 3.17 B). Approximate staining assessments therefore may indicate in an average large blood vessel, 59% may be sympathetic in nature, with 41% as non-sympathetic.

The innervation patterns of nerves within larger vessels could sometimes appear somewhat dissimilar, for instance, in examples from Figure 3.17, the innervation between examples looks slightly different, as does the overall appearance of the vessel. In Figure 3.16 (B), the vessel appears to be wrapped by nerves of both sympathetic and 'other' identity, in a distinct tight and 'wavy' pattern. Whereas in Figure 3.16 (A) the nerves, which appear almost exclusively sympathetic, are extensive but fine and diffuse with more defined flanking nervous tracks long the vessel.

These differences in appearance may be underpinned simply by the size differences of the vessels in the examples, which may also pertain to their subtype (undetermined). It is then likely that innervation pattern may change depending on the vascular identity of the vessel, either venous or arterial.

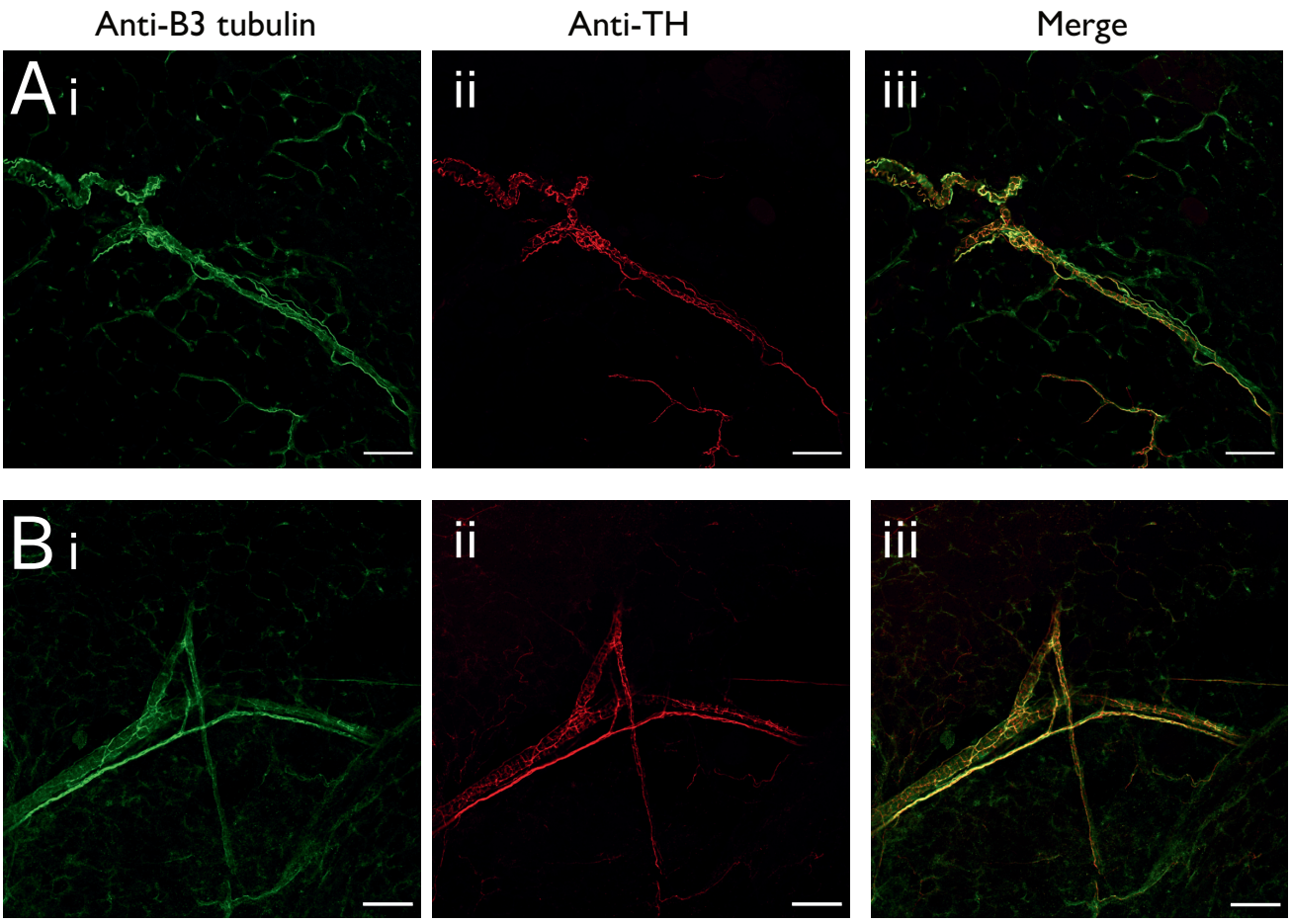

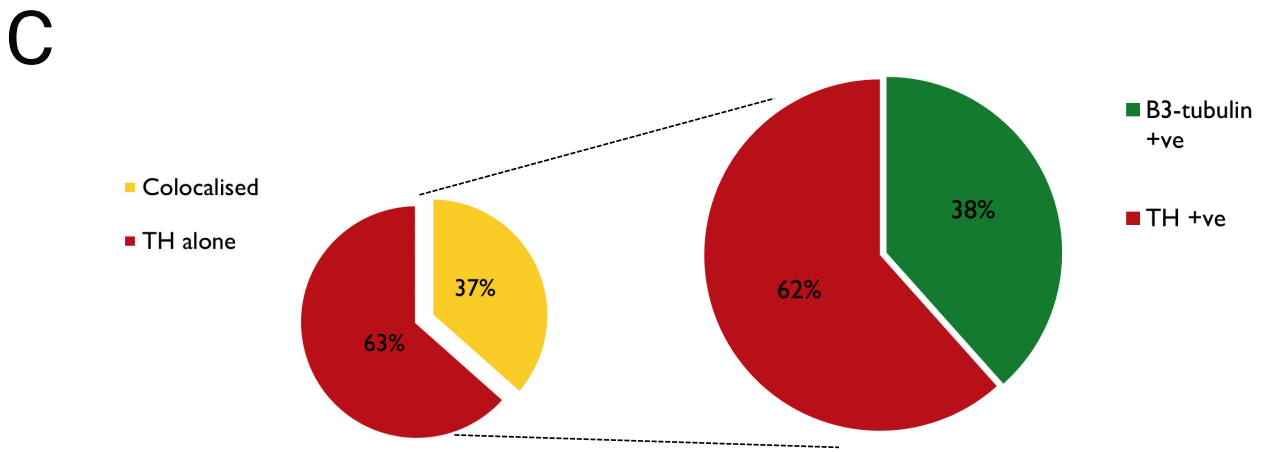

(Figure legend on next page.)

Figure 3.16: Sympathetic and non-sympathetic nerves innervate medium-calibre vessels in the inguinal fat depot. (A) & (B) Representative confocal images of (i) β3-tubulin- stained nerves (green, Alexa 488) and (ii) TH-stained nerves (red, Alexa 647) innervating medium-sized vasculature in the inguinal fat depot and (iii) represents merged channels. Scale bars represent 100 μm and images taken with 10x objective. (N = 3) (C) Approximate proportions of nerve types innervating medium-sized vessels, based on assessments of area coverage for red, green and colocalised yellow channels as percentage of the total fluorescence staining in each example. The main pie chart refers to overall TH-negative and β3-tubulin-positive versus TH-positive (sympathetic), while the smaller pie illustrates the portion of the TH-positive structures that had colocalised with β3-tubulin and those that stained negatively for β3-tubulin (N = 2, n = 3).

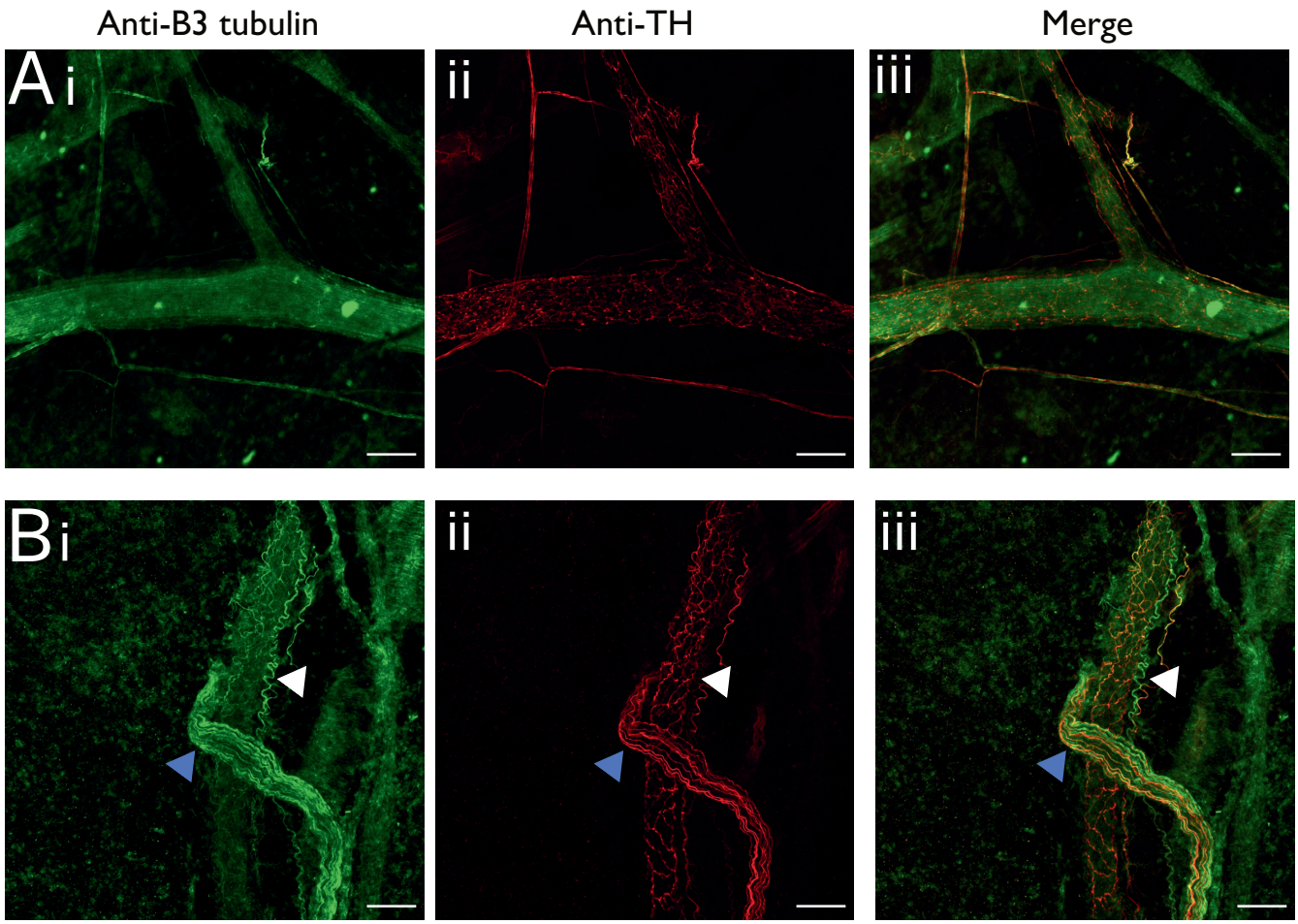

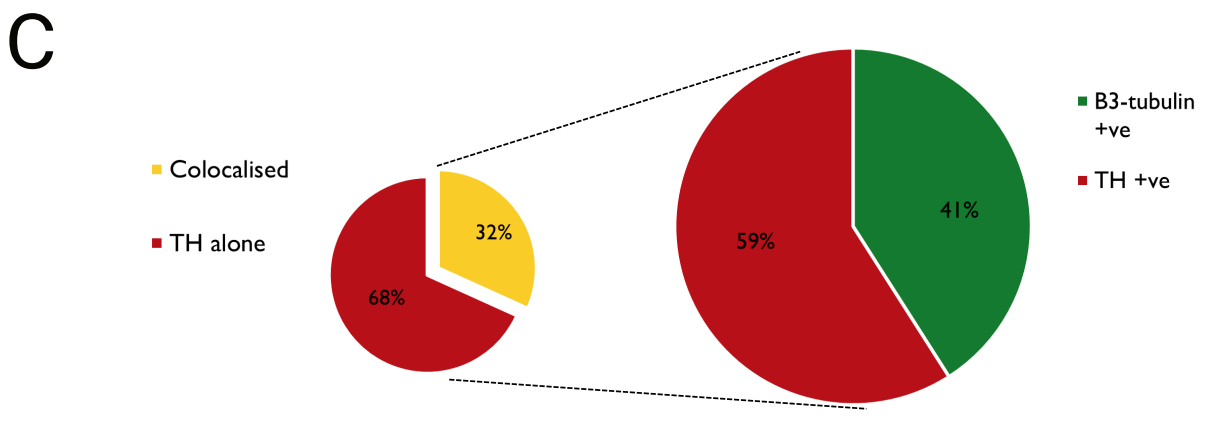

(Figure legend on next page.)

Figure 3.17: Sympathetic and non-sympathetic innervation of large vasculature within the inguinal fat depot. (A) & (B) Representative confocal images of (i) β3-tubulin- stained nerves (green, Alexa 488) and (ii) TH-stained nerves (red, Alexa 647) innervating large vasculature in the inguinal fat depot and (iii) represents merged channels. Blue arrowheads in (B) refer to a nerve bundle while white arrowheads indicate a non-sympathetic nerve. Scale bars represent 100 μm and images taken with 10x objective. (N = 3) (C) Approximate proportions of nerve types innervating large vessels, based on assessments of area coverage for red, green and colocalised yellow channels as percentage of the total fluorescence staining in each example. The main pie chart refers to overall TH-negative and β3-tubulin-positive versus TH-positive, while the smaller pie illustrates the portion of the TH-positive structures that had colocalised with β3-tubulin and those that stained negatively for β3-tubulin (N = 2, n = 3).

3.3.3.1.3 Sympathetic innervation of the parenchyma

As with using the β3-tubulin marker alone in section 3.3.2, evidence of sympathetic nerves innervating away from visible vascular structures was gained (Figure 3.18). Experience from previous experiments informed by using BODIPY and IB4 (markers for adipocytes and vasculature, respectively) enabled for the discern of nerves innervating parenchyma based on innervation characteristics, even without the inclusion of these tools. Medium and large vascular structures are almost always visible to some degree, due to their natural autofluorescence, and nerves that associate with vasculature typically cluster together and wrap the vessel, highlighting vessel shape, further aiding their positive identification. Singular nerves that innervated the parenchyma, meandered in the tissue and were found alone, not clustered or associating with other nerves. Therefore despite the lack of tools to confirm the innervation is away from vasculature and innervates parenchyma definitively, a discerning eye can determine a parenchymal from a neurovascular innervation.

When sympathetic nerves were selectively marked using TH, parenchymal innervation modes were observed with a similar degree of frequency, i.e. fairly frequent, as found in studies with β3-tubulin. The appearance and overall morphology of the sympathetic nerves matched those observed with β3-tubulin (section 3.3.2) (Figure 3.18 A). How-

ever, interestingly, sympathetic classified nerves were the only type observed innervating the parenchyma, with every image taken to showcase/demonstrate parenchymal-type innervation showing some degree of TH positivity, either overlap between β3-tubulin & TH (80% of images), or a singularly stained TH-positive nerve (20% of images) (N = 3, n = 15) (Figure 3.18 E). Over three experiments, using both β3-tubulin alongside TH, the intricate neuro-adipose nexus (likely adipocyte-innervating structures) were observed 8 times (N = 3). In every single instance in which these structures were captured, they were positively stained with TH, with few cases of clear β3-tubulin overlap within part of the webbing stricture. Very frequently, in over 60% of images where observed, these NAN structures did not stain positively for β3-tubulin whatsoever and thus were not visible in the green channel (Figure 3.18 E). This suggests that with the tools and methodology applied here, all neuro-adipose nexus structures are sympathetic in nature.

As previously observed (although perhaps less prominent) in the neuro-adipose nexus structures found with β3-tubulin as a nerve marker, small, defined bulb-like structures were present along the finely innervating axons of TH-stained sympathetic fibres (Figure 3.19). These bulbs were significantly wider than the axon (N = 3, P<0.001, two sample t-test) measuring an average width of 1.38 μm (N = 3, n = 41) compared to the average width of the contiguous axon of 0.91 μm (N = 3, n = 24). Lastly, the bulbs were almost always visible when observing NAN structures using anti-TH antibodies, and were present and most prominent along the more fine axon projections, for the length of the axon captured.

Summary Sympathetic nerves were observed innervating in all 3 modes, as observed with β3-tubulin; In bundles where there was a clear heterogeneous population of nerves and the approximate proportion of TH-positivity in bundles was around a third of the total. Sympathetic nerves were also observed innervating large and medium-calibre vessels with vascular innervation presenting as dominantly sympathetic. Parenchymal innervation and proposed direct adipocyte innervation was found to be exclusively sympathetic. These data provide evidence that sympathetic nerves associate both casually and directly with adipocytes, which serves as a means for nerve-mediated regulation of metabolism.

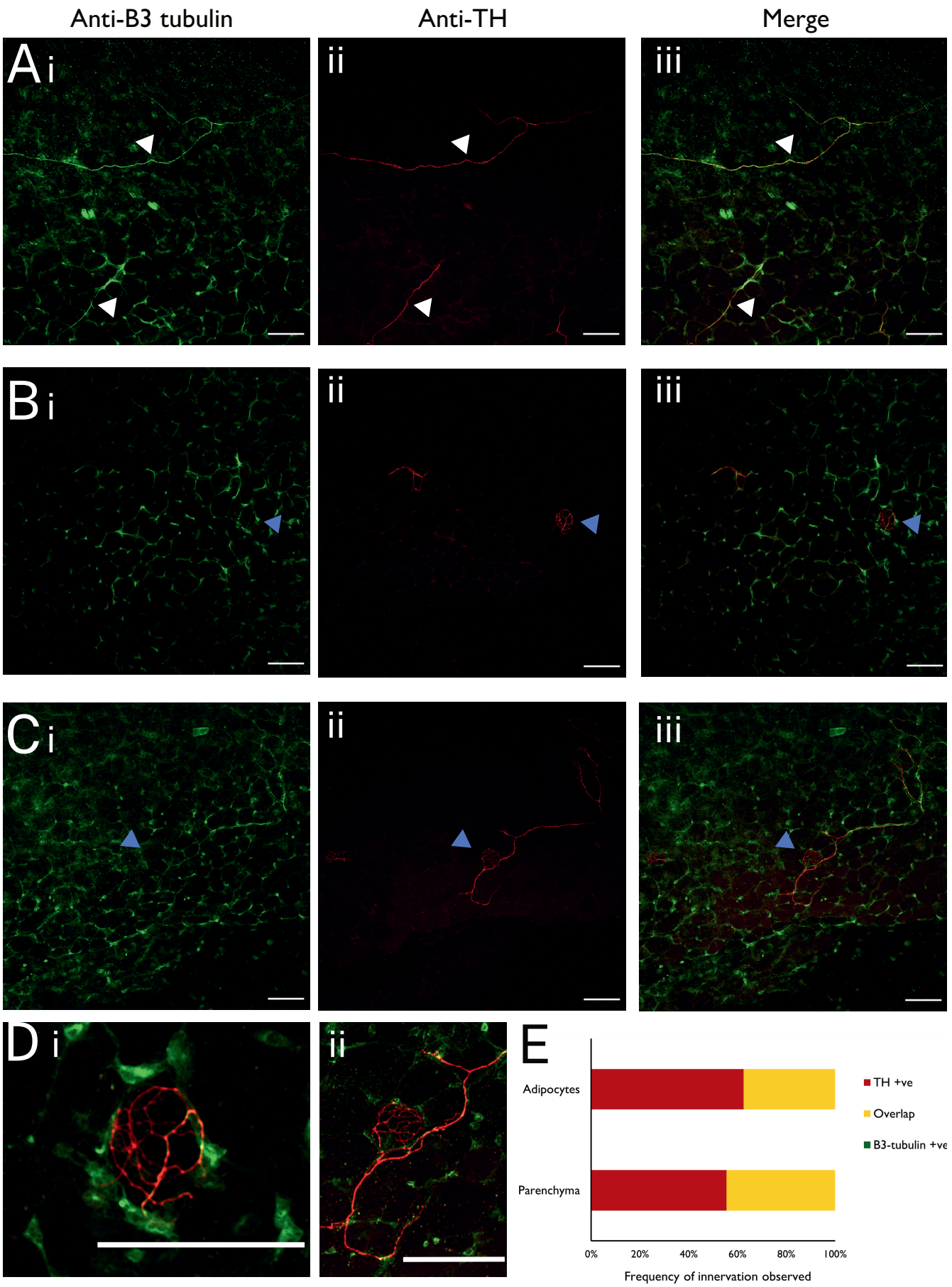

(Figure legend on next page.)

Figure 3.18: Sympathetic nerves innervate parenchyma and adipocytes in the inguinal fat depot. (A) - (C) Representative confocal images of (i) β3-tubulin- stained nerves (green, Alexa 488) and (ii) TH-stained nerves (red, Alexa 647) innervating the parenchyma (A) and adipocytes (B) & (C) in the inguinal fat depot, where (iii) indicates merged channels. (D) (i) and (ii) are digitally zoomed confocal images (5.3x and 3.1x, respectively) of neuro-adipose nexus structures indicted by blue arrowheads in (B) and (C) respectively. White arrowheads indicate parenchymal innervating nerve. Scale bars represent 100 μm. Chart in (E) represents percentage occurrence of parenchymal (N $=$ 3, n $=$ 15) and adipocyte (N $=$ 3, n $=$ 8) innervation in images, where fluorescence signal observed in images were visually assessed for overlap, presence or absence of TH and β3-tubulin positivity and appropriately recorded.

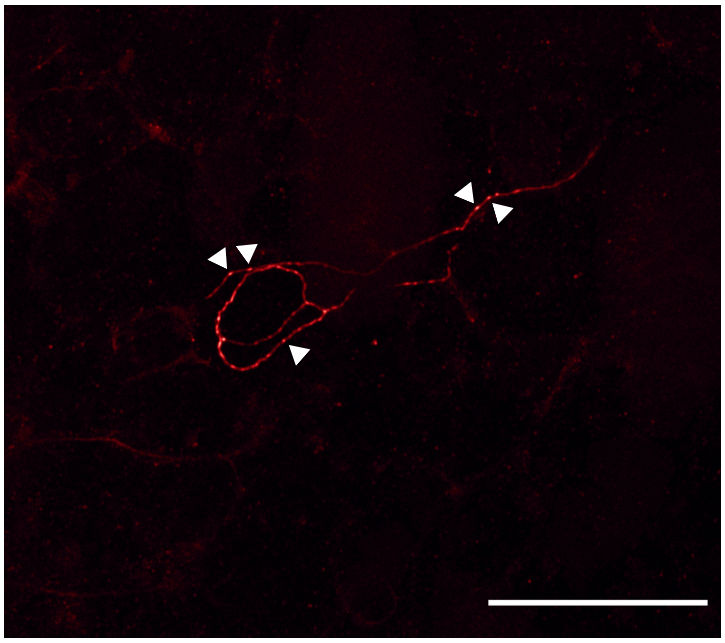

Figure 3.19: Morphology of sympathetic nerves innervating in the neuro-adipose nexus structure. Representative image of TH-stained (red, Alexa 647) sympathetic nerves innervating in the fine, web-like structure of the neuro-adipose nexus, displaying bulbs along the axon. White arrows indicate some examples of bulb-like forms along the length of captured nerve. Images taken with 10x objective with a 2x digital zoom applied and scale bar represents 100 μm.

3.3.3.2 Overall frequency observations

To gather a complete overview of innervation observed within this chapter, this section serves to surmise findings throughout this chapter and to describe the overall frequencies.

Due to the sampling nature, whereby fluorescently labelled structures were actively sought, with no randomisation or structure to sampling, and parenchymal innervation examples were of particular focus, frequencies cannot be accurately ascertained and quantified for each experiment on the basis of % occurrence over a total number of images, due to issues with bias. However, the impressions of frequency based on anecdotal findings of how often and easy structures were to find and frequencies across experiments, is possible.

In agreement with literature (Chi et al. 2018), every experiment performed and in-

cluded/utilised for the description and illustration of nervous innervation had instances of nerve bundles, innervation of vasculature and of parenchyma (N = 13) (Table 3.2). Nerve bundles, and medium-sized vasculature were very frequent and easy to locate within and between experiments and when stained for, small-calibre vessels were always found and unavoidable. Large vasculature was frequent to very frequent and varied across experiments, with some experiments more fruitful than others at producing high-quality examples.

Medium and large sized vasculature were very frequently to almost always innervated by nerves, with variance in innervation existing in medium sized vasculature, with some examples demonstrating little to none. Small calibre vessels only experienced rare examples of innervation.

Overall, parenchymal innervation was considered fairly frequent, with multiple examples found for each experiment, but had varying frequency across experiments, some experiments providing more and clearer examples than others.

All the findings were reproduced when using TH to identify sympathetic nerves, indicating sympathetic innervation is present in all forms. Sympathetic innervation was dominant in vasculature, and less dominant in nerve bundles, where the proportion was biased to non-sympathetic subtypes. Parenchymal innervation however appeared wholly sympathetic. Neuro-adipose nexus structures were overall considered infrequent, with presence of these structures only found in 5 of 13 experiments (38%), with 3 of those 5 being from experiments using TH, representing all experiments where TH was used, suggesting an exclusively sympathetic population. As there was a higher frequency within each experiment and overall using TH (8 examples in N = 3), it is clear that this marker is efficient at detecting these structures over β3-tubulin.

Table 3.2: Types of innervation observed in the inguinal fat depot. The total number of optimised experiments performed using whole mount immunocytochemistry to visualise nervous innervation (N = 13), split into experimental sub-classifications (or 'sets') by markers and categorised by innervation type observed in each case (indicated by '√'); Bundles of nerves, innervation of vasculature, non-vascular parenchymal innervation and direct adipocyte innervation.

		Innervation type			
Marker	**N**	***Bundles***	***Vasculature***	***Parenchyma***	***Adipocytes***
	1	√	√	√	√
β3-tubulin	2	√	√	√	
	3	√	√	√	
	1	√	√	√	
β3-tubulin + IB4	2	√	√	√	
	3	√	√	√	√
	4	√	√	√	
	1	√	√	√	
β3-tubulin + BODIPY	2	√	√	√	
	3	√	√	√	
	1	√	√	√	√
β3-tubulin +	2	√	√	√	√
Tyrosine hydroxylase	3	√	√	√	√

3.4 Discussion and conclusion

3.4.1 The inguinal fat depot is innervated by nerves

Satisfying the first research aim of this chapter, through a systematic approach to optimisation of whole mount immunocytochemistry, evidence of nervous innervation of the inguinal fat depot was gained (Figure 3.20). These data complement observations in literature, while matching image clarity and quality.

3.4.1.0.1 Attenuating autofluorescence

One of the largest obstacles faced when approaching this aim was autofluorescence and thus determination of specific versus non-specific fluorescent signals. It is understood that autofluorescence is generally a large obstacle when imaging in whole mount conditions, but particularly with adipose tissue, due to abundance of highly autofluorescent lipids. The light that travels through a lipid during microscopy is refracted, scattered in multiple directions, to produce the appearance of fluorescence even in the absence of fluorescently labelled antibodies. Additional to autofluorescent lipids, other structures present, such as vasculature, are also highly autofluorescent owing to their elastic fibre content and containment of erythrocytes, which again are autofluorescent due to hemoglobin and its precursors porphyrins within the heme groups (Shrirao et al. 2021). Vascular autofluorescence was largely mitigated here with heparin washes, which acts an an anti-coagulant (via activation of antithrombin III to inhibit formation of fibrin clots) and aids to flush erythrocytes from vessels, particularly larger vessels with wider lumens due to ease of access. Sometimes, this autofluorescence was deliberately exploited for visualisation of larger vessels, weakly or negatively stained by IB4. It is evident in the body of the chapter how prevalent vasculature in all forms is, potentially contributing to and compounding the autofluorescent nature of the tissue. Further sources of autofluorescence arise from lipofuscin, another autofluorescent pigment which is produced by many long-lived post-mitotic cells types, including neurons, and can make unlabelled nerves and other cells appear fluorescent (Di Guardo 2015). This may explain why occasionally, in secondary antibody control images, there appeared to be fluorescence of discrete

structures. The use of young adult mice (typically aged 8-10 weeks) within the present study possibly acted as a benefit in this context, as the nerves had likely not accumulated as much lipofuscin as older animals. A primary solution to essentially attenuate the bulk of autofluorescence was the use of neutral lipid azo dye, Sudan Black B (Qi et al. 2017). As it is slightly basic, Sudan Black B combines with acidic groups in lipids and acts as a mask or block for autofluorescence due to it's light-absorbing capacity (Qi et al. 2017). Although, Sudan Black B is also reported to be a fluorochrome, acting as a lipid dye emitting in the far-red emission spectrum (Sakr et al. 2023; Willows et al. 2021). Therefore caution was used when using far-red secondary fluorophore-conjugated antibodies, although I did not observe increased background staining when using Alexa 647 fluorophores alongside Sudan Black B. Other, more effective autofluorescence-attenuating agents that lack fluorescence in far red spectrum are available and treat issues such as lipofuscin specifically, such as Trueblack™ (also TrueVIEW™, MaxBlock™) (Sakr et al. 2023), but as Sudan Black B seemed adequate for the needs of the present study, other options were not explored.

A secondary challenge in whole mount immunocytochemistry was the thickness of the tissue, which further complicated discernment of specific versus non-specific signals, as faced with autofluorescence. Preserving the full depth of tissue with the use of clearing methods led to substantial amounts of antibody apparently being retained between adipocytes and neurons became more difficult to discern. Reducing the Z-plane of the tissue with Z-depth reduction largely solved this issue, as it reduced the distance for antibodies and wash buffers to diffuse. However, as the thickness of the tissue is reduced approximately from $>$2mm to circa 100 - 300 μm (variable around the span of tissue), inevitable modifications to structural architecture are made, which renders accurate measurements regarding spatial information, inaccurate. Therefore, valuable measurements as to neuron proximity to vasculature and adipocytes etc. have not been made on these premises, presenting a substantial limitation to the methodology. To rectify this, clearing methods in full depth adipose could have been complementarily conducted, as showcased in excellent examples by other researchers using refractive index correcting clearing techniques such as iDISCO (Cao et al. 2018) and CUBIC/HYBRiD (Wang et al. 2022) etc, but I did not optimise such full-depth clearing methods far enough for use.

Further to this, as the nerves were mainly imaged in a 2D format across the tissue,

with occasional examples of Z-stack-produced composite 3D images, maintenance of tissue thickness would allow for a 3D rendering of the whole depot, which other research groups have successfully achieved (Wang et al. 2022). The generation of a 3D reconstruction across the entire depot would better visually describe the innervation extents of the nerves, as they become more traceable.

3.4.1.0.2 PGP9.5 displayed poor selectivity for nerves

Surprisingly, PGP9.5 was not found to be a particularly useful tool for identifying nerves in the inguinal fat depot, unlike other studies where it was suggested to be superior at identifying fine neuronal projections (Willows et al. 2021). Both pan-neuronal antibodies β3-tubulin and PGP9.5 target a cytoplasmic protein ubiquitously expressed in nerves, which ruled out target localisation differences as explanation (i.e. cytoplasmic versus membrane-dwelling targets). However, only one antibody against PGP9.5 was trialled, which may have not been suitable for whole mount immunocytochemistry applications, or was used in insufficient concentrations for full nerve detection and may explain why the antibody was found inadequate. Despite this, β3-tubulin proved to be a sound marker for nerves, with clear examples produced of the innervation and morphology of nerves in the inguinal fat depot.

3.4.2 Nerves of the inguinal fat depot exhibit three main modes of signalling

Nerves were found innervating in three main modes, which fully aligns with literature and satisfies aim 2 of the chapter.

3.4.2.1 Sympathetic and non-sympathetic nerves innervate in bundles

One of the most compelling structures observed when imaging the inguinal fat depot was the large bundles of nerves that appeared to cluster and track coarsely around the entire depot. The bundles were seen tracking alone and alongside larger vasculature, apparently innervating as a cluster, which is parsimonious if the bundles and vasculature innervate from the same entry points. Researchers have previously described the regional anatomy of the inguinal fat depot and described entry points of main vein, artery and

nerve bundle innervation, which do appear to synchronise (Blaszkiewicz et al. 2019a). This may be an example of neurovascular congruence (Manousiouthakis et al. 2014).

The bundles were repeatedly seen innervated or tracked by medium sized vasculature, putative arterioles, which may present a form of vasa nervorum, an extrinsic nutrient artery to provide a vascular-borne supply of nutrients. The delivery of nutrients to peripheral nerves is important for nerve maintenance and function (Boissaud-Cooke et al. 2015), as absence or disruption of vasa nervorum is linked to pathology such as in diabetes (Beggs et al. 1992), and is therefore likely necessary for nerves travelling to peripheries over long distances to prevent loss of integrity or stress due to torsion and compression with movement (Boissaud-Cooke et al. 2015). This may be different for the bundles observed innervating the inguinal fat which are associated with medium sized vessels, but a feasible suggestion.

Nerve bundles appeared completely independent of the small webbing structures of IB4-positive vessels, with no clear interaction between them. Others have appeared to visualise small capillary-sized IB4-positive blood vessels associating longitudinally with the bundle, travelling with the nerves, likely serving as above (Willows et al 2021). However, these interactions were not recorded here, with medium sized vessels (likely arterioles) being those that associated with bundles. It is possible these interactions were missed due to either sampling, the plane of view did not capture the interaction, or there are discrepancies in measurement.

Bundles of nervous tissue have been previously observed innervating the inguinal fat depot and defined as 'lateral cutaneous rami', rising from intercostal nerves from (T12-L1) and "Lateral/anterior femoral nerves" from (L1 - L2) deriving from the lumbar plexus, which track through the depot toward the skin (Huesing et al. 2021) (See Chapter 1 Figure 1.8 for schematic representation). Initially, it was not obvious how these coarse, passive structures may influence vasculature or adipocytes from the perspective of tissue regulation, due to their limited interaction and apparent independence. However, Huesing and colleagues also found that individual sympathetic nerves branch away from the main trunk of the bundles to innervate the inguinal adipose parenchyma, serving as potential origin points for the induction of parenchymal innervation. This bundle-branching has been observed in mouse muscle, where a single neuron can be

observed extending and branching from the intramuscular nerve bundle (Wood et al. 2001). During experiments and optimisation steps, I found (rare) examples of sympathetic branching from nerve bundles, supporting this hypothesis. In an overview image taken of β3-tubulin staining over a large section of fat depot, there appeared to be a bundle branching into individual nerves in a coarse, multiplex manner, but it was not easy to determine whether this was a natural structure or an artefact from during dissection. It therefore remains unclear if these bundle-branching events represent true origin points of parenchymal innervation, or whether singular parenchymal innervations are derived from the sympathetic chain ganglia (ScG) in minor bundles that disseminate into the tissue, or nerves that branch away from innervating vasculature. While this phenomenon was not something actively sought after in data collection, as it was only observed twice during experiments and optimisation, further experiments designed to visualise these interactions are interesting and desirable.

Huesing et al. (2021) also describe a directional innervation pattern to the bundles, where they innervate laterally and longitudinally across the depot from proximal to the spine, outwards toward distal regions where inguinal adipose interfaces with dermal layers and beyond. I did not maintain the orientation of the inguinal tissue post-dissection and did not seek this information whilst imaging, however in one of the half-depot images taken, the bundles could clearly be seen traversing the tissue in a semi-laterally, anterior to posterior direction in a manner that aligns with the description of organisation above. Additionally, the bundles appeared organised and didn't appear to transect each other, appearing to travel in the same, or similar directions. Tissue handling, dissection, orientation and ZDR could all influence the appearance of these bundles, therefore further more intentional experiments following the nerve bundle innervation, orientation and direction would provide clarity to this innervation mode.

Bundles of nerves also positively stained for TH, equating to an approximate third of total nerves present in the few examples assessed, providing evidence of sympathetic identity within the heterogeneous population. My findings somewhat deviated from other reports of a 50% ratio of TH-positive to TH-negative 'non catecholaminergic' nerves in bundles (Zeng et al. 2015). Due to the lack of suitable examples found, and validation through the use of a sensory-specific antibody, conclusions cannot be drawn

as to the proportion of sympathetic identity of these bundles without further data. In fact others have found that there are mixed proportions of nervous identity between different bundles, with some predominantly sensory, with only a few sympathetic nerves within the bundle and others with a greater sympathetic proportion (Blaszkiewicz et al. 2019a). Therefore the deviation between findings here and those by Zeng et al. (2015) may be due to sampling error.

Mixed-identity bundles of spinal nerves are common and expected, as they trace from their respective ganglia, DRG and sympathetic chain ganglia, and mix together in spinal nerves via communicating rami (rami communicantes) and onward via ventral and dorsal rami, toward their destination organs (Huesing et al. 2021). This is more expected since thoroughly conducted research suggests that nerves innervating the inguinal fat depot dorsolumbar region are of thoracic intercostal descent, which are spinal nerves. These further branch from the ventral ramus to the tissue-innervating lateral cutaneous rami. The inguinal portion of the fat depot is further innervated by the lumbar plexus, which is another mixed spinal nerve cluster, which sympathetic post-ganglionic axons feed into and innervate in the form of anterior and lateral cutaneous femoral nerves (Huesing et al. 2021).

It is likely dependent on the destination of the bundles and which ramus they originate/derive from as to the overall subtype proportion observed. Overall, non-sympathetic, putative sensory, neurons were highest in abundance within the bundles compared to any other described modes of innervation.

3.4.2.2 Nervous innervation of vasculature

3.4.2.2.1 Nerves mainly innervate large and medium-sized vasculature

Medium (proposed arterioles and venules) and large-sized vasculature (proposed arteries and veins) were very frequently observed rich with direct nervous innervation.

These findings contribute to a collective body of data that emphasises the dense and close relationship between blood vessels and nerves both generally (Westcott et al. 2013) and within the inguinal fat depot (Cao et al. 2018). Therefore, innervation of medium and larger vessels was expected and compliant with literature.

General perivascular innervation of blood vessels, otherwise known as nervi vasorum, is well established and provides vasomotor control of vascular tone, critical for modifica-

tion of blood flow within the tissue (Westcott & Segal 2013). The innervation pattern of vessels varied between flanks of clustered nerves that tracked the length of the vessel, and fine web-like nervous innervation that appeared to wrap the surface of the vessel (appearing like a sympathetic plexus). The latter mode being critical to control of vascular tone through adjusting lumen size to facilitate incoming oxygen and nutrient supply during periods of fasting, postprandially, and during stressors such as exercise (Baak 2008; Thomas et al. 2004).

There appeared to be differences in appearance of large vasculature, with the largest of vessels displaying greater autofluorescence and a longitudinally striped surface. These are likely to be veins due to their size, however, vessel identity was not selectively stained for to differentiate nervous innervation across veins and arteries. This may prove useful for further lines of investigation, particularly concerning sympathetic/nervous influence on vasculature in normal versus pathological states. Markers such as EphB4 and ephrin-B2 are commonly associated with veins and arteries, respectively, and may be used to distinguish subtypes in future work (Wolf et al. 2019).

Similarly, the mid-sized vessels, considered by size to be arterioles and venules, very frequently displayed neuronal innervation, also potentially allowing for adjustments to vascular tone, which is particularly important to modulate incoming pressure into capillary beds. However innervation was not consistent, with some examples of medium vessels displaying little to no innervation. Venules, which lack smooth muscle, are reportedly not innervated by sympathetic efferents and therefore may account for the discrepancies observed in innervation within medium vasculature (Juan et al. 2019; Thomas 2011). Therefore the medium sized vessels captured with sympathetic innervation are unlikely to be venules. Again, without further differentiation between vessel identities, it is not possible to affirm literature as to whether there is a difference in innervation across arterioles and venules.

As found by similar studies (Cao et al. 2018), the fat depot was dense in highly aborised small calibre vessels, deemed capillaries, across the entire span and depth of tissue. Repeatedly, nerves are found generally absent from capillaries, as previously noted by others (Thomas 2011), due to their function as nutrient/oxygen exchange vessels requiring maximal surface area, thin permeable walls, and as consequence, a lack of contractile smooth muscle. Yet very occasionally, capillaries appeared to be innervated by

neurons. While innervation of microvessels does occasionally occur, it is compliant with literature that these vessels significantly lack innervation compared to larger vessels as above (Thomas 2011). Its possible that these interactions may be formed during periods of neuroplasticity as parsimonious route of extension, using pre-existing vasculature as structural scaffolding, as they also provide growth cues via guidance molecules (Bovetti et al. 2007). Especially since finer individual neurites and capillaries are considered plastic and can undergo extensive remodelling in response to cold stress challenge (Cao et al. 2018). Emphasising this relationship, medical engineering of capillary-like scaffolding to support nerve grafts for guiding axonal growth and development are of interest, as it is understood that vascularisation has a positive influence on nerve regeneration (Saffari et al. 2020; Matsushita et al. 2018). Nerve/axon regeneration and growth was found positively correlated to number of capillaries, and providing nutrients and growth factors, such as VEGF, increased axonal regrowth in a rat sciatic nerve injury model providing scope that nerve-capillary interactions may be both structural and functional (Muangsanit et al. 2018). However, most likely, these innervations may be residual from where the nerve was previously innervating an arteriole and has yet to branch away, as stated by Huang and colleagues (2021), perivascular nerves innervating inguinal fat mostly terminated their association with arterioles prior to inception of the capillary network.

In an alternative explanation, junctions between arterioles and capillaries were thought to have rings of smooth muscle called pre-capillary sphincters, whereby autonomic innervation regulated flow within capillary bed, which offered an explanation of why examples of capillary-nerve interactions were occasionally found. However, precapillary sphincters have been reported as non-universal forms of vascular control across tissues, with a comparative review suggesting their presence and function not extrapolating beyond mesenteric and possibly cerebral vasculature, with authors indicating the contention rising from methodology used to visualise these structures with enough accuracy for positive identification (Sakai et al. 2013). As the capillary innervation, when observed here, were on vessels of the upper maximum of measured widths, they are likely 1st order capillaries or pre-capillary arterioles, which were mistakenly measured/categorised.

Lymph vessel presence in adipose tissue was expected owing to their role: absorption and transport of dietary lipids both to and from the adipose depot and trafficking of

immune cells (Harvey 2008). When found, lymph vessels did not appear to have nervous innervation, although I did not capture clear examples of these structures with enough regularity to explore this fully. While lymph is relatively distinct in autofluorescence pattern, particularly where two fluorophores are used, the reliance on autofluorescence hindered frequent clear capture of the vessels, which are considered to be commonly observed in similar studies (Bachmann et al. 2019). Supporting this, when CD31 (Pecam-1) was trialled as a vascular marker during optimisation, lymph was much easier to capture due to improved endothelial staining (see Appendix Figure 7.1).

Contrary to my findings, literature also suggests lymph vessels are innervated by both sensory nerves (Huang et al. 2021) and sympathetic nerves (Bachmann et al. 2019), particularly in the LN region of the inguinal fat depot. As lymph vessels are transporters of interstitial fluid and immune cells, they have important roles in ensuring adequate tissue drainage and immune cell flux to promote homeostasis (Hampton and Chtanova 2019). Excess pro-inflammatory immune cells are implicated in metabolism dysregulation, which is a hallmark of obesity, so proper control of lymph is important to metabolic maintenance (Hildebrandt et al. 2023). As lymph vessels, particularly collecting vessels, contain smooth muscle and can contract to maintain fluid flow, nervous control of the vessels by induced smooth muscle contractility presents an important prospective player. Evidence of norepinephrine-mediated contractility of lymph has previously been shown in skin-draining lymph vessels of mice, although in a location-dependent manner (Bachmann et al. 2019). It is therefore likely, based on evidence of lymph functional role and from others immunocytochemistry data, that lymph is innervated by nerves and may not have been adequately or accurately captured in this study. As the aim of the project was not especially focused on capturing innervation of lymph vessels in the inguinal fat depot, a selective marker such as Lyve-1 was not used to specifically and clearly label these vessel types. Future work could incorporate these, as others have done, for a more thorough investigation into innervation pattern and neuronal association of lymphatic vasculature.

3.4.2.2.2 Sympathetic innervation outweighed non-sympathetic innervation of vasculature

Meeting aim 4 of the chapter, data here suggests that innervation of medium and larger blood vessels is dominantly sympathetic, with a remaining population of 'other' non-sympathetic nerves. The reported lack of parasympathetic innervation in inguinal fat (Bartness et al. 2014; Giordano et al. 2006) leans toward assumptions that any remaining non-TH-positive nerves are sensory, although sensory-specific markers applied here would aid conclusions to these reports (e.g. CGRP).

Sympathetic nerves innervating vasculature regulate the tone of vessels via the release of norepinephrine, NPY and ATP to nearby vessels, which binds to post-junctional α-adrenoceptors, P2 receptors and Y receptors. The resulting increase in $[Ca^{2+}]i$ induces contraction of vascular smooth muscle (Thomas 2011). There is a degree of vascular tone mediated by tonic activity of vascular-innervating sympathetic nerves that maintains positive pressure throughout the tissue (Thomas 2011), which can be counteracted by the influence of sensory nerves. Therefore, a primary function of nervous innervation of vasculature is control of blood pressure and thereby flow, through the tissue.

Arteries are critical to pressure-dependent delivery of oxygenated and nutrient-rich blood into the tissue. The pressure of delivery must be tightly regulated to avoid damage to capillaries, which is governed by the sympathetic and often sensory nerves innervating their surface, allowing for fine tune of arterial tone. Without sympathetic innervation of vasculature, the arteries and arterioles would lose tone and the blood supply would reduce, slowing down the introduction of oxygen, nutrients, hormones and inversely, the removal of deoxygenated, nutrient-depleted blood via veins. Similarly, vein capacitance is governed by sympathetic tone, perhaps to a lesser degree than arteries (as they possess less smooth muscle) (Sheng et al. 2018). Their capacity for considerable distention allows veins to accommodate large volumes of blood, which constriction via sympathetic nerves serves to mobilise, directly influencing tissue blood volume (Thomas 2011).

Another auxiliary role of nervous innervation of vasculature is induced permeability. Sympathetic activation of α-ARs on blood vessels is also reportedly important for increasing vascular permeability, enabling effective delivery or nutrients and hormones and uptake of FFAs in the blood (Bartness et al. 2014). Local accumulation of FFAs released

from adipocytes during lipolysis can negatively feedback to reduce lipolysis, by reducing the activity of cAMP (Li et al. 2022). The effective uptake and turnover of FFAs can therefore promote lipolysis and healthy function of the adipose tissue (Bartness et al. 2014).

Due to the importance and influence of sympathetic nerves on vasculature, it is not surprising that I found these subtypes to be more abundantly innervating medium and large vasculature. Others have found the innervation of vasculature in iWAT to be dominantly sympathetic (Huesing et al. 2021; Willows et al. 2021). The proportion of sympathetic innervation is likely dependent on location/vascular bed within the body, with some arteries dually innervated by sympathetic and sensory or parasympathetic neurons to mediate vasodilation. As previously mentioned, WAT is accepted to lack parasympathetic innervation (Bartness et al. 2014), leaving sensory-mediated vasodilation via CGRP or sympathetic mechanisms that confer vasodilatory effects. Sympathetic-derived norepinephrine can non-discriminantly activate all postjunctional adrenergic receptors present, to differing extents. Therefore, the outcomes of adrenergic stimulation ultimately depend on subtypes present, and their respective G-protein coupling. Adrenergic receptor subtypes commonly found on vessels and responsible for vasoconstriction are G_q-linked α1-ARs and G_i-linked α2-ARs. α1-ARs activate the inositol pathway to increase intracellular Ca^{2+} via liberation from intracellular stores to induce contraction, while α2-ARs decrease intracellular cAMP which ultimately increases $[Ca^{2+}]i$, promoting contraction. In contrast, other adrenergic subtypes β-ARs in vascular contexts promote vasodilation via intracellular G_s-linked mechanics, increasing levels of cAMP (Sheng et al. 2018). Therefore, the fewer non-sympathetic (sensory) nerve abundance in comparison to sympathetic innervation may indicate a mixed population of adrenergic receptors on the surface of vessels innervating the inguinal fat depot.

While subtypes of vasculature were not identified, from general observations it was clear that populations of the large vascular spectrum were differentially innervated, with the largest appearing to have more obviously dominant sympathetic innervation. Veins may be more likely to have singular innervation by sympathetic nerves, as fine modulation of tone is not as critical for their function like arterial vasculature.

There is a paucity of information regarding the comparative proportion of nerve innervation identity between vascular subtypes in adipose tissue. Therefore, further lines of

investigation as to nervous subtype dominance between venous and arterial vasculature and whether veins do experience less sensory input, is recommended.

In general, findings here demonstrating that blood vessels permeate the inguinal fat depot is valuable to recapitulate the work of others and emphasise their critical role in the delivery and flux of metabolites, O_2 and CO_2 transaction and glucose. Also, critical metabolic regulatory hormones such as insulin and leptin and FFAs all depend on vasculature. The control of delivery is therefore important in regulating lipolysis and lipogenesis, as too much or little input will influence adipocyte responses. Nervous innervation of these structures, particularly sympathetic, represents a key modulator in such transactions. Dysregulation of vasculature is therefore a critical health concern. During obesity where adipose can experience vasculopathy, incoming signals will be limited due to fewer blood vessels, causing potential hypoxia and inflammation (Trayhurn 2013), as well as local lipotoxic effects due to unregulated turnover of FFAs in basal and stimulated lipolysis not being removed by blood (Chait et al. 2020). Local disruptions to lipid storage can then consequently result in spillover to other organs, ultimately perpetuating dysregulation.
In future work, it would be interesting to explore the change in both vascular abundance, as well as vascular nervous innervation in response to diet-induced obesity and diabetes. Both pathologies incur remodelling of WAT architecture, either via expansion which angiogenesis may not be able to match, as well as vasculopathy and neuropathy.

3.4.2.3 Innervation of the parenchyma and adipocytes

A key aim of this PhD project was to ascertain, via qualitative assessment, the extent in which nerves innervated the parenchyma of inguinal fat depot. Generally, terminal synapses are considered elusive structures in the context of the inguinal adipose depot, with little evidence to suggest their appearance up until recently. While not incorporated into methodological design, or directly measured using synapse-specific markers, clear evidence of distinct terminal bouton synapses was not observed. Instead, nerves innervating independently of vasculature appeared to continuously swathe around the tissue, without defined or obvious blunt terminals, instead occasionally wrapping around adipocytes. While not particularly obvious, the neuro-adipose nexus junctions may present as un-

orthodox terminal structures, as the nerves have completed travel through the adipose parenchyma. Nerves in the inguinal fat depot have previously been suggested to present with terminal bouton structures, though the data was difficult to interpret as the authors did not use a synaptic marker (Zeng et al. 2015). Other research has alternatively proposed axonal varicosities as the present and functional mode of synapse found in the inguinal fat depot (Huesing et al. 2021).

Axonal varicosities in this manner would be parsimonious and efficient to cover larger areas of adipocyte parenchyma. If nerves within the tissue were able to release neurotransmitters, such as norepinephrine, from synapses along the entire axon, it would allow for increased diffuse control without increasing nerve number. Such an adaptation would align with the observed frequencies of parenchymal innervation of nerves here, where unlike other studies, I found there to be a more casual association between nerves and adipocytes, with only occasional direct interactions.

During experiments, I regularly observed nodule-like swellings on nerves, often multiple along each axon, which I initially hypothesised may represent axonal varicosities. My initial theories as to the identity of these structures seemed to be validated upon literature review. Others had found similar nerve morphology when staining sympathetic nerves with TH, whereupon analogous nodule-like structures akin to those described here appeared to colocalise with synaptic marker synapsin I (SYN1), indicating their possible synaptic identity (Bachmann et al. 2019). Yet owing to the size of these structures, fairly large in width at around 6 μm, and as axonal synapses are thought to be smaller at around 1 - 2 μm (Willows et al. 2023), their identity remained unclear.

Recent research from the Townsend group clarifies this suggestion, as they indeed have visualised smaller and more frequently punctuating bulb-like axonal varicosities using presynaptic marker SYN1 on along the axons of some (but not all) TH-positive nerves, which also contained synaptic vesicles labelled with synaptic vesicle protein 2 (Sv2). These structures were most densely and clearly expressed in the NAN structures. While the authors propose the NAN structures represent nerve terminals onto adipocytes, their data supports the hypothesised mode of more broad nervous regulation of adipose. However, these bulb-like structures were smaller in appearance compared to the nodules described, only around 1 μm wide. The authors did visualise the larger nodules akin to those I observed, which instead stained positively for Schwann cell marker SOX10,

indicating they may instead be embedded Schwann cells providing potential support for the resident nerves. The finer more regular bead-like swellings I observed and reported in latter sections of this chapter, particularly when using TH to observe the NAN structures, showcased the same morphology that the authors positively identified as axonal varicosities. Therefore, such evidence offers a potential explanation as to both nodule and bulb-like structure identities.

However, while it is feasible that axonal varicosities are present, perhaps in the small bulb-like structures suggested here, which form unorthodox terminals in the NAN structures, data here remains inconclusive. The bulb structures may be artefacts of aberrant/nonuniform antibody staining and not be indicative of synapse morphology and blunt terminal bouton structures may indeed be present within the tissue when appropriately marked. Future experiments should explore the identity of these structures using markers for synapses such as synaptophysin and synaptic vesicles with SV2 alongside the general axonal markers like TH and β3-tubulin.

There are conflicting reports as to the frequency of neuro-adipose associations found in iWAT. Using optical projection tomography techniques to render a 3D image of the intact inguinal fat depot and 2-photon microscopy to visualise sympathetic nerves, some claim a 8% direct association between sympathetic nerve 'bouton' structures and adipocytes (Zeng et al. 2015). Using the same strategies, others found a "sparse" association between TH-positive nerve varicosities and white adipocytes in regions of the inguinal depot (Huesing et al. 2021). While on the other hand, others applying iDISCO clearing techniques with electron and light-sheet microscopy strategies claim up to 91.3% association between nerves and adipocytes (Jiang et al. 2017). In similar HYBRiD techniques, in 3D reconstructions and projections, others claim a "dense parenchymal innervation" of sympathetic nerve fibres with close associations between nerves and adipocytes (although markers for vasculature and adipocytes were not used) (Chi et al. 2018). Overall, I did not quantify the associations between adipocytes and nerves, nor did I produce a suitable 3D reconstruction as facilitation to do so. While evidence of independent parenchymal innervation was found, these interactions were not as common as some researchers have claimed. Abundance of singular, independent nerve innervation in the present study was determined to be fairly frequent, but not as abun-

dant and dense as others suggest (Chi et al. 2018), nowhere near the number to satisfy a 91% neuron to adipocyte relationship (Jiang et al. 2017), using the methodology and antibodies stated here. Contrary to these publications that advocate a direct terminal nerve:adipocyte interaction, I found neurons remained relatively passive through the sample, with only occasional direct adipocyte iterations, in the form of NAN structures. However, what Jiang and colleagues (2017) consider an "interaction" may not be by others. Especially depending on the forms of synapse present. Use of markers for adipocytes and vasculature alongside neuronal markers would also aid context of interactions to this end. Therefore, clarification and standardisation as to what researchers constitute an adipocyte-neuron interaction is required, which can then be translated across studies.

As above, during sampling I occasionally found evidence of direct nerve-adipocyte associations away from vasculature in the NAN structures. Out of 13 total experiments presented as evidence within the chapter, I found examples of these structures across only 5 experiments, with a total of 11 examples found. This presents an important finding, as nerves clearly have capacity to interact directly with adipocytes, but not to the point where every adipocyte is in direct individual association with nerves. It is unclear how frequently these structures are found by other researchers, as this is not explicitly described, it is possible they are also only occasional. As previously mentioned, the deployment of neurotransmitter may be achieved via axonal varicosities, eliminating the need for millions of individual, costly, direct neuro-adipose interactions to regulate metabolism. This infers that neurons are theoretically able to communicate directly with adipocytes via axonal neurotransmitter release, rather than indirectly through influencing vasculature aperture, for example.

The reported infrequency of these interactions observed here may be an artifact of the ZDR method applied, as alluded to by Willows et al (2021), who thoroughly explore the change in structural measurements post-ZDR in the inguinal fat depot. One element of note being adipocyte morphology after ZDR becomes somewhat cuboidal, as the cells expand and fill the extracellular spaces to allow for the physical alteration. The authors instead employed paraffin embedded whole mount techniques to preserve tissue thickness and better capture the neuro-adipose nexus in 3D formats. Loss of adipocyte structure is an issue I certainly encountered using the ZDR approach when attempting to stain with BODIPY, where superficial layers of adipocytes had completely lost their

discrete morphology, potentially lysed in the process. In this case, the loss of space around adipocytes may limit what I am able to interpret as nerve interactions.

Due to the aforementioned artifacts associated with ZDR as described above, it is not possible for definitive conclusions to be drawn on proximity and potential terminal synapsing of neurons on the adipocytes. In order to quash concerns regarding adipocyte visualisation and restricted planes of innervation, other non-distorting whole-mount techniques ought to be considered in future work, to validate casual observations here. Maintaining the entire 3D depth of tissue has drawbacks as already demonstrated and discussed within this chapter, however it does allow for more accurate neuro-adipocyte relationships to be assessed.

When gathering information on tissue depth using Z-stack projections within the tissue, it appeared as though the fine parenchymally-innervating nerves were consistently present in a superficial depth of tissue, while vasculature was spread throughout a fuller dorsal - ventral depth. Nerve bundles and nerves associated with vasculature appeared to innervate deeper. If such interactions are limited to specific planes within the tissue, it certainly limits the capacity for neurotransmitters to reach target receptors on adipocytes deeper within the tissue. Using heat map depth coding, others found that nerves did innervate to greater depths than found here, seemingly capable of spanning the full dorsal - ventral depth. However, it is unclear if these nerves were in association with vasculature, although IB4-positive vessels did seem to correlate in comparative panels (Willows et al. 2021). Similarly, in a whole mount preparation of the inguinal fat depot processed to maintain tissue thickness, sympathetic nerves could be seen penetrating from dorsal to ventral extents of the adipose, yet a vascular marker was not incorporated so it is unclear whether these were owing to associations with vasculature (Chi et al. 2018).
As the post-ganglionic projections that innervate the inguinal adipose tissue also extend to innervate dermal layers, its possible that the nerves visualised are from dorsal facing surfaces where nerves interface with dermis. These restricted planes may therefore represent origin points of innervation of iWAT from nerves innervating the dermis. The origins of fine, parenchymal innervation are still unclear, as discussed previously, nerves have shown branching from bundles, which also serves as a potential alternate inner-

vation origin. While not directly related and non-translatable, researchers found that β3-tubulin positive nerves in the skin of the mouse hind paw were mostly superficial in whole mount preparations, with bundles and perivascular nerves penetrating deeper (Latremoliere et al. 2018).

A likely suggestion is the apparent restricted plane of innervation may be an artefact of ZDR, where outer layers of adipocytes may become damaged which could falsely suggest nerves innervate a superficial depth. It is unknown whether the nature of ZDR in tissue handling is responsible for these findings, however it seems unlikely that compressing the tissue would force the neurons through the parenchyma, to exist in a very limited plane, consistent over multiple Z-stack experiments. If this were the case, significant shearing of fibres and structures within the tissue would be visible, however there is no evidence of this. Therefore, regardless of tissue ZDR, it appears fine nerves independent of vasculature are most abundantly captured in a superficial plane of tissue.

I didn't gather enough data or collect with intentionality to fully explore these interactions, as these were discoveries made post- data collection. The Z-stacks produced were primarily conducted as trials and experimentation with technique and therefore unintentionally differed in quality. With differing numbers of optical 'slices', as well as differing optical section frequency between those slices, the experiments may have not captured the same extent of resolution, full or sparse. Therefore, it is likely that these are not accurate representations of the true innervating capacity of the nerves and remains unresolved. In any case, further work with emphasis on experimental design to explore these findings is required, using a whole mount method that retains full tissue depth, as discussed above, and Z-stack projections with increased slices for increased resolution/visualisation.

3.4.2.3.1 Sympathetic innervation of adipocytes and parenchyma

A key aspect of aim 4 of the chapter was to ascertain the extent that norepinephrine-delivering sympathetic nerves interacted with the parenchyma and adipocytes. I found no definite examples of nerves proposed to be sensory innervating the parenchyma, with all images captured showing TH positivity. Based on findings within the present study, sensory nerves appear restricted to bundles and vasculature, rendering any possible antidromic regulation of lipolysis unlikely, unless via vasculature-mediated effects.

Some have found similar patterns of innervation to those observed here, with parenchymal innervation being "almost exclusively sympathetic" (Willows et al. 2021; Giordano et al. 2006). While conversely, others have found more sensory projections with sympathetic nerves more tightly associated with vasculature, sensory nerves were seen branching into parenchyma, particularly over the lymph node (Huang et al. 2021). Incidentally, I tended to avoid the lymph node due to greater incidence of autofluorescence and noise, making it more challenging to obtain quality images. Therefore, as sampling location was not a methodological parameter kept consistent here, it's possible that regionalisation of the fat depot and observations within discrete regions may alter perceived subtype abundance.

In another publication, clear parenchymal innervations of CGRP-stained sensory nerves are seen in inguinal WAT, but there were no markers for vasculature present, making it difficult to interpret parenchymal from perivascular interactions (Frei et al. 2022). Supportively, another study using anterograde fluorescent labelling techniques in the DRG, in combination with HYBRiD clearing techniques, capture light-sheet microscopy images of sensory nerves innervating the parenchyma and vasculature (Wang et al. 2022). These data therefore suggest that sensory nerves may not be adequately captured in the present and other studies. The use of a sensory-specific marker, such as CGRP, is therefore crucial in future work to fully ascertain the proportion of sensory and sympathetic parenchymal innervation, which is critical to understanding the capacity of nerves to influence the adipocytes.

This is particularly poignant as recent evidence suggests TH antibodies can also stain some sensory neurons, with the aforementioned anterograde-labelled sensory nerves colocalising with TH- labelled nerves, thus potentially falsely inflating the proportion of sympathetic innervation in other studies such as here (Wang et al. 2022). Compounding the unreliability of TH as a sympathetic marker, in a follow-up study, contradicting their initial findings, CGRP-positive neurons have now been identified innervating in NAN structures that previously only TH-positive 'sympathetic' neurons were proposed to demonstrate (Willows et al. 2023). The NAN innervations did still appear to consist mostly of sympathetic neurons in the updated study, but further work is required to develop understandings of sensory parenchymal contribution further with suitable tools. This makes conclusions as to overall proportions of nerve subtypes innervating vascu-

lature, but most notably parenchyma, incredibly challenging in the present study, due to the lack of a sensory-specific marker to improve discern/discrimination. As these issues are based on reports from others, concrete evidence by probing TH antibodies applied here, alongside a sensory-specific marker such as CGRP and trialling alternative sympathetic-specific antibodies is recommended.

3.4.3 Overall limitations and future recommendations

As discussed throughout the thread of the present discussion, the methodological approach taken to answer key aims was fruitful, but did present drawbacks to interpretation. Firstly the method of sampling did not allow for a systematic traceable innervation breakdown by area or region. There was no consistent approach to images being taken, I tracked around the sample until structures that were clear, with limited distortion and noise, were found. This could translate to missing examples of nerve-adipocyte interactions, as the sampling method may have been insufficient to find and capture structures, despite being present. There was no recording of where in the fat depot images were taken, and the fat depot orientation was lost during sample preparation, so dorsal dermis-facing and ventral abdomen-facing sides could not be distinguished. There are reports that clearly demonstrate regionalisation to vascularisation & nervous innervation, as well as adipocyte subtype between central and peripheral areas (particularly concerning sympathetic innervation density [Huesing et al. 2021]), also between subdivisions of the inguinal anatomy; dorsolumbar and inguinal regions (Chi et al. 2018; Huesing et al. 2021; Barreau et al. 2016). Therefore, descriptive information was lost to this end.

Secondly, due to morphology of adipocytes becoming altered post- ZDR processing of the tissue, interactions between nerves and adipocytes were challenging to capture and not possible to measure. Measurements of proximity of any kind were avoided due to the nature of ZDR, which would have been useful to describe vascular, adipose and nerve interactions. As already stated, whole mount techniques that maintain the depth of tissue, that are optimised to reduce non-selective antibody accumulation/noise, alongside a methodology that allows for maintenance of post-excision orientation & traceability of image locations, are favourable steps for future work.

As the whole mount method prevented quantitative measures of proximity and other parameters, I wanted to provide a semi-quantitative facet to compliment images produced

to aid insight. However, the method of estimating colocalisation was performed using samples that best suited measurement and were often in short supply. Further, owing in part to the lack of suitable images, the assessment performed was done so in a simplified format, using selections of wavelengths that best represented the channels and in doing so there may have been data missed or overlapped to slightly inflate/deflate proportions. Additionally, it also doesn't account for background non-specific staining, meaning such staining can contribute to perceived area of 'neuron' presence. Autofluorescent structures were therefore problematic, although the images were cropped to reduce the amount of background to a minimum. Therefore, while the basic assessment of nerve identity by colour channel over total area was helpful to give an overall impression of innervation, there are more sophisticated and statistically-founded measures that future experiments could be designed to accommodate.

Lastly, during experimentation I observed TH-only stained nerves where β3-tubulin was also conjunctionally used. This aberrant β3-tubulin expression pattern was puzzling, as nerves are suggested to ubiquitously express β3-tubulin, hence its widespread use as a pan-neuronal marker (Latremoliere et al. 2018). During literature consultation, I noticed that others had inadvertently encountered this same staining deficit when using the two antibodies conjunctionally, not all TH-positive nerves dually staining with β3-tubulin (Willows et al. 2021). However, these staining patterns were not observed in similar studies using both β3-tubulin and TH antibodies to identify inguinal nervous innervation (Zeng et al. 2015). Therefore, as there is an apparent discrepancy between publications using antibodies against the same targets, it may be an issue with the antibodies used here. To elaborate, it may be poor β3-tubulin antibody staining, where the nerves do stain for β3-tubulin, but weakly. This may either due to a poorly designed antibody which fails to label all targets effectively, an antibody used that was not best suited to a whole mount application, or the antibody may have degraded slightly over time (or during preparation), which failed to stain for all neurons. It may also be occlusion by the presence of the other antibody, which is unlikely as they did demonstrate colocalisation, indicating both antibodies can bind to their respective cytosolic targets concurrently. Another explanation is it may be the plane of view where the image was taken, with the red wavelength being more prominent and diminishing the appearance of green wavelengths. This apparent aberrant staining of β3-tubulin may also explain why I

observed no β3-tubulin only (i.e. sensory) nerves innervating the parenchyma, and may contribute to why examples of the neuro-adipose nexus structures were found more reliably and with increased frequency when using anti-TH antibodies, perpetuating the perception of TH-dominant parenchymal innervation. Use of an alternative pan-neuronal marker such as antibodies targeting neurofilament, alongside TH and/or β3-tubulin, would delineate where the staining discrepancy lies, either antibody or nerve.

3.4.3.1 Conclusive remarks

Using a whole mount immunocytochemistry approach, I have successfully demonstrated ample evidence of general and sympathetic-specific nervous innervation of the inguinal fat depot in various forms, from vasculature and in bundles, to fine parenchymal innervation with direct adipocyte interactions (Figure 3.20). These findings provide scope for nerve stimulation experiments, as adipocytes clearly have access to sympathetic nerves, thereby a source of norepinephrine.

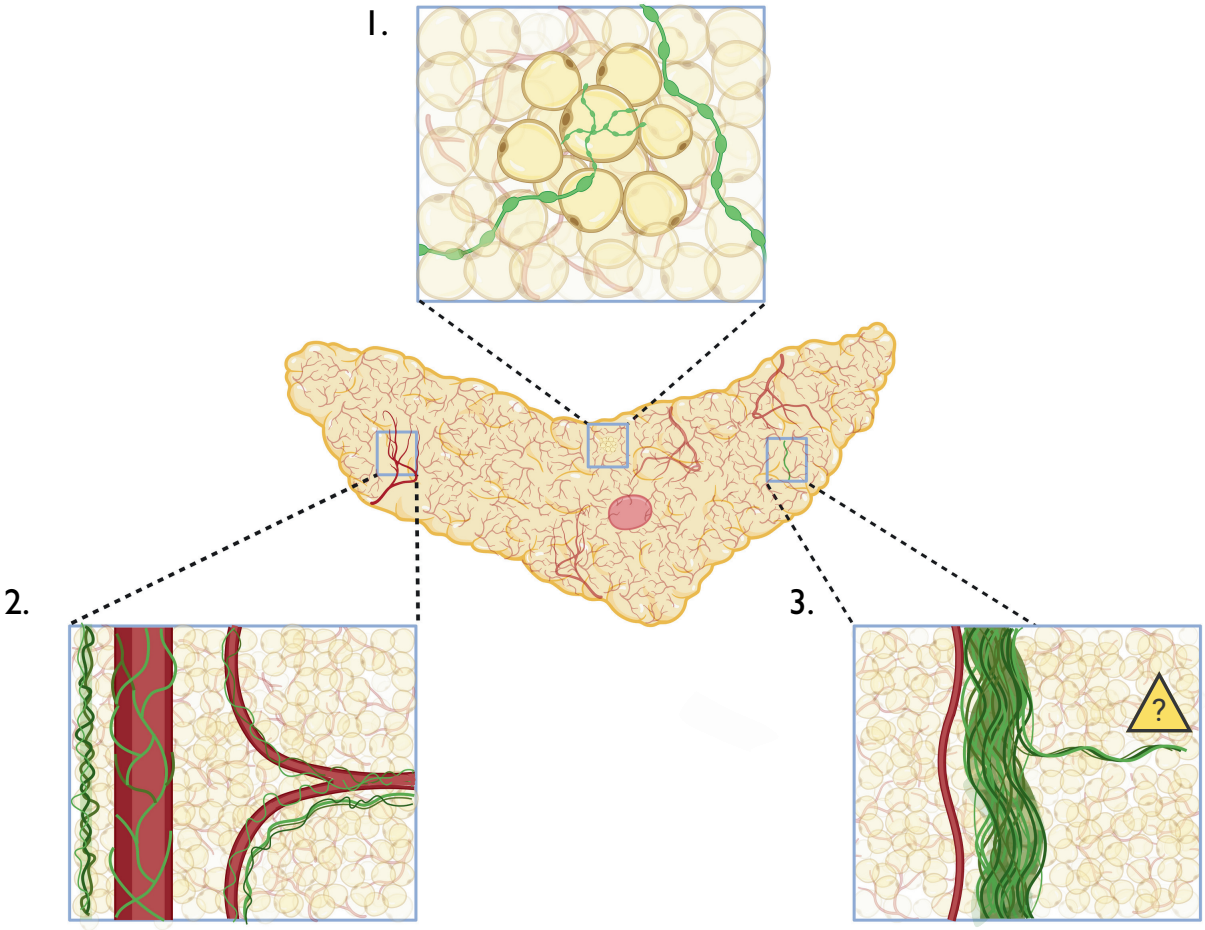

Figure 3.20: Summary of innervation modes of the inguinal fat depot. A diagram illustrating the rich vascularisation and various nervous innervation modes observed in the inguinal fat depot in this PhD project. The middle inguinal fat depot illustrates dense vascularisation with microvessels and numerous branches of large and medium vasculature. **Mode 1.** Parenchymal and adipocyte innervation from sympathetic nerves, **Mode 2.** intensive sympathetic and putative sensory innervation of medium and large vasculature, with the latter often observed tracking together with nerve bundles. **Mode 3.** Large nerve bundles of mixed identity that track through the tissue coarsely, which appear to receive some vascularisation from medium-sized vessels and occasionally branch out from the bundle into finer innervations. The yellow symbol indicates further evidence is required.

Chapter 4

Investigating lipolysis via neurogenic activation *ex vivo*

4.1 Introduction

It is now well established that sympathetic nerves innervating adipose tissue are responsible for metabolic regulation (Bartness et al. 2007). The scientific investigation into neuronally-driven lipolysis began decades ago, with pioneering electrical field stimulation (EFS) experiments, finding increases in FFAs released post- adipose tissue stimulation (Correll 1963). Cementing the neuronal role in lipolysis, researchers found EFS-stimulated sympathetic responses were inhibited by the addition of a β-AR antagonist (Weiss et al. 1965). Activation of nerves via EFS can be a useful tool to study neurogenic effects, however, EFS has previously been found to directly stimulate lipolysis in adipocytes, which limits the use as a tool to measure neurogenic activation of lipolysis (Hamida et al. 2011).

Additionally, most literature investigating lipolysis does so using *in vitro* cultures of cell lines or isolated primary cells. As corollary, such research often has limited physiological validity due to the absence of surrounding stromal vascular components, which invariably influence lipolysis. Harnessing an *ex vivo* model allows for a physiological approach to stimulating lipolysis, with the inclusion of all cell types. Evidence from Chapter 3 clearly indicates the presence of sympathetic and non-sympathetic nerves in the inguinal fat pad, with evidence gained of sympathetic nerves innervating the parenchyma and adipocytes, offering scope for neurogenic activation. Therefore, alternative ap-

proaches of neurogenic activation in conjunction with an *ex vivo* setting offers a useful tool for a more complete and physiologically representative investigation of lipolysis, inclusive of all cell types and endogenous neurotransmitters. These can include sensory neuropeptides, SP and CGRP and sympathetic neurotransmitters typically involved in regulating lipolysis, namely norepinephrine, but also NPY and ATP.

Research by Fredholm found that sympathetic stimulation of white adipose tissue caused release of "adenosine-like material" and inhibition with an α-AR antagonist prevented this release, thus providing a purinergic facet to adipose tissue (Fredholm 1976). ATP is a proposed co-transmitter with norepinephrine and acts as neuromodulatory potentiator in other systems, although there is limited evidence demonstrating this role in inguinal adipose. As already established in Chapter 1, there is a lack of clarity on P2R roles in lipolysis regulation, particularly in contexts of purinergic signalling in neurogenically-driven lipolysis in a more physiological model.

Therefore, development of an *ex vivo* model to study neurogenic activation of white adipose tissue to interrogate the constituent parts in lipolysis, including the role of purinergic signalling, provides value to the research community.

4.2 Aims

1. Establish an *ex vivo* model to stimulate lipolysis with the use of sympathomimetics, and challenge both stimulated and basal lipolysis with sympatholytics.

2. To generate a neurogenic means of activating lipolysis within the *ex vivo* model.

3. To characterise and investigate what neurotransmitters and neuropeptides exist to regulate WAT lipolysis in the context of the model.

4. Investigate the role of P2 purinergic signalling in basal & stimulated lipolysis, as well as nerve output, within the model.

4.3 Results

4.3.1 Mouse inguinal adipose tissue is capable of basal and induced stimulated lipolysis *ex vivo*

In pursuit of investigating the physiology of lipolysis, it was necessary to establish a model in which pharmacological challenge could be easily and reliably applied, then subsequent effects appropriately measured. Other research groups have already established *ex vivo* models which allow for glycerol and/or free fatty acids (FFA) released into media from sections of WAT to be measured as an index of lipolysis (Bridge-Comer et al. 2023; Roy et al. 2022), therefore I adopted an *ex vivo* approach. I chose to limit the measuring variable to glycerol, due to literature emphasising that FFA is a less reliable indicator due to re-uptake, unless measured as a ratio of glycerol:FFA. However, as stated in Chapter 1, glycerol is stable and less readily re-uptaken by adipocytes (owing to WAT expressing low levels of glycerol kinase) (Bridge-Comer et al. 2023). The references to glycerol release values throughout this chapter refer to glycerol corrected to wet tissue weight (μM/mg) in 150 μL total volume of DMEM produced over 3 hours, unless otherwise stated. In the case of isolated adipocyte experiments, values represent total glycerol concentration of response to drug in μM minus basal glycerol values, in 100 μL final volume DMEM produced over 3 hours.

4.3.1.1 Basal lipolysis occurs and is capable of stimulation via sympathomimetics

Initially, in agreement with literature, it was clear that adipose tissue maintained the ability, post-dissection, to undergo basal lipolysis (Figure 4.1 A & B). Explants of adipose released 8.45 $\pm$ 1.05 μM glycerol (N=14) into the supernatant, representing the average basal production of glycerol in a 3 hour period. However the interquartile range indicates basal glycerol values mostly fall within 6-10 μM range, with some tail-end extremes at 4 and 16 μM (N=14; Figure 4.1 B).

Secondly, the tissue retained this basal lipolytic capacity for periods of 4 hours when challenged (and likely beyond, MacDonald et al. 2017) (Figure 4.1 A). Over time, these

basal values remained stable, with a significant increase occurring from 1 to 2 hours (N=3, 2.78 $\pm$ 0.28 μM versus 5.84 $\pm$ 0.44 μM, P<0.01), then no significant change from 2 to 4 hours (N=3, 5.48 μm $\pm$ 0.76 μM versus 5.39 μm $\pm$ 0.9 μM, P>0.05) and appeared to plateau. Overall, cumulative glycerol released by groups after 1 hour, versus those at 4 hours, increased by 2.61 μM.

To both recapitulate literature and verify whether *ex vivo* tissue was also capable of responding to pro-lipolytic signalling cues in the model, exogenous application of well-established agonists of β-adrenergic receptors were applied. After 3 hours, non-selective β-AR agonist isoprenaline applied at concentrations of 10 μM induced a glycerol release of 21.2 $\pm$ 2.3 μM (N=5). Similarly 10 μM concentrations of native adrenergic receptor agonist norepinephrine-induced glycerol release of 27 $\pm$ 5.1 μM (N=5). Both agonists showing significant differences from glycerol released under basal conditions (N=5, 6 $\pm$ 1.3 μM). Therefore, I ascertained that inguinal WAT tissue sections handled *ex vivo* in this manner were successfully able to respond to external lipolytic factors, which culminated on increased glycerol content in the supernatant significantly above basal/vehicle controls (N=5, P<0.001 isoprenaline, P<0.05 norepinephrine) (Figure 4.1 C).

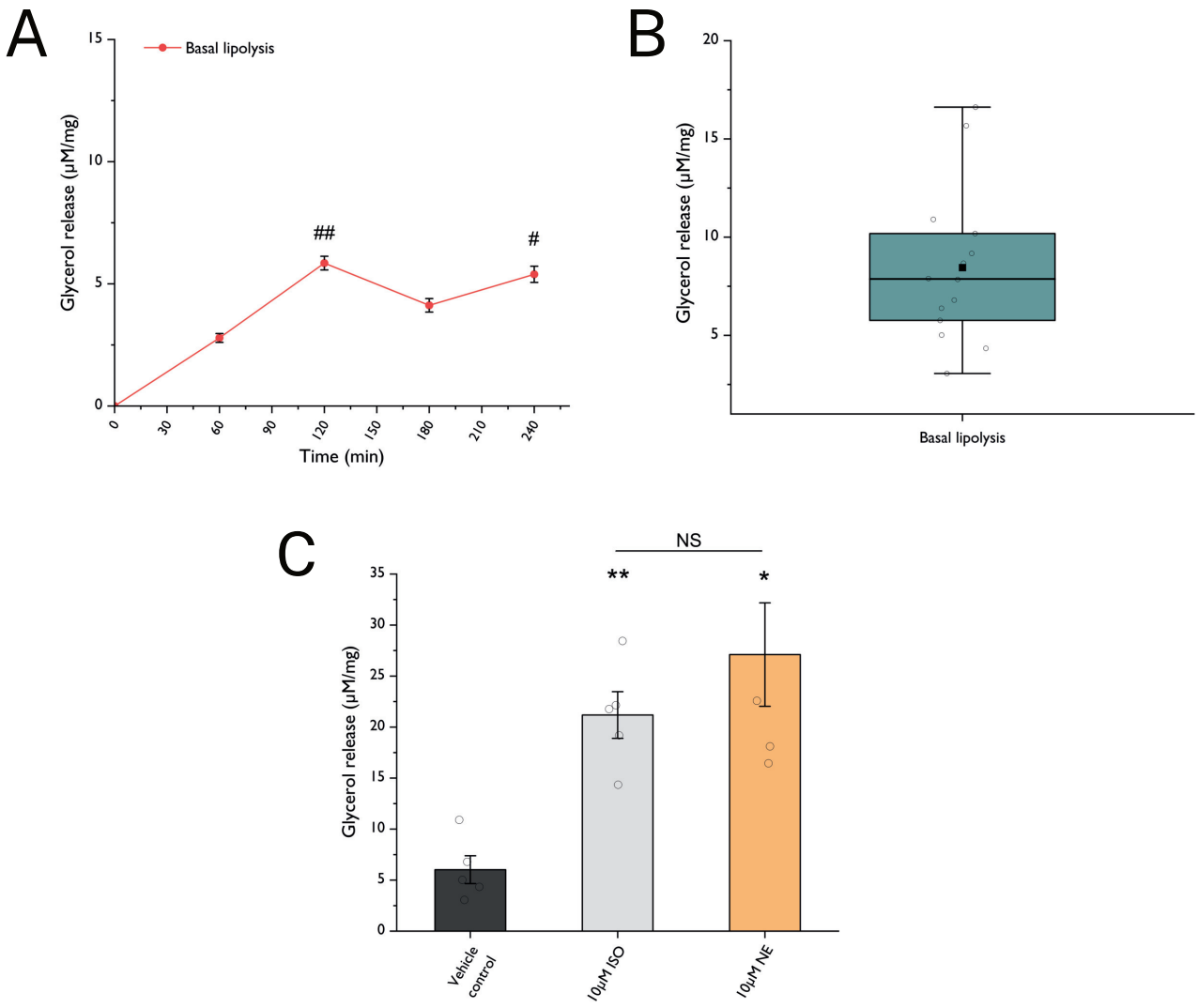

Figure 4.1: White adipose tissue is capable of basal and stimulated lipolysis *ex vivo*. (A) Basal glycerol release values of adipose tissue explants left for either 1, 2, 3 or 4 hours. #P<0.05 ##P<0.001 indicates difference from the respective time point versus 60 minutes (N=3) (ANOVA). (B) Plot indicating the mean (filled square) median (solid black line within box), interquartile range (IQR) (box) and whiskers represent 1.5x IQR (minimum and maximum extremities of data) of glycerol values after 3 hours under basal conditions (N=14). (C) Agonist isoprenaline (ISO) and norepinephrine (NE) stimulated glycerol release after incubation for 3 hours, compared to vehicle controls. Significances denoted by *P<0.05, **P<0.01 versus vehicle controls. Non-significance is denoted by 'NS' (N=5) (Welch's ANOVA). Data represent mean ± SEM of glycerol release corrected to tissue weight. Jitters (open circles) represent each data point (N).

4.3.1.2 Characterisation of norepinephrine-stimulated lipolysis

To accurately and reproducibly explore the model further using the sympathomimetic norepinephrine, it was important to establish parameters in terms of concentration and sampling time. Therefore a dose response curve for norepinephrine was conducted, illustrating norepinephrine increased lipolysis in a concentration-dependent manner (0.1 - 100 μM) which revealed a peak response at 10 μM, which declined at concentrations 30 μM, and a half-maximal concentration (EC50) of 2.4 $\pm$ 1.4 μM (N=5) (Figure 4.2A). Determination of such a concentration was required for enabling glycerol release both above and beyond the norepinephrine response when challenged with other pharmacological agents. Therefore a concentration of 2 μM norepinephrine was used in all other glycerol release experiments from this point onwards.

Secondly, an optimal sampling point was required to achieve a robust lipolytic response, while also allowing time for signalling transduction to fully occur. The sampling time was determined based on comparisons between norepinephrine-stimulated versus vehicle control tissues over a time series, up to 3 hours (Figure 4.2). Both 2 and 3 hours of incubation with norepinephrine increased glycerol release significantly above vehicle controls (N=5, $P<0.001$ and $P<0.001$, respectively). However, while both significant, the largest difference in glycerol release between norepinephrine-stimulated and control tissues was at the 3-hour time point (N=5, 21.5 $\pm$ 1.4 μM versus 6.7 $\pm$ 1.1 μM, respectively, $P<0.001$). Therefore, given the range of basal glycerol release values observed (Figure 4.1 B), to increase the difference between stimulated and non-stimulated groups and limit the future possibility of variation-derived overlap, the 3 hour time point was selected for all future experiments where norepinephrine acts as agonist.

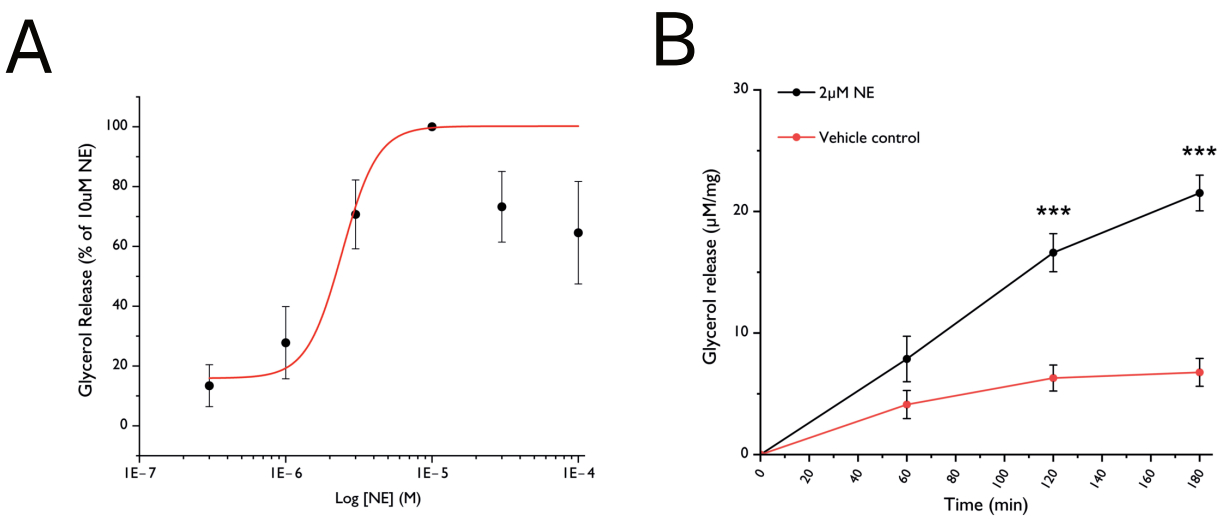

Figure 4.2: Characterisation of the norepinephrine-driven lipolysis. Norepinephrine (NE)-evoked glycerol release values in (A) a dose-dependent manner ranging from 0.1 μM to 100 μM, where 10 μM is peak response & EC50 determined 2.4 $\pm$ 1.4 μM using Hill1 equation and data are normalised to peak response (N=5) and (B) lipolytic response to submaximal NE (black line) over time up to 3 hours compared to vehicle controls (red line). Significance from controls at the corresponding time point denoted using asterisk, where ***P$<$0.001 (N=5) (Welch's ANOVA). Data represented as mean $\pm$ SEM of glycerol release corrected to tissue weight.

4.3.1.3 Lipolysis is inducible via voltage-gated Na^+ channel opener veratridine

After the establishment of an appropriate sympathomimetic agonist and the bounds of application in which to best induce lipolysis, I embarked on the next aim in the project. To increase the physiological validity of the *ex vivo* model employed here and hence investigate the role of neuronal activation of white adipose tissue, it was important to attempt to illicit direct neurogenic-driven lipolysis. Observing such a direct, neuronally-mediated response would provide a more physiologically representative platform, by which pharmacological challenge can be applied to interrogate the involvement of various neurotransmitters, neuropeptides and other signalling molecules in lipolysis. Therefore, for the first time in white adipose tissue, the VGSC opener veratridine was used to attempt induction of neurotransmitter release from resident nerves in the tissue.

The working hypothesis using veratridine was based on published information regarding its mechanism of action; by binding to resident Na_V channels upon nerves, influence their gating properties, allowing Na^+ entry to initiate exocytosis-inducing action potentials.

As veratridine was a novel tool within this *ex vivo* system, literature was assessed as to possible functionally appropriate concentrations. A variety of concentrations between 10 and 100 μM were reported as effective at inducing nervous discharge or altering gating status in various models (Zhang et al. 2018; Hyland et al. 2005; Wada et al. 1992). Therefore I tested some candidate concentrations to ascertain the most appropriate concentration to induce a functional response in the present *ex vivo* model.

Initially with concentrations of 10 μM, veratridine failed to induce glycerol increase significantly above vehicle controls (N=5, P>0.05) (Figure 4.3 A). While 50 μM veratridine induced glycerol release significantly above controls, it was not significantly higher than 10 μM veratridine (N=5, P>0.05), or significantly lower than 100 μM (N=5, P>0.05), risking potential clearance issues from controls in future experiments, if values are subject to variation.

However, 100 μM veratridine was significantly different from vehicle controls and 10 μM concentrations, providing good clearance (N=5, P<0.001 & P<0.05 respectively) (Figure 4.3 A). While glycerol release in response to 100 μM veratridine concentrations did not significantly deviate from those at 50 μM, values were slightly higher and more consistent (N=5, 35.1 $\pm$ 1.7 μM versus 33.2 $\pm$ 3.13 μM, respectively). Other studies have employed veratridine at 100 μM concentrations (Craig et al. 2020; Mohammed et al. 2017). As such, 100 μm veratridine was considered to sufficiently yield a reliable response. Therefore, 100 μM concentration of veratridine was taken forwards in all future experiments.

In experiments comparing stimulants, veratridine elicited glycerol release comparable with those of submaximal concentrations of norepinephrine and was not statistically different (N=5, P>0.05), with values equal to circa 90% of norepinephrine response (N=5, 26.6 $\pm$ 1.3 μM veratridine versus 29.4 $\pm$ 1.3 μM norepinephrine) (Figure 4.3 B).

To further characterise the veratridine response and establish a sampling timepoint, tissues were agonised with veratridine at 100 μM for periods of 1, 2 or 3 hours. The response to veratridine was distinct, with glycerol release increasing by around 13 μM

at each time point (Figure 4.3 C), while vehicle controls increased by nearly 3 times less than these values each time point. As observed in section 4.3.1.2 with exogenous norepinephrine stimulation, veratridine-stimulated tissues were strongly significantly different from vehicle controls after 3 hours exposure ($P<0.001$, $N=5$) and also exhibited the greatest difference in mean glycerol release compared to vehicle controls at this point ($N=5$, 39.9 ± 2.7 μM versus vehicle controls 14.8 ± 1.9 μM) (Figure 4.3 C). Therefore, a sampling time of 3 hours was chosen for all future experiments using veratridine. As veratridine was dissolved in DMSO, effects of 1% DMSO on glycerol release were compared to controls. Under these conditions, there was no significant difference in basal glycerol release with the addition of 1% DMSO ($N = 10$, $P>0.05$) (Figure 4.3 D).

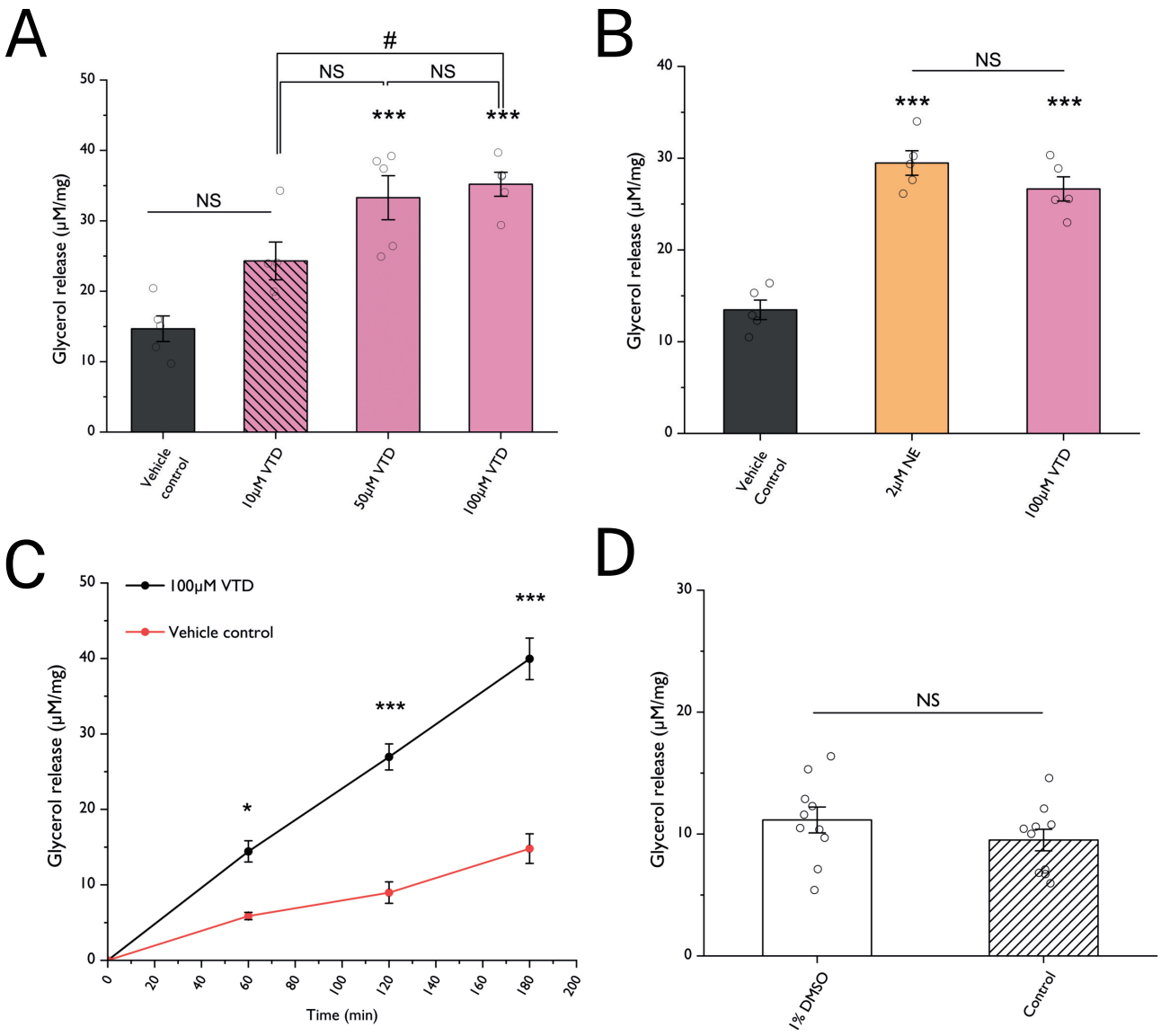

Figure 4.3: Veratridine is capable of inducing lipolysis *ex vivo*. (A) Veratridine (VTD)-induced lipolysis at concentrations of 10 μM, 50 μM and 100 μM (N=5) (ANOVA) and (B) comparison of veratridine and norepinephrine (NE)-stimulated lipolysis (N=5) after 3 hours. ***P<0.001 versus vehicle controls, #P<0.05 between groups indicated by line (ANOVA). (C) Veratridine-stimulated versus basal glycerol release over time (N=5) (ANOVA). (D) Effect of 1% DMSO on basal glycerol release versus controls (N=10) (two sample t-test). Significances denoted by *P<0.05, ***P<0.001 refer to comparisons between stimulated and corresponding basal tissues at the same time point. In all cases, non-significance is denoted by 'NS'. Data represent mean ± SEM of glycerol release corrected to tissue weight. Jitters (open circles) represent each data point (N).

4.3.2 Investigating the receptors involved in veratridine-induced nerve activation

Tetrodotoxin (TTX) is a toxin which binds to VGSCs and prohibits Na^+ entry (Stevens et al. 2011).

TTX has been successfully used to inhibit Na_V channels of excitable cells in many other studies at concentrations of 1 μM (Dobrev et al. 1998; Stacey et al. 2018; Tanaka et al. 1999). To fully establish whether veratridine activity was dependent upon Na_V channels, TTX at 1 μM, was applied to attempt to abolish lipolysis induced by veratridine. Theoretically, if veratridine is acting as hypothesised, pre-exposure of Na_V channels to TTX will prevent veratridine access to its binding site, prohibiting the lipolytic response. Encouragingly, a 30-minute pre-incubation with 1 μM TTX, with subsequent addition of veratridine, abolished the veratridine-induced glycerol release ($N=5$, $P<0.001$) down to values that didn't significantly differ from vehicle controls, after 3 hours exposure ($N=5$, $P>0.05$) (Figure 4.4 A).

Also, TTX applied under basal conditions didn't induce any significant change in glycerol release compared to vehicle controls after 3 hours ($N=6$, $P>0.05$) (Figure 4.4 B), which suggests basal lipolytic processes occur independently of any constitutive or residual nerve excitability, and of Na_V channels, should they be expressed on the adipocytes themselves.

While these data advocate for the response to veratridine being neurogenic, it doesn't eliminate the prospect that adipocytes themselves are responsive to veratridine. While there is currently no published evidence that advocates for the presence of Na_V channels on adipocytes in mice (Pérez-Medina et al. 2012), there is still the possibility that this may be the case and what is being observed.

Therefore, in order to further substantiate the claim that veratridine's lipolysis-inducing action is indeed neurogenic, adipocytes were freshly isolated via enzymatic digestion, then challenged with norepinephrine or veratridine for 3 hours. By removing the surrounding neurons hypothesised to be responsible for conducting veratridine-activated lipolysis, then subsequently challenging remaining adipocytes with norepinephrine or veratridine, I can establish whether isolated adipocytes are firstly viable and able to respond to previously characterised lipolytic signals and secondly, whether veratridine elicits the

same lipolytic responses in absence of its proposed target.

In isolated adipocytes veratridine failed to illicit a significant response and only saw small but insignificant increases in total glycerol release above zero (5.3 $\pm$ 2.5 μM), after 3 hours (N = 5, P>0.05, one sample t-test). Unlike norepinephrine, however, which stimulated a robust glycerol release (155.4 $\pm$ 27.5 μM total glycerol), significantly above that of veratridine (N=5, P<0.01, Figure 4.4 C) . These data build evidence for the neurogenic nature of the veratridine response, with the added reassurance that challenged cells were viable and capable of responding to external lipolytic signals. Extrapolating from this, it again builds evidence that Na_V channels, if expressed by adipocytes, are not responsible for the induction of glycerol release by veratridine in this model.

Summary Taken together, these data indicate that veratridine in this context is acting via Na_V channels, as the lipolysis response is removed when Na_V channels are blocked by TTX. The data also suggests that these observations are not due to direct effects on adipocytes, as veratridine failed to illicit lipolysis in the absence of SVF components, whereas norepinephrine remained capable.

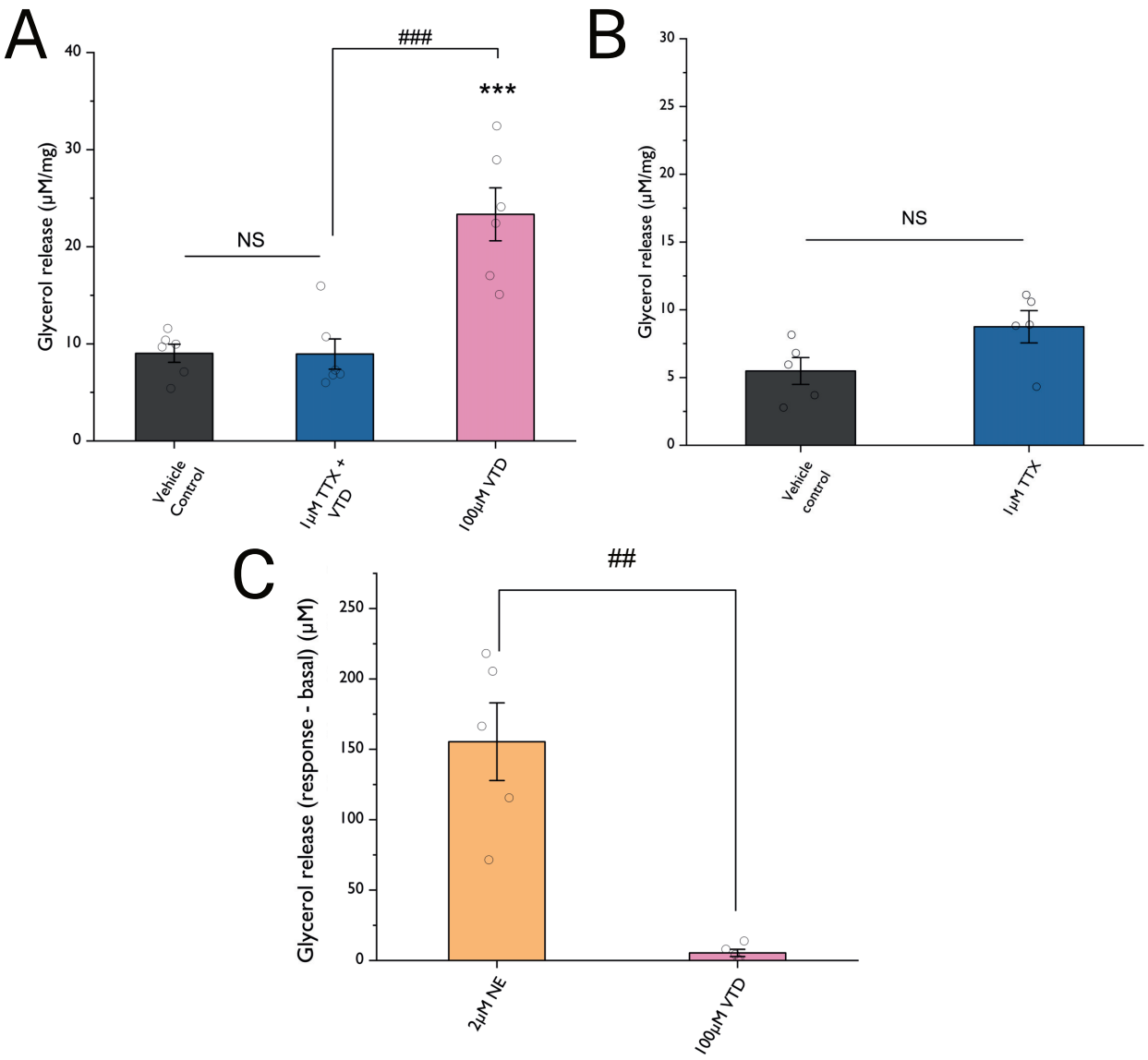

Figure 4.4: Veratridine induced lipolysis is dependent on VGSCs and on the presence of stromal-vascular fraction Tetrodotoxin (TTX) application to (A) veratridine (VTD)-stimulated tissues (N=5) (ANOVA) and (B) basal tissues (N=6) (two sample t-test), where data represent mean ± SEM of glycerol release corrected to tissue weight. (C) Total glycerol release by isolated adipocytes stimulated with norepinephrine (NE) and VTD for 3 hours (N=5) (Mann-Whitney U test), where basal values are subtracted from responses. Significance denoted by ***P<0.001 versus vehicle controls, ##P<0.01, ###P<0.001 between groups indicated by line. Non-significance is denoted by 'NS'. Jitters (open circles) represent each data point (N).

4.3.3 Probing the role of β-adrenergic signalling involvement in veratridine-evoked lipolysis

Further experimental characterisation of the veratridine response was required to affirm the lipolysis outcome was indeed neurogenic. Confirming whether veratridine was acting via a neurotransmitter would eliminate, to an extent, the involvement of other SVF cell types, narrowing possibilities to neurons.

Under the hypothesis that the effector underpinning veratridine responses is a sympathetic-released catecholamine acting at surface membrane β-AR receptors on adipocytes, blocking the prospective target receptors would theoretically reduce or remove the response to veratridine. This section aims to tease apart this aspect of the hypothesis.

4.3.3.1 Lipolysis stimulated by veratridine is abolished by propranolol

To address the identity of the signal involved in veratridine-mediated lipolysis and characterise the receptors involved in subsequent transmission of veratridine signalling, non-selective antagonists of β-adrenergic receptors were applied.

The non-selective β-AR antagonist, propranolol, applied at concentrations of 8 μM in hamster brown adipocytes reduced norepinephrine-stimulated cAMP increases in a dose-dependent manner (Zhao et al. 1997). A concentration of 10 μM propranolol applied in adipocyte 3T3-L1 and bone marrow derived stem cell lines successfully blocked gene expression changes stimulated by isoprenaline (Baek et al. 2014).

Therefore, propranolol at a 10 μM final concentration was applied 30 minutes prior to addition of veratridine.

Propranolol significantly blocked the veratridine-evoked increase in lipolysis after 3 hours, with values of propranolol-treated tissues stimulated with veratridine reduced to 6.3 $\pm$ 0.7 μM from 30.9 $\pm$ 2.3 μM (N=5, P<0.001), reducing glycerol concentrations to values analogous to vehicle controls (9.7 $\pm$ 1.6 μM) (N=5, P>0.05), representing a 79.6% decrease (Figure 4.5 A). There was no significant effect of β-AR antagonism on basal lipolysis when compared to vehicle controls (P>0.05), suggesting that basal lipolysis occurs independently of β-adrenergic receptor input.

The response of tissues to propranolol in the present *ex vivo* model were replicated

when using exogenously applied norepinephrine as a stimulant of lipolysis. Preincubation of tissues with 10 μM propranolol and subsequent stimulation with norepinephrine significantly prevented glycerol release after 3 hours (N=5, P<0.01) (Figure 4.5 B). However, in norepinephrine experiments, propranolol failed to completely abolish the stimulated response, reducing glycerol by 53.7% opposed to 79.6%. Moreover, unlike in veratridine-stimulated conditions, the glycerol values of propranolol-treated tissues remained significantly different from vehicle controls (N=5, P<0.01).

To validate observations that non-selective β-AR antagonism reduces veratridine-stimulated glycerol release in this model, tissues were also treated with alternate non-selective β-AR antagonist, sotalol. Sotalol has been used at relatively high concentrations in other published works; previously used to antagonise agonist-induced activity in CHO cells expressing the human β3-AR receptor, at effective concentrations of 10 μM to 1 mM (in a dose dependent manner) (Baker 2005). Sotalol has also been used in *ex vivo* studies in human tissue at concentrations of 10 and 100 μM (Britton et al. 2017). Therefore, I applied both a higher and lower concentration of sotalol at 10 and 100 μM, respectively.

Concentrations of both 10 (N=5, P>0.05) and 100 μM (N=5, P>0.05) sotalol failed to significantly reduce veratridine-stimulated lipolysis after 3 hours (Figure 4.5 C). Glycerol concentrations from tissues pre-treated with 100 μM sotalol prior to stimulation were slightly reduced compared to veratridine alone (17.8 $\pm$ 2.2 μM versus 22.4 $\pm$ 2.68 μM respectively). As with propranolol, there was no effect of sotalol on basal lipolysis compared to vehicle controls at either concentration (N=5, P>0.05) (Figure 4.5 C).

Summary Propranolol inhibits lipolysis in response to both veratridine and exogenously applied norepinephrine, which suggests the mechanism by which veratridine is inducing lipolysis is β-adrenergic, thus veratridine appears to evoke the neuronal release of a catecholamine that acts on the β-AR suite of receptors.

Sotalol, however, contradicts this hypothesis as it failed to reduce lipolysis under stimulated conditions, suggesting that β-ARs play no role in veratridine-stimulated lipolysis. Therefore a more direct form of enquiry was required to confirm the catecholamine dependence of the veratridine mechanism.

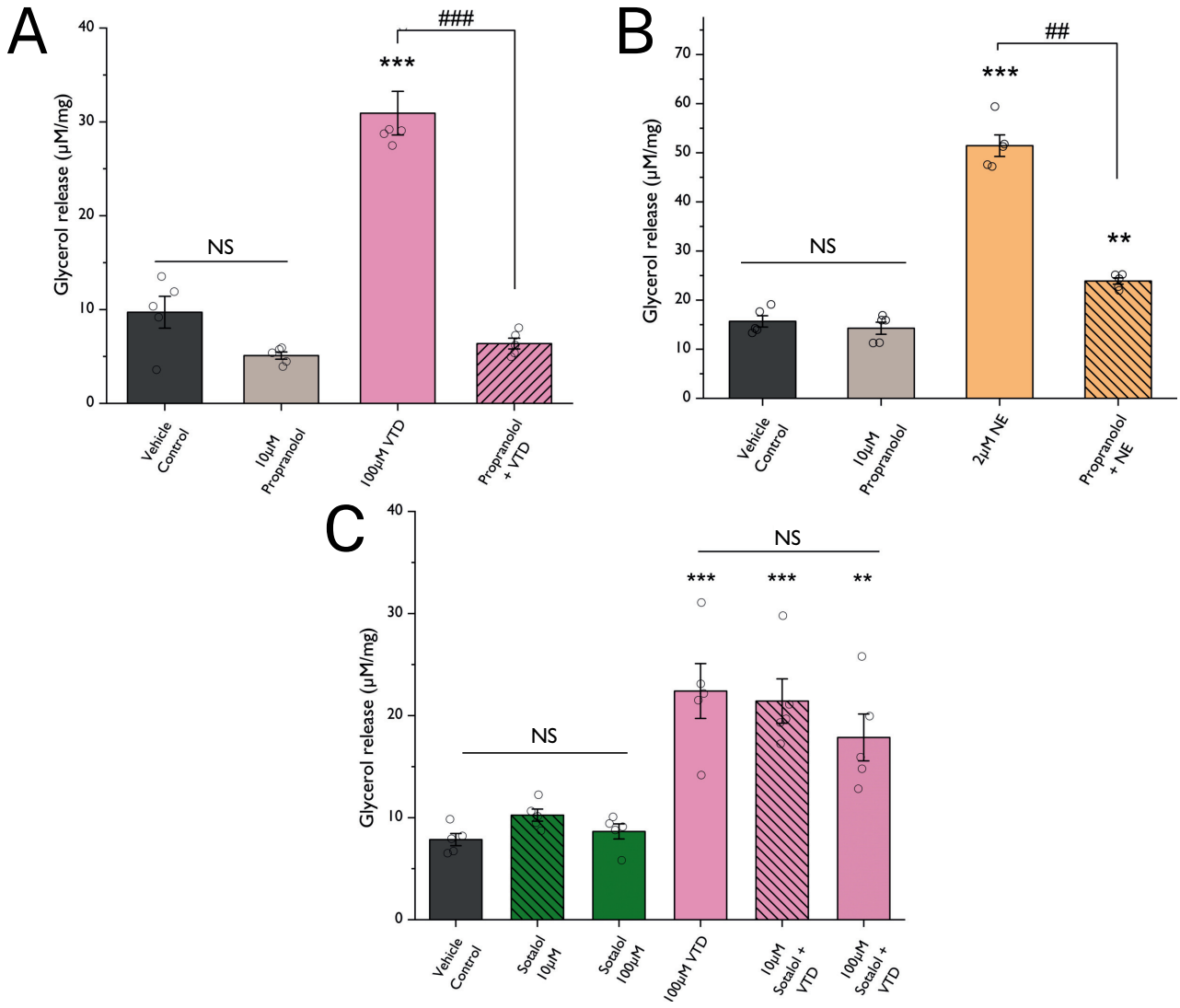

Figure 4.5: Non-selective β-AR antagonism on veratridine and norepinephrine-stimulated lipolysis. Effects of 10 μM propranolol on glycerol release stimulated by (A) veratridine (VTD) (N=5) (ANOVA) and (B) norepinephrine (NE) (N=5) (ANOVA) and (C) effects of sotalol (10 μM) on VTD-stimulated lipolysis (N=5) (ANOVA) after 3 hours. Data represent mean $\pm$ SEM of glycerol release corrected to tissue weight. Significance denoted by **P<0.01 ***P<0.001 versus vehicle controls, ##P<0.01, ###P<0.001 between groups indicated by line. Non-significance is denoted by 'NS'. Jitters (open circles) represent each data point (N).

4.3.4 Characterising the subtypes of β-adrenergic receptor involved in veratridine-evoked lipolysis

To elucidate the mechanism by which veratridine is acting to induce lipolysis, further to general β-AR antagonism, selective antagonism of each β-AR subtype was conducted. Employing the same experimental conditions and antagonist concentrations as in veratridine experiments, each antagonist was additionally stimulated with norepinephrine to validate the observations were equal across lipolytic-inducing regimes and thus underpinned by the same neurotransmitter. I hypothesised that antagonising each β-AR receptor would reveal at least one subtype responsible for neurogenic and exogenously-induced lipolysis.

4.3.4.0.1 Selective β-AR antagonism

Selective β1-AR antagonist CGP 20712 has been used successfully in rat white adipocytes to reduce glycerol release at concentrations of 1 μM (Louis et al. 2000) and in isoprenaline-stimulated mouse white adipocytes at 1 μM (Konkar et al. 1999). In other studies, concentrations of 10 μM have been used to antagonise stimulated responses in rat white adipocytes (Germack et al. 1997).

Selective β2-AR inverse agonist ICI 118551 has been used to block β2-Ars, in different models and tissues at a range of concentrations in published literature to reduce β2-AR signalling, ranging from 1 μM (Louis et al. 2000), to 10 μM in HEK293 cells (Vedel et al. 2015) and 20 μM in keratinocytes (Sivamani et al. 2009).

The β3-AR antagonist L-748337 was found successful at reducing an isoprenaline-stimulated response in experiments with 3T3-L1 cells, at nanomolar concentrations (Jin et al. 2018). L-748337 has also been used in beige and brown populations of human primary adipocytes (Cero et al. 2021) and in 3T3-L1 cell lines (Lim et al. 2019), in both cases at 10 μM with success.

Therefore, each selective β-AR antagonist above was applied at both 1 and 10 μM 30 minutes prior to stimulation with stimulant for 3 hours, to match concentrations reported in literature.

β1-AR antagonism

There was no significant reduction in veratridine-stimulated lipolysis post- β1-AR antagonism with CGP 20712 at either 1 (N=7, P>0.05) or 10 μM (N=7, P>0.05) concentrations, after 3 hours (Figure 4.6 A i). There was also no effect of β1-AR antagonism on basal lipolysis, compared to vehicle controls (N=7, P>0.05)

These findings were mirrored in experiments with exogenously applied norepinephrine as stimulant, where no decrease in lipolysis at either concentration of CGP 20712 was observed after agonism with norepinephrine (N=5, P>0.05) (Figure 4.6 B i). The only deviation between the veratridine and norepinephrine-stimulated datasets is a slight trend of 10 μM CGP 20712 reducing glycerol release by 17% under veratridine-stimulated conditions (Figure 4.6 A i), which is greater than the 5.8% decrease observed in norepinephrine-stimulated conditions. However, this failed to reach significance (N=7, P>0.05).

Lastly, basal lipolysis was unaffected by the addition of CGP 20712 in both veratridine (N=7, P>0.05) and norepinephrine (N=5, P>0.05) experiment sets, compared to vehicle controls, suggesting the β1-AR is not regulating basal lipolysis.

β2-AR antagonism

Antagonism of β2-AR receptors using ICI 118551 before subsequent veratridine stimulation caused a significant reduction in glycerol release, at both 1 (N=5, P<0.01) and 10 μM (N=5, P<0.001), compared to veratridine alone after 3 hours (Figure 4.6 A ii), reducing glycerol values by 19.8% and 40.1% respectively. Under norepinephrine-stimulated conditions, 10 μM ICI 118551 applied (N=5, P<0.01) significantly reduced glycerol release by 37.3% (Figure 4.6 B ii). The main deviation between the norepinephrine and veratridine datasets was 1μM ICI 118551 was not sufficient to significantly reduce lipolysis under norepinephrine-stimulated conditions (N=5, P>0.05), reducing glycerol values by 11.8%.

In both veratridine and norepinephrine-stimulated conditions, 10 μM ICI 118551 did not completely reduce the stimulated response down to basal values, indicating involvement of another receptor subtype responsible in lipolysis.

Basal lipolysis remained unaffected by the addition of ICI 118551 in both veratridine (N=5, P>0.05) and norepinephrine (N=5, P>0.05) datasets compared to vehicle con-

trols, suggesting the β2-AR is not regulating basal lipolysis.

β3-AR antagonism

Surprisingly, attempting to antagonise the β3-AR with either 1 (N=5, P>0.05) or 10 μM (N=5, P>0.05), L-748337 caused no significant reduction in veratridine-stimulated lipolysis after 3 hours (Figure 4.6 A iii). Under norepinephrine-stimulated regimes, neither concentration of L-748337 reached statistical significance (N=5, P>0.05), as observed in veratridine-stimulated conditions.

Interestingly, in both veratridine and norepinephrine datasets, L-748337 application appeared to have a stimulating effect under basal conditions. The effect was most prominent in the veratridine dataset, where L-748337 significantly increased lipolysis over vehicle controls by over 4-fold (N=5, P<0.001 1 μM and P<0.001 10 μM), despite lack of applied stimulant, equating to over 70% of the veratridine response (Figure 4.6 A iii).

The effects of L-748337 on basal lipolysis were shared in norepinephrine experiments, but not to the same extent, as only 10 μM of the antagonist under basal conditions increased lipolysis significantly above vehicle controls, raising glycerol release concentrations to equivalent of 53% of the norepinephrine response (N=5 P<0.05) (Figure 4.6 B iii).

Intriguingly, L-748337 reduced norepinephrine-evoked glycerol values to 30.1 $\pm$ 3.6 μM when applied at 10 μM with norepinephrine, while simultaneously raising them to similar values (24.2 $\pm$ 3 μM) when applied under basal conditions, indicating the possibility of a substitute lipolysis-inducing pathway being triggered (Figure 4.6 B iii).

Lastly, the apparent stimulatory effects of L-748337 did not combine with either stimulant to increase lipolysis above that of the corresponding stimulant applied alone.

Adipocytes + selective antagonists

There is little published evidence of the application of these selective β-AR antagonists in adipose tissue under *ex vivo* conditions. To ensure the responses observed were not due to effects of the *ex vivo* model, experiments were subsequently conducted on freshly isolated adipocytes, using norepinephrine as stimulant of lipolysis. Antagonist applications were all confined to a single final concentration of 1 μM. Adipocytes were responsive to norepinephrine in each antagonist experiment set to a similar degree, releasing around 100

μM total glycerol (Figure 4.6 C i, ii, iii). However, 30-minute preincubation of adipocytes with each antagonist for β1-AR: CGP 20712 (N=5, P>0.05) (Figure 4.6 C i), β2-AR: ICI 118551 (N=5, P>0.05) (Figure 4.6 C ii) or β3-AR: L-748337 (N=5, P>0.05) (Figure 4.6 C iii) did not significantly reduce lipolysis evoked by norepinephrine, after 3 hours. While the lack of significant effect after β1 and β3-AR antagonism matched the *ex vivo* veratridine and norepinephrine datasets, the lack of response to β2-AR antagonist ICI 118551 marked a deviation in antagonist response pattern between approaches.

Consistently, as observed in both veratridine and norepinephrine datasets, the adipocytes experienced increased lipolysis under basal conditions after exposure to β3-AR antagonist L-748337. The glycerol values were increased to an extent that was not significantly different from glycerol produced by norepinephrine-stimulated adipocytes (N=5, P>0.05), equating to 81.9% of the norepinephrine response (Figure 4.6 C iii). Again, the stimulatory effects of L-748337 did not combine with norepinephrine to increase lipolysis when used conjunctionally.

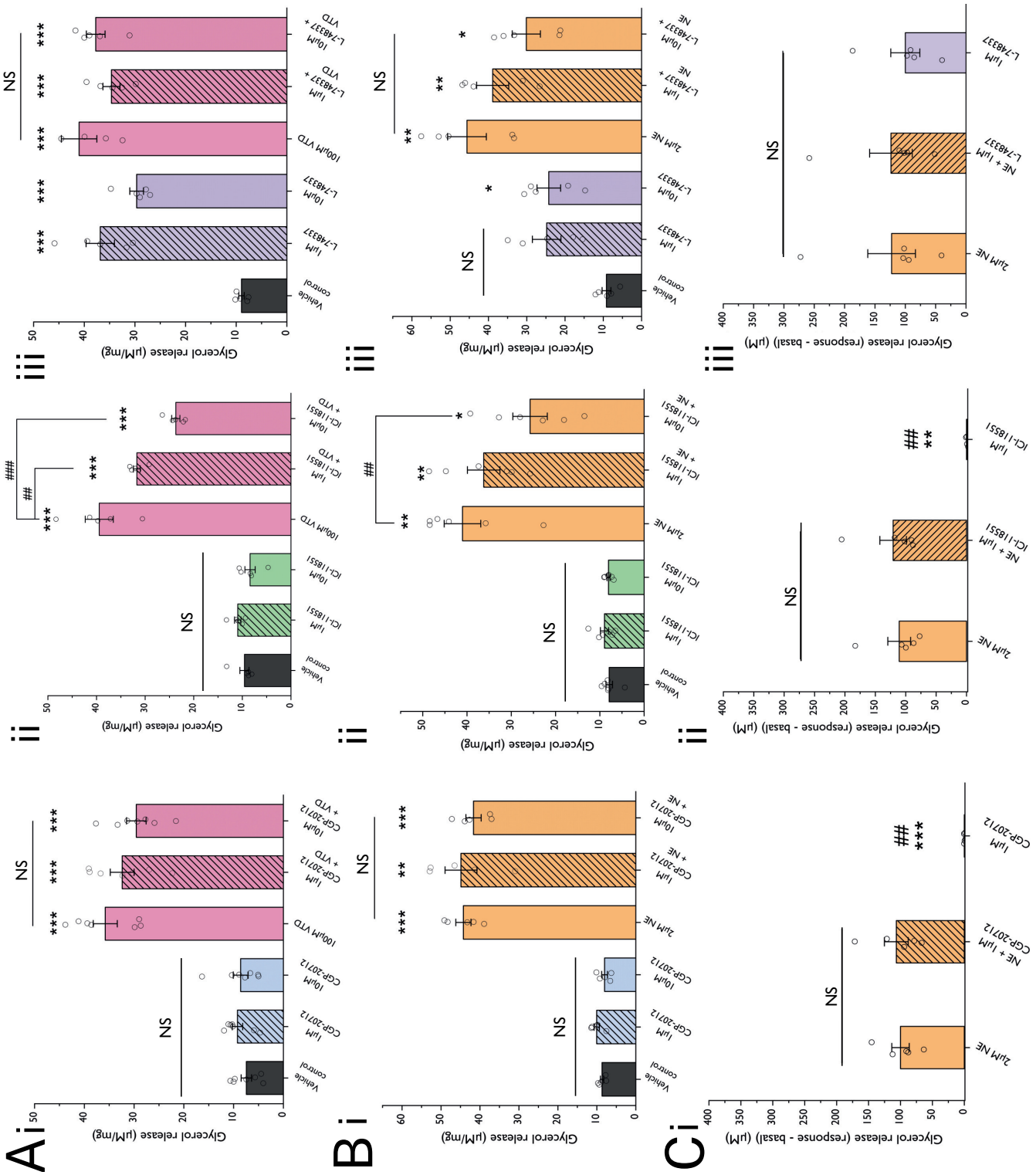

(Figure legend on next page.)

Figure 4.6: Selective antagonism of β-AR subtypes under veratridine or norepinephrine-stimulated conditions *ex vivo* and in isolated adipocytes. Effects of selective β-AR antagonists for (i) **β1-AR**; CGP 20712, (ii) **β2-AR**; ICI 118551 and (iii) **β3-AR**; L-748337 on basal and (A) veratridine (VTD) (B) norepinephrine (NE)-evoked lipolysis *ex vivo* and (C) on isolated adipocytes stimulated with NE, after 3 hours, where *ex vivo* data represent mean $\pm$ SEM of glycerol release corrected to tissue weight and isolated adipocytes data represents total glycerol release of groups, minus basal values. Significance in *ex vivo* experiments denoted by *P$<$0.05, **P$<$0.01 ***P$<$0.001 versus vehicle controls, #P$<$0.05, ##P$<$0.01, ###P$<$0.001 between groups indicated by line. In isolated adipocytes **P$<$0.01 ***P$<$0.001 denotes difference from NE alone, and ##P$<$0.01 from NE with antagonist versus antagonist applied alone. In all cases, non-significance is denoted by 'NS'. Jitters (open circles) represent each data point (N). All experiments are N=5, except A(i) (N=7) and B(ii) (N=6). Welch's ANOVA used in A(i) and B (i), (ii), (iii). ANOVA used in A(ii), (iii) and C(i), (ii), (iii).

4.3.4.0.2 L-748337 + propranolol

To investigate the stimulatory effect L-748337 had under basal conditions, basal tissues were pre-incubated with 10 μM propranolol 30 minutes prior to the addition of 10 μM L-748337. If the antagonist was agonising a β-AR via the canonical lipolysis pathway, theoretically propranolol exposure would remove this response.

However, pre-exposure to propranolol failed to significantly reduce glycerol release evoked by L-748337, after 3 hours (N=5, P>0.05) (Figure 4.7). Both groups exposed to L-748337, alone (N=5, P<0.01) or with propranolol (N=5, P<0.001), demonstrated glycerol release values significantly above that of vehicle controls (Figure 4.7). Therefore, the effect of β3-AR antagonist L-748337 was not considered sensitive to the previously effective β-AR antagonist activity of propranolol.

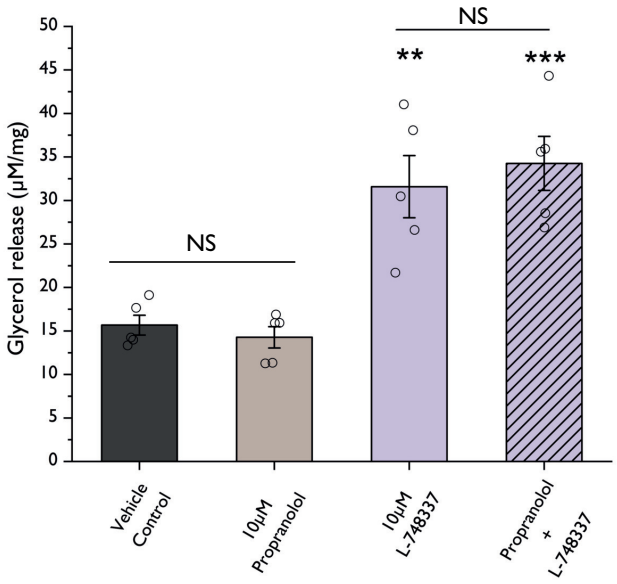

Figure 4.7: Propranolol failed to inhibit glycerol release induced by β3-antagonist L-748337. Effects of propranolol on L-748337-evoked glycerol release applied under basal conditions after 3 hours (N=5) (ANOVA). Significance denoted by **P<0.01 ***P<0.001 versus vehicle controls. Non-significance is denoted by 'NS'. Data represent mean ± SEM of glycerol release corrected to tissue weight. Jitters (open circles) represent each data point (N).

4.3.4.0.3 Alternative β3-AR antagonist

Given that application of widely used β3-AR antagonist L-748337 failed to reproduce lipolysis-antagonising effects observed in literature, I wanted to explore whether the lack of effects observed were due to antagonist efficacy and performance, opposed to effects of the model. Therefore I antagonised β3-ARs in both veratridine and norepinephrine *ex vivo* conditions, as well as in isolated adipocytes (under norepinephrine stimulation), using the only other β3-AR antagonist commercially available, SR59230A. SR59230A has previously been used at concentrations of 1 μM in perivascular adipose (Saxton et al. 2019), and 10 μM in 3T3-L1 cell lines (Mizuno et al. 2002) & mouse embryonic stem cells (Calvani et al. 2018). Therefore, concentrations of 1 and 10 μM SR59230A were applied in *ex vivo* conditions, and at 1 μM in isolated adipocyte experiments.

Preincubation of tissues with 10 μM SR59230A significantly antagonised lipolytic responses induced by norepinephrine after 3 hours (N=5, P<0.001) (Figure 4.8 B), but not in veratridine stimulated-conditions (N=5, P>0.05).

Although, neither norepinephrine- (N=5, P>0.05) or veratridine-stimulated (N=5, P>0.05) lipolysis was significantly reduced after exposure to 1 μM concentrations of SR59230A. Similarly, norepinephrine-stimulated adipocytes preincubated with 1 μM SR59230A experienced no significant reduction in glycerol release, compared to norepinephrine alone (N=3, P>0.05) (Figure 4.8 C).

As observed with the first β3-AR antagonist L-478337, SR59230A applied under basal conditions also increased glycerol release, in all experiments (Figure 4.8). These effects appeared more moderate, as in all experiments, basal groups exposed to either 1 or 10 μM concentrations of SR59230A increased glycerol release above controls by less than 2-fold, opposed to over 3- and 4-fold, as observed with L-748337. Again, the lipolysis increasing effects of SR59230A did not combine with either stimulant to increase glycerol release over that of stimulant alone, under any conditions.

Summary Reinforcing the case that veratridine is operating via induced release of norepinephrine, use of selective β-AR antagonists with veratridine and norepinephrine in *ex vivo* preparations showed similar patterns of response: Both stimulating conditions were unaffected by β1-AR antagonism, yet showed sensitivity to β2-AR antagonism. However, the β2-AR antagonist did not abolish lipolysis completely in either

case, indicating the potential role of another receptor. Both stimulatory regimes lacked a significant reduction in glycerol release using β3-AR antagonist L-748337. However, use of an alternative antagonist for β3-AR, SR59230A, achieved a significant reduction in lipolysis, but only under exogenously applied norepinephrine-stimulated conditions *ex vivo*. Further, contrary to antagonist patterns established *ex vivo*, selective antagonism of any β-AR receptor failed to reduce norepinephrine-stimulated lipolysis when applied in adipocyte preparations.

Under basal conditions, application of β1 and β2-AR antagonists did not alter basal lipolysis in *ex vivo* veratridine and norepinephrine datasets, indicating that basal lipolysis occurs independently of β-AR activation, supporting data from section 4.3.3. However, conversely, antagonism of β3-AR with either antagonist under basal conditions induced glycerol release in all cases, with effects of L-748337 being more prominent. The lipolysis-enhancing effects of both antagonists did not combine with stimulants to increase lipolysis above that when stimulants were applied alone, in either regime. The lipolysis-inducing effects of the antagonist L-748337 were not abolished by propranolol.

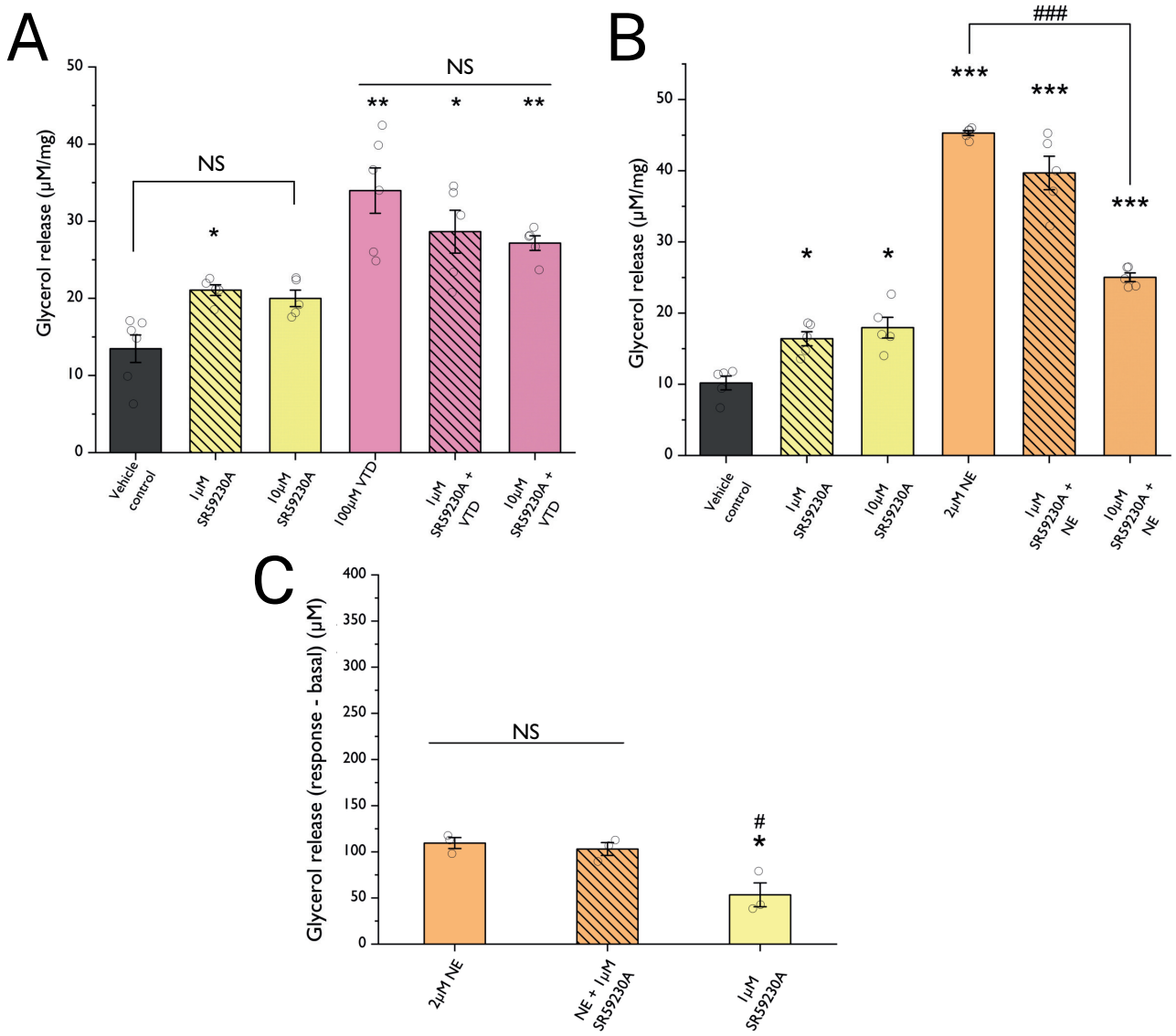

Figure 4.8: Alternative β3-AR antagonist SR59230A effects on basal and stimulated lipolysis *ex vivo* and in isolated adipocytes. Effects of β3-AR antagonist SR59230A on basal, (A) veratridine (VTD) (N=5) (Welch's ANOVA) and (B) norepinephrine (NE) (N=5) (Welch's ANOVA) evoked lipolysis *ex vivo* and (C) isolated adipocyte basal and NE-stimulated lipolysis (ANOVA), after 3 hours. *ex vivo* data represent mean $\pm$ SEM of glycerol release corrected to tissue weight and isolated adipocyte data represents total glycerol release of groups, minus basal values. *P$<$0.05 ***P$<$0.001 versus vehicle controls,

###P$<$0.001 between groups indicated by line. In isolated adipocytes *P$<$0.05 denotes difference from NE alone, and #P$<$0.05 from NE with antagonist, versus antagonist alone. Non-significance is denoted by 'NS'. Jitters (open circles) represent each data point (N).

4.3.5 Investigating Ca^{2+} dependency of veratridine-evoked lipolysis

As discussed in Chapter 1, the canonical approach of neuronal exocytosis of transmitter from prejunctional synapses is regarded as Ca^{2+}-dependent. Briefly, action potentials confer excitability to voltage-gated calcium channels on the presynapse (VGCC) which induces a conformational change, allowing calcium entry via the channel into the synapse. Calcium entry sequentially catalyses a series of calcium-dependent steps, causing fusion of vesicles containing neurotransmitter to be released into the post-synaptic space. With the understanding of this mechanism and it's role in regulated exocytosis, it was necessary to probe whether the veratridine response was sensitive to VGCC interference, as to characterise exocytosis in the hypothesised veratridine mechanism of action. Theoretically, by preventing calcium entry into the neuron synapse, vesicles of neurotransmitter release should be subsequently abrogated.

4.3.5.1 Investigating the role of VGCCs in veratridine-evoked lipolysis

N-type VGCCs

Expression of voltage-gated calcium channels of the N-type (Ca_V 2.2) are generally most involved in the nervous system (hence their nomenclature, 'neuronal' type) (Westenbroek et al. 1992). Using well-established cone-snail (*Conus geographus*) derived neurotoxin ω-conotoxin-GVIA to block Ca_V channels, I attempted to further interrogate the mechanism underlying the veratridine response. ω-conotoxin-GVIA is reportedly selective for the N-type Ca_V channel subtypes (Whorlow et al. 1996). Under the theory of the proposed mechanism of action, I hypothesised that glycerol release would decrease in tissues challenged with veratridine that had been pre-incubated with ω-conotoxin-GVIA. Concentrations of GVIA applied in literature suggest 1 μM as effective in blocking veratridine-evoked dopamine release (in combination with other toxins) in rat brain (Dobrev et al. 1998). Other work illustrates concentrations from 0.33 μm up to 12 μM were effective at reducing Ca^{2+} current in electrically-stimulated frog sympathetic neurons, in a dose-dependent manner (Boland et al. 1994). Therefore, concentrations of 1 μM and 10 μM were taken forward for use in this model.

Preincubation of tissues with 1 μM (N=3, P>0.05) or 10 μM (N=3, P>0.05) ω-conotoxin-GVIA, did not prevent glycerol release in tissues after subsequent exposure to veratridine after 3 hours (Figure 4.9 A). There was also no effect of either concentration on basal lipolysis (N=3, P>0.05, Figure 4.9 A). These data suggest that the action of veratridine is not mediated by Ca_V 2.2 N-type channels.

P & Q type VGCCs

It is generally accepted that calcium channels of the broader Ca_V 2 family can also be expressed in peripheral nerves, which includes P/Q-type Ca_V channels (Ca_V 2.1) (Dolphin et al. 2020; Motagally et al. 2009). Indeed, studies have shown P- and Q-type Ca_Vs to have significant roles in sympathetic release of neurotransmitter in rat mesenteric arteries (Tanaka et al. 1999). Given the possibility that in the previous experiment, ω-conotoxin-GVIA was missing a suite of active members of the Ca_V family, an antagonist for the remaining possible subtypes were employed.

ω-conotoxin-MVIIC blocks P & Q as well as N-type (Ca_V 2.1 and 2.2) channels and has been successfully used in other studies to block EFS-stimulated nervous discharge in Guinea pig atria (Serone et al. 1999), and reduce EFS-stimulated norepinephrine release from mouse vas deferens (Waterman 1997). In EFS-evoked contraction of the rat mesenteric artery, 3 μM ω-conotoxin-MVIIC was efficient at blocking contractility (Tanaka et al. 1999). Lower concentrations within nanomolar ranges have been used in single cell-based assays, with a predicted full inhibition at circa 0.82 μM (Hanlon et al. 2016). Therefore, in both veratridine-stimulated and basal conditions, I tested ω-conotoxin-MVIIC at concentrations of 1 μM and 10 μM to span the range in literature, and provide a higher alternative concentration. This is informed by researchers who noted that ω-conotoxin-MVIIC required longer exposure and higher concentrations to alter inward calcium currents than alternative conotoxin subtypes (Xu et al. 1996).

Preincubation of both 1 (N=3, P>0.05) or 10 μM (N=3, P>0.05) ω-conotoxin-MVIIC failed to significantly reduce veratridine-evoked lipolysis after 3 hours (Figure 4.9 B). There was also no significant change when ω-conotoxin-MVIIC was applied under

basal conditions (N=3, P>0.05).

Small molecule Ca^{2+} antagonists

As conotoxins GVIA & MVIIC are relatively large molecules, and the model here is explant based, the conotoxins may have been ineffectual at accessing their target within adipose tissue. Therefore, to eliminate the possibility that molecule size prevented antagonist access to, and subsequent blockade of, target channels, alternative smaller compounds were tested. Cilnidipine is an N- and L-type (Ca_V 1) Ca^{2+} channel blocker (Chandra et al. 2013), and is used in Japan as treatment for hypertension (Kario et al. 2013). A study using isolated sympathetic neurons in rats found cilnidipine effectively suppressed N-type Ca^{2+} currents (Uneyama et al. 1999). Cilnidipine has been previously used in cultured vascular smooth muscle cells at concentrations of 1 & 10 μm (Hu et al. 2001), and applications of 1 μM successfully attenuated norepinephrine release from sympathetic neurons in isolated rabbit aorta (Nap et al. 2004). Therefore tissues were pre-incubated with 1 & 10 μM cilnidipine prior to stimulation with veratridine, in an attempt to inhibit hypothesised VGCC-mediated vesicle fusion.

Additionally, although considered to be located in neurons within the CNS (Moore et al. 2020; Roca-Lapirot et al. 2018), to singularly re-probe the involvement of L-type channels in veratridine-stimulated neurotransmitter release, nifedipine was selected. Nifedipine has been used in human neuroblastoma cells to reduce veratridine-induced Ca^{2+} entry (Vetter et al. 2012), and others found concentrations ranging from 10 - 100 μM to be effective in reducing neurotransmission in Guinea pig celiac ganglion neurons (Zhai et al. 1991). Therefore experimental concentrations of nifedipine were applied at 10 and 100 μM.

Interestingly, exposure to either 1 (N=3, P>0.05) or 10 μM (N=3, P>0.05) cilnidipine did not significantly reduce veratridine-stimulated lipolysis (Figure 4.9 C). Nor was there any significant effect of cilnidipine application on basal lipolysis compared to vehicle controls (N=3, P>0.05).

Similarly, veratridine-evoked lipolysis was unaffected by 10 (N=3, P>0.05) or 100 μM (N=3, P>0.05) nifedipine after 3 hours (Figure 4.9 D) and had no significant effect on basal lipolysis at either concentrations (N=3, P>0.05).

Irrespective of molecule size of the antagonists applied, N and L-type channels do

not appear involved in the veratridine mechanism.

Summary Blockade of N- P- Q- and L-type Ca_V channels had no impact on veratridine-evoked lipolysis, suggestive of a mode of action that does not depend on VGCCs for release of neurotransmitter.

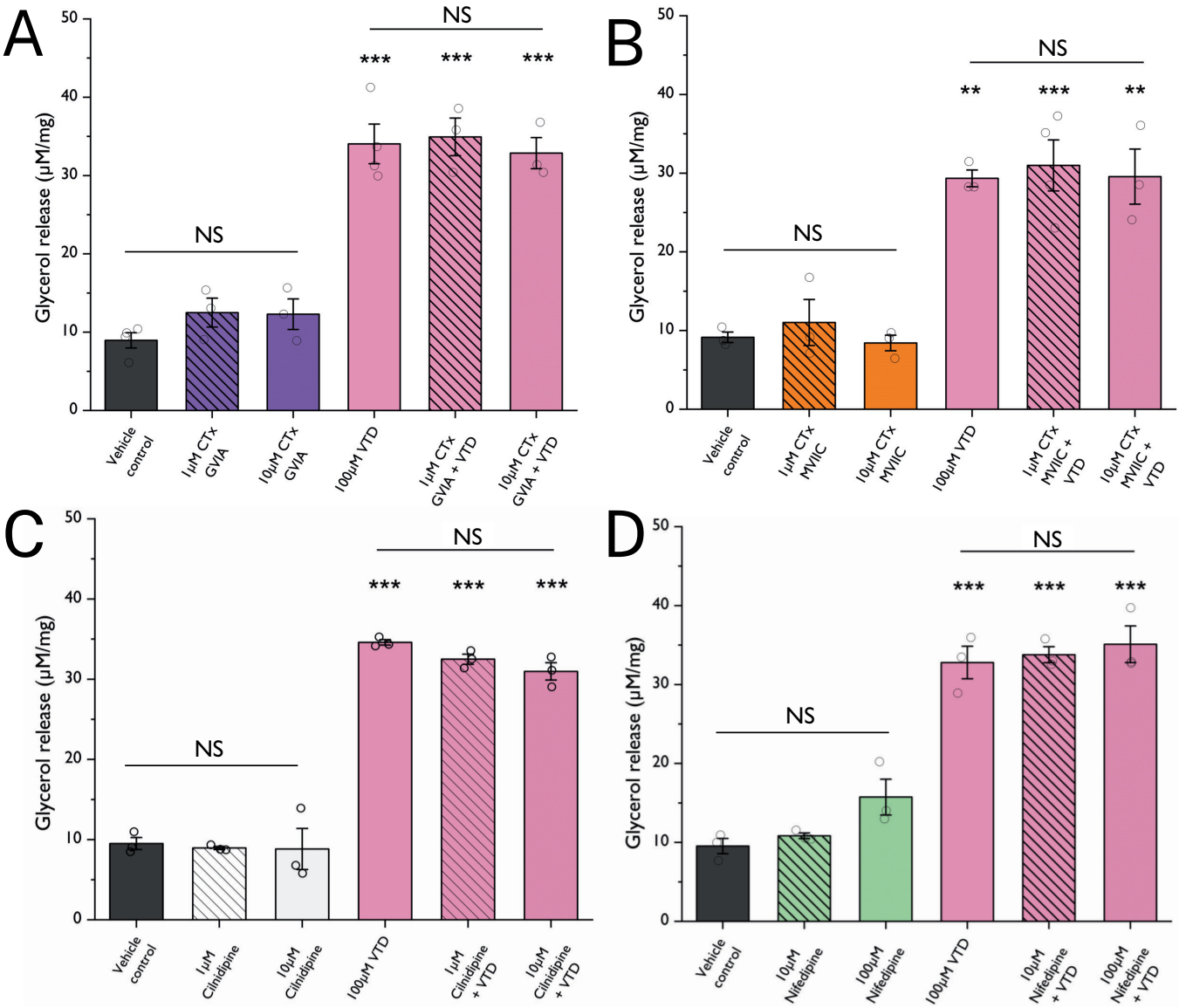

Figure 4.9: No role for VGCCs in veratridine-stimulated lipolysis. Veratridine-(VTD) stimulated lipolysis antagonised by (A) ω-conotoxin-GVIA (CTx GVIA) (N=3) (ANOVA), (B) ω-conotoxin-MVIIC (CTx MVIIC) (N=3) (ANOVA), and small molecule inhibitors (C) cilnidipine (N=3) (Welch's ANOVA) and (D) nifedipine (N=3) (ANOVA) after 3 hours. Significance denoted by **P<0.01 ***P<0.001 versus vehicle controls. Non-significance is denoted by 'NS'. Data represent mean ± SEM of glycerol release corrected to tissue weight. Jitters (open circles) represent each data point (N).

4.3.5.2 Inhibition of alternate routes of Ca^{2+} entry

Given that blocking VGCCs offered no candidate Ca_V subtypes that underpin veratridine-evoked neurotransmitter release, the canonical assumptions of the hypothesised release of neurotransmitter were reconsidered.

Evidence from seminal studies using veratridine as a tool for nervous excitation have indicated that veratridine effects were less dependent on extracellular Ca^{2+} and moreso on the effects of extracellular Na^+. The authors hypothesised that veratridine-driven neurotransmission was instead contingent on an intracellular source of Ca^{2+} liberated by Na^+, such as from mitochondrial stores (Cunningham et al. 1981). Therefore to establish whether veratridine in this model was operating via the liberation of mitochondrial stores of Ca^{2+}, inhibitor of the mitochondrial Na^+/Ca^{2+} exchanger (NCLX) CGP 37157, was applied. This inhibitor has previously been used in human astrocytes at 10 μM (Cabral-Costa et al. 2023), in isolated rat neurons at 10 μM (Ruiz et al. 2014) and in mouse astrocytes at 20 μM concentrations (Parnis et al. 2013). In line with concentrations utilised in literature, concentrations of 10 and 20 μM CGP 37157 were applied within the model.

In other studies, a similar phenomenon regarding apparent independence of veratridine on VGCC activity was observed, but conversely was still found dependent on extracellular calcium (Platel et al. 2005). Blockade of reverse-mode of the plasma-dwelling Na^+/Ca^{2+} exchanger (NCX) via 1 μM KB-R7943 in mouse pre-plate (cortex) cells, blocked veratridine-stimulated responses (Platel et al. 2005). In bovine chromaffin cells, veratridine-stimulated Ca^{2+} uptake and catecholamine release was successfully inhibited with concentrations of KB-R7943 up to 10 μM, in a dose-dependent manner (Soma et al. 2006).

Therefore, concentrations of 1 and 10 μM KB-R7943 were applied to tissues 30 minutes prior to veratridine. I hypothesised that disruption of either of these reported alternative routes of Ca^{2+} entry would result in reduced veratridine-mediated lipolysis.

However, inhibition of mitochondrial sources of Ca^{2+} with CGP 37157 at 10 (N=3, $P>0.05$) or 20 μM (N=3, $P>0.05$) concentrations did not reduce veratridine-evoked lipolysis after 3 hours (Figure 4.10 A). Application of CGP 37157 under basal conditions also had no significant effect compared to vehicle controls (N=3, $P>0.05$, Figure 4.10 A). Additionally, inhibition of external Ca^{2+} entry via reverse mode of the plasmalemmal

Na^+/Ca^{2+} exchanger caused no significant reduction in lipolysis in veratridine-stimulated tissues pre-exposed to 1 (N=3, P>0.05) or 10 μM (N=3, P>0.05) KB-R7943, after 3 hours (Figure 4.10 B). The addition of KB-R7943 to basal tissues appeared to slightly increase glycerol release above vehicle control values, particularly at 10 μM, however this did not reach significance (N=3, P>0.05) (Figure 4.10 B).

Summary Antagonism of either of the elected alternative routes of veratridine-induced Ca^{2+} increases, neither mitochondrial or plasmalemmal Na^+/Ca^{2+} exchangers, caused any reduction in veratridine-evoked lipolysis, suggesting that veratridine action is independent of Ca^{2+}.

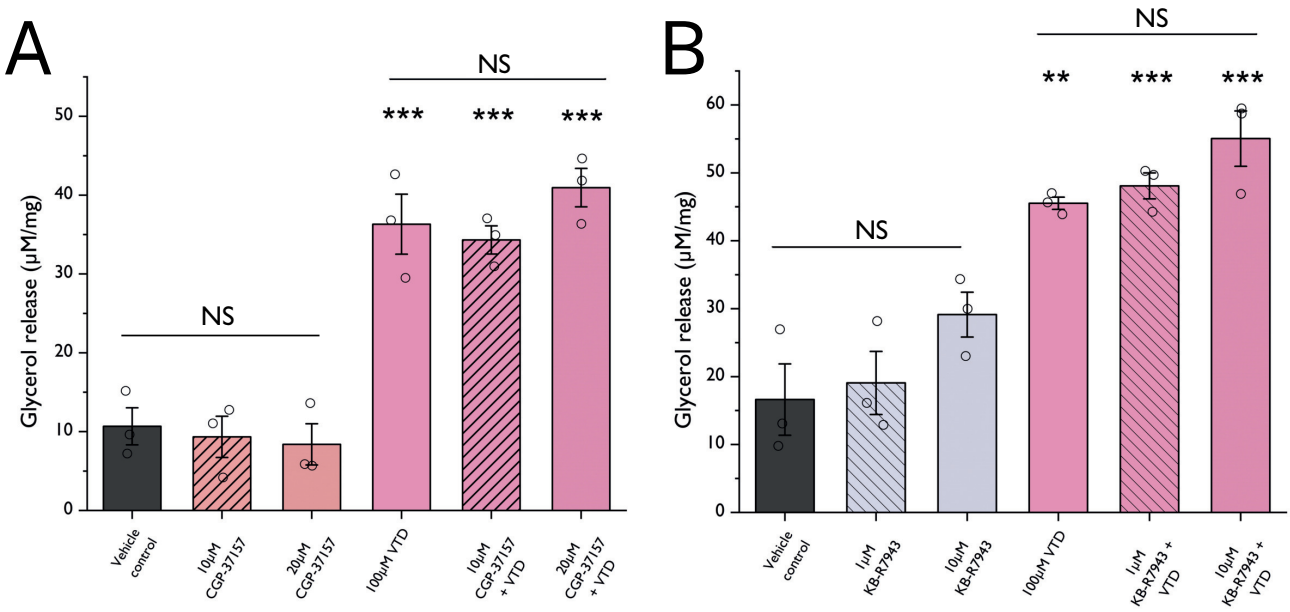

Figure 4.10: Lack of role for alternative Ca^{2+} entry mechanisms via Na^{+}/ Ca^{2+} exchangers on veratridine-evoked lipolysis. Veratridine (VTD) evoked lipolysis challenged with (A) mitochondrial Na^{+}/Ca^{2+} exchange inhibitor CGP 37157 (N=3) (ANOVA) and (B) plasma membrane Na^{+}/Ca^{2+} exchange inhibitor KB-R7943 (N=3) (ANOVA). Significance denoted by **P<0.01 ***P<0.001 versus vehicle controls. Non-significance is denoted by 'NS'. Data represent mean ± SEM of glycerol release corrected to tissue weight. Jitters (open circles) represent each data point (N).

4.3.6 Exploring the role of receptors commonly found prejunctionally in regulating veratridine-stimulated lipolysis

4.3.6.1 α2 adrenergic receptors

In other systems, prejunctionally expressed G_i-linked α2-ARs have been found to be involved in negative regulation of neuronal output, reducing the release of norepinephrine from nerves, for example in control of vascular tone (Hill et al. 2001; Kubes et al. 1992). Rodent white adipocytes are reported to have negligible expression of α2-ARs (Merlin et al. 2018; Valet et al. 2000; Chusyd et al. 2016), offering a route of antagonism that is independent of adipocyte responses. To investigate whether the α2-AR had any role in the regulation of veratridine-evoked lipolysis, the α2-AR antagonist yohimbine was used, possessing high selectivity for α2-AR over α1-AR.

Yohimbine has previously been used at concentrations of 1 μM to increase nerve outflow in rat brain sections (Hagan et al. 1986) and concentrations including 10 μM in corpus cavernosum tissue sections (Filippi et al. 2002).

Therefore, yohimbine at 1 and 10 μM concentrations was used to challenge veratridine-evoked lipolysis. I hypothesised addition of yohimbine would increase the norepinephrine output induced by veratridine, and therefore increase glycerol release.

Yohimbine at 1 (N=3, P>0.05) and 10 μM (N=3, P>0.05) concentrations had no significant effect on veratridine-stimulated lipolysis (Figure 4.11). When applied under basal conditions, yohimbine at 1 or 10 μM also had no effect compared to vehicle controls (N=3, P>0.05).

Under the conditions within the present model, α2-ARs appear to have no role in the regulation of veratridine-stimulated lipolysis, if these receptors are expressed prejunctionally.

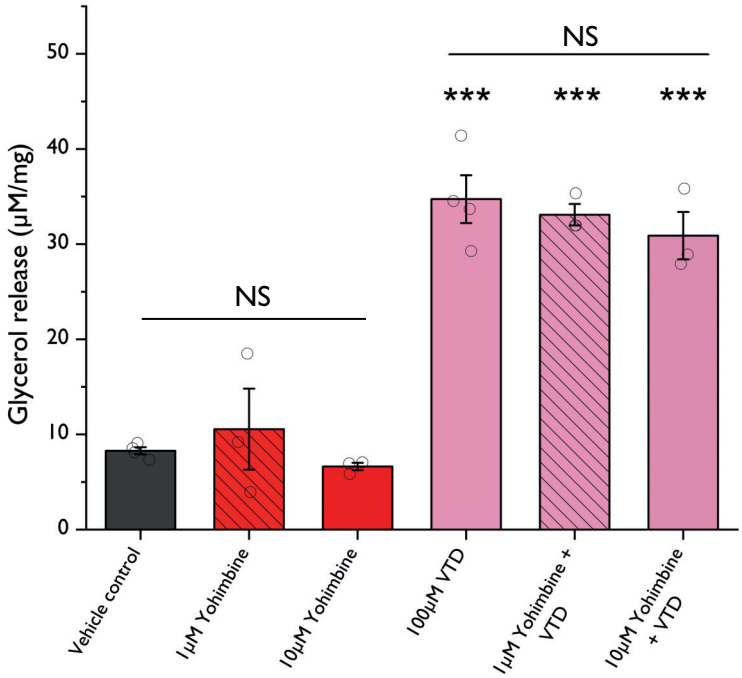

Figure 4.11: Lack of effect of α2-AR antagonism on veratridine-evoked lipolysis Veratridine (VTD) stimulated lipolysis challenged with α2-AR antagonist yohimbine for 3 hours (N=3) (ANOVA). Significance denoted by ***P<0.001 versus vehicle controls. Non-significance is denoted by 'NS'. Data represent mean $\pm$ SEM of glycerol release corrected to tissue weight. Jitters (open circles) represent each data point (N).

4.3.6.2 P2X3 & P2X2/3 receptors

A goal of this PhD project was to understand whether purinergic signalling played any role in white adipose lipolysis regulation, from the perspective of the peripheral nervous system. As ATP is available from multiple sources within adipose tissue, as mentioned in Chapter 1, it offers opportunity for neuromodulatory feedback mechanisms in this system.

P2X3 and heterotrimeric P2X2/3 prejunctional receptors are commonly expressed in sympathetic neurons in other tissues, with roles in modulating neurotransmission (Cockayne et al. 2005; Sperlágh et al. 2007). For example, in Guinea pig atria P2X3 & P2X2/3 receptors on cardiac sympathetic neurons are suggested to potentiate neurotransmitter release via enhancement of sympathetic transmission (Sperlágh et al. 2000). Similarly, P2X3 and P2X2/3 receptors were found to be involved in facilitatory modulation of nore-

pinephrine outflow in rat sympathetic nerves of the vas deferens (Queiroz et al. 2003). Literature reviewed suggests P2X2 and P2X3 receptor subunits are not readily expressed on mouse white adipocytes, offering a potential target independent of adipocytes.

Investigation into the contribution of these receptors in neuromodulation have been conducted using antagonists in various models. For example, antagonist A-317491 was found to be effective at blocking α-β-ATP mediated inward current increases in voltage-clamped mouse astrocytes (Lee et al. 2018). Additionally, 10 μM of selective antagonist A-317941 was found to effectively and selectively antagonise P2X3 and P2X2/3 receptors, to reduce nerve injury and nociceptive perception in rats (Jarvis et al. 2002).

Therefore, to ascertain whether these receptors had a functional role in this model, purinergic receptors P2X3 and P2X2/3 were selectively antagonised with A-317491 at concentrations of 10 μM, in line with literature. I hypothesised, given results in other tissues using this compound successfully, I may expect blockade of these receptors (if found prejunctionally) to result in reduced glycerol release.

There was no significant change in glycerol release in tissues exposed to A-317491 under veratridine-stimulated conditions (N=5, P>0.05), or when applied under basal conditions compared to vehicle controls (N=5, P>0.05) (Figure 4.12 A). These data suggest the receptors have no role.
During research post-data collection, a piece of literature was found suggesting mouse nerve terminals lack neuromodulatory P2X receptors (Norenburg et al. 2001). Therefore, I performed immunocytochemistry using anti-P2X2 and anti-P2X3 antibodies to target protein expression of these receptors, while co-staining for putative sympathetic nerves with anti-TH antibodies.

Using whole mount immunocytochemistry approaches to investigate the presence of P2X2 and P2X3 protein, there appeared to be a lack of P2X2 (N=3) and P2X3 (N=2) positive staining observed in sympathetic nerves of the inguinal fat pad (Figure 4.12 B). The antibodies when applied to human astrocytoma 1321N1 cell lines overexpressing P2X2 or P2X3, respectively, positively stained for P2X2 (N=3) and P2X3 (N=3), indicating the primary antibody was able to detect the protein when present (Figure 4.12 C). There was a lack of staining in secondary-antibody only controls, indicating the antibody

was selective for the P2X2 and P2X3 receptor, and DAPI staining indicates cells were present (Figure 4.12 C).

Summary Together these data indicate that P2X3 & P2X2/3 receptors have no role in modulating veratridine-stimulated lipolysis as they appear not to be prejunctionally expressed, using the conditions and techniques applied here.

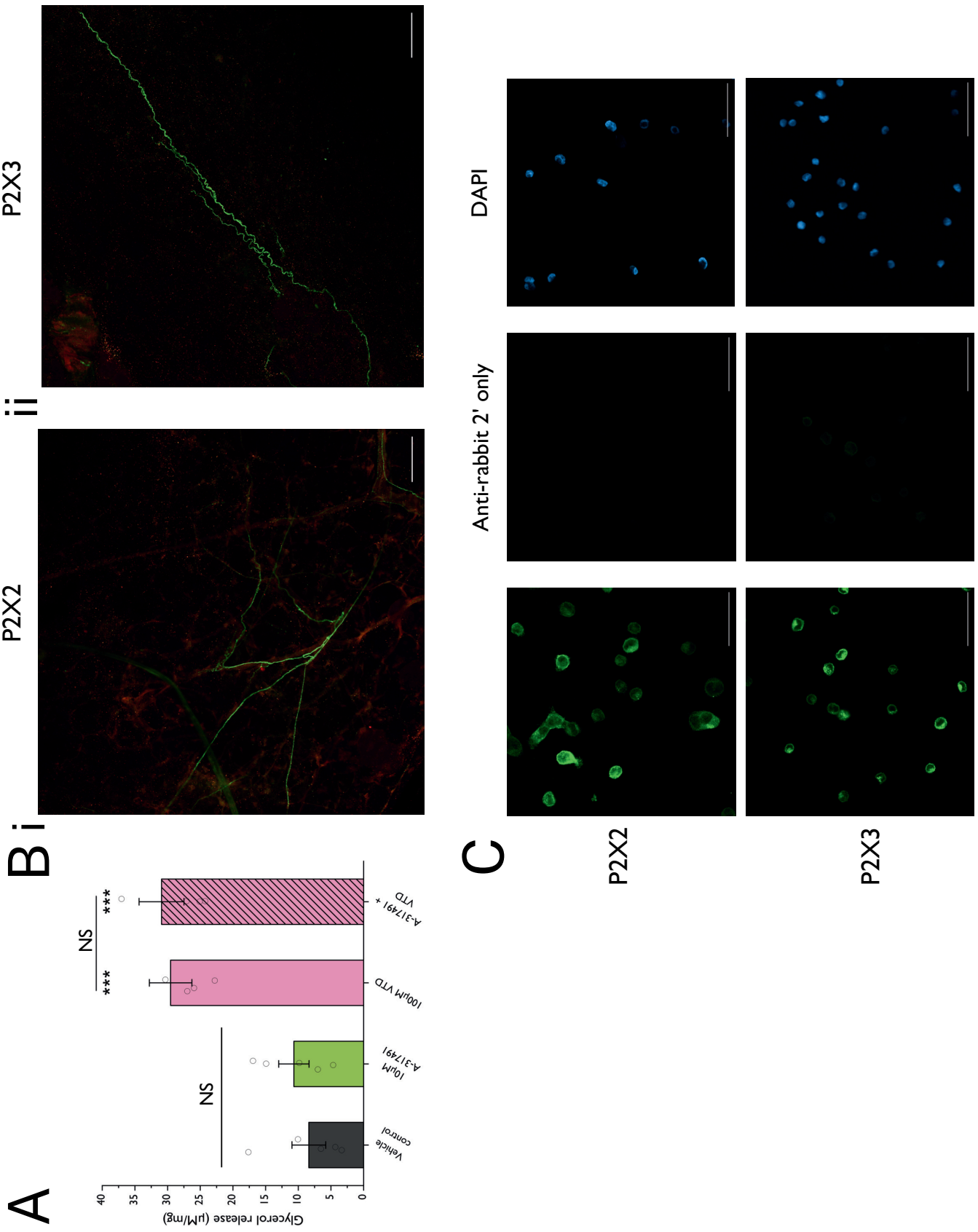

(Figure legend on next page.)

Figure 4.12: Lack of function and expression of P2X3 P2X2/3 receptors on nerves innervating the inguinal fat pad. (A) Effects of P2X3 P2X2/3 antagonism using A-317491 on veratridine (VTD) stimulated lipolysis (N=5) (ANOVA). Significance denoted by ***P<0.001 versus vehicle controls. Non-significance is denoted by 'NS'. Data represent mean ± SEM of glycerol release corrected to tissue weight. Jitters (open circles) represent each data point (N). (B) Representative images of whole mount immunocytochemical staining for (i) P2X2 (N=3) and (ii) P2X3 (N=2) receptors (both red, Alexa 647), alongside tyrosine hydroxylase staining for sympathetic nerves (green, Alexa 488). (C) Representative images for human astrocytoma cell lines over-expressing P2X2 and P2X3 and stained with antibodies against P2X2 (N=3) and P2X3 (N=3) (green, Alexa 488). Dapi staining of cell nuclei in blue. Cell images are representative of at least 3 fields of view (n) from 3 culture wells (N) of cells. Scale bars represent 100 μm in (B) and 50 μm in (C).

4.3.7 Investigating the role of sensory neuropeptides in veratridine-evoked lipolysis

Veratridine, as previously discussed in this chapter, targets Na_V channels, which are found along the axonal projections of both sympathetic and sensory peripheral neurons, with overlapping expression of TTX-sensitive subtypes e.g. Na_V 1.7 (Ruiz et al. 2015). As found in Chapter 3, there exists a heterologous population of neurons in the *ex vivo* sections of tissue used within this work, which may equally possess veratridine-sensitive Na_V channels. As veratridine non-discriminately stimulates the population of neurons in the tissue, there could be both a sympathetic and sensory discharge of transmitter, which both contribute to the lipolytic response. While data from Chapter 3 suggests these non-sympathetic, putative sensory subtypes were not found to innervate away from vasculature and bundles into the parenchyma, it is still possible that antidromic release of neuropeptides could affect populations of adipocytes proximal to points of innervation, for example vasculature.

Receptors for sensory neuropeptides, both SP and CGRP, are found expressed on white adipocytes (Miegueu et al. 2013; Liu et al. 2017; Halloran et al. 2020). Studies have demonstrated that SP induces lipolysis in primary adipocyte cultures (Miegueu et al.

2013). Conversely, studies have shown that the other main transmitter of sensory origin, CGRP, has an anti-lipolytic role in mice (Liu et al. 2017). While other studies have indicated CGRP having a lipolytic role in 3T3-L1 cells (Walker et al. 2014). Therefore, it is important to delineate the effects observed and clarify what neurotransmitter components are responsible for the lipolytic response observed post-veratridine stimulation.

Potent and selective antagonists of both SP receptors (CP-96345) and CGRP receptors (BIBN 4096) have been shown to be effective in the nanomolar range; CP-96345 IC50 34 nM in COS-7 cells (Vrecl et al. 2004), BIBN 4096 IC50 10 nM in rat neuroblastoma cells (Doods et al. 2000). Also, both have been used at 1 μM concentrations; CP-96345 1 μM in mouse pulmonary tissue *ex vivo* (Manzini 1992), BIBN 4096 1 μM in mouse brain sections (Liu et al. 2020). Therefore, 100 nM and 1 μM concentrations were used for both CP-96345 and BIBN 4096 in veratridine-stimulated conditions, to determine whether blockade of either receptor causes a change in glycerol release.

Tissues antagonised with at 100 nM (N=5, P>0.05) or 1 μM (N=5, P>0.05) concentrations of BIBN 4096 experienced no significant change in glycerol release post-veratridine exposure compared to veratridine alone, after 3 hours (Figure 4.13 A). Application of BIBN 4096 under basal conditions at either concentration did not alter glycerol release compared to vehicle controls (N=5, P>0.05) (Figure 4.13 A). Similarly, there was no significant change observed in glycerol release when tissues were antagonised with 100 nm (N=5, P >0.05) or 1 μM (N=5, P >0.05) CP-96345, under veratridine-stimulated conditions after 3 hours (Figure 4.13 B). Nor was there an effect of CP-96345 at either concentration applied under basal conditions, compared to vehicle controls (N=5, P>0.05) (Figure 4.13 B).

Summary It can be surmised based on these data that the antagonism of receptors for two main neuropeptides of sensory origin, SP and CGRP, are not involved in the observed veratridine-stimulated glycerol release response in this model.

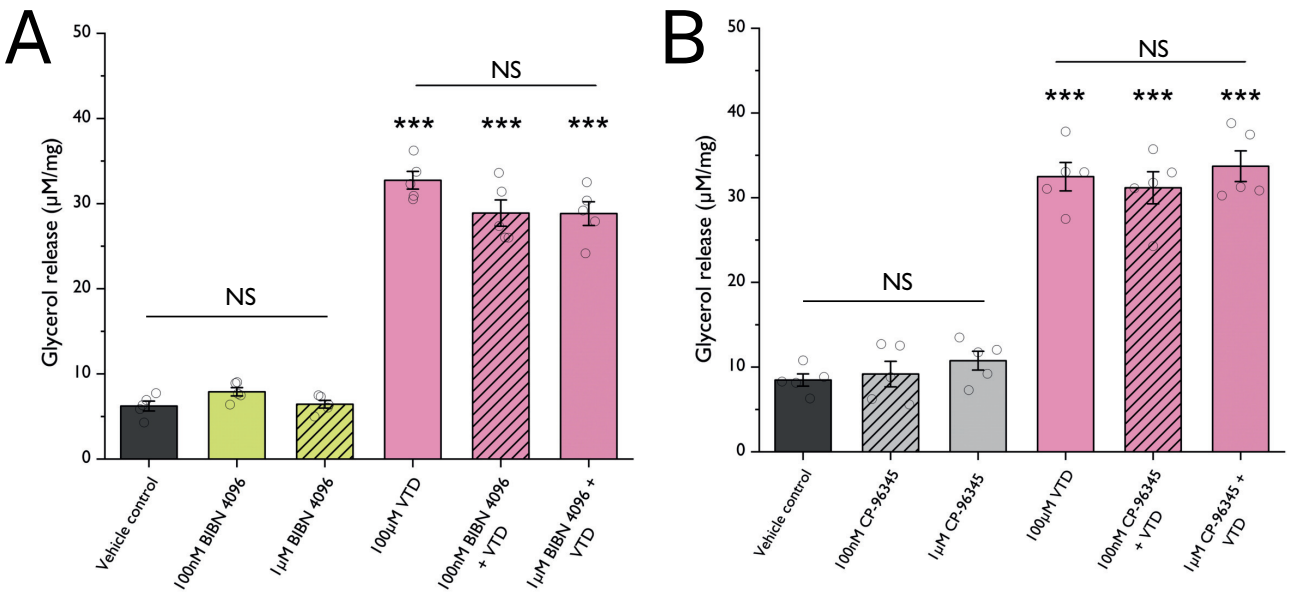

Figure 4.13: Antagonism of CGRP and SP receptors had no impact on veratridine-stimulated lipolysis. Antagonism of veratridine (VTD) stimulated lipolysis with (A) CGRP receptor antagonist BIBN 4096 (N=5) (Welch's ANOVA) and (B) SP receptor antagonist CP-96345 (N=5) (ANOVA) after 3 hours. Significance denoted by ***P<0.001 versus vehicle controls. Non-significance is denoted by 'NS'. Data represent mean ± SEM of glycerol release corrected to tissue weight. Jitters (open circles) represent each data point (N).

4.3.8 Investigating the role of other sympathetic-derived neurotransmitters in veratridine-evoked lipolysis

A strength of the neurogenic approach is that veratridine theoretically stimulates non-discriminatory deployment of transmitter from sympathetic neuron synapses, which are generally accepted to wield multiple transmitter subtypes, such as ATP and NPY alongside principle catecholamine, norepinephrine (Burnstock 2009). Therefore a core aim in the development of the present study was to determine the contribution of the transmitters to the stimulated lipolysis response observed.

4.3.8.1 NPY receptors

NPY receptors are heavily implicated in CNS-level feeding and appetite control, but evidence also suggests function on adipocytes directly (Zhang et al. 2014). According to literature, the common receptor subtypes found on white adipocytes are Y1 and Y2 (Kuo et al. 2007; Wittrisch et al. 2020; Loh et al. 2015) and therefore represent candidates for antagonism in the veratridine model. Given literature suggests NPY reduces lipolysis in favour of lipid accumulation and adipocyte differentiation (Zhang et al. 2014; Chao et al. 2011) and leads to decreased lipolysis under stimulated conditions (Turtzo et al. 2001), its possible NPY released conjunctionally with norepinephrine acts to balance and tune lipolysis. Therefore, I hypothesised antagonism of the NPY receptors may show an increased glycerol release if they indeed act as negative regulators.

To investigate NPY contribution to lipolysis, I therefore employed BIBO 3304 and BIIE 0246, which act as potent antagonists of Y1 and Y2 receptors, respectively. Y1 receptor antagonist BIBO 3304 has previously been used at 300 nM in an *ex-vivo* model using colon tissue preparations stimulated with veratridine (Hyland et al. 2005), while other studies have used 1 μm in mouse pancreatic islet cells (Yang et al. 2022) and in rat brain (Dumont et al. 2000). Similarly, Y2 receptor antagonist BIIE 0246 has been used at concentrations of 1 μM (Hyland et al. 2005). Other studies have used BIIE 0246 at 1 μM, in human hepatoma cells (Kaji et al. 2016), and in mouse podocytes (Lay et al. 2020). Therefore, a final concentration of 1 μM BIBO 3304 and BIIE 0246 was selected for use to investigate NPY signalling in veratridine-stimulated lipolysis.

Antagonism of Y1 receptors using BIBO 3304 had no significant effect on veratridine-stimulated lipolysis (N=5, P>0.05) (Figure 4.14 A). Similarly, antagonism of Y2 receptors with BIIE 0246 also saw no change in lipolysis in veratridine-stimulated conditions (N=5, P>0.05) (Figure 4.14 B). Neither antagonist BIBO 3304 (N=5, P>0.05) or BIIE 0246 (N=5, P>0.05) had any significant effect when applied under basal conditions compared to vehicle controls (Figure 4.14 A & B).

These data suggest that if NPY is released onto surrounding adipocytes upon veratridine stimulation, it has limited action, at least via Y1 and Y2 receptors, in regulating stimulated lipolysis. It is possible that Y1 & Y2 receptors are not the functionally dominant subtype in this system and have less contribution compared to others. Researchers have emphasised that NPY influences metabolic function in peripheral tissues via Y1 and Y2 but also less commonly, Y5 receptor signalling. While generally considered to be more localised and functional within the CNS, the Y5 receptor offers another candidate NPY receptor subtype to explore in adipose (Turtzo et al. 2001; Long et al. 2015; Zhang et al. 2014).

A range of studies have employed selective Y5 antagonist L-152804 to investigate the functional role of Y5 receptor and as a obesity-reducing target. Literature has displayed a wide range of concentrations in different biological applications, with concentrations of 100 nM in rats and 3T3-L1 cell lines (Kanatani et al. 2000; Long et al. 2015), concentrations of 1 & 100 μM in the DRG (Santos-Carvalho et al. 2013) and 1 μM up to 30 μM concentrations in sections of rat brain (Silva et al. 2007).

Therefore, next I antagonised the Y5 receptor subtype using potent and selective L-152804 at concentrations of 1 and 10 μM, representing middling values of the array of concentrations observed in literature.

There was no significant effect of Y5 antagonism on glycerol release in veratridine-stimulated at 1 (N=5, P>0.05) or 10 μM (N=5, P>0.05) concentrations after 3 hours (Figure 4.14 C). Nor was there an effect on basal lipolysis compared to vehicle controls (N=5, P>0.05). The NPY Y5 receptor therefore appears to have no role in veratridine-stimulated lipolysis in this model.

Summary At the concentrations and conditions applied here, with the combined

results from antagonism of Y1, Y2 and Y5 , these data indicate that NPY may not be released in veratridine induced nervous excitation, or if it is, it does not have any measurable impact on adipocyte lipolysis via these receptors.

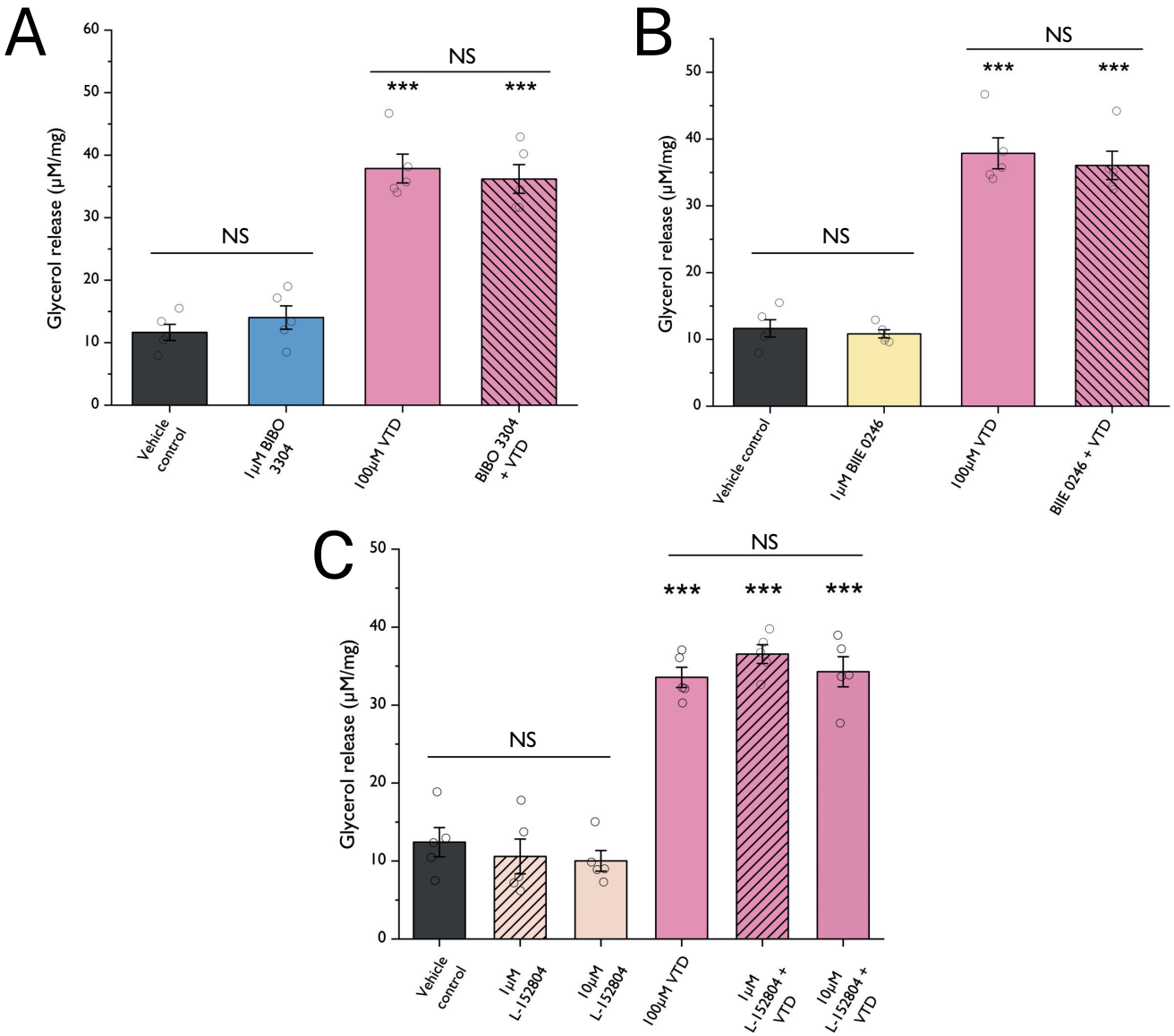

Figure 4.14: Antagonism of NPY receptors Y1, Y2 and Y5 has no effect on veratridine-stimulated lipolysis. Effects of antagonising NPY signalling via (A) Y1 receptor (BIBO 3304) (N=5) (ANOVA), (B) Y2 receptor (BIIE 0246) (N=5) (ANOVA) and (C) Y5 receptor (L-152804) (N=5) (ANOVA) on veratridine (VTD) stimulated lipolysis, after 3 hours. Significance denoted by ***P<0.001 versus vehicle controls. Non-significance is denoted by 'NS'. Data represent mean ± SEM of glycerol release corrected to tissue weight. Jitters (open circles) represent each data point (N).

4.3.8.2 ATP

Having already established a lack of role for P2X3 and P2X2/3 purinergic receptors in the present model (section 4.3.6.2), the next experiments intended to establish whether potentially co-released ATP had a postjunctional role, as observed in other tissues. This may apply in adipose tissue to modulate the lipolysis-inducing activity of norepinephrine. Harnessing the development of the *ex vivo* model and neuro-stimulatory tool throughout this chapter, and to satisfy initial aims of the project, the role of P2 purinergic signalling under neurogenic *ex vivo* conditions was investigated.

To explore the role of potentially released ATP in veratridine-driven lipolysis, broad spectrum antagonists of purinergic receptors were applied.
Suramin is a non-selective competitive antagonist of P2 receptors (Lambrecht et al. 1992). Suramin has been utilised as a tool for general purinergic blockade in many studies. For example, suramin has been used to antagonise purinergic signalling at 200 μM in rat fundus preparations (Jenkinson et al. 2000) and 100 μM in murine cell cultures (Lin et al. 2008). Therefore concentrations of 100 μM suramin were applied under veratridine-stimulated conditions.

Pyridoxalphosphate-6-azophenyl-2',4'-disulfonic acid (PPADS) is another broad-spectrum P2R inhibitor (Billington et al. 2007). PPADS has been used as a general purinergic antagonist in other systems. For example, 100 μM was used to reduce ATP- and EFS-induced responses in rat and Guinea pig intestine (Windscheif et al. 1995), and to suppress depolarisation of rat nodose ganglion cells (Bobryshev et al. 2012). Therefore, 100 μM PPADS was endogenously applied to tissues to antagonise purinergic receptors in the present model.

Preincubation of tissues with suramin at 100 μM had no significant impact on veratridine-stimulated lipolysis (N=5, P>0.05) after 3 hours, and there was no effect observed of suramin applied under basal conditions compared to vehicle controls (N=5, P>0.05) (Figure 4.15 A).

Similarly, there was no significant change in glycerol release observed in veratridine-stimulated tissues when preincubated with 100 μM PPADS after 3 hours (N=5, P>0.05). No effects were observed with PPADS application in unstimulated conditions compared

to vehicle controls (N=5, P>0.05) (Figure 4.15 B). These data suggest P2 purinergic signalling has no role in lipolysis, or that veratridine may not induce ATP release from nerves.

In response to the lack of effects of PPADS in veratridine-evoked lipolysis, to validate the results attained with veratridine, 100 μM PPADS was subsequently applied under a submaximal concentration of norepinephrine.

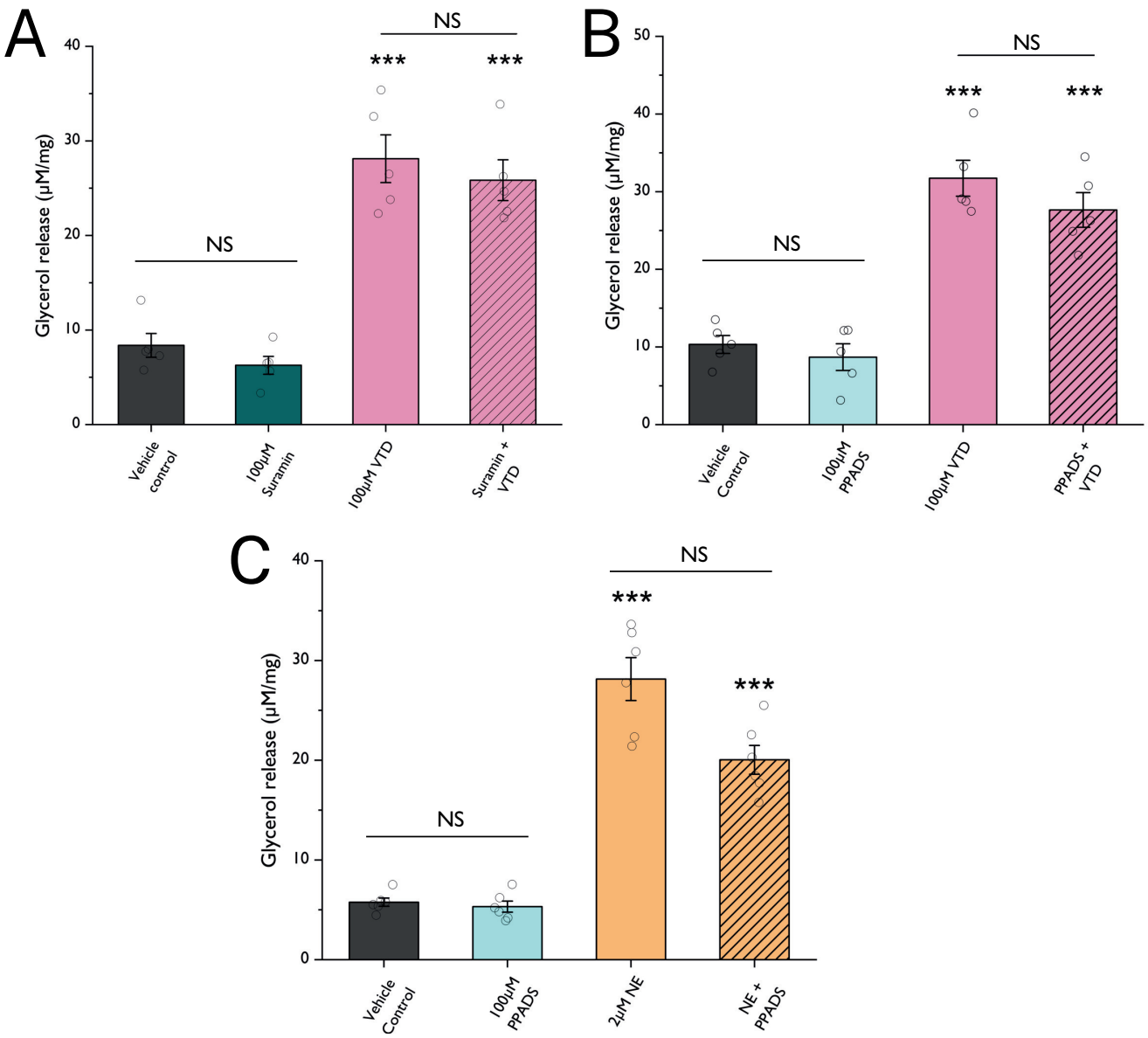

Figure 4.15: Non-selective antagonism of purinergic signalling had no effect on veratridine or norepinephrine stimulated lipolysis. Effect of suramin on (A) veratridine (VTD)-evoked lipolysis (N=5) (ANOVA) and the effect of PPADS on (B) veratridine (N=5) (ANOVA) and (C) norepinephrine (NE)-evoked lipolysis (N=6) (Welch's ANOVA), after 3 hours. Significance denoted by ***P<0.001 versus vehicle controls. Non-significance is denoted by 'NS'. Data represent mean ± SEM of glycerol release corrected to tissue weight. Jitters (open circles) represent each data point (N).

4.3.8.2.1 Selective P2R antagonism

General P2R antagonists suramin and PPADS are known to have unequal antagonistic activity across the P2R subtypes (Ralevic et al. 1998). To have a more direct approach to investigate purinergic role in lipolysis, total RNA of freshly isolated adipocytes was examined to identify specific subtypes expressed.

Firstly, to establish that isolated adipocytes were free from contamination of other cell types of the stromal vascular fraction (SVF) and ensure any observed expression of purinergic receptors was therefore restricted to adipocytes, extracted adipocyte mRNA was pre-screened for purity using a panel of SVF markers (Chapter 2, Table 2.2). The SVF markers were effective at detecting bands of the expected size when used in whole fat tissue (Figure 4.16 A). Only RNA of 'pure' populations of adipocytes were further probed for purinergic receptor expression, which revealed the presence of mRNA for the *P2x4* receptor in 5/5 experiments, and *P2y6* receptor in 3/5 experiments (N=5) (Figure 4.17 A). Purinergic receptor mRNA expression in the whole adipose extracts illustrated that all receptors with the exception of *P2y1* (2/4) and *P2y4* (1/4) receptors were found expressed consistently over 4 repeats (N=4) (Figure 4.17 B). The positive expression of housekeeping gene *Gapdh* in each iteration confirmed that quality cDNA was present and reverse-transcriptase negative controls indicate a lack of genomic DNA contamination.

In order to determine whether the purinergic receptors revealed in pure adipocyte RT-PCR preparations had any role in veratridine-stimulated or basal lipolysis, specific antagonists of P2X4 and P2Y6 receptors were employed in the present model. PSB-12062 is a selective antagonist of the P2X4 receptor, previously used within the Fountain lab at 10 μM concentrations (Layhadi et al. 2018). Therefore, PSB-12062 was applied at 10 μM.

The selective P2Y6 receptor antagonist MRS 2578 has been used repeatedly in various models including rodent cardiomyocytes (Nishida et al. 2008), and in neutrophils (Zheng et al. 2018), all at 10 μM concentrations. Therefore 10 μm was the elected concentration applied under veratridine-stimulated conditions.

Based on the identity of the receptors identified and slightly anti-lipolytic leaning reports in literature, I hypothesised there may be an increase in glycerol release when these receptors were antagonised.

There was no significant change in glycerol release from tissues pre-incubated with the P2X4 receptor antagonist PSB-12062 under veratridine-stimulated conditions (N=5, P>0.05) (Figure 4.18 A). Similarly, there was no significant change in glycerol release in tissues pre-exposed to the P2Y6 receptor antagonist MRS 2578 under veratridine-stimulated conditions (N=5, P>0.05) (Figure 4.18 B). There was no significant change in lipolysis when PSB-12062 (N=5, P>0.05) or MRS 2578 (N=5, P>0.05) was applied under basal conditions compared to respective vehicle controls.
These data suggest no role for P2X4 or P2Y6 in basal or stimulated lipolysis regulation.

Summary Under these conditions, application of neither broad (PPADS and suramin) or selective (PSB-12062 & MRS 2578) antagonists of purinergic receptors had no effect on stimulated or basal lipolysis, suggesting that P2 purinergic signalling does not act to meaningfully regulate lipolysis within this model.

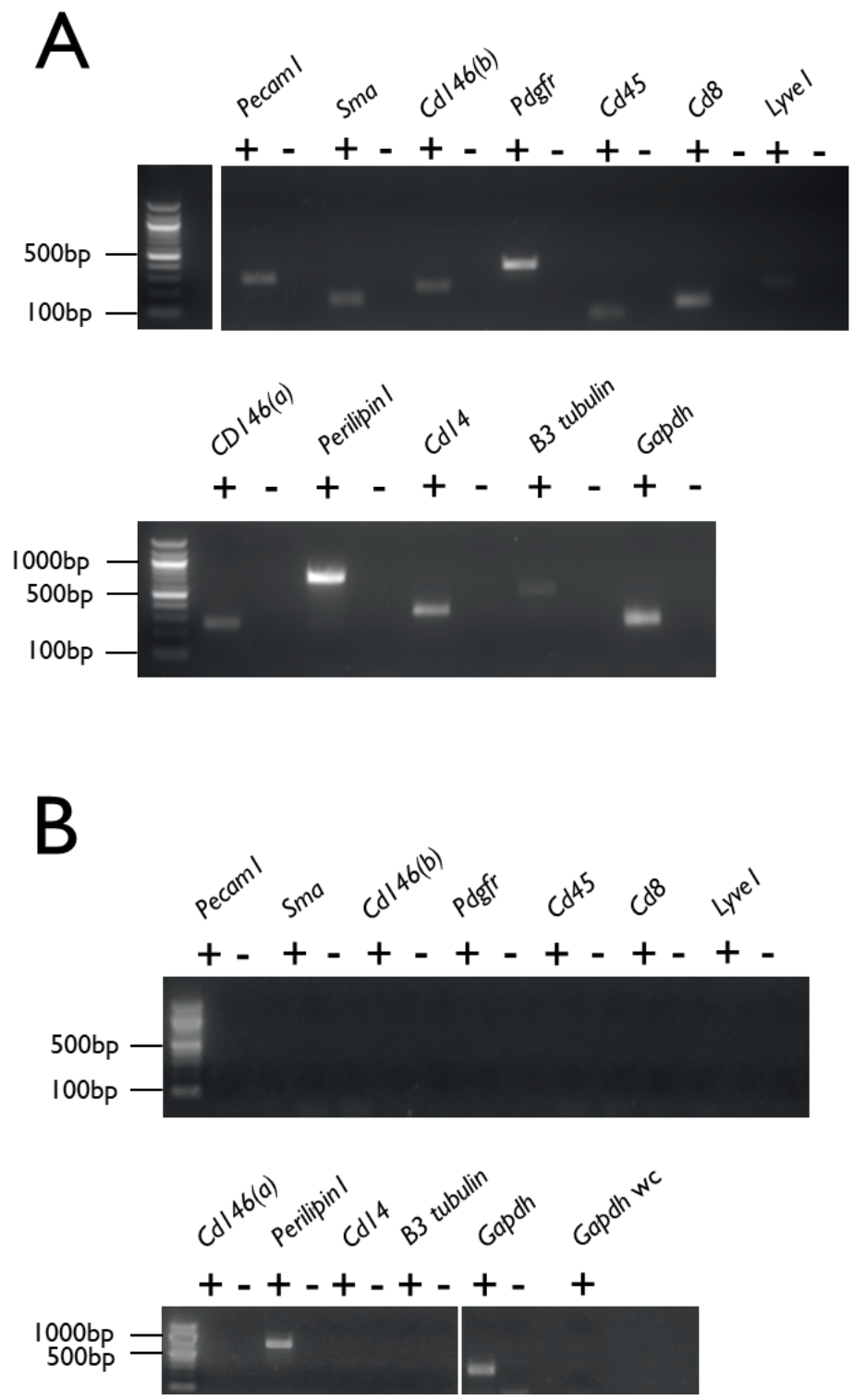

(Figure legend on next page.)

Figure 4.16: Non-quantitative RT-PCR indicating absence of stromal-vascular components in isolated white adipocytes compared to whole fat. Representative gels showing detection of stromal vascular fragment components; *Pecam1* (273 bp), α-*Sma* (144bp), *Cd146* a (261 BP) & b (211 BP), *Pdgfrb* V2 (PDGFR) (367 bp), *Cd45* (71 bp), *Cd8* (121 bp), *Lyve1* (214 bp), *perilipin1* (705 bp), *Cd14* (350 bp), *B3tubulin* (534 bp) and housekeeper gene *Gapdh* (266 bp) in (A) whole white adipose (N = 4) or (B) isolated white adipocytes (N = 10), from inguinal fat pads. Where '+' refers to presence and '-' to absence (and thus negative control for genomic contamination) of reverse transcriptase (RT) cDNA samples. *Gapdh* water control (WC) refers to samples containing all reagents, *Gapdh* primers and RT, but without cDNA (as control for reagent contamination).

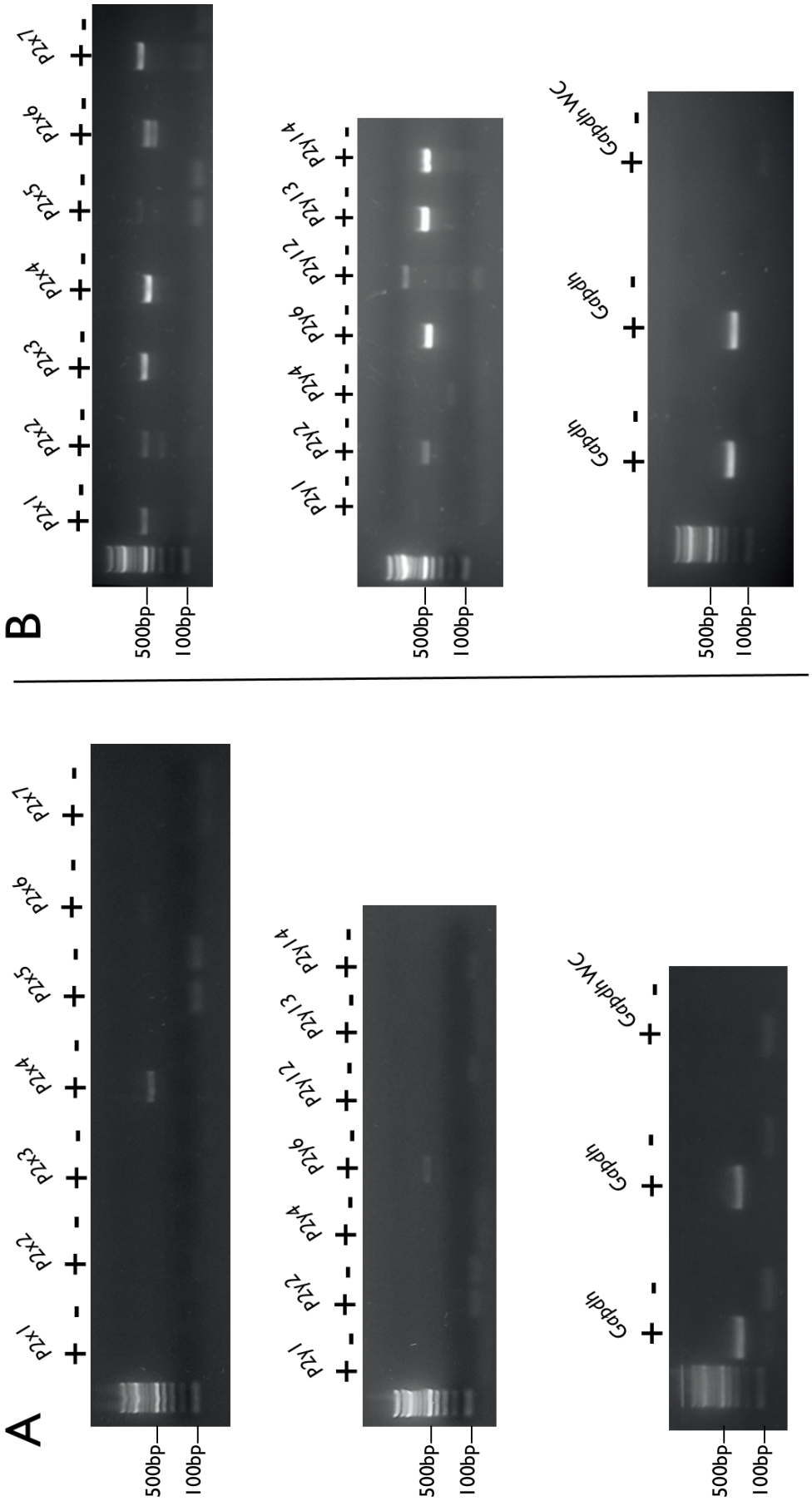

(Figure legend on next page.)

Figure 4.17: Non-quantitative RT-PCR expression of P2R receptors in isolated adipocytes and whole fat. Representative gels showing detection of P2 receptor mRNA; *P2x1* (505 bp) *P2x2* (499 bp), *P2x3* (533 bp), *P2x4* (500 bp), *P2x5* (647 bp), *P2x6* (566 bp), *P2x7* (712 bp), *P2y1* (668 bp) *P2y2* (516 bp), *P2y4* (492 bp), *P2y6* (500 bp), *P2y12* (978 bp), *P2y13* (591 bp), *P2y14* (571 bp), housekeeper gene *Gapdh* (266 bp) in (A) pre-screened populations of isolated white adipocytes (N = 5) and (B) in whole white adipose (N = 4) from inguinal depots. Where '+' refers to presence and '-' to absence (and thus negative control for genomic contamination) of reverse transcriptase (RT) cDNA samples. *Gapdh* water control (WC) refers to samples containing all reagents, *Gapdh* primers and RT, but without cDNA (as control for reagent contamination).

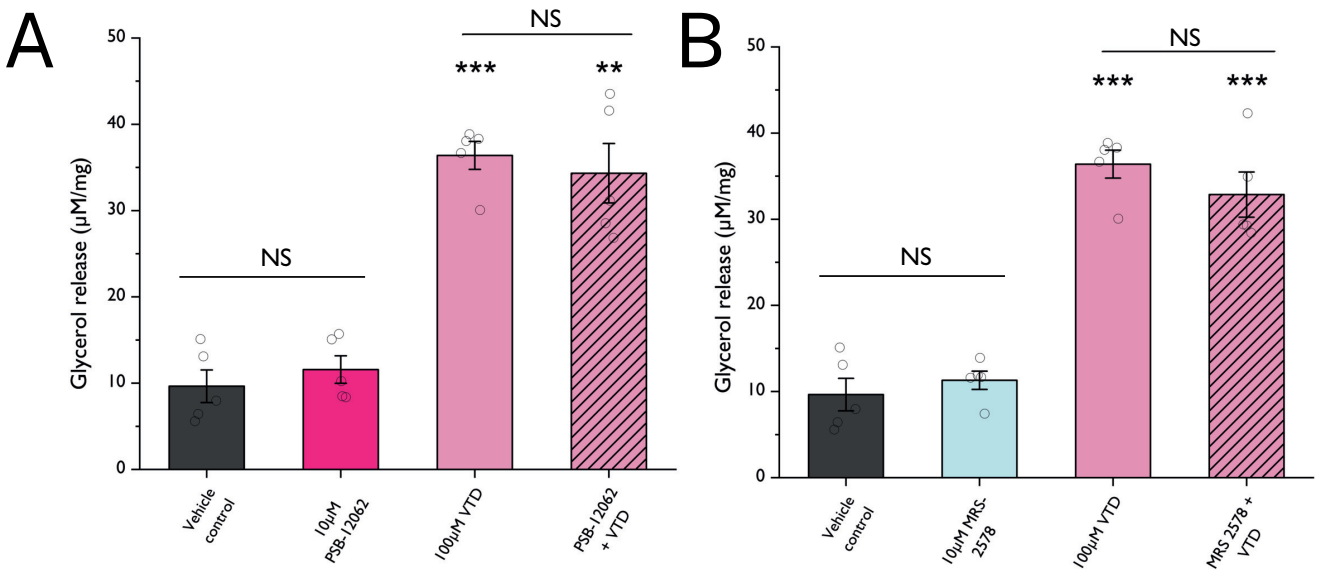

Figure 4.18: Selective antagonism of P2X4 and P2Y6 receptors had no effect on veratridine-stimulated lipolysis. Effect of (A) P2X4 antagonism (PSB-12062) (N=5) (Welch's ANOVA) and (B) P2Y6 antagonism (N=5) (MRS 2578) (ANOVA) on basal and veratridine (VTD)-stimulated lipolysis after 3 hours. Significance denoted by **P<0.01 ***P<0.001 versus vehicle controls. Non-significance is denoted by 'NS'. Data represent mean ± SEM of glycerol release corrected to tissue weight. Jitters (open circles) represent each data point (N).

4.3.9 Investigating the role of purinergic signalling in basal and stimulated lipolysis

To further explore the role of purinergic signalling in this model, a more deliberate approach was needed to ascertain the influence, if any, purinergic signalling had on lipolysis from the perspective of the adipocytes. ATP release by veratridine remains theoretical and may have not been released in previous experiments as hypothesised, thus the expected outcomes of P2 receptor activation had not been fully ascertained. As such this necessitated exogenous addition of nucleotides with removal of nervous influence, thus detangling the response, without the additional complexities of neurogenic stimulation. This approach also allows for observations of receptor activation under basal conditions.

4.3.9.1 Exogenous application of nucleotides to challenge basal and norepinephrine stimulated lipolysis

To perform a complete interrogation, both tri- and di-phosphate forms of adenosine and uridine nucleotides were applied to activate P2 purinergic subtypes present, in order to investigate the role of P2-implicated purinergic signalling in basal and stimulated lipolysis. The use of both adenosine and uridine-based nucleotides accommodates for differential receptor affinities, as P2X receptors have preferential affinity for adenosine-based nucleotides, while most P2Y receptors generally have more affinity for uridine-based nucleotides. Uridine based nucleotides were therefore introduced to eliminate preferential ligand biases and to activate P2Y receptors identified in Section 4.3.8.2 (Jain et al. 2022).

Literature has demonstrated that exogenous application of 100 μM L^{-1} ATP increased glycerol release over basal controls in CH3H10T1/2-derived white adipocyte cell lines (Tozzi et al. 2020) and 100 μM ATP has also been applied to isolated rat white adipocytes (Lee et al. 2005). Concentrations of 100 μM ATP and UTP have been used with endothelial cells (Moerenhout et al. 2001) and by previous PhD student Dr Seema Ali to experimentally challenge stromal cells (Ali 2018). Therefore, to establish the role of purinergic signalling under basal and stimulated conditions in an *ex vivo* model, all nucleotides were applied at high concentrations 100 μM and also 1 mM 30 minutes prior

to incubation with or without norepinephrine. I hypothesised that given literature leans toward more anti-lipolytic roles for the subtypes previously identified here, perfusion with nucleotides may reduce lipolysis.

Under basal conditions, there was no significant alteration in glycerol release observed in tissues exposed to nucleotides ATP, ADP, UTP or UDP at 100 μM (N=4, P>0.05) or 1 mM (N=5, P>0.05), compared to vehicle controls (Figure 4.19 A & C). Under stimulated conditions, there was also no significant change observed in norepinephrine-stimulated tissues pre-exposed to ATP, ADP, UTP and UDP at 100 μM (N=4, P>0.05) or 1 mM (N=5, P>0.05), compared to norepinephrine alone (Figure 4.19 B & D).
In support of data from Section 4.3.8.2, these data suggest that introduction of nucleotides does not reduce lipolysis in basal or stimulated conditions and nor does it evoke lipolysis.

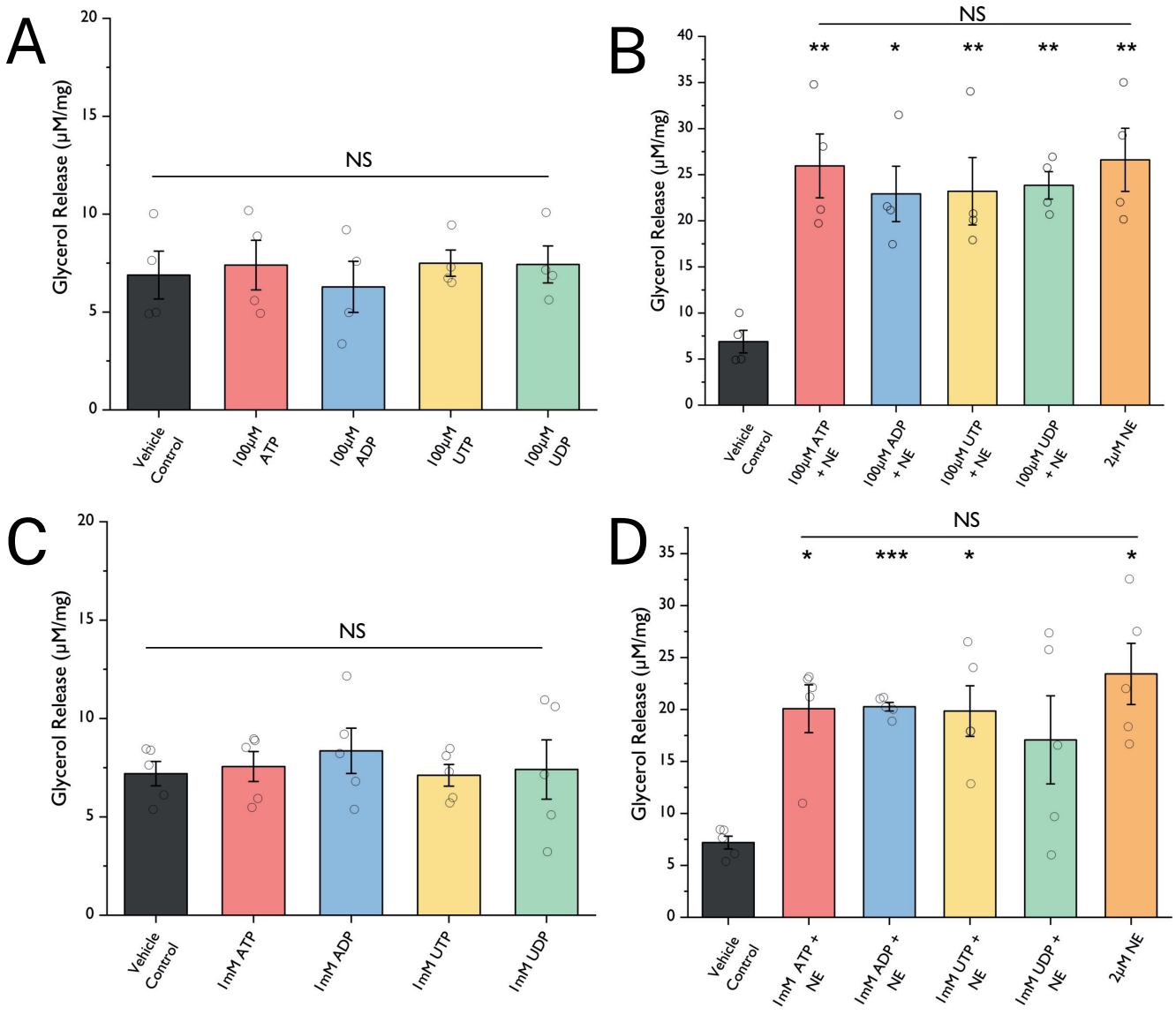

Figure 4.19: Lack of effect of exogenous nucleotide application on basal and norepinephrine-stimulated lipolysis. Effects of 100 μM (A & B) (N=5) and 1 mM (C & D) (N=4) nucleotides ATP, ADP, UTP or UDP on basal (A & C) and norepinephrine (NE) stimulated (B & D) lipolysis after 3 hours. Significance denoted by *P<0.05, **P<0.01, ***P<0.001 versus vehicle controls. Non-significance is denoted by 'NS'. Data represent mean $\pm$ SEM of glycerol release corrected to tissue weight. Jitters (open circles) represent each data point (N). ANOVA used in A, B and C and Welch's ANOVA in D.

4.3.9.1.1 Effect of ectonucleotidase inhibitors on basal lipolysis and nucleotide-supplemented tissue lipolysis

Nucleotides, particularly ATP, are rapidly hydrolysed at 37°C by resident membrane-bound ectonucleotidases expressed on the surface of a multitude of cell types (Pfeifer et al. 2024). The *ex vivo* nature of the experiment may allow for endogenous ectonucleotidase activity to persist, as the adipocytes are still surrounded by their native matrix, especially given tissues are incubated at 37°C. Therefore, the addition of ectonucleotidase inhibitors was required to eliminate this potential.

The chief ectonucleotidase responsible for the breakdown of extracellular ATP and UTP to their respective monophosphates is NTPDase/CD39 (Robson et al. 2006; Giuliani et al. 2021). ARL 67156 is considered the only commercially available competitive ectonucleotidase-inhibitor that acts effectively at CD39 without interfering to a great extent on the purinergic receptors themselves (Robson et al. 2006; Schäkel et al. 2020). ARL 67156 has been previously used in Guinea pig vas deferans at concentrations of 100 μM (Westfall et al. 1996). Therefore, a concentration of 100 μM was taken forward, alongside the application of 100 μM nucleotides or norepinephrine. In consideration of the previous hypothesis, I hypothesised inhibition of ectonucleotidases to result in decreased glycerol release.

Under basal conditions, there was no significant change in glycerol release of tissues exposed to 100 μM ATP, ADP, UTP, UDP compared to their respective groups in the presence of 100 μM ARL 67156 (N=5, P>0.05) (Figure 4.20 A). None of the nucleotide-supplemented groups with or without ARL 67156 deviated from vehicle controls (N=5, P>0.05).

In the absence of exogenous supplementation of nucleotides, there was also no significant difference observed in lipolysis in norepinephrine-stimulated tissues when 100 μM ARL 67156 was present (N=5, P>0.05), and lastly, there was no change in basal lipolysis in tissues sans added nucleotides with exposure to ARL 67156, compared to vehicle controls (N=5, P>0.05) (Figure 4.20 B).

These data infer either nucleotides are not being hydrolysed in previous experimental conditions, or their theoretical preservation using an ectonucleotidase inhibitor has no

impact due to a lack of a role for P2 purinergic signalling on basal or stimulated lipolysis, in support of outcomes in Section 4.3.8.2 & 4.3.9.1.

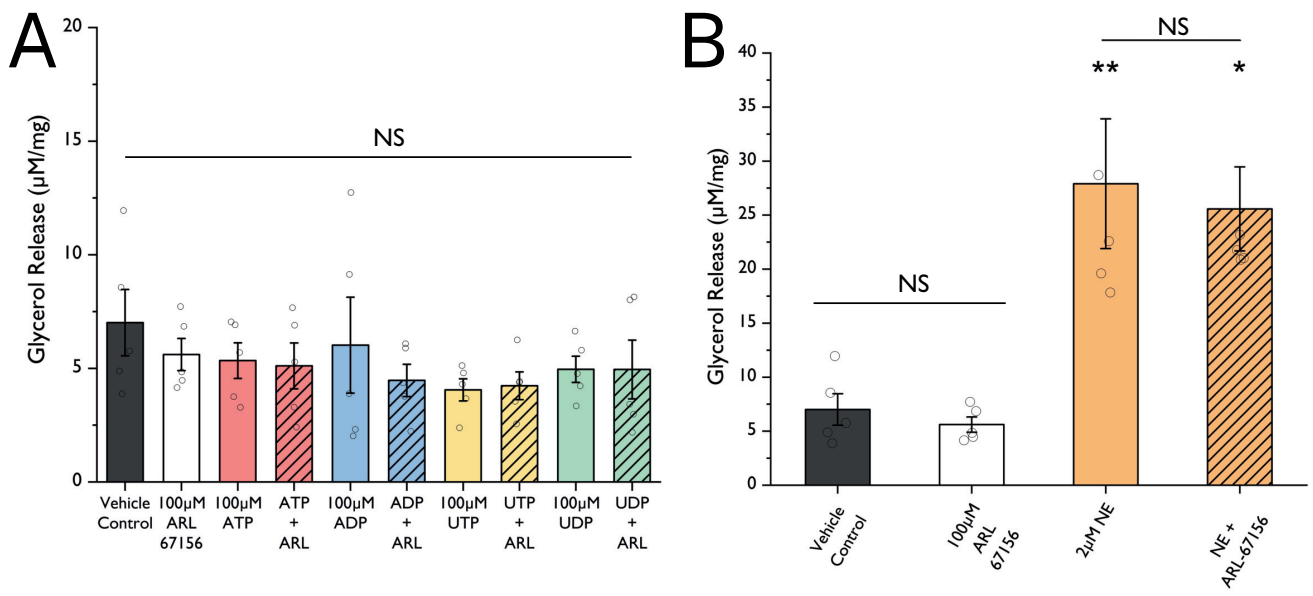

Figure 4.20: Addition of ARL 67156 had no effect on lipolysis under basal conditions with or without nucleotide-supplementation or norepinephrine-stimulated conditions. Effects of ARL 67156 to (A) basal lipolysis of tissues exposed to 100 μM ATP, ADP, UTP or UDP (N=5) (Welch's ANOVA) or (B) basal and norepinephrine (NE)-stimulated lipolysis sans nucleotides (N=5) (ANOVA), after 3 hours. Significance denoted by *P<0.05, **P<0.01 versus vehicle controls. Non-significance is indicated by 'NS'. Data represent mean ± SEM of glycerol release corrected to tissue weight. Jitters (open circles) represent each data point (N).

4.3.9.2 Removal of endogenous nucleotides

The previous data suggesting nucleotides are not impaired by intrinsic ecto-enzyme activity due to the lack of effect of the ectonucleotidase inhibitor, could also imply that nucleotides are already at saturating concentrations under native conditions and may underpin the lack of response, as there are other sources of nucleotides in WAT. Given this model allows tissues to remain intact in sections, there may be constitutive release and persistent activity of associated purinergic receptors, therefore removing the possibility for additional activation.

To compliment and conclude the previous set of purinergic antagonism experiments conducted with veratridine (section 4.3.8.2), I explored enzymatic removal of existing nucleotide signalling opposed to receptor blockade. It was necessary to eliminate

veratridine-stimulated potential of increased nucleotide concentrations, therefore experiments were conducted under norepinephrine-stimulated and basal conditions.

Therefore, in order to fulfill the next step of the investigation, the enzyme apyrase was introduced to hydrolyse nucleotides into their monophosphate forms (ATP and UTP to AMP and UMP respectively) and thereby theoretically reduce P2 signalling cascades. Apyrase has been used at concentrations of 10 U/mL to remove ATP-induced secretion in mouse neutrophils (Karmakar et al. 2016) and in bovine arterial endothelial cells to ablate Ca^{2+} signalling (Moerenhout et al. 2001). Therefore, 10 U/mL was taken forward in the present model. I hypothesised that the addition of apyrase may result in increased glycerol release.

However, the addition of 10 U/mL apyrase had no effect on norepinephrine-stimulated lipolysis (N=5, P>0.05), nor did apyrase have any affect on basal lipolysis compared to vehicle controls (N=5, P>0.05) (Figure 4.21). Again, these data support those observed in Section 4.3.8.2 and prior experiments in the present section suggestive of a lack of role for P2 purinergic signalling in regulation of lipolysis.

Summary Supplementation with adenosine or uridine nucleotides (tri- or di-phosphates) had no impact on stimulated or basal lipolysis and inhibition of potential nucleotide-hydrolysing enzymes also had no effect. This suggests responses to nucleotides under veratridine and norepinephrine-stimulated, or basal conditions, are not impaired by any intrinsic enzymatic activity. Removal of endogenous nucleotides with apyrase appeared to have no effect on glycerol release. These data collectively suggest there is no role for P2 purinergic signalling in regulating lipolysis under conditions applied in the present *ex vivo* model, as presence or absence of nucleotides appears inconsequential to basal or stimulated lipolysis.

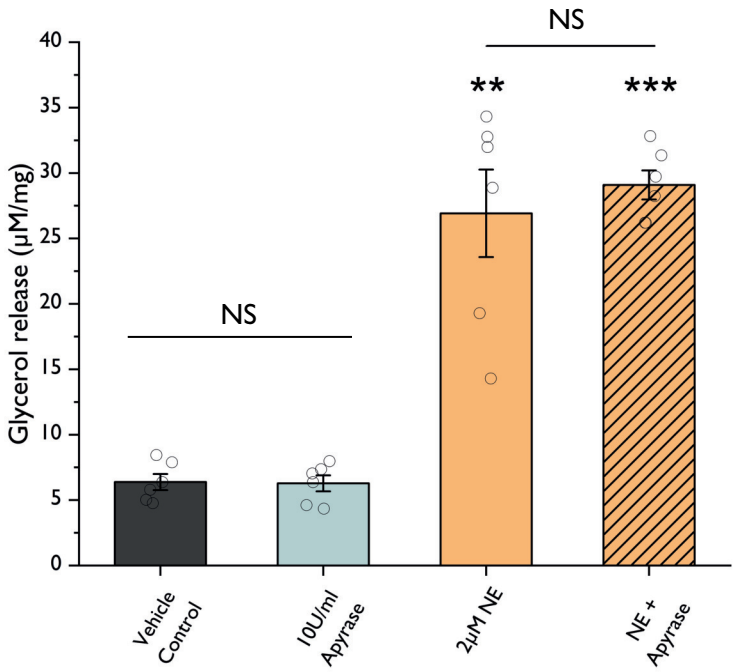

Figure 4.21: Removal of endogenous nucleotides with apyrase had no effect on norepinephrine-stimulated lipolysis. Effect of apyrase on basal and norepinephrine-stimulated lipolysis after 3 hours (N=5) (Welch's ANOVA). Significances denoted by **P<0.01 ***P<0.001 versus vehicle controls. Non-significance is denoted by 'NS'. Data represent mean ± SEM of glycerol release corrected to tissue weight. Jitters (open circles) represent each data point (N).

4.4 Discussion

4.4.1 Veratridine provides a tool to induce lipolysis *ex vivo*

In the beginning of this chapter, I established that *ex vivo* preparations of white adipose tissue from the mouse inguinal fat depot were responsive to exogenous application of both synthetic and natural lipolytic stimulants, which was a critical foundation to the project and satisfied aim 1 of this chapter. Other researchers have already well established similar *ex vivo* models to investigate lipolysis in this manner (Bridge-Comer et al. 2023; Roy et al. 2022), however, none have done so using a neurogenic approach, excluding EFS. EFS when applied to isolated adipocytes has previously been shown to increase the release of glycerol and in some stimulation protocols, to equal or greater extents than that of isoprenaline (Hamida et al. 2011). Therefore the introduction of a simpler model, without the potential direct stimulatory effects on adipocytes, was desired.

Veratridine has previously been used to induce the release of endogenous norepinephrine in other tissue preparations, such as in the rat vas deferens (Bönisch & Trendelenburg 1987), mesenteric arteries (Park et al. 2023) and in isolated nerves (Blaustein et al. 1972). For the first time in white adipose tissue, using veratridine, I was able to successfully meet aim 2 of the chapter and induce lipolysis to the same extent of the other common and well-cited agonists in the field of metabolic research (isoprenaline and norepinephrine). This apparent neurogenic activation of lipolysis then provided a platform for further inquisition as to the roles of various constituents influencing lipolysis, in a more holistic/physiologically valid manner.

The characterisation of the neurogenic lipolytic response was required to fully understand the validity of veratridine as a tool. Figure 4.22 represents the initial working hypothesis.

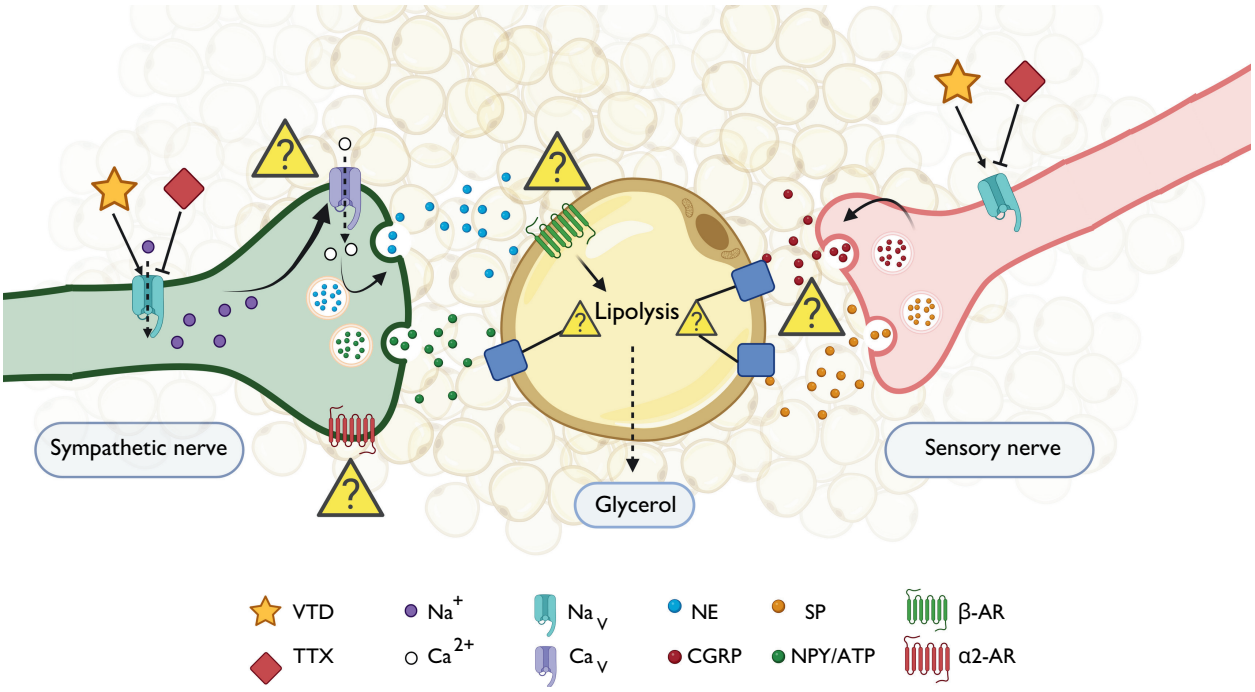

Figure 4.22: Initial proposed hypothesis of veratridine-evoked lipolysis. Illustration of the initial hypothesised route in which veratridine acts to induce lipolysis. Veratridine acting on voltage-gated sodium (Na_V) channels propagates an action potential that results in voltage gated calcium (Ca_V) channel-mediated release of a catecholamine neurotransmitter, which binds to β-adrenergic receptors (ARs) receptors on adipocytes to induce lipolysis. Indicated by the yellow triangle symbol are the areas demanding characterisation, such as involvement of other neurotransmitters, from either sympathetic neuropeptide Y (NPY) and adenosine triphosphate (ATP) or sensory origin substance P (SP) and calcitonin gene-related peptide (CGRP), the specific β-AR receptors involved, and the role of prejunctional neuromodulatory receptors (α2-ARs and P2X2 P2X2/3 receptors) in the response.

4.4.2 Veratridine evoked lipolysis is mediated by VGSCs on a non-adipocyte cell type

To establish whether veratridine was activating neurons as hypothesised, I first targeted VGSCs which are known transducers of action potential conductance (Erickson et al. 2018).

As established in Chapter 1, Na_V 1.1, 1.2, 1.3, 1.4, 1.6, 1.7 & NaX are TTX-sensitive, and Na_V 1.5, Na_V 1.8, & Na_V 1.9 are TTX-insensitive (Zhang et al. 2018). The

Na_V channel subtype commonly found on peripheral sympathetic neurons is Na_V 1.7 (Wang et al. 2017) and Na_V 1.7 & Na_V 1.8 on sensory neurons (Blaszkiewicz et al. 2019a). Encouragingly, through the application of TTX, it was clear that veratridine was acting via Na_V channels, as the veratridine response was completely removed by TTX, suggestive of neuronal activity. Additionally, the lack of effect of TTX on basal lipolysis suggests regulation of basal lipolysis is independent of nerves, in line with literature and by default, independent of Na_V channels (Bartness et al. 2014).

However, Na_V channels can also be expressed on non excitable cell types (Black et al. 2013). For example, Na_V 1.5 has been demonstrated as important to macrophage phagocytosis (Carrithers et al. 2007). While there is no current evidence published to suggest white adipocytes express Na_V channels (Pérez-Medina et al. 2012), there remained a possibility that veratridine was directly stimulating adipocytes, rather than via neurogenic activation. Encouragingly, veratridine failed to illicit lipolysis in isolated adipocytes, while norepinephrine was able to induce robust lipolytic responses, indicating functional retention of a lipolysis pathway. Therefore, this limited the expression of the veratridine-sensitive Na_V channels involved to other components of the stromal vascular fraction.

Nonetheless, I did not directly experimentally deduce and demonstrate the exact component of SVF responsible. Yet, supportive of my results, in a plethora of other models/systems, veratridine has been demonstrated to act via nerves to increase excitation and activity in a TTX-sensitive manner. TTX successfully removed veratridine-induced contractility in mouse mesenteric arteries (Park et al. 2023). In preparations of mouse colon, TTX also reduced veratridine-induced nerve depolarisation and subsequent anion secretion from colon mucosa epithelial cells (Hyland et al. 2005). In rat striatal preparations, veratridine-evoked radiolabelled dopamine release was completely removed with the addition of TTX (Dobrev et al. 1998). These studies are demonstrative of the nerve-mediated and TTX-sensitive nature of veratridine activity, which builds credibility that veratridine is operating in an analogous way, via neurons, within the present model.

A fruitful line of enquiry unresolved in the present work is the determination of the specific Na_V subtype(s) involved in the transduction pathway of veratridine. Although, the TTX-sensitive nature of the veratridine response ruled out Na_V 1.5, Na_V 1.8 and

Na_V 1.9 (TTX-resistant) subtypes.

This still leaves a multitude of candidates though, as literature suggests that veratridine has some capacity to activate most Na_V subtypes, with varying degrees of efficacy, with Na_V 1.8 to a lesser extent than others (Vetter et al. 2012). However Na_V 1.2, Na_V 1.4, Na_V 1.6 and Na_V 1.7 have been demonstrated to respond to veratridine (Zhang et al. 2018) and recently Na_V 1.5 was demonstrated as veratridine-sensitive in human cardiac myocytes (Gulsevin et al. 2022). Given expression of Na_V channels commonly found within the peripheral sympathetic nervous system are most extensively Na_V 1.7, which are TTX-sensitive, they present likely candidates (McDermott et al. 2019; Erickson et al. 2018). Indeed, recent research has identified functional Na_V 1.7 channels expressed on sympathetic nerves in both Guinea pig and humans, which were TTX-sensitive (Kin et al. 2024). Research has also directly linked veratridine activity to the Na_V 1.7 channel in efforts in drug discovery, further increasing the probability that Na_V 1.7 is a likely candidate within this model (Chernov-Rogan et al. 2018). Future work should confirm protein expression of likely candidate Na_V channels using western blot or immunocytochemistry. For functional enquiry, Na_V-subtype selective inhibition of the most likely subtypes, for example Na_V 1.7 using GNE8493 or PF 05089771, whilst challenging with veratridine would provide clarity by either confirming or eliminating its role.

4.4.3 Veratridine operates via β-adrenergic receptors

In section 4.3.3 the veratridine response was found to be propranolol-sensitive, removing veratridine-induced lipolysis, which was a characteristic matched when applied to norepinephrine-stimulated tissues. These responses infer that veratridine is operating through the same suite of β-AR receptors that norepinephrine acts upon and further substantiates that veratridine induces neurogenic release of norepinephrine, in concurrence with what others have shown in literature (Dobrev et al. 1998). Additionally, basal lipolysis persisted in incubation with propranolol, indicating basal lipolysis occurs independently of β-ARs, in line with literature and supports the findings of the TTX-insensitive and thus nerve-independent nature of basal lipolysis.

It has been suggested that propranolol can target other class B GPCRs, as observed in the gut (Pasznik et al. 2019). Therefore the action of propranolol may be promiscuous

and the effects observed above may be due to interruption of other signalling pathways. This granted, glucose-dependent insulinotropic polypeptide (GIP) receptors are members of the class B GPCR family, which can be found on adipocytes (Campbell et al. 2022). As these receptors are GPCRs that can couple to a G_s subunit, their activity may increase lipolysis via AC-mediated cAMP increases (Laurindo et al. 2022), analogous to β-ARs, which could be impacted by propranolol. Additionally, there are reports that propranolol may also block Na_V channels, as it is considered a "membrane stabilising" agent. Researchers have found specifically Na_V 1.5 and Na_V 1.7 are impacted by propranolol (Wang et al. 2010), which may be why the effects with veratridine were more drastic compared to effects with norepinephrine, as it could impede the discharge of neurotransmitter alongside β-AR blockade. Therefore there is a possibility that if other receptors and channels are affected by propranolol activity, it may be responsible, at least in part, for the observed decrease in glycerol release.

In light of this, sotalol was therefore introduced as a second pan-β blocker to validate results observed in propranolol, owing to the potential off-target effects considered above. Both propranolol and sotalol lack intrinsic sympathomimetic activity, neither acting as agonists of β-ARs, which was an important parameter to consider (Embaby et al. 2022). Furthermore propranolol and sotalol reportedly share a similar antagonistic profile with respect to β-receptor order of potency; both are generally more selective for β1 and β2-AR over β3-ARs (Vrydag et al. 2007; Baker 2005). There were limited examples of sotalol used as a β-blocker in literature for non-medical applications, and propranolol appeared to be the more common β-blocker used in experimental studies, particularly in those associated with adipose (Vrydag et al. 2007; Cannon et al. 2004). Despite the similarities in the pharmacological targets of the drugs, the results showed complete insensitivity of veratridine-driven lipolysis to the addition of sotalol. While the expectation was not of a complete blockade as observed in propranolol, based on it's performance in literature (Baker 2005), it remained surprising.

However, sotalol has low lipophilicity i.e. hydrophilic, whereas propranolol is hydrophobic and considered to have high lipophilicity (Embaby et al. 2022). As such, medical practitioners can avoid negative side effects of β-blockers in the brain by prescribing sotalol, as it cannot effectively cross the blood brain barrier into lipid-dense brain tissue

(Cojocariu et al. 2021). Use of sotalol in literature where it has been exogenously applied to lipid-dense tissues, such as in brain, found the drug be less effective and had a high IC50 compared to alternatives such as timolol (Mueller et al. 1982). Therefore it may explain why there was little observed response of tissues to preincubation with sotalol versus propranolol, as within the *ex vivo* nature of this model, sotalol may have had difficulty penetrating though the adipose to β-ARs deeper within the tissue.

Furthermore, sotalol use as a treatment stems from its potent blocking activity at K^+ channels, categorised as a class III anti-arrhythmic agent (Zanetti 1993). This may mean K^+ channels on cell membranes in the tissue were affected by sotalol, which could have altered outcomes in lipolysis. A study found that subtypes of K^+ channels expressed on brown adipocytes negatively regulated thermogenesis, with K^+ channel KO resulting in increased thermogenesis (Chen et al. 2017). If this were to apply in white adipocytes, the effect of K^+ channel blockade would theoretically increase lipolysis if exposed to an agent such as sotalol.

For future consideration and to address this limitation, I could have challenged isolated adipocytes with sotalol to ascertain whether removal of the tissue obstacle improved the efficacy of sotalol as a β-antagonist.

Additionally, further clarification could be achieved through the use of timolol as an alternative to sotalol, as timolol is also non-selective β-AR antagonist lacking sympathomimetic activity, with high lipophilicity similar to propranolol (Cojocariu et al. 2021).

As already established, neither of the β-blockers, propranolol or sotalol, have equal antagonistic activity across the suite of β-ARs. Generally, β1 and β2 ARs are more sensitive to the action of pan β-blockers as "many classical β-AR antagonists have low affinity for β3-ARs" (Schena & Caplan 2019). Therefore it remained unclear which receptors specifically were involved in veratridine-evoked lipolysis, which warranted investigation into the subtypes involved using selective antagonists.

4.4.4 β3-AR appears less critical than β2-ARs in stimulated lipolysis *ex vivo*

4.4.4.0.1 Deviations in responses to antagonists between stimulation regimes

Use of the selective antagonists for each β-AR subtype in veratridine-stimulated lipolysis revealed surprising results that contradicted those observed in literature. The only antagonist to yield a significant reduction in lipolysis was the β2-AR antagonist ICI 118551. To eliminate the possibility that veratridine was inducing some mechanistic deviation in typical responses to selective β-AR antagonists observed in literature, I applied the same selective β-AR antagonists while stimulating with norepinephrine. This means of sympathomimetic stimulation in itself may not reflect the native mosaic of lipogenic signalling as it's a 'clean' stimulation (with respect to the targets of norepinephrine being limited and no other potential neurotransmitters indirectly introduced in the process). However, it allowed for determination of whether veratridine-induced lipolysis mechanistically differs in some way which influences receptor contributions.

While the observed responses to selective β-AR antagonism were largely matched in both stimulation regimes, there were some deviations between responses. A minor difference being that 1 μM of β2-AR antagonist ICI 118551 was not sufficient to significantly reduce norepinephrine-stimulated lipolysis, as observed in veratridine. It is unclear why the lipolytic response to 1 μM ICI 118551 deviated between the stimulants, given the hypothesis that ultimately they are one and the same, but the answer may be due to the reactive nature of the neurogenic mechanism.

Norepinephrine clearance is important in regulation of signalling and various cell types within adipose are reportedly capable of scavenging norepinephrine, such as vasculature (Horvath et al. 2003) and adipocytes (Ryuid et al. 2019). Additionally, if the nerves prompted by veratridine are capable, induced re-uptake of norepinephrine released by sympathetic nerves may substantially reduce the acute load of agonist present, as some reports suggest up to 90% is reuptaken by nerves (Ryu & Buettner 2019). In essence, if clearance mechanisms do differ, it's possible that exogenously applied norepinephrine may overcome the effects of the antagonist ICI 118551 when it is applied at lower concentrations such as 1 μM. Indeed Louis et al. (2000) found differences in response patterns to antagonists when agonist concentrations were altered (relating to β1-AR

specifically).
It is also likely that there is pre-existing disparity in agonist concentration between the two regimes, one agonist is exogenously applied at 2 μM consistently across experiments, the other is induced and will depend on relative abundance of nerves present within each adipose explant section. This represents a feature of the model which has been unquantified and ought to be considered in future work. The differences in response to ICI 118551 may be therefore underpinned by unequal loads of neurotransmitter present for different periods, with β-AR receptors thereby being differentially activated.
However, the theory of exogenous norepinephrine application overcoming antagonist activity appears contradicted by the response pattern observed with the β3-AR antagonists. While it is prudent to consider that concentrations of neurotransmitter will alter minor responses to antagonists, it alone is unlikely to explain the contrast in response to the β3-AR antagonists.

The responses to β3-AR antagonism represents the main deviation between veratridine and norepinephrine datasets. β3-AR antagonism using L-748337 or SR59230A did not produce a significant reduction in veratridine-induced lipolysis at either concentration and was surprising given the litany of published works describing it's paramount role in lipolysis. However, in norepinephrine-stimulated conditions, application of β3-AR antagonist SR59230A did significantly reduce lipolysis, and while not reaching significance, L-748337 produced a clear downward trend in lipolysis. Such trends were less prominent in the veratridine-stimulated tissues, particularly with regard to the L-748337 antagonist. If, as suggested above, the concentration of exogenous norepinephrine applied overcomes antagonist activity, then the β3-AR antagonists would potentially be similarly affected. However this is not the case and there is a clearer relationship of β3-AR to lipolysis with exogenous norepinephrine stimulation, which is less sensitive in veratridine-stimulated conditions.

In spite of a lack of clear role for β3-AR underpinning veratridine-stimulated lipolysis, the *ex vivo* application of norepinephrine therefore aligns more with literature, given the slightly more typical response using β3-AR antagonists, particularly SR59230A. Other models and studies using exogenous agonists to stimulate lipolysis in cell lines or primary cell cultures, also observe the β3-AR bias.
Its challenging to dissect the disparity in the findings between veratridine and nore-

pinephrine *ex vivo*, yet the more typical response found with norepinephrine indicates the *ex vivo* nature of the model itself doesn't account for the disparity in β3-AR role between literature and the veratridine-stimulated response. Instead it implies that the discrepancy is underpinned by the veratridine mechanism. Therefore its more reasonable to assume that the veratridine mechanism is more complex and the nature of neurogenic activation may introduce other signalling molecules that translate to influence lipolysis. While evidence here suggests these may not be those investigated here, there are potentially other signalling molecules introduced. For example, in a recent Nature publication, Li and colleagues demonstrate that oxytocin potentiates isoprenaline-induced glycerol release from cultured adipocytes and adipose explants in humans and mice via an MEK/ERK axis. They progress to demonstrate oxytocinergic populations of sympathetic nerves innervate the tissue. Activation of these sympathetic nerves via 'designer receptor exclusively activated by designer drugs' (or DREADD) techniques, led to increased oxytocin accumulation within the inguinal adipose tissue, indicating it's release (Li et al. 2022). These data may contribute to understanding why veratridine-stimulated tissues were less responsive to β3-AR antagonism, owing to the potential oxytocin increased MEK/ERK lipolysis axis potentiating veratridine-stimulated norepinephrine signalling. Therefore veratridine may be eliciting a dual induction of two independent lipolytic pathways, one of which independent of the G_s-linked β3-AR pathway, which could result in antagonism of the receptor being insufficient to reduce overall lipolysis. However, this needs further substantiation within the contexts of the present methodology to prove, for example it should be established whether these two pathways can be concurrently active to produce a greater lipolytic output, as literature suggests (Collins 2012). Especially since these pro-lipolytic effects were apparently not observed in β2-AR antagonism. These specific complexities are unexplored in the present β-AR study and future experiments could explore this possibility.

Additionally, an experimental pitfall may be explained by the solvents the agonists and antagonists were dissolved in. Where possible, neutral solvents such as water, were used as preference. Exceptions are where manufacturers instructions recommend solvents such as DMSO due to the hydrophobic nature of the drug. Veratridine is dissolved in DMSO, while norepinephrine is dissolved in dH_2O. Both of the β3-AR antagonists

are dissolved in DMSO, meaning that veratridine experiments had a final DMSO concentration of 2%, while the norepinephrine dataset had a 1% final concentration. While I found no effect of 1% DMSO on basal lipolysis, I failed to determine whether there was a concentration-dependent relationship, or investigate the effects of DMSO under stimulated conditions. Essentially, these effects were not accounted for and may explain why effects of antagonists differed between datasets. DMSO can have wide-ranging effects and without further experimentation, it is unclear how these may have implicated lipolysis here, although literature strongly indicates DMSO exposure potentiates lipolysis incurred by stimulants such as norepinephrine (Wieser et al. 1977). It would be useful to explore this further in dose-response experiments.

Additionally, there is limited evidence where selective β-AR antagonists have been used in conjunction with other neurogenic-activation models, such as EFS. Therefore, it remains unclear whether the apparent redundancy in β3-AR is an artefact of the use of veratridine, an odd effect which is not representative of that *in vivo*, or a reflection that neurogenic activation is more complex and results in lipolysis that culminates on different receptors which contradicts current published literature.

4.4.4.0.2 Antagonists applied to adipocytes

As discussed above, a possible explanation as to the less clearly defined role for β3-AR in lipolysis compared to literature, was that there was limited literature available where these antagonists had been applied to adipose in an *ex vivo* setting. There are reports in literature that suggest antagonists have differential effects depending on the model in which they are applied. For example, the β3-AR antagonist SR59230A apparently has different effects when used in tissue compared to isolated cells (Perrone et al. 2008). The antagonists selected for use in this study were done so through a review of literature using them to attenuate lipolysis, or some alternative comparative measure. However, it is worthy of note that the experiments involving use of these antagonists to abrogate lipolysis are typically done using primary cultured adipocytes, or 3T3-L1 adipocyte cell lines. Isolated cells, without the context of the extracellular matrix (ECM) and other cell types surrounding them, have their membrane bound receptors exposed and are consequently an easily accessible target for exogenously applied pharmacological agents to

interact (Stylianopoulos et al. 2010). This may generally explain why higher concentrations of antagonists in tissue are required to generate the same or equivalent responses observed at lower concentrations in isolated cells. Furthermore, without neighbouring cells and ECM, any regulatory processes that these cells and matrix provide to tune norepinephrine-mediated stimulation by β-ARs are no longer operational. Conversely, given this point, when the same antagonists were applied to isolated adipocytes, there was no observed reduction in lipolysis in response to antagonism of any of the β-AR subtypes, which was unusual based on literature in similar models. The concentration of 1 μM for each applied antagonist was found in examples in literature, and some studies used the antagonists in cell lines with even lower concentrations (Merlin et al. 2018). Therefore it is unlikely that the concentration of antagonist was insufficient.

There is a possibility that the adipocyte isolation protocol used may have impacted the adipocytes ability to respond to antagonists, as disturbances during isolation such as shear stress can affect receptor sensitivities in other cells (Dufau et al. 2021; Paz et al. 2017; Choi et al. 2017). As adipocytes were isolated and used immediately with no conditioning period (other than 30 minutes of preincubation with antagonists), the stress may have impacted cellular responses. Other researchers frequently isolate and then culture primary adipocytes before use in experiments, which may serve to regulate responses. During this work, culture of adipocytes was avoided due to potential affects on receptor expression and intracellular signalling pathways, particularly in 2D culture systems, which can ultimately alter the true the native/physiological response of cells leading to non-translatable conclusions (Klein et al. 2022; Jensen et al. 2020). Also, it has been accepted that isolation methods can alter outcomes on cell responsiveness (Thompson et al. 2012; Bajek et al. 2017). Exposure to factors such as enzymatic digestion and mechanical disturbance in the isolating procedure have been previously shown to increase proinflammatory cytokine release (IL-6, TNF-α) which induced downregulation of multiple genes (Thompson et al. 2012). Complications such as these which were not considered, checked or mitigated for, may have ultimately influenced adipocyte responses.

Upon reflective literature review, other researchers incorporate adenosine deaminase (ADA) in media when isolating primary white adipocytes. ADA is responsible for purine metabolism, converting adenosine into inosine, which reduces the accumulation of adeno-

sine as a product of the isolation procedure (Preite et al. 2016). Adenosine accumulation can reportedly have varied effects upon the isolated cells, including reducing viability, impairing responses to pharmacological agents and initiating a stress response (Preite et al. 2016). P1 receptors are also known to regulate lipolysis in WAT and some subtypes found on adipocytes directly increase lipolysis via G_s-linked cAMP increases, for example A2B receptors (Tozzi et al. 2017). As I did not incorporate ADA whilst isolating adipocytes, it may possibly have contributed to the lack of response to antagonists. In order to determine whereupon the incongruency between findings in literature and the present results lies, it would be valuable to use a cell line regularly used in such studies, such as 3T3-L1 adipocytes. In doing so, it would ascertain whether the adipocytes in my preparation are unresponsive, or if it is an antagonist-related issue. Additionally, adipocytes could be antagonised with propranolol as a broad positive control to challenge general response to general β-AR antagonism.

4.4.4.0.3 Role of β2-AR

Rodents express all three β-AR subtypes on white adipocytes (Evans et al. 2019; Vetter et al. 2012), with consensus that β3-AR are proportionally the highest subtype expressed and reportedly possess the most dominant role in the induction of lipolysis (Valentine et al. 2022; Dwaib et al. 2023; Louis et al. 2000). The β2-AR has been previously considered unimportant in the induction of lipolysis in investigations of stimulated lipolysis in rat white adipocytes (Louis et al. 2000; Germack et al. 1997). Others have shown it to be less important than β1-AR in lipolysis in pig white adipocytes (Mills 2000). Even explicit declarations in review articles suggest "no role for the β2-AR [in lipolysis] despite its detection in WAT" in rodents (Evans et al. 2019). Therefore, these results represent an interesting finding in an *ex vivo* model, where outcomes are potentially more reflective of true physiological roles/responses.

Unsurprisingly, evidence of β2-AR involvement in lipolysis is sparse, particularly in rodents. Studies have alluded to a potential role in lipolysis, where pigs that have undergone β2-AR agonism experienced upregulated lipoproteins and transcription of genes associated with metabolism, pertaining to a role in metabolic regulation (Zhang et al. 2007). Work has shown that the β2-AR may have important roles in phenotypic regulation, with chronic β2-AR stimulation in mice leading to increased beiging (Ohyama

et al. 2016). Due to the focus on β3-AR in lipolysis, particularly in rodent models, many publications overlook the role of β1 and β2-AR subtypes, instead direct efforts toward antagonising or knocking out β3-AR and observing effects, often altogether neglecting antagonists for the β1 and β2-ARs. However, evidence for the role of β1 and β2-ARs can be inferred indirectly from research that has a β3-AR focus.

In an optogenetics-based murine experiment looking at the involvement of leptin-stimulated and nerve-mediated lipolysis, overall whole body fat composition of mice lacking β1 and β2-ARs (adipose-specific KO) was modestly increased by 10% when β3 was also removed (Zeng et al. 2015). While not directly comparable, due to a lack of WT controls to compare for baseline body fat values in the presence of all β-ARs, the results from data here show a similar trend; that β3-AR may have a more modest influence on lipolysis when a physiological approach of nervous agonism *in vivo* is applied.
In other β3-AR KO studies, when looking at their results in the absence of added adenosine A1 receptor agonist phenylisopropyladenosine (PIA), adipocytes from mice lacking the β3-AR receptor remained capable of isoprenaline-stimulated lipolysis, up to 75% of WT maximum and β3-AR$^{(-/-)}$ mice gained just 34% in total body fat (Susulic et al. 1995; Schena & Caplan 2019).
In a similar study, β3-AR KO male mice gained 42% total body fat over WT mice under chow dietary conditions, which does indicate impairment of the β3-AR leads to less well regulated lipolysis (Revelli et al. 1997). However, what both of these KO studies lack is a comparison to a β1- or β2-AR KO, or indeed a triple KO (ideally specifically restricted to adipocytes), to contextualise the effects of β3-AR removal and establish relative contributions of each receptor subtype. This is somewhat demonstrated in work by Preitner and colleagues (1998), where lipolytic responses to epinephrine in β3-AR KO mouse adipocytes were blunted, which convincingly suggests dominance of the β3-AR. However, the selective agonists for β1 and β2-ARs were previously able to robustly induce lipolysis in WT, but not in β3-AR KO adipocytes. These deductions indicate possible non-selectivity of the agonists, or β3-AR KO inadvertently affected the other receptors and is thus inflating the β3-AR role.

In other studies using antagonists, oral administration of β3-AR antagonist SR59230A in mice did blunt the total amount of weight lost in response to calorie restriction, but

those mice still lost weight, only experiencing a circa 5% difference compared to those without the antagonist at day 12 (Sipe et al. 2017).
Obese mice, demonstrated to have no mRNA expression of the β3-AR, experienced blunted AC activity in response to adrenergic stimulation compared to lean controls, suggestive of a prominent role for β3-AR in lipolysis. However, even in lean mice, β3-AR selective agonist BRL 37344 failed to reach peak of epinephrine response, equating to around 75%, leaving room for involvement of another receptor. Recapitulation with selective β3-AR agonist BRL 37344 in β3-AR-lacking obese mice demonstrated there was no response to β3-AR selective agonism, as expected. Yet, the response to epinephrine was retained, which was found sensitive to β2-AR antagonist ICI 188551. These data infer a role for the β2-AR in mouse lipolysis (Collins et al. 1994).

Additionally, research in other species demonstrated an incomplete removal of stimulated lipolysis when β3-AR antagonist L-748337 was used in isolated human adipocytes compared to the effects of propranolol, suggesting involvement of another β-AR subtype (Cero et al. 2021).
Others have echoed the importance β2-AR has in regulating lipolysis in humans (Fernandes et al. 2014). Studies in humans have shown the β2-AR as being important in lipolysis, as decreased expression of β2-AR correlated with decreased sensitivity to catecholamines (Lonnqvist et al. 1992). While species-specific differences in roles of β-AR subtypes are well acknowledged in literature, with β3-AR being less important in humans than rodents, it still provides evidence that other subtypes have influence and are not completely redundant (Dwaib et al. 2023).
Furthermore, it is not possible to untangle the relative contribution of the non-β3-AR subtypes involved in lipolysis in these indirect examples. The β1-AR may well be of greater influence in the examples above, as others have suggested compensatory upregulation of β1-AR when β3-AR is disrupted (Schena & Caplan 2019). Due to the lack of specific antagonists or receptor knock-outs used for all three subtypes in these studies, it is not possible to conclusively determine.

Therefore, β2-ARs found to be involved at all, considering literature claims their insignificance in lipolysis regulation, is an interesting finding in this project. Literature has repeatedly demonstrated the expression of rodent β2-AR, and the presence of a receptor that is completely redundant is unlikely. Yet, β2-AR has the highest affinity for

epinephrine, circa 20 times greater than that for norepinephrine (Goldstein 2010). Circulating epinephrine, once regarded the be the sole source of regulating lipolysis, it is now relegated to minor influences on routine lipolysis regulation (Bartness et al. 2007; Bartness et al. 2014). However, it is possible that the expression of β2-ARs on adipocytes is adaptive, allowing for fight-or-flight induced increases in circulating epinephrine to engage access to stored energy, bypassing the strictly regulated hypothalamus-sympathetic axis. Further experimentation and *in vivo* models would allow for exploration of this theory.

Additionally, isoprenaline is often the favored agonist of choice in equivalent studies investigating lipolysis, which invariably conclude that β3-AR has dominance in controlling lipolysis. Yet, it is important to note that the order of potency isoprenaline is fairly equal between subtypes, and considered as a full agonist for all three, with a general greater potency overall than norepinephrine (Hoffmann et al. 2004; Vrydag et al. 2007). Comparatively, norepinephrine has a order of potency of $\beta 1 > \beta 3 > \beta 2$ (Vrydag et al. 2007) and therefore, studies that use isoprenaline in favour of native ligand norepinephrine may be inflating the importance of the β3-AR as they stimulate it beyond its typical capacity. Together, these points may contribute to why here, the link of β3-AR to lipolysis is less clear under norepinephrine-stimulated and in particular, neurogenically-stimulated conditions.

To investigate the contribution of β2 and β3-ARs further in this model (until β3-AR selective inverse agonists are commercially available), tissue specific knockout of β3-AR in conjunction with veratridine stimulation compared with a control, would help elucidate true β-AR contributions.

4.4.4.0.4 Antagonist issues

It seems paradoxical that given norepinephrine has the lowest potency at β2-ARs, it would have such an integral role in lipolysis within the present model. A possible explanation as to the surprising role of β2-AR in this model is that ICI 118551 used to antagonise the receptor, is an inverse agonist. These types of inhibitor are reportedly more efficient at blocking receptors, as they 'lock' the receptor in an inactive state, removing any constitutive or induced activity (Perrone et al. 2010). Therefore the potency of ICI

118551 compared to the other antagonists, may have inflated the β2-AR role in lipolysis within this model.

In fact, supporting this, Perrone and colleagues discuss the overlap and limited selectivity of selective β-AR antagonists, and studies researching β3-AR antagonists suggest that inverse agonist ICI 118551 may have circa 30% inverse agonist activity at the β3-AR too (Perrone et al. 2010). Corroborating this, there are reports that β2-AR antagonist ICI 118551, particularly at higher concentrations (10 μM), counteracted lipolysis stimulated with isoprenaline but also selective β3-AR agonist BRL 37344 (Germack et al. 1997). This infers that ICI 118551 may act to inhibit activity of other, if not all, β-AR subtypes. Therefore, due to these apparent non-selective effects, the use of β2-AR inverse agonist may also be acting on β3-ARs, which may falsely inflate the importance of β2-AR in stimulated lipolysis here. To address this within the present model, tissues could be antagonised with ICI 118551 followed by a β3 and/or β1-AR selective agonist to induce lipolysis and measure changes in glycerol release relative to non-antagonised controls, in order to rule out whether those subtypes are indeed impacted by ICI 118551.

Secondly, as alluded to throughout this thesis, GPCRs also have the propensity and capacity for alternate coupling (Collins 2022; Soeder et al. 1999). Alternate coupling can depend on the ligand in a phenomenon termed "ligand directed signalling bias" and is thought to be governed by changes in the receptor conformation via differential activation of the same receptor (Wootten et al. 2018; Michel et al. 2010). This may influence how antagonists are responded to, as antagonists may shunt the intracellular signalling pathway & allow for activity to occur, whereas an inverse agonist effectively locks the receptor in its inactive state, preventing alternate pathway induction (Sato et al. 2016; Perrone et al. 2008).

Therefore, it is possible the type of antagonists that were applied to β3-AR here failed to remove any potential ligand bias shifted activity and possibly encouraged it, giving the appearance that the β3-AR has a diminutive role and thereby not providing an accurate capture of the role of the receptor in regulating stimulated lipolysis (Schena et al. 2019, Collins 2022). As such, it infers that the receptor may be at least partially activating one of the lipolysis pathways when β3-AR antagonists are introduced, illustrated by the modest glycerol reduction observed under "antagonised" stimulated conditions, and increased glycerol release under antagonised "basal" conditions (discussed further below).

It would be valuable to re-challenge the role of β3-AR in this model with the use of an inverse agonist, particularly due to the ambiguous role of the receptor in stimulated lipolysis here. Unfortunately, there is no commercially available inverse agonist for the β3-AR, specifically. In fact, there is an agreed lack of selective antagonists available in general for the β3-AR, and the two commercially available, particularly SR59230A, have both been criticized regarding their selectivity and efficacy (Schena et al. 2019; Nastasi et al. 2022; Sato et al. 2008). SR59230A has been termed "essentially non-selective" with cases where it has a lower affinity for human β3-AR than it does for β1 and β2-ARs, and additional reports of agonist activity at the β3-AR (Schena & Caplan 2019). L-748337 is reportedly the better option and has highest efficacy when used on human β3-ARs, however, has a reported 100 times reduced potency at rat β3-ARs (Schena & Caplan 2019). Therefore using the L-748337 β3-AR antagonist in mouse tissue under these conditions may have produced a result reflective of it's poor selectivity, or lack of efficacy, at the mouse β3-AR. Therefore its important to acknowledge that the antagonist may not be performing in its proposed parameters.

As previously mentioned, there is not an abundance of specific examples where these antagonists have been used to investigate lipolysis in mouse adipocytes, lest in *ex vivo* tissue preparations. Of the limited examples found, there is clear ambiguity relating to the efficacy of the antagonists. Jin et al. (2018) used both L-748337 and SR59230A to attempt to abolish isoprenaline-stimulated glycerol release from 3T3-L1 cells and found differential efficacy of these antagonists, with SR59230A failing to remove stimulated responses.

4.4.4.0.5 Stimulatory effect of β3-AR antagonists

In addition to the lack of clear role of β3-AR based on response to antagonists, I also observed increased basal lipolysis with application of both antagonists. These effects were more pronounced in the veratridine datasets, which is potentially due to the compounding presence of DMSO.

As previously discussed, there is conflicting evidence on the validity/efficacy of the selective β3-AR antagonists currently available, with there being only two options. There have previously been reports of β3-AR antagonist SR59230A having agonist-like prop-

erties at the β3-AR in other models (Perrone et al. 2008; Hutchinson et al. 2005). Therefore it was not an unexpected finding based on such reports. However, literature seemed to suggest that unlike SR59230A, L-748337 was "devoid of agonist activity" when used human β-ARs (Candelore et al. 1999; Vrydag et al. 2007). Therefore, the results indicating lipolysis induction in basal conditions with both antagonists, were surprising. However, thorough examination of literature revealed that while L-748337 has been found to inhibit the canonical G_s-linked pathway in CHO (Chinese hamster ovary) cells expressing the human β3-AR, it subsequently engages the G_i pathway which in turn activates the MEK/ERK axis with "exquisitely high potency" (Sato et al. 2008).
Also, literature discussed in Chapter 1 has indicted that β3-AR is a particularly promiscuous receptor, as it can alternately couple to G_i or G_s proteins depending on the ligand profile and this links to alternate lipolytic pathways, such as MEK/ERK (Collins 2012). In fact researchers have indicated that use of antagonists of the β3-AR have dually affected the receptor, reducing cAMP accumulation as desired, but increasing lipolysis via alternate intracellular pathways (Sato et al. 2016).

The β3-AR alternate coupling to the G_i and G_s pathways in ligand-directed signalling bias may explain much of the effects observed here. The G_s axis stimulates the canonical cAMP-PKA route and the G_i linked pathway activates an alternate route of lipolysis via induction of the MEK/ERK axis. Interestingly, research by Hong et al. (2018) found MEK/ERK signalling was linked to the β3-AR, where it phosphorylates residues of the receptor to engage the pathway and interruption of this axis significantly reduced lipolysis induced by a β3-AR-selective agonist (Hong et al. 2018).

Therefore, it is possible that the β3-AR antagonists as applied under basal conditions in the present study are paradoxically stimulating lipolysis via the alternate MEK/ERK pathway. The fact that L-748337 applied in norepinephrine experiments both raised glycerol release in basal conditions and lowered it in norepinephrine-stimulated conditions to nearly equal values, indicates an alternate pathway, different to that typically instigated by norepinephrine, is being induced. To substantiate this theory and claim that the MEK/ERK pathway is being induced under β3-AR antagonism in both stimulated and basal lipolysis, future studies ought to use MEK/ERK inhibitor PD 0325901 alongside these antagonists to see whether these lipolytic effects are removed. To also establish

a link between the antagonist and proposed G_i-linked lipolysis pathway, incubation of tissues with G_i-inhibiting pertussis toxin, under conjunctional challenge with the β3-AR antagonists, would illuminate whether this is indeed the connecting axis.

4.4.4.0.6 Antagonist stimulatory effects are not propranolol sensitive

In order to investigate whether the stimulating effects of the β3-AR antagonists were contingent on the β3-AR receptor, I used propranolol to attempt to block the stimulatory L-748337 effects under basal conditions. Propranolol didn't abolish the agonist-like response to L-748337 under basal conditions. Due to the lack of effectiveness of propranolol it could lead to a conclusion that these stimulatory effects are independent of the β3-AR, via some alternative route. However, this agonist-like effect was also observed in a study using SR59230A which was also unable to be removed with propranolol (Horinouchi et al. 2001). Another study found selective β3-AR agonism led to increases in the MEK/ERK signalling cascade, which was propranolol-insensitive (Soeder et al. 1999). Propranolol is known for having a poorer efficacy at the β3-AR receptor (Collins 2022) as all non-selective β blockers are. These points considered, it may explain the insensitivity of L-748337 stimulatory effects to propranolol and therefore doesn't eliminate the receptor from being involved in the antagonist-driven response, particularly as others have observed these effects in β3-AR antagonists.

It may be that a pathway such as MEK/ERK has an association with the receptor which is resistant to propranolol, for example intracellular receptor modifications that propranolol binding cannot affect.

4.4.5 Veratridine-evoked transmitter release is Ca^{2+} independent

It was important to try and establish a full working scheme of how veratridine was inducing lipolysis in this model, with regard to the initial hypothesis. Results so far have established a convincing case that veratridine operates via nerves to release norepinephrine, which in turn activates β2 adrenergic receptors. However there was little information gained as to how veratridine was able to induce the neurotransmitter release. VGCCs are typically a critical component to canonical nerve transmission. Therefore to assess whether members of VGCCs may be involved in mediating the observed response to ve-

ratridine, I challenged the veratridine-induced lipolytic response with pretreatment with various antagonists of the VGCC subtypes; ω-conotoxin-GVIA to block N-type channels, ω-conotoxin-MVIIC to block N- P- & Q-type channels. However, in this system both conotoxins failed to prevent or even diminish veratridine-stimulated lipolysis, which was unexpected, given conotoxins GVIA and MVIIC target the majority of the Ca_V channel subtypes between them.

These results were initially surprising, as other studies have successfully used conotoxins to abrogate neurotransmitter release in other neurogenic models (Pruneau et al. 1990; Boland et al. 1994). Considering the application of these toxins in literature, I noted that they were often conducted in isolated neurons/cells. For example, ω-conotoxin-GVIA has been used to reduce Ca^{2+} currents in electrically-stimulated isolated sympathetic neurons in frogs (Boland et al. 1994). Therefore the *ex vivo* segments of tissue within this model presented a potential explanation as to why there may have been a lack of response to conotoxins GVIA and MVIIC. Given the molecular weight of ω-conotoxin-GVIA (3037) and ω-conotoxin-MVIIC (2749) is nearly 7-fold larger than any other compound/drug exogenously applied in these tissue preparations, it may have proven too large to diffuse through tight pericellular spaces (Yang et al. 2017; Duggan et al. 2009). This is compounded by the natural hydrophobic nature of adipose tissue, making it more likely to repel larger molecules (Duggan et al. 2009), especially when dissolved in H_2O, as they were. While the use of the DMEM incorporating BSA acted as a carrier to some extents, perhaps the addition of turpenes or some other penetration-enhancing agent could ameliorate these potential effects (Yang et al. 2017). However, this theory was quashed after small molecule alternatives, cilnidipine and nifedipine, were used to to block both N-& L- and L-type channels, respectively. The lack of reduction in lipolysis in response to VGCC antagonism persisted irrespective of molecule size. In this investigation, however, I neglected to challenge P & Q-types with small molecule alternatives, it remains that if such antagonists were applied they may have demonstrated a role. However expression isn't ubiquitous, nor translatable model to model and therefore I cannot be certain that any of these subtypes are present without further investigation, such as expression at the protein level via western blot or immunocytochemistry.

Literature has shown that VGCCs are expressed on white adipocytes in multiple model organisms, for example L & T types (Zhai et al. 2020). In terms of relation

to lipolysis, L-type Ca_V 1.2 and Ca_V 1.3 identified on rat white adipocytes, where the former illustrated a role in regulating basal lipolysis (Fedorenko et al. 2020). Similar outcomes have been found in mice, where blockade of Ca^{2+} entry through Ca_V channels in adipocytes blunted stimulated lipolysis (Chen et al. 2017). Therefore, evidence implies that administration of whole-tissue antagonists in an attempt to block nerves alone, may inadvertently affect Ca^{2+} fluxes at an adipocyte level, which may alter the overall net lipolytic effect. After using a battery of VGCC-specific antagonists, the veratridine-mediated lipolysis response was unchanged, whilst crucially also having no significant effect on basal. As evidence suggests blocking or removal of Ca^{2+} through such mechanisms would either reduce, or increase (Garca-Barrado et al. 2001) lipolysis, and neither effect was observed on basal tissues here, it's unlikely that responses were masked by direct effects on adipocytes and therefore cannot account for the lack of response under veratridine-stimulated conditions. Deducing this, it also indicates that if the VGCCs are expressed on white adipocytes as literature suggests, they may not have roles in regulating basal lipolysis either, at least within the model and context applied here. The only potential trend observed was in response to 10 μM nifedipine, which caused a slight increase in basal lipolysis. This contradicts evidence elsewhere suggesting disruption of Ca^{2+} via L-type Ca_V channel blockade may reduce lipolysis, as seen with alternative L-type blocker verapamil (Fedorenko et al. 2020).

While there are studies (such as those previously mentioned) that successfully use VGCC antagonists to remove or reduce transmitter release in other models, studies that employ veratridine as a tool for neurogenic activation have found general insensitivity to VGCC blockade. For example, after application of various VGCC blockers, including ω-conotoxin-GVIA, the only one that had any effect on dopamine release in rat brain slices was ω-conotoxin-MVIIC (in combination with other inhibitors) (Dobrev et al. 1998). The apparent veratridine insensitivity to VGCC blockade has been echoed across other studies (Platel et al. 2005; Rungta et al. 2015; Vetter et al. 2012), suggesting the results gained in the present study are not wholly unorthodox.

4.4.5.1 Non-canonical Ca^{2+} sources

Evidence from early published literature utilising veratridine as a tool to increase Na_V channel permeability indicated there was a non-canonical mechanism involved in the

subsequent release of neurotransmitter, which was not dependent on extracellular Ca^{2+}, but on Na^{+} (Cunningham & Neal 1981). Building on this, others reported complete independence of extracellular Ca^{2+} in veratridine-mediated transmitter release, suggesting instead a Na^{+} gradient was responsible. Supporting this theory, veratridine was found to induce neuronal swelling through increases of Na^{+} and Cl^{-} influx into the axon (Rungta et al. 2015). Linking this, others found that while there is an extracellular Ca^{2+}-independence and Na^{+} dependence, the response to veratridine did remain contingent on intracellular Ca^{2+} sources. Researchers found Ca^{2+} release form an internal store was blockable with the addition of mitochondrial Na^{+}/Ca^{2+} exchanger antagonist CGP 37157 (Palty et al. 2010).

Conversely, other researchers found that veratridine was in fact contingent on extracellular Ca^{2+}, but were independent of VGCCs in other models, as when Ca^{2+} was removed from media, veratridine failed to induce responses in pre-plate cells of the mouse neocortex (Platel et al. 2005). Blockade of the reverse mode of plasmalemmal Na^{+}/Ca^{2+} exchangers (via KB-R7943) replicated the effects of extracellular Ca^{2+} removal, ablating the response to veratridine and thus suggesting that ionic gradients i.e. Na^{+} introduction, governed veratridine action and facilitated Ca^{2+} entry (Platel et al. 2005; Soma et al. 2006).

The mechanism underpinning calcium entry in these examples is therefore likely a result of the depolarising effect of the Na^{+} influx into the axon. The surge of Na^{+} into the axon results in a difference in potential, which Na^{+}/Ca^{2+} exchangers act to rectify, exchanging calcium and extruding sodium. The consequential effect resulting in a sodium-driven, but ultimately calcium-mediated, exocytosis event.

Yet converse to findings and mechanisms described above, I saw no effect of Ca^{2+} challenge via these alternative mechanisms when stimulating with veratridine, which was puzzling. The differing results in literature suggest non-linearity in the veratridine mechanism, i.e. contention as to calcium dependency and possible sources, clearly illustrating that veratridine mechanisms may slightly differ depending on the model on which it is applied. Therefore, conformation of the exocytosis mechanism underpinning veratridine-driven lipolysis in the inguinal fat pad remains outstanding.

As already discussed with the use of conotoxins in whole tissue, the validity of the Na^{+}/Ca^{2+} exchanger antagonists applied in this *ex vivo* model is questionable, due to

the reported nature of both channels ubiquitously expressed in other cell types, notably adipocytes, and therefore one cannot easily detangle the effects of calcium mechanics in other cells, versus neurons (as described previously). As previously stated, evidence suggests blocking Ca^{2+} channels on adipocytes may reduce basal lipolysis and blunt stimulated responses (Fedorenko et al. 2020; Chen et al. 2017) or conversely increase lipolysis (Xue et al. 2001; Garca-Barrado et al. 2001; Ali et al. 2018a), thus endangering procurement of a false positive or negative result. Therefore, without further scrupulous research, the exact (and likely complex) effects of disrupting these channels at the adipocyte level cannot be determined.

4.4.5.2 Alternative Ca^{2+} independent route of exocytosis

The apparent Ca^{2+}-independent effects of veratridine may be a unique characteristic of the veratridine mechanism of action, as in other models of neurogenic stimulation in tissues, such as via EFS, the effects were conotoxin-sensitive and thus VGCC-dependent. For example, ω-conotoxin-MVIIC has been used used at low concentrations in EFS-stimulated Guinea pig atria (Serone et al. 1999), and to reduce EFS-stimulated contraction of rat mesenteric arteries (Tanaka et al. 1999). Waterman and colleagues (1997) successfully used both ω-conotoxin-GVIA and MVIIC to reduce EFS-stimulated neurotransmitter outflow in mouse vas deferens. These studies all harness an *ex vivo* approach, therefore it was unlikely to be the whole *ex vivo* sections of tissue in this model that explained the lack of responsiveness to VGCC challenge. Given the clear unorthodox nature of veratridine exocytosis presented in literature, with mixed conclusions on the role of Ca^{2+}, its likely that this is a feature of veratridine.

A Ca^{2+}independent route for exocytosis is proposed to be via protein-kinase phosphorylation. Specifically, serine-threonine protein kinases, which group includes PKA, PKC and CAMK (Hille 1999). Protein kinases typically need a 'trigger' to become activated, to avoid inappropriate and unregulated activation of cellular processes. Hille et al (1999) proposed that activation of these kinases could initiate downstream activation of exocytosis via liberation of Ca^{2+} from intracellular stores, or by acting directly on presynaptic vesicles that are in a 'primed' state in a reserve pool. An example given is mucin secretion from bronchial epithelial cells can be stimulated by agents that activate PKC,

such as ATP, A1 antagonists and muscarinic agonists (Park et al. 2007). Veratridine therefore may be triggering activation of protein kinases within the neuron, directly or via voltage transmission, that induces intracellular Ca^{2+}, or interacts with vesicles and causes subsequent exocytosis.

The third explanation may be 'calcium-independent but voltage dependent exocytosis' (CiVDS), which induces exocytosis via voltage sensation and subsequent channel modification rather than via the canonical Ca^{2+} route. Initial work from Zhang & Zhou (2002) showed that in single-neuron patch clamp assays with rat DRG neurons, membrane capacitance upon stimulation did not change when both intra- and extracellular Ca^{2+} was removed. In future work, Huang et al. (2019) recapitulated these findings in sympathetic neurons from the superior cervical ganglia, showing extrapolation between neuronal populations. Their work and others (Chai et al. 2017) concluded in their hypothesis, that while Ca_V 2.2 channels (N-type) were not inducing exocytosis via Ca^{2+} influx, they were conducting the action potential-derived voltage intracellularly, with some mechanical conformational change, which induces signalling cascades and results in exocytosis. Veratridine could then theoretically activate exocytosis through this manner. However, the authors in the referenced suite of literature demonstrate the pivotal role of Ca_V 2.2 channels in transmitting the voltage into intracellular changes by successfully blocking the response with ω-conotoxin-GVIA. Therefore as I failed to see this inhibition with ω-conotoxin-GVIA or ω-conotoxin-MVIIC it is less likely that CiVDS explains findings here.

For future work, it is recommended to challenge the veratridine response with Na^+ free media, as others have, to see if veratridine is indeed dependent on Na^+. Similarly, a Ca^{2+} free- challenge would illuminate whether the effects are truly independent of all Ca^{2+} (yet this again complicates responses with potential direct effects adipocytes). Alternatively, experiments such as calcium imaging in response to veratridine stimulation on isolated neurons cultured from ganglia that are known to supply inguinal tissue.

4.4.6 Lack of neuromodulatory roles in veratridine mechanism

4.4.7 α2 adrenergic receptors

α2-ARs are G_i- linked GPCRs and recognised as being expressed prejunctionally, to negatively regulate neurotransmission (Giovannitti et al. 2015). Their activity has been found to modulate nerve output in other systems, such as in vasculature (Westcott et al. 2013).

There is currently no evidence to suggest a convincing role for α2-ARs in "authentic" rodent white adipocytes (Evans et al. 2019). In mouse primary white adipocytes, mRNA for α2-AR was negligible, while the α1-AR was present, but not to a great extent (Merlin et al 2018). Others have concurred with the lack of adipocyte expression of α2-ARs (Valet et al. 2000; Chusyd et al. 2016). Therefore the use of an α2-AR antagonist avoided potential direct effects on adipocytes. In this system, the use of yohimbine did not affect the lipolytic response to veratridine, suggesting that there was not a role for prejunctional α2-ARs, if expressed on the nerves within the tissue. There is a possibility that there could have been complexities in using yohimbine, as Hagan and Hughs (1986) found higher concentrations (10 μM) of yohimbine had opposing effects and increased nerve outflow in rat brain, suggesting via another receptor type. However, the concentrations used within this work spanned both a lower and higher concentration, neither of which produced any effect.

Indirect evidence for the lack of a role in this system comes from systemic administration of α-AR blockers in mice that lack β-ARs, as there was no change in body weight when α-ARs were also antagonised (Zeng et al. 2015). However it is not possible to directly suggest that prejunctional α2-ARs had no role due to the whole-body effects. Importantly, these receptors are expressed in other tissues, and I did not prove that α2-ARs were indeed expressed prejunctionally, or rule out their presence elsewhere. I therefore cannot conclusively determine prejunctional effects as inhibition of the receptor elsewhere may have influenced outcomes.

In any case, it appears that veratridine-induced release of norepinephrine is not affected by α2-AR antagonism in this system.

4.4.7.1 P2X3 & P2X2/3 receptors

Prejunctionally expressed P2Rs were discussed in Chapter 1 and have important roles in many systems in the control of nervous output. A key aim of the PhD project was to investigate the role of purinergic signalling in lipolysis. The establishment of the veratridine-based neurogenic response made it possible to interrogate the effects of prejunctional P2Rs in an *ex vivo* setting. Research has indicated that the most abundantly expressed prejunctional P2X receptors on peripheral sympathetic nerves are P2X3 and P2X2 subunits (Cockayne et al. 2005). P2X3 and the heterotrimeric P2X2/3 have been found on sympathetic neurons (Cockayne et al. 2005; Sperlágh et al. 2000). Although generally, P2X3 subunit expression is considered less abundant in sympathetic than sensory nerves (Cockayne et al. 2005). These receptors expressed prejunctionally would act to potentiate neurotransmitter release through the introduction of extracellular Ca^{2+} into the synapse (Sperlágh et al. 2007). Norenburg et al. (2001) stated that there was expression of P2X neuromodulatory channels in rat, but not mouse sympathetic neurons, based on responses to nucleotides. This work was contradicted by Cockayne et al. (2000) who found expression and function of these receptors in mouse using immunohistochemistry and electrophysiology techniques. Both mouse sympathetic and sensory ganglion neurons contained ATP-sensitive P2X receptors that were dependent on the P2X2 and P2X3 subunits. Mice genetically lacking P2X2 and P2X3 receptors sustained reduced urinary bladder reflexes, suffering hypoflexia, indicating the role of the receptors in sympathetic-mediated responses.

Yet, when applying immunocytochemistry techniques in the whole mount model, the P2X2 and P2X3 receptors were not found present on sympathetic neurons innervating the inguinal fat depot. The antibodies were validated using human astrocytoma cell lines overexpressing P2X2 or P2X3 receptors, indicating their capacity to detect the protein when present. Evidence in RT-PCR work in section 4.3.8.2 indicated that P2X2 and P2X3 mRNA was being detected within the whole adipose depot, although it was undetermined which cell types were expressing the mRNA. Also, the mRNA may not translate into protein, as in whole mount immunocytochemistry work, there appeared to be limited background P2X2 or P2X3-positive staining in other non-nervous cell types. Without further investigation, it is likely that the functional investigation of P2X3 and P2X2/3 receptors in veratridine-stimulated lipolysis did not show effects due to the lack

of expression of these receptors in the resident nerves in this tissue.

It is likely that peripheral sympathetic neurons have some degree of heterologous receptor expression depending on which tissue they innervate, and this provides an angle for deeper investigation comparing receptor expression of sympathetic nerves from different locations.

It would be interesting to challenge α2-ARs and other potential neuromodulatory roles using a different mode of neurogenic activation, to establish whether the lack of effects observed are veratridine related. Especially since section 4.4.5 suggests the mechanisms underpinning veratridine-mediated exocytosis are apparently non-canonical. These non-canonical features may therefore extend to other signalling mechanisms in the neuron, such as neuromodulation. Therefore, while these mechanisms may indeed play a role under normal circumstances, their involvement may be masked by the non-canonical nature of veratridine evoked neurotransmitter release.

4.4.8 Sensory neuropeptides have no role in veratridine-mediated lipolysis

Veratridine, as previously established, is commonly employed to activate sympathetic nerves, but has also been used to stimulate sensory nerves (Stacey et al. 2018; Mohammed et al. 2017). Additionally, the TTX-sensitive Na_V 1.7 channel appeared to be a likely candidate target of veratridine in this model, as others have found (Zhang et al. 2018; Vetter et al. 2012), which is dually expressed in both sympathetic and sensory nerves (Chang et al. 2018). Furthermore, I made a case for the sensory signalling phenomenon of antidromic signalling in Chapter 1, meaning the sensory nerves within the tissue may possess the ability to signal anti-dromically 'backwards' to release their synaptic contents onto adipocytes (Mishra et al. 2024). Therefore, due to the global application of veratridine in an *ex vivo* model where a heterologous population of both sympathetic and proposed sensory nerves exist, there may have been harmonised release of both sympathetic and sensory transmitters.

As previously described, adipocytes possess receptors for CGRP and SP, which have been demonstrated to regulate lipolysis (Halloran et al. 2020; Liu et al. 2017; Miegueu et al. 2013; Walker et al. 2014). However, these studies do not directly illustrate that

an antidromic mechanism of sensory nerves is responsible for the deployment of these neurotransmitters in white adipose tissue, to routinely regulate lipolysis or homeostasis. Indeed studies typically observe effects of exogenous application of the transmitters on adipocytes, or cell lines. Therefore the role of these receptors on adipocytes is unclear. Antagonism of either receptor made no impact on veratridine-stimulated lipolysis. These results therefore may not be unexpected as antidromic signalling within adipose tissue hasn't been conclusively demonstrated. Additionally, evidence from Chapter 3 suggested that the nerves observed tracking though the tissue and in closest association to adipocytes are of sympathetic origin. Therefore, even if the nerves become stimulated by veratridine to release neurotransmitter antidromically, they are likely doing so proximal to vasculature, or within bundles where most of the 'non-sympathetic' innervation was observed. Therefore there may be a limitation to the potential effects of sensory stimulation in influencing lipolysis, which may contribute to why there was a lack of response observed antagonising the respective receptors.

Alternatively, veratridine stimulation may not have induced the antidromic release of sensory release of neuropeptides that may otherwise naturally occur *in vivo*. For instance, in other studies in comparisons of nervous stimulation, veratridine failed to induce release of CGRP, while successfully inducing SP and VIP release form isolated rat neurons (Belai et al. 1988).

In any case, in answer to aim 3 of this chapter, it can be concluded that veratridine stimulation of potentially global nervous discharge within the tissue is not inducing sensory-derived neurotransmitter activation of the tissue in a way that impacts glycerol release, even partially. It remains unclear whether antidromic release of sensory neuropeptides does occur in this model and further neuro-centric experiments are required to determine this definitively. Additionally, in future to provide a baseline of expected outcomes on lipolysis, exogenous application of CGRP or SP together with a stimulant of norepinephrine would demonstrate a positive control of what to expect if these peptides were present.

4.4.9 Other sympathetic-derived neurotransmitters appear to have no impact on veratridine-stimulated lipolysis

4.4.9.1 NPY

The majority of reports that explore the role of NPY in adipose tissue regulation are focused on its role in the central nervous system. To reiterate, literature suggests adipocytes can express Y1 Y2 and Y5 receptors, which have been implicated in anti-lipolytic and lipogenic pathways (Kuo et al. 2007; Turtzo et al. 2001; Gericke et al. 2009; Singer et al. 2013; Yang et al. 2022).

Veratridine activation of nerves has previously shown a consequential release of NPY in other models, such as in colon preparations (Hyland et al. 2005). Therefore it was hypothesised under reasonable assumption that NPY may also be released upon veratridine activation of nerves. The investigation into the role of NPY was a key aim within the PhD project, as there is limited evidence where a physiological approach has been used to study the effects of NPY in adipose tissue metabolism. However, answering aim 3 of the chapter, under the conditions applied within the model, none of the receptors targeted appeared to play a role in regulating lipolysis. This suggests either NPY is not released by veratridine stimulation, or it is and does not contribute meaningfully to lipolysis regulation. The absence of effect of Y5 receptor antagonism is unsurprising, as there is very limited evidence for the role of the receptor at the adipocyte level. Yet the lack of effect of Y1 and Y2 receptor antagonism was surprising. These data therefore contradict a suite of literature implicating NPY in anti-lipolytic mechanisms at the peripheral adipose level (Labelle et al; Shi et al; Kuo et al. 2007).

However, I did not establish whether these, or other, receptors were expressed on adipocytes within the tissue preparations used here. Therefore I cannot be certain of the presence of NPY receptors on the adipocytes within the adipose tissue, which could explain the lack of response.

Also, while NPY receptors are generally G_i-linked, evidence has suggested Y1 and Y2 receptors may be G_q-linked in some cell types, as found in rabbit SMCs (Misra et al. 2004). Therefore its possible that adipocyte-expressed Y1 receptors had some deviation/duplicity in their signalling pathways and instead increased Ca^{2+} may have altered the ultimate outcome. Also, the surge of norepinephrine released in this novel model

may overcome the mitigating capacity of the negative-regulatory receptors such as NPY receptors.

Another possible explanation is that neuropeptides are generally slow acting, so an incubation period of 3 hours could be insufficient to observe effects (Hodges et al. 2009). Finally, in early experiments using veratridine, researchers proposed it may have a differential effect on exocytosis of various neurotransmitters, with those such as GABA & glutamate being released in response to a Na^+ gradient, forcing vesicles to the synapse, and others more dependent on Ca^{2+} (Levi et al. 1980). The non-canonical and complex nature of the veratridine mechanism of exocytosis has been a continuous thread throughout this chapter. Therefore its possible that under veratridine stimulated conditions, NPY was not being effectively released from nerves. Supporting this theory, researchers have suggested that NPY is released during "higher stimulation frequencies", due to storage in large core dense vesicles (Hill et al. 2001; Labelle et al. 1997). As the stimulation frequency or depolarising characteristics of veratridine were not established in the present work, it remains possible veratridine under these conditions failed to induce NPY release. Further work is required to establish the bounds of these ideas, such as challenging nerves with a different stimulatory technique like EFS to verify the role of endogenous NPY. Also, to serve as a reference comparison, it would be interesting to observe the effects of exogenous NPY application under norepinephrine-stimulated conditions and observe whether adipocytes possess capacity to respond in an *ex vivo* setting, as other studies typically use 3T3-L1 cell lines (Long et al. 2015; Turtzo et al. 2001).

4.4.9.2 ATP

ATP is a well-established co-transmitter in sympathetic nerves of other tissues. A key aim of the PhD was to investigate the effects of ATP postjunctionally, under the hypothesis that veratridine induces release of neuronal ATP.

Tackling aim 4 of this chapter, during the investigation into postjunctional roles of ATP, I found there was a lack of effect of general P2 purinergic blockade on lipolysis with suramin or PPADS. Suramin and PPADS are competitive inhibitors, therefore, increased concentrations of natural ligands may out-compete introduced antagonists (Billington et

al. 2007; Jenkinson et al. 2000). Supporting this hypothesis, a similar response has been noted with suramin in research by Jenkinson et al. (2000) who found suramin failed to block ATP-induced responses, in fact potentiated them. The authors proposed suramin may have preserved ATP from degradation by inhibiting ectonucleotidases and there was a negative correlation between suramin efficacy and ATP concentration. Effectively, higher concentrations of substrate reduce efficacy and capacity of the antagonist.

More specific experiments are required to prove that ATP is being released from sympathetic nerves upon veratridine stimulation within this tissue, as the current data cannot confirm this.

4.4.9.2.1 Selective antagonism of P2X4 and P2Y6 had no effect on veratridine-stimulated lipolysis

Both antagonists, suramin and PPADS, are also known for having promiscuous and pleiotropic effects across other receptors, which cannot be ruled out from affecting the overall net lipolysis and indeed contributing to trends described above. For example suramin is implicated as an inhibitor of enzymes involved in the citric acid cycle, as well as at Na^+/K^+ ATPases and other GPCRs (Wiedemar et al. 2019). PPADS has been suggested to have inhibitory effects at NAADP receptors (Billington & Genazzani 2007). These complications prompted and justified a more direct approach. Given that the RT-PCR results revealed expression of P2X4 and P2Y6 receptors and these pan P2R antagonists have unequal antagonistic action across the suite of P2 receptors, its reasonable to assume that they may have unequal affinity for the receptors expressed on the adipocytes. Indeed, PPADS is found to have higher potency at the human versus the rat P2X4 receptor (Ralevic et al. 1998) and was suggested to have limited activity at the mouse P2X4. However this has been contradicted and mouse P2X4 was experimentally determined to be PPADS-sensitive, however the same study also finding that P2X4 was suramin-insensitive (Jones et al. 2000). Suramin and PPADS have been suggested to only have 'slight' antagonistic action at rat P2Y6 receptors (Abbracchio et al. 2006; Ralevic et al. 1998). While these are not translational to mouse, it does suggest the results may not be reflective of the true involvement of these receptors when these broader antagonists are applied.

However, selective antagonists of P2X4 and P2Y6 receptors had no significant effect on veratridine-evoked lipolysis either, suggesting there was no involvement of these receptors in regulating lipolysis. This was unsurprising as literature converges on either neutral or more anti-lipolytic roles for P2 purinergic signalling in general.

The P2Y6 receptor has been found expressed in adipocytes (Chapter 1 Table 1.2), with roles reported in glucose uptake (Balasubramanian et al. 2014) and gene regulation, which correlates with maintenance of the white adipocyte phenotype in mice (Jain et al. 2022). Therefore the detected presence of P2Y6 receptor falls in line with literature describing its positive expression in mice. The lack of role of P2Y6 receptor in lipolysis regulation observed in the present model is likely a true reflection of the P2Y6

receptor contribution to basal and stimulated lipolysis because, as previously stated, the P2Y6 receptor has limited claims of involvement in regulation of lipolysis. Jain et al. (2020) reported that the P2Y6 receptor "did not play a significant role in lipolysis" in either basal or stimulated conditions, instead was implicated in maintaining the white adipocyte phenotype through gene regulation. Crucially, the P2Y6 receptor is not activated by ATP, so the results may be reflective of veratridine having no agonist-driven influence, thus rendering antagonism redundant. It also suggests endogenous levels of UDP, the recognised ligand for the P2Y6 receptor, may not activate the receptor enough to manifest in alterations to lipolysis, or the outcomes are unrelated to lipolysis.

The P2X4 receptor is not a receptor commonly reported present on white adipocytes, with limited literature describing its presence and possible function. Tian and colleagues found P2X4 expressed in mouse primary white adipocytes, but conclude little in terms of function of the receptor in the context of lipolysis (Tian et al. 2020). Therefore, the apparent redundancy of the P2X4 receptor in lipolysis regulation within this model may support absence of literature suggesting its expression and function in white adipocyte cell types, and therefore may not present an unexpected result.

In the case of both receptors, other measurables such as adipocyte number, adipokine secretion, glucose uptake and transcriptional patterns may be altered in response to receptor antagonism, but not in a way that translates to glycerol release and therefore, missed. For example, research has suggested that both ATP (via P2Y2 receptors) and norepinephrine conjunctionally regulate adiponectin release from white mouse adipocytes (Musovic et al. 2022b). It is also possible that the receptors may influence lipogenesis as opposed to lipolysis, which was not investigated. Additionally, the effects on lipolysis may occur on a longer timescale which evades detection in the short-term study here.

Overall, the receptor subtypes found present and absent were surprising, as they largely contradicted literature. Other studies, including work within the Fountain lab (Ali et al. 2018ba), have found a plethora of purinergic receptor subtypes on human and mouse white adipocytes, using techniques to detect both RNA and protein (Chapter 1, Table 1.2). For example, P2X5 (Ussar et al. 2014; Tian et al. 2020) & P2X7 (Li et al. 2022) receptors have all been found expressed in mouse primary white adipocytes from visceral or subcutaneous depots. Additionally, P2Y1 (Laplante et al. 2010), P2Y2

(Musovic et al. 2022; Zhang et al. 2020; Negri et al. 2020), P2Y4 (Lemaire et al. 2017), P2Y13 (Duparc et al. 2024; Laplante et al. 2010) and P2Y14 (Jain et al. 2021; Xu et al. 2012) receptors have been identified in mouse primary white adipocyte and 3T3-L1 cell lines, as well as in whole adipose tissue. However these receptor subtypes were not detected here, and may have been beyond limit of detection using the selected methods. Additionally, most of these studies use cultured adipocytes, or fail to provide evidence of a 'pure' population of a fresh preparation of adipocytes, free from components of the SVF (See Chapter 1, Table 1.2). A complimentary and conformational experimental approach recommended for future work is RNA sequencing. RNA-seq would provide an accurate and thorough screening system for SVF contamination, as well as detection and quantification of mRNA potentially missed by RT-PCR here. Also, as solely mRNA was investigated, its possible that the receptors are latent and untranslated to protein and therefore don't possess a functional role. Assessment of protein for these receptors by western blot or immunocytochemistry is recommended.

Collectively the data suggests that if ATP is a co-transmitter in sympathetic nerves of white adipose tissue in mice, it may not influence lipolysis. Data also aligns with the lack of response to general antagonism observed with suramin and PPADS as these receptor subtypes are not renowned for roles in lipolysis. This largely conforms with literature, whereupon P2 receptor roles are generally restricted to adipogenesis, phenotype maintenance and adipokine secretion, unless the receptor is coupled with a G protein that interacts with adenylyl cyclase.

Lastly, again it must also be considered that veratridine may not have induced the release of neuronal ATP, if indeed it is present as a co-transmitter in this tissue, and thus the receptors were not sufficiently "agonised". These mechanistic aspects were not determined or investigated here and present important steps for future enquiry.

4.4.10 P2 purinergic signalling plays no role in basal or stimulated lipolysis

The P2Rs identified may not have been being activated under veratridine stimulation as, despite the trend with norepinephrine and PPADS, there is limited direct evidence to

suggest ATP is being released by veratridine. Thus it was necessary to agonise the receptors to establish a positive control and also to characterise activation of the receptors under basal conditions, without the induction and potential complication of introduced signalling molecules from neurogenic stimulation. While a strength of the model is the prospect of a complete deployment of sympathetic transmitters, it also adds complexity to responses, making aspects such as roles for nucleotides hard to detangle.
Therefore, to fully and thoroughly establish whether P2 purinergic signalling possessed any role in lipolysis in this *ex vivo* model, exogenous application of nucleotides was necessary and were applied at two concentrations under both a basal and norepinephrine-stimulated conditions to activate P2 receptors identified. This is especially important since P2Y6 was likely unstimulated in the veratridine experiments.

There is an apparent bimodality of effects observed in literature when applying nucleotides in this manner, albeit in other models. Tozzi et al (2019) reported that exogenously applied ATP potentiated lipolysis. Additionally, Lee et al (2005) found increased lipolysis in rat white adipocytes after ATP and UTP perfusion. Others found that broad purinergic activation increased lipogenesis, with no role in regulating lipolysis (Schödel et al. 2004). Owing to the general consensus in literature of a neutral or anti-lipolytic leaning role of P2Rs (discussed in Chapter 1), with the subtypes identified, my expectation was for lipolysis to decrease.

Despite my hypothesis, the lack of effect after nucleotide supplementation to diminish or conversely, promote lipolysis under stimulated or basal conditions, was unsurprising given the collective outcomes in previous experiments.
To offer an explanation, its possible that the concentrations of nucleotides applied were too high and could have desensitised the receptors, yet researchers have used these concentrations previously and induced signalling cascades (Cockayne et al. 2005). Given the lack of change in glycerol release after exposure to high concentrations of nucleotides, it would be reasonable to conclude P2 purinergic signalling plays no role in the potentiation or attenuation of either stimulated or basal lipolysis in this model/context.
Its also possible that any nucleotide-induced responses that impact lipolysis occur on a discrete timescale than sampled here, and the rate of glycerol release may instead be transiently altered, but not the overall total. A time series comparing nucleotide-exposed

versus control tissues may prove fruitful to this end.
Another explanation is that application of nucleotides in an *ex vivo* preparation of adipose is not a common approach, as there is limited literature employing this methodology. As such, it is possible this reflects a more physiological perspective of purinergic signalling than experiments with isolated cells.

4.4.10.1 No effect of ectonucleotidase inhibitors on basal lipolysis with and without exogenous nucleotides or in norepinephrine-stimulated lipolysis

In the interest of a thorough investigation, it was necessary to ensure nucleotides were not being hydrolysed. NTPDases are enzymes chiefly responsible for hydrolysing triphosphates into monophosphates and they exist on the surface of many cell types (Giuliani et al. 2021). Their ubiquitous nature and manner of expression ensure that associated signalling is negatively regulated, preventing persistent activation of signalling pathways which may otherwise have nefarious effects (Haas et al. 2021). Due to the likelihood that endogenous NTPDase activity was still occurring given the *ex vivo* approach, reducing the enzymatic breakdown of nucleotides within the tissue, in combination with nucleotide supplementation was necessary. The goal was to increase the concentration of nucleotides, should they be hydrolysed too rapidly for effects to be observed.
However I failed to see any effect of ARL 67156 alone, or alongside nucleotides, on basal lipolysis. Nor did the addition of ARL 67156 to basal or norepinephrine-stimulated tissues with only endogenous sources of nucleotides have any effect.

There are different subtypes of NTPDase (CD39) 1,2,3 AND 8 (Robson et al. 2006). In WAT, the most likely subtypes present are NTPDase 2, as it is expressed on many cells such as pericytes, myofibroblasts and glial cells, and NTPDase 3 as it is reportedly expressed in the peripheral nervous system (Sandhu et al. 2021). Generally, ARL 67156 is considered a selective CD39 inhibitor, but researchers investigated the subtypes most affected and found ARL 67156 acts as an inhibitor of NTPDases 1, 2, 3 and 8 and NPP 1 & 3 and ecto-5'-nucleotidase to varying degrees of efficacy, depending on concentration applied (Lévesque et al. 2007). Ultimately NTPDase2, NTPDase8, NPP3 and ecto-5' -nucleotidase activities were found to be the most affected. There is little information

currently available that definitively suggests the ecto enzyme subtypes most likely to be present in WAT, lest specifically in mouse inguinal WAT. Therefore, based on the evidence above, its possible that ARL 67156 was not able to quench endogenous ecto enzyme activity to its full extent, particularly if resistant types are dominant in this tissue. While there is likely overlap of the subtypes of NTPDase found present in adipose and those that are sensitive to ARL 67156, further investigation would provide additional clarity and certainty.

Additionally, researchers found the efficacy of ARL 67156 reduced when concentrations of NTPDase substrate were high, likely due to it being a competitive inhibitor (Schäkel et al. 2020). In other words, the higher the concentration of ATP, the less effective ARL was at inhibiting the enzyme activity of NTPDase. For example, in mouse, NTPDase1, 3 and 8 saw a 50% inhibition with 100 μM ARL 67156 when ATP was 10 μM, which halved as the concentration of ATP was increased to 100 μM, then again at 500 μM. NTPDase 2 inhibition by ARL 67156 was reduced even at low ATP concentrations (10 μM). Therefore, as I was also exposing the tissue to 100 μM of substrate under basal conditions, it potentially reduced the efficacy of ARL 67156 at preventing their hydrolysis. However, I also saw no response when applying ARL 67156 to basal and stimulated tissues without the exogenous application of nucleotides where, presumably, the nucleotide concentrations are lower meaning the above may not explain the results. Therefore, as the theoretical protection of either endogenous or exogenous sources of nucleotides had no significant impact on lipolysis, the results support the previous data, that P2 receptors are not important in the regulation of lipolysis under these conditions.

There are reports that other ectonucleotidase inhibitors may be more selective against ATP degradation such as POM-1 (Durnin et al. 2016), which may be valuable to explore in future experiments. Additionally, the use of a non-hydrolysable alternative to ATP, such as ATP-γ -S may equally provide clarity.

4.4.10.2 Removing endogenous nucleotides had no effect on lipolysis

To conclude the investigation into the role of purinergic signalling, apyrase was used complimentary to experiments where P2 purinergic receptors were antagonised. As nucleotides can derive from multiple sources in WAT, it was possible that the receptors were already saturated. Apyrase offered removal/reduction of endogenous nucleotide

signalling via hydrolysis into monophosphate forms, without blocking the receptors.

The lack of effect of apyrase observed in basal conditions may indicate that there is no role of purinergic signalling at the basal level, as hydrolysis of existing nucleotides had no effect. This was unsurprising, given the previous outcomes using selective antagonists for the identified receptors under basal conditions.

It is plausible that the biological effects of applying nucleotide-hydrolysing enzymes, such as apyrase, are complex as they hydrolyse triphosphates into their monophosphate form, it is likely increasing the proportion of adenosine, if resident ecto-5'-nucleotidases are present and active. The resulting adenosine generated post-enzyme action may drive P1 receptor signalling in adipocytes. P1 receptors are typically G_i or G_s-linked receptors which can either increase or decrease AC signalling. There are reportedly A1 (G_i/G_q), A2A (G_s) and A3 (G_i/G_q) P1 receptor subtypes on white adipocytes (Tozzi et al. 2017). However, I failed to see indications of this, as basal and norepinephrine-stimulated glycerol release of apyrase-exposed tissue remained similar to that of tissues without apyrase exposure. The outcomes may depend on the expression and abundance of the adenosine receptors on the adipocytes, which were not investigated in this work. If there were a greater expression of G_s-linked A2A adenosine receptors, then any lipolysis-reducing effect of blocking P2Rs may be overcome by a shunt toward the adenosine G_s pathway. The overall effects of apyrase may therefore have resulted in a net effect of lipolysis that matched stimulated controls, yet further investigation is recommended to clarify the effects described above.

Again, the results therefore support the other suite of experiments demonstrating a lack of role for P2 purinergic signalling in lipolysis in mouse WAT, as well as literature (Jain et al. 2022; Garca-Barrado et al. 2001; Schödel et al. 2004; Laplante et al. 2010). Ultimately, the signalling outcomes depend on the overall effect of Ca^{2+} signalling and its contribution to lipolysis. Interestingly, norepinephrine and ATP have been both shown to increase $[Ca^{2+}]_i$ in rat white adipocytes to a similar degree, with a rise to around 300 nM, clearly indicating some degree of relationship (Kelly et al. 1989). Its clear from literature that Ca^{2+} is generally important to adipocytes due to expression and constitutive activity of Ca_V channels (Fedorenko et al. 2020). Yet this may mean that additional Ca^{2+} introduction would have to overcome existing Ca^{2+} tone to elicit effects.

In summary of the investigation into P2 purinergic involvement in lipolysis, to investigate whether there was a role, I tackled with four main approaches, general & specific blockade, nucleotide supplementation, theoretical preservation and removal via hydrolysis. In light of subsets of evidence in literature described in Chapter 1, I may have found the purinergic receptors identified to possess a negative regulatory role in lipolysis. However, with the combined information from veratridine, norepinephrine and basal studies, there appears to be no role for P2 purinergic signalling in this model for regulation of lipolysis, which aligns with another suite of literature suggestive of a lack of role. The trend observed in norepinephrine stimulated lipolysis in response to PPADS is likely to be an anomaly which would require additional investigation to fully establish. Impacts on gene expression, adipokine secretion and other cell processes may have been impacted, but were not investigated. Although P1 receptor signalling was not explored in this model, investigation into P1Rs may produce more conclusive outcomes.

4.4.11 Conclusive remarks

In this chapter, I have presented that lipolysis can be induced *ex vivo* by the action of Na^+ channel opener veratridine, and provided a convincing case this is operating via nerve-mediated release of neurotransmitter norepinephrine. This work has shown that the β2-AR was most important in conveying the lipolytic signal, which presents an intriguing finding, contradicting the β3-AR-dominant narrative presented in literature. The mechanism of veratridine-induced release of norepinephrine is apparently Ca^{2+} independent. In the model here, the mechanism of induced lipolysis was also independent of influence from other neurotransmitters and neuropeptides of sympathetic or sensory origin. To elaborate, contrary to literature, NPY had no negative regulatory role in lipolysis under these conditions. P2 purinergic signalling provided no role in *ex vivo* basal or stimulated lipolysis, whether pharmacologically or neurogenically stimulated.

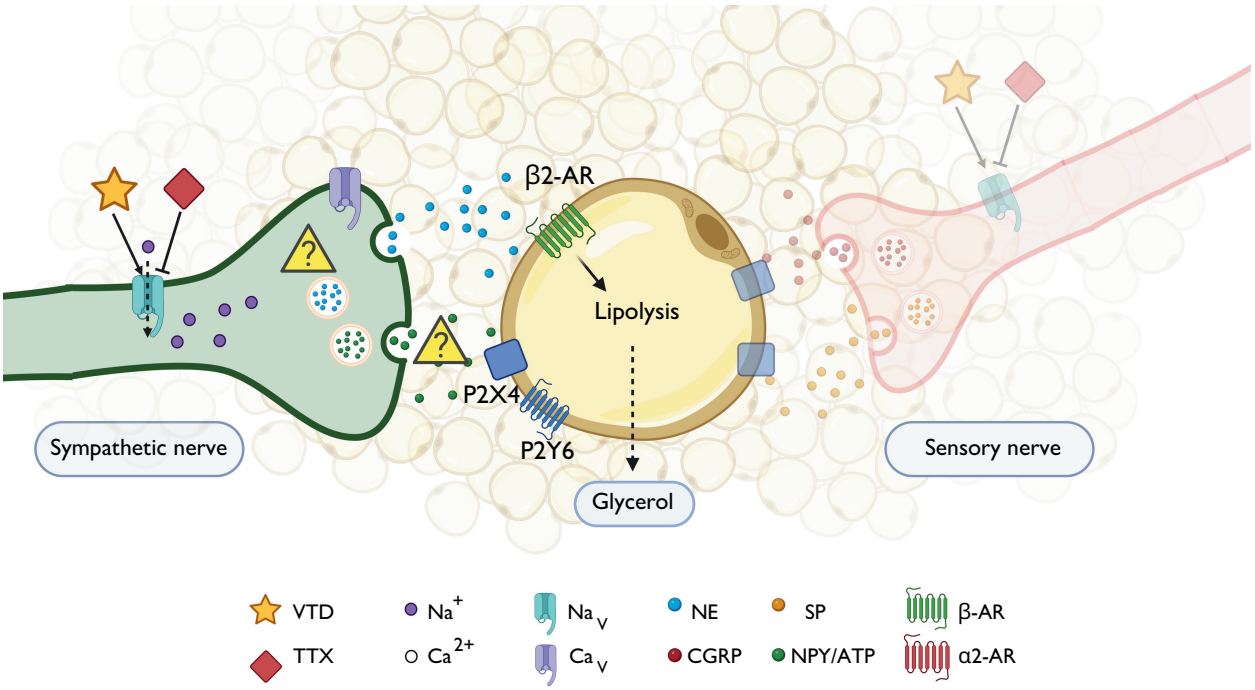

Figure 4.23: Illustration of the present understanding of veratridine-evoked lipolysis. Illustrative diagram of the current understanding of veratridine-evoked lipolysis in an *ex vivo* model at the end of this PhD project. Veratridine appears to act on voltage gated sodium (Na_V) channels, and induces lipolysis independently of voltage gated calcium (Ca_V) channels. Veratridine induces the release of an apparently catecholamine neurotransmitter that acts on β-adrenergic receptors (ARs), specifically β2-ARs. Sensory neuropeptides substance P (SP) and calcitonin gene-related peptide (CGRP) and other sympathetic co-transmitters neuropeptide Y (NPY) and adenosine triphosphate (ATP) appear to have no involvement in lipolysis. Yellow triangular symbols refer to where further characterisation is required, for example determining Na^+-dependence of veratridine exocytosis and whether NPY/ATP is being released effectively.

Chapter 5

General discussion

The aims and objectives outlined in Chapter 1 Section 1.6 have been addressed within the research presented in this thesis. Within each chapter discussion, I have offered theories and hypothesis for the results obtained, alongside suggestions for future work relating to specific experiments. The purpose of the present chapter is to highlight overall benefits and drawbacks of the approaches and research in the context of the wider world and suggestions of critical next steps for scientific benefit.

5.1 Innervation of inguinal WAT

Using a novel approach of whole-mount immunocytochemistry (Townsend method, Willows et al. 2021) and selective antibodies against nerves, as well as a vascular stain, evidence of vascularisation and neuronal innervation of the inguinal fat depot was gained. There was dominance of TH-positive 'sympathetic' neurons found innervating the parenchyma and vasculature, however literature offers this may have been falsely inflated by the fact that a population of sensory nerves can also apparently stain positively for TH (Willows et al. 2023; Wang et al. 2022). Investigating this possibility is a crucial immediate step in order to accurately comprehend the sympathetic innervation of adipose, especially since many researchers use these markers to form conclusions on innervation. Validation via conjunctional use of a sensory-specific marker alongside TH would aid identification of sympathetic, versus sensory TH-positive.

As laid out in Chapter 1, both vascular dysfunction and neuropathy occur in patho-

logical states of obesity. Loss of these structures serves to perpetuate the obese state and increase inflammation, leading to tissue dysfunction. Therefore, in combination with markers for sensory and sympathetic nerves, to fully explore neurovascular relationships, future immunocytochemistry experiments should include specific markers for the detection and distinction of larger vasculature; veins, arteries and lymph vessels. In doing so, this would provide clear evidence of differential innervation patterns across vascular beds. Ultimately, application of the method in obese models will allow for chronologically tracked observations of how these structures change in response to obesity. For example, is there an order to dysfunction? Do nerves innervating the blood vessel deteriorate in response to vascular dysfunction, or vice versa? Within Chapter 3, I described how bundles of nerves appeared to receive vascularisation, prospectively a form of vasa nervorum. Nerve bundles have recently been suggested as origin branch points for parenchymal innervation of the depot (Huesing et al. 2021) and was something that was observed on rare occasions here. Do these vessels also become dysregulated during obesity and does this mean that potential origins of nervous innervation reduce as consequence?
In tandem with this, next experiments ought to compare parenchymal and adipocyte level innervation across obese, diabetic and ageing models, and concurrently determine the extent lipolytic output is altered as consequence. Others have shown obesity-driven recession of nerves innervating WAT (Blaszkiewicz et al. 2019a). Could alterations such as these contribute to why there is a paradox between overall increased sympathetic drive in obesity (Kalil & Haynes 2012), but adiposity is maintained (Duncan et al. 2007)?

Crucially, future work ought to apply this whole mount approach to human subcutaneous explants to investigate whether innervation patterns described here are consistent across species. Others have already performed whole mount approaches using human tissue to observe sympathetic nerves (Perdikari et al. 2022). However harnessing the knowledge from the present project, it would be valuable to determine whether human depots share the same degree of sympathetic innervation. Also, whether neuroadipose interactions occur at the same frequency and also present with axonal varicosities which terminate in a NAN structure. Literature has suggested vascularisation between human and mice SAT in certain depots may differ, owing to differences in baseline size of adipocytes (Ledoux et al. 2008; Song et al. 2016; Börgeson et al. 2022). There appears to be less information specifically comparing nervous innervation between analogous de-

pots of mice and humans. In doing so, this would build strength in translatability when using a mouse model, as access to human tissue can be difficult for researchers.

5.2 Neurogenic activation of lipolysis by veratridine *ex vivo*

5.2.1 Prestige, promise and pitfalls

5.2.1.1 Prestige and promise

Veratridine has been utilised in many models to stimulate nerves and study the effects of subsequently released neurotransmitter. Specifically, veratridine has been used to successfully stimulate nerve activity in *ex vivo* models, such as in colon preparations (Hyland et al. 2005), in mesenteric arteries (Park et al. 2023) and in slices of striatal brain tissue (Dobrev et al. 1998).

However, at the time of writing, there has been no published application of veratridine to stimulate neurogenic activation of lipolysis in white adipose tissue *ex vivo*, presenting a novel research approach. Therefore, for the first time in white adipose tissue, veratridine was exogenously applied to sections of inguinal adipose tissue *ex-vivo*, to attempt induction of action potentials in resident neurons, and thus result in neurotransmitter release.

The *ex vivo* model used here to study a complex biological process is attractive, as it is a simple, economical and relatively swift way to measure lipolysis without the need for large, specialised equipment or facilities. The key benefit of employing such a system is it allows for all native cell types to be included in the context of the responses observed. This is a critical aspect that many 2D-culture *in vitro* studies lack. Studies have shown that 2D cultured cells do not typically share native characteristics/responses (Jensen et al. 2020). Relating to this, immortalised mouse adipocyte cell lines such as 3T3-L1 & C3H10T1/2 offer limited translatability to cells or tissues freshly obtained from the living organism, as culture environments can impact on receptor expression (Jensen et al. 2020). Cell lines, while providing important benefits for the research community, simply don't fully represent native adipocytes and their discrete gene expression patterns, which

reportedly vary depot-to-depot (Thompson et al. 2012; Bajek et al. 2017; Harms et al. 2019). Primary adipocytes are widely and notoriously known for being challenging to culture successfully, due to their fragility, buoyancy and short life-span *in vitro* (Harms et al. 2019; Lafontan 2012; Dufau et al. 2021). Yet the alternative of using pre-adipocyte cells and differentiating them *in vitro* is still not a direct substitute, as they often present with entirely different morphology once differentiated. Differentiated adipocytes are reportedly smaller without the characteristic unilocular white adipocyte appearance due to issues with lipid uptake and expansion, which again is not reflective of the analogous differentiated adipocyte *in vivo* (Lauschke et al. 2023).

3D cell culture models are emerging which do provide better and more valid representation, although often use cell lines and rely on exogenous application of immune molecules to replicate the obese state (Avelino et al. 2024). Recent developments using freshly isolated adipocytes in 'membrane mature adipocyte aggregate cultures' (MAAC) are providing even more useful data (Harms et al. 2019).

However, exciting scientific advancements have provided alternative *in vivo* optogenetic approaches, which offer the most valuable and translatable results. Herein, animals such as mice are genetically modified to express light-sensitive opsin channels along nerve axons, which can be "switched on" upon exposure to a laser, allowing for endogenous nerve activation at specific sites. However optogenetic approaches can be unattainably costly, time-consuming, with additional animal licensing requirements & ethics considerations and therefore not a viable option for many research groups.

Therefore, the present model using veratridine as a tool to stimulate lipolysis, offers a more physiological halfway house between *in vitro* cell culture with limited translatability, and *in vivo* optogenetic approaches.

Directly linked to this, another key benefit of the approach is flexibility, allowing for easy application to different disease contexts. For example, use in obese mice to study the implications on lipolysis in a model which may allow for full immunological retention, for a comprehensive disease state. This is a key aspect *in vitro* cell-culture studies often lack. Application in disease models, in harmony with investigating the innervation changes via immunocytochemistry, presents a key imminent step for future work using this system, to investigate how stimulated lipolysis changes within different disease and

age backgrounds. For instance, to more deeply examine obesity-driven catecholamine resistance and diabetic neuropathy.

Importantly, the data gained using veratridine was stable and consistent, with a reliable induction of lipolysis. Reproducibility is a general concern within scientific research and this approach may hopefully offer a reproducible platform for future work by different groups. Next steps should ensure it is reproducible across different adipose depots, as there are reportedly differences in lipolytic potential across depots (Roy et al. 2022). Therefore it would be prudent to validate veratridine-induced lipolysis among WAT depots such as axiliary SAT and then to visceral depots such as epididymal/perigonadal VAT. There is also the potential for veratridine to be used in studies of thermogenesis in brown adipose depots, which requires experimentation to verify and a new measure of temperature as output. As only male mice were used here, it is important to characterise the responses in female mice and investigate sex-based deviations in response and verify this method is reproducible in females.

The results gained here in mouse will not be immediately representative of other species physiology without further experimentation. Therefore the current results cannot be extrapolated to understanding human nervous control of white adipose tissue, which ultimately research using models such as these, aims to bridge. However, relating to both reproducibility and flexibility of the model, this approach can easily be applied across species and should be assessed for interspecific reproducibility in humans to gain more physiologically translatable and relevant data.

Comparing how relatable mouse versus human adipose explant responses are in terms of lipolysis would also clarify and potentially solidify the validity of rodent models to effectively study for, ultimately, human-centric issues. While there are known key differences between human and mouse lipolysis such as adipocyte α2-AR expression and role, literature has suggested that inguinal and human abdominal adipose is "comparable" in terms of results (Börgeson et al. 2022). Further work applying this model in such comparisons would develop (either prove or disprove) this narrative. As previously mentioned, further comparison of responses between species may serve to eliminate, or at least reduce, the need for access to human tissue which can be challenging for many research groups, while rodents are generally more accessible (provided the identified differences are ac-

counted for).

Moreover, application of this approach in humans can potentially insight and generate mitigative opportunities to target issues such as aforementioned catecholamine resistance, often seen in human obesity. For instance it could help tease apart catecholamine resistance and reveal whether nerve output is dysfunctional, alongside whether receptors on adipocyte cell surfaces are desensitised, as others found (Valentine et al. 2022; Reynisdottir et al. 1994; Arner 2005), or whether it relates to top-down signalling through altered adipokine secretion. More than likely, it is a complex combination and insight using human tissue of obese patients may offer new targets for intervention.

Relating to this, at present, there have been three main approaches to mitigating obesity in humans. Pharmacotherapies such as dinitrophenol (DNP) (sympathomimetic) and sibutramine (serotonin-norepinephrine reuptake inhibitor) have been historically used in an attempt to increase lipolysis via the β-adrenergic axis. However these imposed complex side effects, with the use of DNP linked to fatalities and sibutramine having serious cardiovascular side effects (Grundlingh et al. 2011). Mirabegron has been trialled as a β3-AR agonist for the induction of thermogenesis in BAT, but was found largely ineffective in obese patients (Dabrowska et al. 2023). NICE-approved pharmacological treatments for obesity include orlistat, a lipase inhibitor to reduce the efficiency of lipid metabolism and thereby calorie reduction (NICE.org). However orlistat is associated with issues relating to gastric motility and fat-soluble vitamin absorption (Filippatos et al. 2008).

A recent and high-profile introduction to pharmaceutical weight loss intervention has been semaglutide (Ozempic ®) and liraglutide diabetic medications, which target GLP-1 receptors in the CNS to reduce appetite and stimulate insulin release (NICE.org). These drugs are effective, with rapid weight loss, yet often results in weight loss relapse, with one study suggesting patients gained two-thirds of their weight loss back after a year of semaglutide withdrawal (Wilding et al. 2022). At present, aside from diet and exercise for weight management, bariatric surgeries present the most efficient and long-lived means of weight intervention for obesity (BMJ 2023 guidance).

Therefore, in consideration of the above and in light of the projected increases in obesity

and associated health & economic costs outlined in Chapter 1, there is an apparent need for developing alternative mitigative treatments for obesity management. Veratridine as a tool for neurogenic activation in an *ex vivo* model can therefore be used as a promising platform for assessing existing pharmaceuticals in pre-clinical trials, opposed (or additional to) to *in vitro* cell culture, for responses in a more valid, dynamic setting.
Further to this, additional research exploring the involvement of other receptors and signalling molecules not investigated here, may illuminate potential new targets for intervention.

Also, through research into nervous innervation and more physiologically representative lipolysis in adipose tissue, we can develop alternative techniques to overcome the obesity crisis. For example, there are already suggestions for nerve-stimulating electrotherapies to target nerves and stimulate lipolysis, as has already been applied to treat conditions such as Parkinson's disease and rheumatoid arthritis, among others (François et al. 2018).

As mentioned within Chapter 2, a promising and fruitful step for future work is to harness this platform to investigate the impact of veratridine stimulation on measureables other than lipolysis. Particularly with regard to purinergic involvement, as some literature that suggests no role in relation to lipolysis, instead find roles relating to a plethora of other cell processes such as adipokine secretion, gene regulation or lipogenesis (Ali et al. 2018a; Jain et al. 2022; Musovic et al. 2022a; Laplante et al. 2010; Schödel et al. 2004). Future work should verify whether veratridine-stimulated tissues secrete adipokines, as has been found in other models in response to application of norepinephrine (Musovic et al. 2022).

5.2.1.2 Pitfalls

Firstly, the mechanism underpinning veratridine-induced exocytosis remains unresolved, with findings indicating a Ca^{2+}-independent mechanism. The response is potentially contingent on Na^{+} ions, which remains to be established and is recommended research for follow-up studies. This could mean that other characteristics, such as complete neurotransmitter deployment, alongside reuptake and neuromodulatory mechanisms, differ from *in vivo* conditions. Therefore, veratridine-stimulated neurotransmitter release per-

haps does not represent accurate physiology as desired, and may present a pitfall without further characterisation.
Other studies using veratridine as a stimulant while applying antagonists typically look for effects within the same excitable cell type in question, rather than look for evidence of neurogenic effects on other cells (Soma et al. 2006; Platel et al. 2005). Therefore characterising veratridine exocytosis is challenging when applying antagonists or Ca^{2+}/ Na^{+}-free media challenge to the whole tissue and isolated nerves may provide more straightforward means to characterise the mechanism. For example culturing nerves from sympathetic ganglia that have been shown to innervate the tissue to conduct experiments on Na^{+} dependency.

Leading from this, this project did not provide evidence that neurotransmitters were released. While I systematically built a solid case, I have not unequivocally shown that veratridine causes norepinephrine release from neurons, nor have I established what quantities of norepinephrine are released. Further experiments using the culture of neurons described above and subsequent norepinephrine spillover assays would provide more direct evidence. The release of other co-transmitters was less convincing, therefore in the same manner, I could also observe whether veratridine does in fact induce NPY or ATP release in similar spillover studies.
Less specific assays can be performed with the existing methodology to measure the general quantity of norepinephrine in supernatant, which can be used to detect levels pre- and post-veratridine stimulation, providing proof of its liberation.

An additional characterisation of the veratridine response after proving release of norepinephrine would be to probe whether release occurs in pulses, or whether it is exhaustive. The stimulatory characteristics of veratridine may manifest as continuous bursts of neurotransmitter release over the 3-hour duration of incubation, or a single exhaustive expulsion of norepinephrine. If veratridine induces a complete discharge of neurotransmitter at a timepoint early within the incubation period, neuromodulatory mechanisms will be redundant, as there is not a continuation of exocytosis events to regulate. Therefore, what is being observed with veratridine may not be a true reflection of discrete physiological and regulatory processes that occur within the tissue.

To challenge this, norepinephrine reuptake mechanisms can be antagonised with the use of agents such as cocaine to disrupt nerve-mediated norepinephrine reuptake, which can indicate whether the response is dynamic (Zhu et al. 2022). More direct experimental measures could be applied, such as initiating the veratridine response, measuring glycerol release, washing and then re-agonising tissues with veratridine to see whether the response is repeatable.

In light of the above, a consideration of the model overall which ought to be investigated in future work using veratridine, is that it could be inducing damage to the nerves, which would make for one single large release. Other studies have exploited veratridine to this end (Zou et al. 2013). This may potentially explain why there are not apparent effects of inhibiting exocytosis or any signs of neuromodulatory mechanisms occurring, as nerves are damaged and releasing their contents in an unregulated fashion. To identify whether this is occurring, measurement of lactate dehydrogenase content in the tissue versus a positive and negative control may indicate whether this theory is correct. Additionally, immunocytochemistry with nerve markers TH or β3-tubulin can be performed on the tissue post-veratridine exposure to inspect the appearance of the nerves for signs of damage compared to norepinephrine and controls.
Regardless of whether the nerves are damaged and permeabilised by veratridine, the application still elicits lipolysis via a, convincingly, catecholamine stimulant. If this is the case, while not relevant for investigations relating to neuronal feedback mechanisms, stimulated lipolysis can still be investigated using veratridine to liberate endogenous stores of norepinephrine, opposed to exogenously applied.

A limitation of the present study, opposed to a pitfall, is that I did not investigate the role of intracellular calcium signalling at the adipocyte level in general. I thereby did not determine a baseline for what the overall effects of calcium are in regulating lipolysis in adipocytes in this system, which complicates interpretation of the purinergic role. This project therefore has not contributed to understanding the involvement of Ca^{2+} in lipolysis regulation with specific systematic experiments, which would have provided value to the scientific community.
To determine the general role of Ca^{2+} in lipolysis regulation in tissue of the inguinal fat

pad, stimulation of isolated adipocytes at basal or with norepinephrine under Ca^{2+}-free conditions, will determine whether the lipolytic response is blunted. Then to challenge the role of intracellular calcium cascades, artificially increasing/decreasing [Ca^{2+}]i using drugs such as ryanodine or caffeine/NAADP tetrasodium salt which inhibit or liberate release of intracellular endoplasmic reticulum stores of Ca^{2+}, respectively, and measure glycerol release in response. Understanding general Ca^{2+} effects on lipolysis allows for understanding purinergic receptor involvement. Using isolated adipocytes would provide additional clarity as to the roles of the specific P2 purinergic receptors in lipolysis at a more discrete level than was considered here. Perhaps also probing functionality of the identified receptors by using FURA-2 AM fluorescent dye to determine whether Ca^{2+} levels change in response to receptor agonism.

In more general terms, to fully understand the effects of intracellular Ca^{2+} in mouse white adipocytes, subtypes of adenylyl cyclase present should be identified, as there are different isoforms of AC which have differing sensitivities to Ca^{2+}, resulting in different outcomes to activity. For example, AC5 and AC6 are inhibited by Ca^{2+} presence, which would reduce AC-mediated lipolysis (Cooper 2005; Devasani & Yao 2022), meaning Ca^{2+} signalling in these cases would inhibit cAMP-driven lipolysis. Ultimately, in reflection of data presented here, adipocyte-level Ca^{2+} effects may be negated when in context of all other cell types and signalling mechanisms, resulting in no net observable effect on lipolysis.

This again links back to the fact that lipolysis was the only outcome considered here, as previously mentioned as a promising future study, but a present pitfall. Experiments where application of pharmacological agents had no effect on lipolysis, may instead have effected other cellular processes. Any pharmacological challenge applied must have an effect on glycerol release for approximation of it's role. For example, while I found peptides like NPY or P2 purinergic receptors appeared to have no impact on lipolysis, there may be important changes to secretory patterns in adipokine release, which are critical in top-down signaling signalling, rather than acute alterations in lipolysis (e.g. leptin and adiponectin). Therefore array assays to detect levels of various adipokines would be a complimentary line of investigation for a more systemic perspective of metabolic regulation in white adipose tissue. Additionally, in cases where other researchers have reported a drug as "having an effect" on lipolysis, they may be measuring intracellular

AC activity by cAMP increases, or other downstream indicators of lipolysis aside from glycerol release, which I haven't measured. If changes in intracellular mechanisms occur post-exposure to a given drug, unless they have a direct effect on the amount of glycerol released within the 3-hour incubation period, they will not be detected, which is a limitation of the study.

As briefly mentioned at the beginning of this section, a pitfall that befalls any whole-tissue experiment is detangling the responses when applying compounds, such as veratridine and antagonists, to the whole tissue. The associated complexities of using a physiologically representative *ex vivo* model are the equal and opposite drawbacks of the positives, as without a cell-specific target, the impacts of pharmacological agents will be shared among other cell types in the tissue. Therefore, in light of the above, characterising the roles of each neurotransmitter should also occur on isolated adipocytes or using aforementioned 3D culture models to determine approximate response baselines, as compliment to the whole-tissue approach.

Finally, is veratridine a sound and valid tool for the neurogenic activation of lipolysis? There are, of course, limitations in any scientific approach, as a model is always a model. Overall, the model is promising, provided further work is applied to fully characterise the mechanisms underpinning veratridine as a tool within it. As evidenced throughout this thesis and chapter, characterisation of exocytosis mechanisms, the stimulatory profile of veratridine (exhaustive or pulses) and whether or not it induces the release of all neurotransmitters, are all outstanding. Discovery of these outstanding points will determine whether or not this mechanism is sufficiently representative of *in vivo* conditions, and could potentially provide a promising alternative to cell culture approaches of investigating metabolism. Therefore, comparison of key findings attained by veratridine could be validated by repeating in another neurogenic-based model, such as EFS. While the EFS technique is not free of its own pitfalls, these comparisons would help understand the veratridine mechanism of action and to ascertain whether this approach represents a truly valid model. For example, the release and roles of other neurotransmitters, β-AR receptor subtype involvement and neuromodulatory mechanisms. Validation work using opotogenetic approaches offers the most physiologically sound way of determining

a baseline of responses of native neurogenic activation *in vivo*, with limited introduction of variables associated with *ex vivo* work. Optogenetics combined with a tissue-specific KO model for a given receptor type would allow for *in vivo* observations of lipolysis and thereby provide comparison for the veratridine *ex vivo* response.

5.3 Conclusive remarks

To conclude, the data presented within this PhD thesis suggest that veratridine operates solely via sympathetic nerves identified via immunocytochemistry within the tissue. Veratridine appears to act via a VGSC, releasing, independently of canonical Ca^{2+} mechanisms, what characteristically appears to be norepinephrine, as it acts via β-ARs . Specifically, veratridine-evoked lipolysis appears to be contingent on β2-AR subtypes. This presents an interesting finding and the first reported example where β2-AR has been the most critical subtype in rodent lipolysis, contrary to literature. No other neurotransmitter investigated was influential on lipolysis, and purinergic signalling appeared dispensable to lipolysis regulation overall.

Data also suggests that these inductions of lipolysis by norepinephrine are conducted in a diffuse manner, as immunocytochemistry revealed a casual neuroadipose relationship, which also appears to be exclusively sympathetic.

Future students and researchers should aim to further characterise the innervation and neurogenic activation of white adipose tissue, as per the provided suggestions, to fully develop these techniques for wider use in disease models and human adipose. The collective data from this project, with particular emphasis on veratridine as a tool in an *ex vivo* model, could be harnessed as a platform for drug development instead of, or complimentary to, existing *in vitro* cell culture methods, as well as for novel target identification.

Chapter 6

Bibliography

Abbracchio, Maria P., Geoffrey Burnstock, Jean Marie Boeynaems, Eric A. Barnard, José L. Boyer, Charles Kennedy, Gillian E. Knight, Marta Fumagalli, Christian Gachet, Kenneth A. Jacobson, and Gary A. Weisman (2006). "International Union of Pharmacology LVIII: Update on the P2Y G protein-coupled nucleotide receptors: From molecular mechanisms and pathophysiology to therapy". In: *Pharmacological Reviews* 58.3, pp. 281–341. ISSN: 00316997. DOI: 10.1124/pr.58.3.3.

Ali, Seema (2018). "Purinergic signalling in human adipose-derived mesenchymal stromal cells and in vitro differentiated adipocytes". PhD thesis.

Ali, Seema, Jeremy Turner, and Samuel Fountain (2018a). "Constitutive P2Y2 receptor activity regulates basal lipolysis in human adipocytes". In: *Journal of Cell Science* 131.22. ISSN: 14779137. DOI: 10.1242/jcs.221994.

Ali, Seema, Jeremy Turner, and Samuel J Fountain (2018b). "P2Y 2 and P2Y 6 receptor activation elicits intracellular calcium responses in human adipose-derived mesenchymal stromal cells". In: *Purinergic Signalling* 14.4, pp. 371–384. ISSN: 15739546. DOI: 10.1007/s11302-018-9618-3.

Anderson, Christopher M and Fiona E Parkinson (1997). "Potential signalling roles for UTP and UDP: sources, regulation and release of uracil nucleotides". In: *TiPS* 18, p. 7.

Angiolillo, Dominick J., Fabiana Rollini, Robert F. Storey, Deepak L. Bhatt, Stefan James, David J. Schneider, Dirk Sibbing, Derek Y.F. So, Dietmar Trenk, Dimitrios Alexopoulos, Paul A. Gurbel, Willibald Hochholzer, Leonardo De Luca, Laurent Bonello, Daniel Aradi, Thomas Cuisset, Udaya S. Tantry, Tracy Y. Wang, Marco

Valgimigli, Ron Waksman, Roxana Mehran, Gilles Montalescot, Francesco Franchi, and Matthew J. Price (2017). "International expert consensus on switching platelet P2Y12 receptor-inhibiting therapies". In: *Circulation* 136.20, pp. 1955–1975. ISSN: 15244539. DOI: 10.1161/CIRCULATIONAHA.117.031164.

Araújo-Vilar, D. and F. Santini (2019). "Diagnosis and treatment of lipodystrophy: a step-by-step approach". In: *Journal of Endocrinological Investigation* 42.1, pp. 61–73. ISSN: 17208386. DOI: 10.1007/s40618-018-0887-z.

Arch, Jonathan R.S. (Aug. 2008). *The discovery of drugs for obesity, the metabolic effects of leptin and variable receptor pharmacology: Perspectives from β3- adrenoceptor agonists*. DOI: 10.1007/s00210-008-0271-1.

Armstrong, Clay M and Bertil Hille (1998). *Voltage-Gated Ion Channels Review and Electrical Excitability*. Tech. rep., pp. 371–380.

Arner, P (2005). "Human fat cell lipolysis: Biochemistry, regulation and clinical role". In: *Best Practice & Research Clinical Endocrinology & Metabolism* 19.4, pp. 471–482.

Ashraf, Javed M and Paramdeep Baweja (2013). "Obesity: The 'Huge' Problem in Cardiovascular Diseases". In: *Missouri Medicine* 110.6, pp. 499–504.

Avelino, Thayna Mendonca, Marta García Arévalo Provencio, Luis Antonio Peroni, Romênia Ramos Domingues, Felipe Rafael Torres, Paulo Sergio Lopes de Oliveira, Adriana Franco Paes Leme, and Ana Carolina Migliorini Figueira (2024). "Improving obesity research: Unveiling metabolic pathways through a 3D In vitro model of adipocytes using 3T3-L1 cells". In: *PLoS ONE* 19.5. ISSN: 19326203. DOI: 10.1371/journal.pone.0303612.

Aveseh, Malihe, Maryam Koushkie-Jahromi, Javad Nemati, and Saeed Esmaeili-Mahani (2018). "Serum calcitonin gene-related peptide facilitates adipose tissue lipolysis during exercise via PIPLC/IP3 pathways". In: *Endocrine* 61.3, pp. 462–472. ISSN: 15590100. DOI: 10.1007/s12020-018-1640-2.

Baak, Marleen A. van (May 2008). "Meal-induced activation of the sympathetic nervous system and its cardiovascular and thermogenic effects in man". In: *Physiology and Behavior* 94.2, pp. 178–186. ISSN: 00319384. DOI: 10.1016/j.physbeh.2007.12.020.

Bachmann, Samia B., Denise Gsponer, Javier A. Montoya-Zegarra, Martin Schneider, Felix Scholkmann, Carlotta Tacconi, Simon F. Noerrelykke, Steven T. Proulx, and

Michael Detmar (2019). "A Distinct Role of the Autonomic Nervous System in Modulating the Function of Lymphatic Vessels under Physiological and Tumor-Draining Conditions". In: *Cell Reports* 27.11, pp. 3305–3314. ISSN: 22111247. DOI: 10.1016/j.celrep.2019.05.050.

Bae, Jaehyun and Byung Wan Lee (2023). *Association between Impaired Ketogenesis and Metabolic-Associated Fatty Liver Disease*. DOI: 10.3390/biom13101506.

Baek, Kyunghwa, Hyun Jung Park, Hyo Rin Hwang, and Jeong Hwa Baek (2014). "Propranolol attenuates calorie restriction- and high calorie diet-induced bone marrow adiposity". In: *BMB Reports* 47.10, pp. 587–592. ISSN: 1976670X. DOI: 10.5483/BMBRep.2014.47.10.176.

Bajek, Anna, Natalia Gurtowska, Joanna Olkowska, Małgorzata Maj, Łukasz Kaźmierski, Magdalena Bodnar, Andrzej Marszałek, Robert Debski, and Tomasz Drewa (May 2017). "Does the Harvesting Technique Affect the Properties of Adipose-Derived Stem Cells? The Comparative Biological Characterization". In: *Journal of Cellular Biochemistry* 118.5, pp. 1097–1107. ISSN: 10974644. DOI: 10.1002/jcb.25724.

Baker, Jillian G. (Feb. 2005). "The selectivity of β-adrenoceptor antagonists at the human β1, β2 and β3 adrenoceptors". In: *British Journal of Pharmacology* 144.3, pp. 317–322. ISSN: 00071188. DOI: 10.1038/sj.bjp.0706048.

Balasubramanian, Ramachandran, Bernard Robaye, Jean Marie Boeynaems, and Kenneth A. Jacobson (2014). "Enhancement of glucose uptake in mouse skeletal muscle cells and adipocytes by P2Y6 receptor agonists". In: *PLoS ONE* 9.12, pp. 1–19. ISSN: 19326203. DOI: 10.1371/journal.pone.0116203.

Barella, Luiz F., Shanu Jain, Takefumi Kimura, and Sai P. Pydi (Apr. 2021). *Metabolic roles of G protein-coupled receptor signaling in obesity and type 2 diabetes*. DOI: 10.1111/febs.15800.

Barnett, Mark W, Philip M Larkman, M W Barnett, and P M Larkman (2007). "The action potential". In: *Pract Neurol* 7, pp. 192–197.

Barreau, Corinne, Elodie Labit, Christophe Guissard, Jacques Rouquette, Marie Laure Boizeau, Souleymane Gani Koumassi, Audrey Carrière, Yannick Jeanson, Sandra Berger-Müller, Cécile Dromard, Franck Plouraboué, Louis Casteilla, and Anne Lorsignol (2016). "Regionalization of browning revealed by whole subcutaneous adipose

tissue imaging". In: *Obesity* 24.5, pp. 1081–1089. ISSN: 1930739X. DOI: 10.1002/oby.21455.

Bartness, Timothy J., Yang Liu, Yogendra B. Shrestha, and Vitaly Ryu (Oct. 2014). *Neural innervation of white adipose tissue and the control of lipolysis*. DOI: 10.1016/j.yfrne.2014.04.001.

Bartness, Timothy J. and C. K. Song (2007). "Sympathetic and sensory innervation of white adipose tissue". In: *Journal of Lipid Research* 48.8, pp. 1655–1672. ISSN: 00222275. DOI: 10.1194/jlr.R700006-JLR200.

Bartness, Timothy J., C. Kay Song, Haifei Shi, Robert R. Bowers, and Michelle T. Foster (Feb. 2005). "Brain–adipose tissue cross talk". In: *Proceedings of the Nutrition Society* 64.1, pp. 53–64. ISSN: 0029-6651. DOI: 10.1079/pns2004409.

Basciani, Sabrina, Stefania Mariani, Mario Arizzi, Marina Brama, Andrea Ricci, Christer Betsholtz, Cecilia Bondjers, Giulia Ricci, Angela Catizone, Michela Galdieri, Giovanni Spera, and Lucio Gnessi (2004). "Expression of Platelet-Derived Growth Factor (PDGF) in the Epididymis and Analysis of the Epididymal Development in PDGF-A, PDGF-B, and PDGF Receptor β Deficient Mice". In: *Biology of Reproduction* 70.1, pp. 168–177. ISSN: 00063363. DOI: 10.1095/biolreprod.103.019232.

Baskin, Alison S., Joyce D. Linderman, Robert J. Brychta, Suzanne McGehee, Esti Anflick-Chames, Cheryl Cero, James W. Johnson, Alana E. O'Mara, Laura A. Fletcher, Brooks P. Leitner, Courtney J. Duckworth, Shan Huang, Hongyi Cai, H. Martin Garraffo, Corina M. Millo, William Dieckmann, Vladimir Tolstikov, Emily Y. Chen, Fei Gao, Niven R. Narain, Michael A. Kiebish, Peter J. Walter, Peter Herscovitch, Kong Y. Chen, and Aaron M. Cypess (Oct. 2018). "Regulation of human adipose tissue activation, gallbladder size, and bile acid metabolism by A b3-adrenergic receptor agonist". In: *Diabetes* 67.10, pp. 2113–2125. ISSN: 1939327X. DOI: 10.2337/db18-0462.

Beck, B. (2006). "Neuropeptide Y in normal eating and in genetic and dietary-induced obesity". In: *Philosophical Transactions of the Royal Society B: Biological Sciences* 361.1471, pp. 1159–1185. ISSN: 09628436. DOI: 10.1098/rstb.2006.1855.

Beggs, J, P C Johnson, A Olafsen, and C J Watkins (1992). "Innervation of the vasa nervorum: changes in human diabetics". In: *J Neuropathol Exp Neurol* 51.6, pp. 612–641. DOI: 10.1097/00005072.

Belai, A and G Burnstock (1988). "Release of calcitonin gene-related peptide from rat enteric nerves is Ca2+-dependent but is not induced by K+ depolarization". In: *Regulatory Peptides* 23, pp. 227–235.

Bennett, M. R., A. Cheung, and K. L. Brain (Sept. 1998). *Sympathetic neuromuscular transmission at a varicosity in a syncytium*. DOI: 10.1002/(SICI)1097-0029(19980915)42:6<433::AID-JEMT6>3.0.CO;2-N.

Bentley, Donna C, Pawitra Pulbutr, Sue Chan, and Paul A Smith (2014). "Etiology of the membrane potential of rat white fat adipocytes". In: *Am J Physiol Endo-crinol Metab* 307, pp. 161–175. DOI: 10.1152/ajpendo.00446.2013.-The.

Berridge, M J (1997). "The AM and FM of calcium signalling". In: *Nature* 386, pp. 759–760.

Berridge, Michael J (2016). "The Inositol Trisphosphate/Calcium Signaling Pathway in Health and Disease". In: *Physiol Rev* 96, pp. 1261–1296. DOI: 10.1152/physrev.00006.2016.-Many.

Bezaire, Véronic, Aline Mairal, Carole Ribet, Corinne Lefort, Amandine Girousse, Johan Jocken, Jurga Laurencikiene, Rodica Anesia, Anne Marie Rodriguez, Mikael Ryden, Britta M. Stenson, Christian Dani, Gérard Ailhaud, Peter Arner, and Dominique Langin (2009). "Contribution of adipose triglyceride lipase and hormone-sensitive lipase to lipolysis in hMADS adipocytes". In: *Journal of Biological Chemistry* 284.27, pp. 18282–18291. ISSN: 1083351X. DOI: 10.1074/jbc.M109.008631.

BHF (2024). *Global Heart & Circulatory Diseases Factsheet*. Tech. rep., pp. 1–12.

Billington, Richard A. and Armando A. Genazzani (2007). "PPADS is a reversible competitive antagonist of the NAADP receptor". In: *Cell Calcium* 41.6, pp. 505–511. ISSN: 01434160. DOI: 10.1016/j.ceca.2006.10.002.

Black, Joel A. and Stephen G. Waxman (2013). "Noncanonical roles of voltage-gated sodium channels". In: *Neuron* 80.2, pp. 280–291. ISSN: 08966273. DOI: 10.1016/j.neuron.2013.09.012.

Blaszkiewicz, Magdalena, Jake W. Willows, Amanda L. Dubois, Stephen Waible, Kristen DiBello, Lila L. Lyons, Cory P. Johnson, Emma Paradie, Nicholas Banks, Katherine Motyl, Merilla Michael, Benjamin Harrison, and Kristy L. Townsend (2019a). "Neuropathy and neural plasticity in the subcutaneous white adipose depot". In: *PLoS ONE* 14.9, pp. 1–27. ISSN: 19326203. DOI: 10.1371/journal.pone.0221766.

Blaszkiewicz, Magdalena, Jake W. Willows, Cory P. Johnson, and Kristy L. Townsend (2019b). "The importance of peripheral nerves in adipose tissue for the regulation of energy balance". In: *Biology* 8.1, pp. 1–23. ISSN: 20797737. DOI: 10.3390/biology8010010.

Blaustein, Mordecai P, Eugene M Johnson, and Philip Needleman (1972). *Calcium-Dependent Norepinephrine Release from Presynaptic Nerve Endings In Vitro (veratridine/K +/tetrodotoxin/synaptosomes/rat/pargyline)*. Tech. rep. 8, pp. 2237–2240.

Blaustein, Mordecai P and W Jonathan Lederer (1999). "Sodium/Calcium Exchange: Its Physiological Implications". In: *Physiological Reviews* 79.3, pp. 763–854.

BMJ (2023). *Referral criteria and assessment for bariatric surgery: summary of updated NICE guidance*. DOI: https://doi.org/10.1136/bmj.p1880.

Bobryshev, A Yu, E A Petrushenko, and O A Krishtal (2012). *Effect of of ATP on Neurons of the Rat Intact Nodose Ganglion*. Tech. rep. 6, pp. 506–510.

Boehm, Stefan (1999). "ATP stimulates sympathetic transmitter release via presynaptic P2X purinoceptors". In: *Journal of Neuroscience* 19.2, pp. 737–746. ISSN: 02706474. DOI: 10.1523/jneurosci.19-02-00737.1999.

Boissaud-Cooke, Matthew, Thomas Edward Pidgeon, and Richard Tunstall (Apr. 2015). "The Microcirculation of Peripheral Nerves: The Vasa Nervorum. The Vasa Nervorum". In: *Nerves and Nerve Injuries*. Vol. 1. Elsevier Ltd, pp. 507–523. ISBN: 9780124104471. DOI: 10.1016/B978-0-12-410390-0.00039-1.

Boland, Linda M, James A Morrill, and Bruce P Bean (1994). *w-Conotoxin Block of N-Type Calcium Channels in Frog and Rat Sympathetic Neurons*. Tech. rep. 8, pp. 501–5027.

Bönisch H and Trendelenburg U (1987). "Veratridine-induced outward transport of 3H-noradrenaline from adrenergic nerves of the rat vas deferens". In: *Naunyn Schmiedebergs Arch Pharmacol.* 336, pp. 621–630.

Bootman, M D, M J Berridge, and L H Roderick (2002). "Calcium signalling: More Messengers More Channels, More Complexity". In: *Current Biology* 12, pp. 563–565.

Bora, Pablo and Anish S. Majumdar (2017). "Adipose tissue-derived stromal vascular fraction in regenerative medicine: A brief review on biology and translation". In: *Stem*

Cell Research and Therapy 8.1, pp. 1–10. ISSN: 17576512. DOI: 10.1186/s13287-017-0598-y.

Börgeson, Emma, Jeremie Boucher, and Carolina E. Hagberg (2022). "Of mice and men: Pinpointing species differences in adipose tissue biology". In: *Frontiers in Cell and Developmental Biology* 10. ISSN: 2296634X. DOI: 10.3389/fcell.2022.1003118.

Boutari, Chrysoula and Christos S Mantzoros (Aug. 2022). *A 2022 update on the epidemiology of obesity and a call to action: as its twin COVID-19 pandemic appears to be receding, the obesity and dysmetabolism pandemic continues to rage on*. DOI: 10.1016/j.metabol.2022.155217.

Bovetti, Serena, Yi Chun Hsieh, Patrizia Bovolin, Isabelle Perroteau, Toida Kazunori, and Adam C. Puche (May 2007). "Blood vessels form a scaffold for neuroblast migration in the adult olfactory bulb". In: *Journal of Neuroscience* 27.22, pp. 5976–5980. ISSN: 02706474. DOI: 10.1523/JNEUROSCI.0678-07.2007.

Bowers, Robert R, William T L Festuccia, C Kay Song, Haifei Shi, Renato H Migliorini, Timothy J Bartness, and Timothy J Bartness Sym (2004). "Sympathetic innervation of white adipose tissue and its regulation of fat cell number". In: *Am J Physiol Regul Integr Comp Physiol* 286, pp. 1167–1175. DOI: 10.1152/ajpregu.00558.2003.-White.

Braun, Katharina, Josef Oeckl, Julia Westermeier, Yongguo Li, and Martin Klingenspor (2018). "Non-adrenergic control of lipolysis and thermogenesis in adipose tissues". In: *Journal of Experimental Biology* 121, pp. 1–14. ISSN: 00220949. DOI: 10.1242/jeb.165381.

Bridge-Comer, Pania E. and Shannon M. Reilly (2023). "Measuring the Rate of Lipolysis in Ex vivo Murine Adipose Tissue and Primary Preadipocytes Differentiated In Vitro". In: *Journal of Visualized Experiments* 193.193, pp. 1–21. ISSN: 1940087X. DOI: 10.3791/65106.

Britton, Oliver J., Najah Abi-Gerges, Guy Page, Andre Ghetti, Paul E. Miller, and Blanca Rodriguez (Aug. 2017). "Quantitative comparison of effects of dofetilide, sotalol, quinidine, and verapamil between human ex vivo trabeculae and in silico ventricular models incorporating inter-individual action potential variability". In: *Frontiers in Physiology* 8.AUG. ISSN: 1664042X. DOI: 10.3389/fphys.2017.00597.

Brose, N, A G Petrenko, T C Sudhof, and R Jahn (1992). "Synaptotagmin: a calcium sensor on the synaptic vesicle surface". In: *Science* 256, pp. 1021–1025.

Burns, Marie E and George J Augustine (1995). *Synaptic Structure and Function: Dynamic Organization Yields Architectural Precision*. Tech. rep., pp. 187–194.

Burnstock, G and V Ralevic (1994). "New insights into the local regulation of blood flow by perivascular nerves and endothelium". In: *Brirish Journal of Plasnc Surgery* 47, pp. 527–543.

Burnstock, G., G. Campbell, D. Satchell, and A Smythe (1970). "Evidence that adenosine triphosphate or a related nucleotide is the transmitter substance released by non-adrenergic inhibitory nerves in the gut". In: *British Journal of Pharmacology* 40.4, pp. 668–688. ISSN: 14765381. DOI: 10.1111/j.1476-5381.1970.tb10646.x.

Burnstock, Geoffrey (2006). "Historical review: ATP as a neurotransmitter". In: *Trends in Pharmacological Sciences* 27.3, pp. 166–176. ISSN: 01656147. DOI: 10.1016/j.tips.2006.01.005.

Burnstock, Geoffrey (Apr. 2007). *Physiology and pathophysiology of purinergic neurotransmission*. DOI: 10.1152/physrev.00043.2006.

Burnstock, Geoffrey (2009a). "Purinergic cotransmission". In: *Experimental Physiology* 94.1, pp. 20–24. ISSN: 1469445X. DOI: 10.1113/expphysiol.2008.043620.

Burnstock, Geoffrey (2009b). "Purinergic regulation of vascular tone and remodelling". In: *Autonomic and Autacoid Pharmacology* 29.3, pp. 63–72. ISSN: 14748665. DOI: 10.1111/j.1474-8673.2009.00435.x.

Burnstock, Geoffrey (2012). "Purinergic signalling: Its unpopular beginning, its acceptance and its exciting future". In: *BioEssays* 34.3, pp. 218–225. ISSN: 02659247. DOI: 10.1002/bies.201100130.

Burnstock, Geoffrey (2018). "Purine and purinergic receptors". In: *Brain and Neuroscience Advances* 2, pp. 1–10. ISSN: 2398-2128. DOI: 10.1177/2398212818817494.

Cabral-Costa, João Victor, Carlos Vicente-Gutiérrez, Jesús Agulla, Rebeca Lapresa, John W. Elrod, Ángeles Almeida, Juan P. Bolaños, and Alicia J. Kowaltowski (May 2023). "Mitochondrial sodium/calcium exchanger NCLX regulates glycolysis in astrocytes, impacting on cognitive performance". In: *Journal of Neurochemistry* 165.4, pp. 521–535. ISSN: 14714159. DOI: 10.1111/jnc.15745.

Callaghan, Brian C., Evan Reynolds, Mousumi Banerjee, Ericka Chant, Emily Villegas-Umana, and Eva L. Feldman (July 2020). "Central Obesity is Associated With Neuropathy in the Severely Obese". In: *Mayo Clinic Proceedings* 95.7, pp. 1342–1353. ISSN: 19425546. DOI: 10.1016/j.mayocp.2020.03.025.

Calvani, Maura, Lorenzo Cavallini, Annalisa Tondo, Valentina Spinelli, Luisa Ricci, Amada Pasha, Gennaro Bruno, Daniela Buonvicino, Elisabetta Bigagli, Marina Vignoli, Francesca Bianchini, Laura Sartiani, Maura Lodovici, Roberto Semeraro, Filippo Fontani, Francesco De Logu, Massimo Dal Monte, Paola Chiarugi, Claudio Favre, and Luca Filippi (2018). "B3-adrenoreceptors control mitochondrial dormancy in melanoma and embryonic stem cells". In: *Oxidative Medicine and Cellular Longevity* 2018, pp. 1–11. ISSN: 19420994. DOI: 10.1155/2018/6816508.

Campbell, Jonathan E., Jacqueline L. Beaudry, Berit Svendsen, Laurie L. Baggio, Andrew N. Gordon, John R. Ussher, Chi Kin Wong, Fiona M. Gribble, David A. D'alessio, Frank Reimann, and Daniel J. Drucker (2022). "GIPR Is Predominantly Localized to Nonadipocyte Cell Types Within White Adipose Tissue". In: *Diabetes* 71.5, pp. 1115–1127. ISSN: 1939327X. DOI: 10.2337/DB21-1166.

Candelore, M R, L Deng, L Tota, X M Guan, A Amend, Y Liu, R Newbold, M A Cascieri, and A E Weber (1999). "Potent and Selective Human β3-Adrenergic Receptor Antagonists". In: *Journal of Pharmacology and Experimental Therapeutics* 290.2, pp. 649–655.

Cannon, Barbara and Jan Nedergaard (2004). "Brown Adipose Tissue: Function and Physiological Significance". In: *Physiological Reviews* 84, pp. 277–359. DOI: 10.1152/physrev.00015.2003.-The.

Cao, Ying, Huanhuan Wang, Qi Wang, Xiangli Han, and Wenwen Zeng (2018). "Three-dimensional volume fluorescence-imaging of vascular plasticity in adipose tissues". In: *Molecular Metabolism* 14.June, pp. 71–81. ISSN: 22128778. DOI: 10.1016/j.molmet.2018.06.004.

Caron, Alexandre, Syann Lee, Joel K. Elmquist, and Laurent Gautron (2018). "Leptin and brain-adipose crosstalks". In: *Nature Reviews Neuroscience* 19.3, pp. 153–165. ISSN: 14710048. DOI: 10.1038/nrn.2018.7.

Carpéné, Christian, Alain Bousquet-Mélou, Jean Galitzky, Michel Berlan, and Max Lafontan (May 1998). "Lipolytic effects of β1-, β2 and β3-adrenergic agonists in white

adipose tissue of mammals". In: *Annals of the New York Academy of Sciences* 839, pp. 186–189. ISSN: 00778923. DOI: 10.1111/j.1749-6632.1998.tb10756.x.

Carrithers, Michael D, Sulayman Dib-Hajj, Lisette M Carrithers, Gouzel Tokmoulina, Marc Pypaert, Elizabeth A Jonas, and Stephen G Waxman (2007). "Expression of the Voltage-Gated Sodium Channel NaV1.5 in the Macrophage Late Endosome Regulates Endosomal Acidification 1". In: *The Journal of Immunology* 178.12, pp. 7822–7832.

Catterall, William A. (2011). "Voltage-gated calcium channels". In: *Cold Spring Harbor Perspectives in Biology* 3.8, pp. 1–23. ISSN: 19430264. DOI: 10.1101/cshperspect.a003947.

Catterall, William A., Sandrine Cestèle, Vladimir Yarov-Yarovoy, Frank H. Yu, Keiichi Konoki, and Todd Scheuer (2007). "Voltage-gated ion channels and gating modifier toxins". In: *Toxicon* 49.2, pp. 124–141. ISSN: 00410101. DOI: 10.1016/j.toxicon.2006.09.022.

Cavaliere, Gina, Fabiano Cimmino, Giovanna Trinchese, Angela Catapano, Lidia Petrella, Margherita D'Angelo, Lucio Lucchin, and Maria Pina Mollica (2023). "From Obesity-Induced Low-Grade Inflammation to Lipotoxicity and Mitochondrial Dysfunction: Altered Multi-Crosstalk between Adipose Tissue and Metabolically Active Organs". In: *Antioxidants* 12.1172, pp. 1–23. ISSN: 20763921. DOI: 10.3390/antiox12061172.

Cero, Cheryl, Hannah J. Lea, Kenneth Y. Zhu, Farnaz Shamsi, Yu Hua Tseng, and Aaron M. Cypess (June 2021). "β3-Adrenergic receptors regulate human brown/beige adipocyte lipolysis and thermogenesis". In: *JCI Insight* 6.11. ISSN: 23793708. DOI: 10.1172/jci.insight.139160.

Cestèle, Sandrine and William A Catterall (2000). "Molecular mechanisms of neurotoxin action on voltage-gated sodium channels". In: *Biochimie* 82, pp. 883–892.

Chai, Zuying, Changhe Wang, Rong Huang, Yuan Wang, Xiaoyu Zhang, Qihui Wu, Yeshi Wang, Xi Wu, Lianghong Zheng, Chen Zhang, Wei Guo, Wei Xiong, Jiuping Ding, Feipeng Zhu, and Zhuan Zhou (Dec. 2017). "CaV2.2 Gates Calcium-Independent but Voltage-Dependent Secretion in Mammalian Sensory Neurons". In: *Neuron* 96.6, pp. 1317–1326. ISSN: 10974199. DOI: 10.1016/j.neuron.2017.10.028.

Chait, Alan and Laura J. den Hartigh (Feb. 2020). *Adipose Tissue Distribution, Inflammation and Its Metabolic Consequences, Including Diabetes and Cardiovascular Disease*. DOI: 10.3389/fcvm.2020.00022.

Chandra, K. Sarat and G. Ramesh (Dec. 2013). "The fourth-generation Calcium channel blocker: Cilnidipine". In: *Indian Heart Journal* 65.6, pp. 691–695. ISSN: 00194832. DOI: 10.1016/j.ihj.2013.11.001.

Chang, Wonseok, Temugin Berta, Yong Ho Kim, Sanghoon Lee, Seok Yong Lee, and Ru Rong Ji (Feb. 2018). "Expression and Role of Voltage-Gated Sodium Channels in Human Dorsal Root Ganglion Neurons with Special Focus on Nav1.7, Species Differences, and Regulation by Paclitaxel". In: *Neuroscience Bulletin* 34.1, pp. 4–12. ISSN: 19958218. DOI: 10.1007/s12264-017-0132-3.

Chao, Pei Ting, Liang Yang, Susan Aja, Timothy H. Moran, and Sheng Bi (May 2011). "Knockdown of NPY expression in the dorsomedial hypothalamus promotes development of brown adipocytes and prevents diet-induced obesity". In: *Cell Metabolism* 13.5, pp. 573–583. ISSN: 15504131. DOI: 10.1016/j.cmet.2011.02.019.

Chapman, E R (2018). "A Ca2+ sensor for exocytosis". In: *Trends in Neurosciences* 41.6, pp. 327–330.

Chen, Rong and Shin Ho Chung (2014). "Mechanism of tetrodotoxin block and resistance in sodium channels". In: *Biochemical and Biophysical Research Communications* 446.1, pp. 370–374. ISSN: 10902104. DOI: 10.1016/j.bbrc.2014.02.115.

Chen, Yi, Xing Zeng, Xuan Huang, Sara Serag, Clifford J. Woolf, and Bruce M. Spiegelman (Nov. 2017). "Crosstalk between KCNK3-Mediated Ion Current and Adrenergic Signaling Regulates Adipose Thermogenesis and Obesity". In: *Cell* 171.4, pp. 836–848. ISSN: 10974172. DOI: 10.1016/j.cell.2017.09.015.

Chernov-Rogan, Tania, Tianbo Li, Gang Lu, Henry Verschoof, Kuldip Khakh, Steven W. Jones, Maureen H. Beresini, Chang Liu, Daniel F. Ortwine, Steven J. McKerrall, David H. Hackos, Daniel Sutherlin, Charles J. Cohen, and Jun Chen (2018). "Mechanism-specific assay design facilitates the discovery of Nav1.7-selective inhibitors". In: *Proceedings of the National Academy of Sciences of the United States of America* 115.4, E792–E801. ISSN: 10916490. DOI: 10.1073/pnas.1713701115.

Chi, Jingyi, Zhuhao Wu, Chan Hee J. Choi, Lily Nguyen, Saba Tegegne, Sarah E. Ackerman, Audrey Crane, François Marchildon, Marc Tessier-Lavigne, and Paul Cohen (Jan. 2018). "Three-Dimensional Adipose Tissue Imaging Reveals Regional Variation in Beige Fat Biogenesis and PRDM16-Dependent Sympathetic Neurite Density". In:

Cell Metabolism 27.1, pp. 226–236. ISSN: 19327420. DOI: 10.1016/j.cmet.2017.12.011.

Choe, Sung Sik, Jin Young Huh, In Jae Hwang, Jong In Kim, and Jae Bum Kim (2016). "Adipose tissue remodeling: Its role in energy metabolism and metabolic disorders". In: *Frontiers in Endocrinology* 7.30, pp. 1–16. ISSN: 16642392. DOI: 10.3389/fendo.2016.00030.

Choi, Jongyun, Sei Young Lee, Yeong Min Yoo, and Chi Hyun Kim (Mar. 2017). "Maturation of Adipocytes is Suppressed by Fluid Shear Stress". In: *Cell Biochemistry and Biophysics* 75.1, pp. 87–94. ISSN: 10859195. DOI: 10.1007/s12013-016-0771-4.

Chusyd, Daniella E., Donghai Wang, Derek M. Huffman, and Tim R. Nagy (2016). "Relationships between Rodent White Adipose Fat Pads and Human White Adipose Fat Depots". In: *Frontiers in Nutrition* 3.10, pp. 1–12. ISSN: 2296861X. DOI: 10.3389/fnut.2016.00010.

Cirera, Susanna (2013). "Highly efficient method for isolation of total RNA from adipose tissue". In: *BMC Research Notes* 6.472, pp. 1–5.

Clapham, David E. (2007). "Calcium Signaling". In: *Cell* 131.6, pp. 1047–1058. ISSN: 00928674. DOI: 10.1016/j.cell.2007.11.028.

Cockayne, Debra A, Philip M Dunn, Yu Zhong, Weifang Rong, Sara G Hamilton, Gillian E Knight, Huai Zhen Ruan, Bei Ma, Ping Yip, Philip Nunn, Stephen B. McMahon, Geoffrey Burnstock, and Anthony P.D.W. Ford (2005). "P2X2 knockout mice and P2X2/P2X3 double knockout mice reveal a role for the P2X2 receptor subunit in mediating multiple sensory effects of ATP". In: *Journal of Physiology* 567.2, pp. 621–639. ISSN: 00223751. DOI: 10.1113/jphysiol.2005.088435.

Cojocariu, Sabina Alexandra, Alexandra Maștaleru, Radu Andy Sascău, Cristian Stătescu, Florin Mitu, and Maria Magdalena Leon-Constantin (2021). "Neuropsychiatric consequences of lipophilic beta-blockers". In: *Medicina (Lithuania)* 57.2, pp. 1–13. ISSN: 16489144. DOI: 10.3390/medicina57020155.

Collins, Sheila (2012). "β-Adrenoceptor signaling networks in adipocytes for recruiting stored fat and energy expenditure". In: *Frontiers in Endocrinology* 3.102, pp. 1–7. ISSN: 16642392. DOI: 10.3389/fendo.2011.00102.

Collins, Sheila (2022). "Annual Review of Physiology β-Adrenergic Receptors and Adipose Tissue Metabolism: Evolution of an Old Story". In: DOI: 10.1146/annurev-physiol-060721.

Collins, Sheila, Kiefer W Daniel, Elizabeth M Rohlfs, Vickram Ramkumart, Ian L Taylor, and Thomas W Gettys (1994). "Impaired Expression and Functional Activity of the p3-and ,&-Adrenergic Receptors in Adipose Tissue of Congenitally Obese (C57BL/6J ob/ob) Mice". In: *Molecular Endocrinology* 8.4, pp. 518–527.

Cooper, D M F (2005). "Compartmentalization of adenylate cyclase and cAMP signalling". In: *Biochemical Society Transactions*, pp. 17–21.

Corliss, Bruce A., Corbin Mathews, Richard Doty, Gustavo Rohde, and Shayn M. Peirce (2019). "Methods to label, image, and analyze the complex structural architectures of microvascular networks". In: *Microcirculation* 26.5, pp. 1–24. ISSN: 15498719. DOI: 10.1111/micc.12520.

Correll, J (1963). "Adipose Tissue: Ability to Respond to Nerve Stimulation in vitro". In: *Science* 140, pp. 387–388.

Craig, Robert A., Catherine E. Garrison, Phuong T. Nguyen, Vladimir Yarov-Yarovoy, and J. Du Bois (Feb. 2020). "Veratridine: A Janus-Faced Modulator of Voltage-Gated Sodium Ion Channels". In: *ACS Chemical Neuroscience* 11.3, pp. 418–426. ISSN: 19487193. DOI: 10.1021/acschemneuro.9b00621.

Crowley, Vivion E.F. (2008). "Overview of human obesity and central mechanisms regulating energy homeostasis". In: *Annals of Clinical Biochemistry* 45.3, pp. 245–255. ISSN: 00045632. DOI: 10.1258/acb.2007.007193.

Cunningham, J O and M J Neal (1981). "On the mechanism by which veratridine causes a calcium-independent release of y-aminobutyric acid from brain slices". In: *Br. J. Pharmac* 73, pp. 655–667.

Dabrowska, Anna Maria and Jarosław Dudka (2023). "Mirabegron, a Selective β3-Adrenergic Receptor Agonist, as a Potential Anti-Obesity Drug". In: *Journal of Clinical Medicine* 12.21, pp. 1–12. ISSN: 20770383. DOI: 10.3390/jcm12216897.

Daubner, S. Colette, Tiffany Le, and Shanzhi Wang (Apr. 2011). *Tyrosine hydroxylase and regulation of dopamine synthesis*. DOI: 10.1016/j.abb.2010.12.017.

Despoix, Nicolas, Thierry Walzer, Nathalie Jouve, Marcel Blot-Chabaud, Nathalie Bardin, Pascale Paul, Luc Lyonnet, Eric Vivier, Francoise Dignat-George, and Frédéric Vély

(2008). "Mouse CD146/MCAM is a marker of natural killer cell maturation". In: *European Journal of Immunology* 38.10, pp. 2855–2864. ISSN: 15214141. DOI: 10.1002/eji.200838469.

Devasani, Karan and Yao Yao (2022). "Expression and functions of adenylyl cyclases in the CNS". In: *Fluids and Barriers of the CNS* 19.1. ISSN: 20458118. DOI: 10.1186/s12987-022-00322-2.

Di Guardo, Giovanni (2015). "Lipofuscin, lipofuscin-like pigments and autofluorescence". In: *European Journal of Histochemistry* 59.1, pp. 1–2. ISSN: 20388306. DOI: 10.4081/ejh.2015.2485.

Diabetes UK (n.d.). *How many people in the UK have diabetes?, https://www.diabetes.org.uk/about-us/about-the-charity/ our-strategy/statistics, accessed 22/07/2024.*

Dobrev, Dobromir, Alexander S Milde, Klaus Andreas, and Ursula Ravens (1998). "Voltage-activated calcium channels involved in veratridine-evoked [3 H]dopamine release in rat striatal slices". In: *Neuropharmacology* 37, pp. 973–982.

Dolphin, Annette C. and Amy Lee (Apr. 2020). *Presynaptic calcium channels: specialized control of synaptic neurotransmitter release*. DOI: 10.1038/s41583-020-0278-2.

Doods, Henri, Gerhard Hallermayer, Dongmei Wu, Michael Entzeroth, Klaus Rudolf, Wolfhard Engel, and Wolfgang Eberlein (2000). "Pharmacological profile of BIBN4096BS, the first selective small molecule CGRP antagonist". In: *British Journal of Pharmacology* 129, p. 423.

Dreisig, Karin and Birgitte Rahbek Kornum (Sept. 2016). "A critical look at the function of the P2Y11 receptor". In: *Purinergic Signalling* 12.3, pp. 427–437. ISSN: 15739546. DOI: 10.1007/s11302-016-9514-7.

Dufau, Jer emy, Joanne X. Shen, Morgane Couchet, Thais de Castro Barbosa, Niklas Mejhert, Lucas Massier, Elena Griseti, Etienne Mouisel, Ez Zoubir Amri, Volker M. Lauschke, Mikael Ryden, and Dominique Langin (2021). "In vitro and ex vivo models of adipocytes". In: *American Journal of Physiology - Cell Physiology* 320.5, pp. C822–C841. ISSN: 15221563. DOI: 10.1152/ajpcell.00519.2020.

Duggan, Peter J., Richard J. Lewis, Y. Phei Lok, Natalie G. Lumsden, Kellie L. Tuck, and Aijun Yang (May 2009). "Low molecular weight non-peptide mimics of ω-conotoxin GVIA". In: *Bioorganic and Medicinal Chemistry Letters* 19.10, pp. 2763–2765. ISSN: 0960894X. DOI: 10.1016/j.bmcl.2009.03.130.

Dumont, Yvan, Alain Cadieux, Henri Doods, Alain Fournier, Rémi Quirion, Y Dumont, R Quirion, A Cadieux, H Doods, and A Fournier (2000). "Potent and selective tools to investigate neuropeptide Y receptors in the central and peripheral nervous systems: BIBO3304 (Y1) and CGP71683A (Y5) 1". In: *J. Physiol. Pharmacol* 78, pp. 116–125.

Duncan, Robin E., Maryam Ahmadian, Kathy Jaworski, Eszter Sarkadi-Nagy, and Hei Sook Sul (2007). *Regulation of lipolysis in adipocytes*. DOI: 10.1146/annurev.nutr.27.061406.093734.

Duparc, Thibaut, Emilia Gore, Guillaume Combes, Diane Beuzelin, Julie Pires Da Silva, Vanessa Bouguetoch, Marie Adeline Marquès, Ana Velazquez, Nathalie Viguerie, Geneviève Tavernier, Peter Arner, Mikael Rydén, Dominique Langin, Nabil Sioufi, Mohamad Nasser, Cendrine Cabou, Souad Najib, and Laurent O. Martinez (2024). "P2Y13 receptor deficiency favors adipose tissue lipolysis and worsens insulin resistance and fatty liver disease". In: *JCI Insight* 9.8. ISSN: 23793708. DOI: 10.1172/jci.insight.175623.

Durnin, L., N. Moreland, A. Lees, and V. N. Mutafova-Yambolieva (Sept. 2016). "A commonly used ecto-ATPase inhibitor, ARL-67156, blocks degradation of ADP more than the degradation of ATP in murine colon". In: *Neurogastroenterology and Motility* 28.9, pp. 1370–1381. ISSN: 13652982. DOI: 10.1111/nmo.12836.

Dwaib, Haneen S. and Martin C. Michel (2023). *Is the β3-Adrenoceptor a Valid Target for the Treatment of Obesity and/or Type 2 Diabetes?* DOI: 10.3390/biom13121714.

Embaby, Alaa, Lisanne van Merendonk, Neeltje Steeghs, Jos Beijnen, and Alwin Huitema (Sept. 2022). "Beta-adrenergic receptor blockade in angiosarcoma: Which beta-blocker to choose?" In: *Frontiers in Oncology* 12. ISSN: 2234943X. DOI: 10.3389/fonc.2022.940582.

Erickson, Andelain, Annemie Deiteren, Andrea M. Harrington, Sonia Garcia-Caraballo, Joel Castro, Ashlee Caldwell, Luke Grundy, and Stuart M. Brierley (Mar. 2018). *Voltage-gated sodium channels: (Na V)igating the field to determine their contribution to visceral nociception*. DOI: 10.1113/JP273461.

Evans, Bronwyn A., Jon Merlin, Tore Bengtsson, and Dana S. Hutchinson (2019). "Adrenoceptors in white, brown, and brite adipocytes". In: *British Journal of Pharmacology* 176, pp. 2416–2432.

Fedorenko, Olena A., Pawitra Pulbutr, Elin Banke, Nneoma E. Akaniro-Ejim, Donna C. Bentley, Charlotta S. Olofsson, Sue Chan, and Paul A. Smith (2020). "CaV1.2 and CaV1.3 voltage-gated L-type Ca2+ channels in rat white fat adipocytes". In: *Journal of Endocrinology* 244.2, pp. 369–381. ISSN: 14796805. DOI: 10.1530/JOE-19-0493.

Fernandes, Gustavo W., Cintia B. Ueta, Tatiane L. Fonseca, Cecilia H.A. Gouveia, Carmen L. Lancellotti, Patrícia C. Brum, Marcelo A. Christoffolete, Antonio C. Bianco, and Miriam O. Ribeiro (2014). "Inactivation of the adrenergic receptor β2 disrupts glucose homeostasis in mice". In: *Journal of Endocrinology* 221.3, pp. 381–390. ISSN: 14796805. DOI: 10.1530/JOE-13-0526.

Filippatos, Theodosios D, Christos S Derdemezis, Irene F Gazi, Eleni S Nakou, Dimitri P Mikhailidis, and Moses S Elisaf (2008). *Orlistat-Associated Adverse Effects and Drug Interactions A Critical Review*. Tech. rep. 1, pp. 53–65.

Filippi, S, M Luconi, S Granchi, A Natali, P Tozzi, G Forti, F Ledda, and M Maggi (2002). "Endothelium-dependency of yohimbine-induced corpus cavernosum relaxation". In: *International Journal of Impotence Research* 14, pp. 295–307. DOI: 10.1038=sj.ijir.3900890.

Filippov, Alexander K., Roy C.Y. Choi, Joseph Simon, Eric A. Barnard, and David A. Brown (Sept. 2006). "Activation of P2Y1 nucleotide receptors induces inhibition of the M-type K+ current in rat hippocampal pyramidal neurons". In: *Journal of Neuroscience* 26.36, pp. 9340–9348. ISSN: 02706474. DOI: 10.1523/JNEUROSCI.2635-06.2006.

François, Marie, Emily Qualls-Creekmore, Hans Rudolf Berthoud, Heike Münzberg, and Sangho Yu (2018). "Genetics-based manipulation of adipose tissue sympathetic innervation". In: *Physiology and Behavior* 190, pp. 21–27. ISSN: 1873507X. DOI: 10.1016/j.physbeh.2017.08.024.

Fredholm, B B (1976). "Release of adenosine-like material from isolated perfused dog adipose tissue following sympathetic nerve stimulation and its inhibition by adrenergic alpha-receptor blockade". In: *Acta physiologica Scandinavica* 96.3, pp. 122–130. DOI: 10.1111/j.1748-1716.1976.tb10211.x.

Fredholm, B B (1978). "Effect of adenosine, adenosine analogues and drugs inhibiting adenosine inactivation on lipolysis in rat fat cells." In: *Acta Physiologica Scandinavica* 102, pp. 191–198.

Frei, Irina C., Diana Weissenberger, Danilo Ritz, Wolf Heusermann, Marco Colombi, Mitsugu Shimobayashi, and Michael N. Hall (Nov. 2022). "Adipose mTORC2 is essential for sensory innervation in white adipose tissue and whole-body energy homeostasis". In: *Molecular Metabolism* 65. ISSN: 22128778. DOI: 10.1016/j.molmet.2022.101580.

Frühbeck, Gema, Leire Méndez-Giménez, José Antonio Fernández-Formoso, Secundino Fernández, and Amaia Rodríguez (2014). "Regulation of adipocyte lipolysis". In: *Nutrition Research Reviews* 27.1, pp. 63–93. ISSN: 14752700. DOI: 10.1017/S095442241400002X.

Fryklund, Claes, Mathis Neuhaus, Björn Morén, Andrea Borreguero-Muñoz, Richard Lundmark, and Karin G. Stenkula (Sept. 2022). "Expansion of the Inguinal Adipose Tissue Depot Correlates With Systemic Insulin Resistance in C57BL/6J Mice". In: *Frontiers in Cell and Developmental Biology* 10. ISSN: 2296634X. DOI: 10.3389/fcell.2022.942374.

Gaur, Shikha, Hiroshi Yamaguchi, and H Maurice Goodman (1996). "Growth hormone regulates cytosolic free calcium in rat fat cells by maintaining L-type calcium channels". In: *Cell Physiol* 39, pp. 1478–1484.

Geppert, Martin, Yukiko Goda, Robert E Hammer, Cai Li, Thomas W Rosahi, Charles F Stevens, and Thomas C Siiclhof' (1994). "Synaptotagmin I: A Major Ca2+ Sensor for Transmitter Release at a Central Synapse". In: *Cell* 79, pp. 717–727.

Gericke, Martin T., Joanna Kosacka, Daniela Koch, Marcin Nowicki, Thomas Schröder, Albert M. Ricken, Karen Nieber, and Katharina Spanel-Borowski (2009). "Receptors for NPY and PACAP differ in expression and activity during adipogenesis in the murine 3T3-L1 fibroblast cell line". In: *British Journal of Pharmacology* 157.4, pp. 620–632. ISSN: 00071188. DOI: 10.1111/j.1476-5381.2009.00164.x.

Germack, ReneÂ, Anna B Starzec, Roger Vassy, and GeÂ Y rard Perret (1997). "b-Adrenoceptor subtype expression and function in rat white adipocytes". In: *British Journal of Pharmacology* 120, pp. 201–210.

Gervasi, Noreen M., Shane S. Scott, Armaz Aschrafi, Jenna Gale, Sanah N. Vohra, Margaret A. Macgibeny, Amar N. Kar, Anthony E. Gioio, and Barry B. Kaplan (June 2016). "The local expression and trafficking of tyrosine hydroxylase mRNA in the axons of sympathetic neurons". In: *RNA* 22.6, pp. 883–895. ISSN: 14699001. DOI: 10.1261/rna.053272.115.

Giacovazzo, Giacomo, Paola Fabbrizio, Savina Apolloni, Roberto Coccurello, and Cinzia Volonté (2019). "Stimulation of P2X7 Enhances Whole Body Energy Metabolism in Mice". In: *Frontiers in Cellular Neuroscience* 13.August, pp. 1–9. ISSN: 16625102. DOI: 10.3389/fncel.2019.00390.

Giordano, Antonio, C. Kay Song, Robert R. Bowers, J. Christopher Ehlen, Andrea Frontini, Saverio Cinti, and Timothy J. Bartness (2006). "White adipose tissue lacks significant vagal innervation and immunohistochemical evidence of parasympathetic innervation". In: *American Journal of Physiology - Regulatory Integrative and Comparative Physiology* 291.5. ISSN: 03636119. DOI: 10.1152/ajpregu.00679.2005.

Giovannitti, Joseph A, Sean M Thoms, and James J Crawford (2015). "Alpha-2 Adrenergic Receptor Agonists: A Review of Current Clinical Applications". In: *American Dental Society of Anesthesiology* 62, pp. 31–38.

Giuliani, Anna Lisa, Alba Clara Sarti, and Francesco Di Virgilio (Feb. 2021). *Ectonucleotidases in Acute and Chronic Inflammation*. DOI: 10.3389/fphar.2020.619458.

Goddard, Kayleigh (2021). "Consequences of an obesogenic diet can be prevented by knockout of P2Y6 purinergic receptor in mice". In: *Purinergic Signalling* 17.3. ISSN: 15739546. DOI: 10.1007/s11302-021-09793-8.

Goldstein, David S (Sept. 2010). "Adrenaline and Noradrenaline". In: *Encyclopedia of Life Sciences*. Wiley. DOI: 10.1002/9780470015902.a0001401.pub2.

Gov.uk (2022). *New obesity treatments and technology to save the NHS billions,https://www.gov.uk/government/news/new-obesity-treatments-and-technology -to-save-the-nhs-billions, accessed, 22/07/2024.*

Gov.uk (2023). *Government plans to tackle obesity in England, https://healthmedia.blog.gov.uk/2023/06/07/government-plans-to-tackle-obesity-in- england/, accessed 22/07/2024.*

Grabner, Gernot F., Hao Xie, Martina Schweiger, and Rudolf Zechner (2021). "Lipolysis: cellular mechanisms for lipid mobilization from fat stores". In: *Nature Metabolism* 3.11, pp. 1445–1465. ISSN: 25225812. DOI: 10.1038/s42255-021-00493-6.

Grahn, Tan Hooi Min, Rajween Kaur, Jun Yin, Martina Schweiger, Vishva Mitra Sharma, Mi Jeong Lee, Yasuo Ido, Cynthia M. Smas, Rudolf Zechner, Achim Lass, and Vishwajeet Puri (2014). "Fat-specific protein 27 (FSP27) interacts with adipose triglyceride lipase (ATGL) to regulate lipolysis and insulin sensitivity in human adipocytes". In: *Journal of Biological Chemistry* 289.17, pp. 12029–12039. ISSN: 1083351X. DOI: 10.1074/jbc.M113.539890.

Granade, Mitchell E., Stefan R. Hargett, Daniel S. Lank, Michael C. Lemke, Melissa A. Luse, Brant E. Isakson, Irina M. Bochkis, Joel Linden, and Thurl E. Harris (Sept. 2022). "Feeding desensitizes A1 adenosine receptors in adipose through FOXO1-mediated transcriptional regulation". In: *Molecular Metabolism* 63. ISSN: 22128778. DOI: 10.1016/j.molmet.2022.101543.

Granneman, James G., Hsiao Ping H. Moore, Rukmani Krishnamoorthy, and Miloni Rathod (2009). "Perilipin controls lipolysis by regulating the interactions of AB-hydrolase containing 5 (Abhd5) and adipose triglyceride lipase (Atgl)". In: *Journal of Biological Chemistry* 284.50, pp. 34538–34544. ISSN: 00219258. DOI: 10.1074/jbc.M109.068478.

Grant, Ryan W. and Jacqueline M. Stephens (2015). "Fat in flames: Influence of cytokines and pattern recognition receptors on adipocyte lipolysis". In: *American Journal of Physiology - Endocrinology and Metabolism* 309.3, E205–E213. ISSN: 15221555. DOI: 10.1152/ajpendo.00053.2015.

Greenberg, Andrew S., Wen Jun Shen, Kizito Muliro, Shailja Patel, Sandra C. Souza, Richard A. Roth, and Fredric B. Kraemer (2001). "Stimulation of Lipolysis and Hormone-sensitive Lipase via the Extracellular Signal-regulated Kinase Pathway". In: *Journal of Biological Chemistry* 276.48, pp. 45456–45461. ISSN: 00219258. DOI: 10.1074/jbc.M104436200.

Griffin, Michelle F., Heather E. desJardins-Park, Shamik Mascharak, Mimi R. Borrelli, and Michael T. Longaker (2020). *Understanding the impact of fibroblast heterogeneity on skin fibrosis*. DOI: 10.1242/dmm.044164.

Grubb, Søren, Changsi Cai, Bjørn O. Hald, Lila Khennouf, Reena Prity Murmu, Aske G.K. Jensen, Jonas Fordsmann, Stefan Zambach, and Martin Lauritzen (Dec. 2020). "Precapillary sphincters maintain perfusion in the cerebral cortex". In: *Nature Communications* 11.1. ISSN: 20411723. DOI: 10.1038/s41467-020-14330-z.

Grundlingh, Johann, Paul I. Dargan, Marwa El-Zanfaly, and David M. Wood (Sept. 2011). *2,4-Dinitrophenol (DNP): A Weight Loss Agent with Significant Acute Toxicity and Risk of Death*. DOI: 10.1007/s13181-011-0162-6.

Guardia, Lucio Della and Andrew C. Shin (2024). *Obesity-induced tissue alterations resist weight loss: A mechanistic review*. DOI: 10.1111/dom.15637.

Guilherme, Adilson, Joseph V. Virbasius, Vishwajeet Puri, and Michael P. Czech (2008). "Adipocyte dysfunctions linking obesity to insulin resistance and type 2 diabetes". In: *Nature Reviews Molecular Cell Biology* 9.5, pp. 367–377. ISSN: 14710072. DOI: 10.1038/nrm2391.

Gulsevin, Alican, Andrew M. Glazer, Tiffany Shields, Brett M. Kroncke, Dan M. Roden, and Jens Meiler (Feb. 2022). "Veratridine Can Bind to a Site at the Mouth of the Channel Pore at Human Cardiac Sodium Channel NaV1.5". In: *International Journal of Molecular Sciences* 23.4. ISSN: 14220067. DOI: 10.3390/ijms23042225.

Guo, James, Andrew Nguyen, Derek A. Banyard, Darya Fadavi, Jason D. Toranto, Garrett A. Wirth, Keyianoosh Z. Paydar, Gregory R.D. Evans, and Alan D. Widgerow (2016). "Stromal vascular fraction: A regenerative reality? Part 2: Mechanisms of regenerative action". In: *Journal of Plastic, Reconstructive and Aesthetic Surgery* 69.2, pp. 180–188. ISSN: 18780539. DOI: 10.1016/j.bjps.2015.10.014.

Haas, Clarissa Branco, Marianna Lovászi, Elizandra Braganhol, Pál Pacher, and György Haskó (May 2021). "Ectonucleotidases in Inflammation, Immunity, and Cancer". In: *The Journal of Immunology* 206.9, pp. 1983–1990. ISSN: 0022-1767. DOI: 10.4049/jimmunol.2001342.

Hachmane, Mickaël F El, Anna Ermund, Cecilia Brännmark, and Charlotta S. Olofsson (2018). "Extracellular atp activates store-operated Ca2+ entry in white adipocytes: functional evidence for STIM1 and ORAI1". In: *Biochemical Journal* 475.3, pp. 691–704. ISSN: 14708728. DOI: 10.1042/BCJ20170484.

Hagan, R. M. and I. E. Hughes (1986). "Yohimbine affects the evoked overflow of neurotransmitters from rat brain slices by more than one mechanism". In: *Journal of Pharmacy and Pharmacology* 38.3, pp. 195–200. ISSN: 20427158. DOI: 10.1111/j.2042-7158.1986.tb04543.x.

Halloran, Jonathan, Alexandre Lalande, Mandy Zang, Harshita Chodavarapu, and Céline E. Riera (Dec. 2020). "Monoclonal therapy against calcitonin gene-related peptide

lowers hyperglycemia and adiposity in type 2 diabetes mouse models". In: *Metabolism Open* 8, p. 100060. ISSN: 25899368. DOI: 10.1016/j.metop.2020.100060.

Hamida, Zied Haj, Alain S. Comtois, Michel Portmann, Jean P. Boucher, and Roland Savard (2011). "Effect of electrical stimulation on lipolysis of human white adipocytes". In: *Applied Physiology, Nutrition and Metabolism* 36.2, pp. 271–275. ISSN: 17155312. DOI: 10.1139/h11-011.

Hammond, Constance (2015). *Cellular and Molecular Neurophysiology*. Ed. by Constance Hammond. 4th ed. Academic Press, pp. 55–91. ISBN: 978-0-12-397032-9. DOI: https://doi.org/10.1016/C2011-0-07267-8.

Hampton, Henry R. and Tatyana Chtanova (2019). "Lymphatic migration of immune cells". In: *Frontiers in Immunology* 10, pp. 1–10. ISSN: 16643224. DOI: 10.3389/fimmu.2019.01168.

Hanlon, Katherine E., Alysia N. Lozano-Ondoua, Puja J. Umaretiya, Ashley M. Symons-Liguori, Anupama Chandramouli, Jamie K. Moy, William K. Kwass, Patrick W. Mantyh, Mark A. Nelson, and Todd W. Vanderah (Apr. 2016). "Modulation of breast cancer cell viability by a cannabinoid receptor 2 agonist, JWH-015, is calcium dependent". In: *Breast Cancer: Targets and Therapy* 8, pp. 59–71. ISSN: 11791314. DOI: 10.2147/BCTT.S100393.

Harms, Matthew J., Qian Li, Sunjae Lee, Cheng Zhang, Bengt Kull, Stefan Hallen, Anders Thorell, Ida Alexandersson, Carolina E. Hagberg, Xiao Rong Peng, Adil Mardinoglu, Kirsty L. Spalding, and Jeremie Boucher (2019). "Mature Human White Adipocytes Cultured under Membranes Maintain Identity, Function, and Can Transdifferentiate into Brown-like Adipocytes". In: *Cell Reports* 27.1, pp. 213–225. ISSN: 22111247. DOI: 10.1016/j.celrep.2019.03.026.

Harrell, Maria I., Brian M. Iritani, and Alanna Ruddell (2008). "Lymph node mapping in the mouse". In: *Journal of Immunological Methods* 332.1-2, pp. 170–174. ISSN: 00221759. DOI: 10.1016/j.jim.2007.11.012.

He, Rongfang, Juan Zhang, Yiyan Yu, Laluo Jizi, Weizhong Wang, and Miaoling Li (July 2018). "New Insights Into Interactions of Presynaptic Calcium Channel Subtypes and SNARE Proteins in Neurotransmitter Release". In: *Frontiers in Molecular Neuroscience* 11. ISSN: 16625099. DOI: 10.3389/fnmol.2018.00213.

Hemmings, H. C. (2009). "Sodium channels and the synaptic mechanisms of inhaled anaesthetics". In: *British Journal of Anaesthesia* 103.1, pp. 61–69. ISSN: 14716771. DOI: 10.1093/bja/aep144.

Herold, Jacqueline and Joanna Kalucka (2021). *Angiogenesis in Adipose Tissue: The Interplay Between Adipose and Endothelial Cells*. DOI: 10.3389/fphys.2020.624903.

Hildebrandt, Ximena, Mohamed Ibrahim, and Nieves Peltzer (Feb. 2023). "Cell death and inflammation during obesity: "Know my methods, WAT(son)"". In: *Cell Death and Differentiation* 30.2, pp. 279–292. ISSN: 14765403. DOI: 10.1038/s41418-022-01062-4.

Hill, Caryl E., Jacqueline K. Phillips, and Shaun L. Sandow (2001). "Heterogeneous control of blood flow amongst different vascular beds". In: *Medicinal Research Reviews* 21.1, pp. 1–60. ISSN: 01986325. DOI: 10.1002/1098-1128(200101)21:1<1::AID-MED1>3.0.CO;2-6.

Hille (1999). "The mainstream analysis in endocrine cells and synapses". In: *Journal of Physiology* 520.1, pp. 23–31.

Hodges, Gary J, Dwayne N Jackson, Louis Mattar, John M Johnson, and J Kevin Shoemaker (2009). "Neuropeptide Y and neurovascular control in skeletal muscle and skin". In: *Am J Physiol Regul Integr Comp Physiol* 297, pp. 546–555. DOI: 10.1152/ajpregu.00157.2009.-Neuropeptide.

Hoffmann, C., M. R. Leitz, S. Oberdorf-Maass, M. J. Lohse, and K. N. Klotz (Feb. 2004). "Comparative pharmacology of human β-adrenergic receptor subtypes - Characterization of stably transfected receptors in CHO cells". In: *Naunyn-Schmiedeberg's Archives of Pharmacology* 369.2, pp. 151–159. ISSN: 00281298. DOI: 10.1007/s00210-003-0860-y.

Hong, Shangyu, Wei Song, Peter James H. Zushin, Bingyang Liu, Mark P. Jedrychowski, Amir I. Mina, Zhaoming Deng, Dimitrije Cabarkapa, Jessica A. Hall, Colin J. Palmer, Hassan Aliakbarian, John Szpyt, Steven P. Gygi, Ali Tavakkoli, Lydia Lynch, Norbert Perrimon, and Alexander S. Banks (June 2018). "Phosphorylation of Beta-3 adrenergic receptor at serine 247 by ERK MAP kinase drives lipolysis in obese adipocytes". In: *Molecular Metabolism* 12, pp. 25–38. ISSN: 22128778. DOI: 10.1016/j.molmet.2018.03.012.

Horinouchi, T. and K. Koike (2001). "Agonistic activity of SR59230A at atypical b-adrenoceptors in guineapig gastric fundus and duodenum". In: *European Journal of Pharmacology* 416.1-2, pp. 165–168.

Horvath, Gabor, Zoltan Sutto, Aliza Torbati, Gregory E. Conner, Matthias Salathe, and Adam Wanner (Oct. 2003). "Norepinephrine transport by the extraneuronal monoamine transporter in human bronchial arterial smooth muscle cells". In: *American Journal of Physiology - Lung Cellular and Molecular Physiology* 285.4 29-4. ISSN: 10400605. DOI: 10.1152/ajplung.00054.2003.

Hostrup, Morten, Johan Onslev, M Hostrup, and J Physiol (2022). "The beta 2-adrenergic receptor-a re-emerging target to combat obesity and induce leanness?" In: *The Journal of Physiology* 600, pp. 1209–1227. DOI: 10.1113/JP281819{\#}support-information-section.

Hsiao, Wen Yu and David A. Guertin (Nov. 2019). *De Novo Lipogenesis as a Source of Second Messengers in Adipocytes*. DOI: 10.1007/s11892-019-1264-9.

Hu, Wen-Yang, Noboru Fukuda, Jin-Zi Su, and Katsuo Kanmatsuse (2001). *Effects of the L-and N-Type Calcium Channel Blocker Cilnidipine on Growth of Vascular Smooth Muscle Cells from Spontaneously Hypertensive Rats*. Tech. rep.

Huang, Siyi, Carly G.K. Ziegler, John Austin, Najat Mannoun, Marko Vukovic, Jose Ordovas-Montanes, Alex K. Shalek, and Ulrich H. von Andrian (Jan. 2021). "Lymph nodes are innervated by a unique population of sensory neurons with immunomodulatory potential". In: *Cell* 184.2, pp. 441–459. ISSN: 10974172. DOI: 10.1016/j.cell.2020.11.028.

Huesing, Clara, Emily Qualls-Creekmore, Nathan Lee, Marie François, Hayden Torres, Rui Zhang, David H. Burk, Sangho Yu, Christopher D. Morrison, Hans Rudolf Berthoud, Winfried Neuhuber, and Heike Münzberg (May 2021). "Sympathetic innervation of inguinal white adipose tissue in the mouse". In: *Journal of Comparative Neurology* 529.7, pp. 1465–1485. ISSN: 10969861. DOI: 10.1002/cne.25031.

Hutchinson, Dana S, Masaaki Sato, Bronwyn A Evans, Arthur Christopoulos, and Roger J Summers (Mar. 2005). "Evidence for pleiotropic signaling at the mouse β3- adrenoceptor revealed by SR59230A [3-(2-ethylphenoxy)-1-[(1,S)-1,2,3,4- tetrahydronapth-1-ylamino]-2s-2-propanol oxalate]". In: *Journal of Pharmacology and Experimental*

Therapeutics 312.3, pp. 1064–1074. ISSN: 00223565. DOI: 10.1124/jpet.104.076901.

Hyland, Niall P. and Helen M. Cox (Nov. 2005). "The regulation of veratridine-stimulated electrogenic ion transport in mouse colon by neuropeptide Y (NPY), Y 1 and Y 2 receptors". In: *British Journal of Pharmacology* 146.5, pp. 712–722. ISSN: 00071188. DOI: 10.1038/sj.bjp.0706368.

Jain, Shanu and Kenneth A. Jacobson (Apr. 2022). "Adipocyte purinergic receptors activated by uracil nucleotides as obesity and type 2 diabetes targets". In: *Current Opinion in Pharmacology* 63. ISSN: 14714973. DOI: 10.1016/j.coph.2022.102190.

Jain, Shanu, Sai P Pydi, Young-Hwan Jung, Mirko Scortichini, Efrat L Kesner, Tadeusz P Karcz, Donald N Cook, Oksana Gavrilova, Jürgen Wess, and Kenneth A. Jacobson (2021). "Adipocyte P2Y14 receptors play a key role in regulating whole-body glucose and lipid homeostasis". In: *JCI insight* 6.10, pp. 1–15.

Jarvis, Michael F, Edward C Burgard, Steve Mcgaraughty, Prisca Honore, Kevin Lynch, Timothy J Brennan, Alberto Subieta, Tim Van Biesen, Jayne Cartmell, Bruce Bianchi, Wende Niforatos, Karen Kage, Haixia Yu, Joe Mikusa, Carol T Wismer, Chang Z Zhu, Katharine Chu, Chih-Hung Lee, Andrew O Stewart, James Polakowski, Bryan F Cox, Elizabeth Kowaluk, Michael Williams, James Sullivan, Connie Faltynek, and John W Daly (2002). "A-317491, a novel potent and selective non-nucleotide antagonist of P2X 3 and P2X 2/3 receptors, reduces chronic inflammatory and neuropathic pain in the rat". In: *PNAS* 99.26, pp. 17179–17184.

Jenkinson, Karl M. and Julianne J. Reid (2000). "The P2-purinoceptor antagonist suramin is a competitive antagonist at vasoactive intestinal peptide receptors in the rat gastric fundus". In: *British Journal of Pharmacology* 130.7, pp. 1632–1638. ISSN: 00071188. DOI: 10.1038/sj.bjp.0703482.

Jensen, Caleb and Yong Teng (Mar. 2020). "Is It Time to Start Transitioning From 2D to 3D Cell Culture?" In: *Frontiers in Molecular Biosciences* 7. ISSN: 2296889X. DOI: 10.3389/fmolb.2020.00033.

Jiang, Haochen, Xiaofan Ding, Ying Cao, Huanhuan Wang, and Wenwen Zeng (2017). "Dense Intra-adipose Sympathetic Arborizations Are Essential for Cold-Induced Beig-

ing of Mouse White Adipose Tissue". In: *Cell Metabolism* 26.4, pp. 686–692. ISSN: 19327420. DOI: 10.1016/j.cmet.2017.08.016.

Jin, Jiyu, Chunxiao Miao, Zhilong Wang, Wanli Zhang, Xiongwen Zhang, Xin Xie, and Wei Lu (Apr. 2018). "Design and synthesis of aryloxypropanolamine as β3-adrenergic receptor antagonist in cancer and lipolysis". In: *European Journal of Medicinal Chemistry* 150, pp. 757–770. ISSN: 17683254. DOI: 10.1016/j.ejmech.2018.03.032.

Johnston-Cox, Hillary, Milka Koupenova, Dan Yang, Barbara Corkey, Noyan Gokce, Melissa G. Farb, Nathan LeBrasseur, and Katya Ravid (July 2012). "The A2b adenosine receptor modulates glucose homeostasis and obesity". In: *PLoS ONE* 7.7. ISSN: 19326203. DOI: 10.1371/journal.pone.0040584.

Jones, C A, I P Chessell, J Simon, E A Barnard, K J Miller, A D Michel, and P P A Humphrey (2000). "Functional characterization of the P2X 4 receptor orthologues". In: *British Journal of Phamacology* 129.2, pp. 388–394.

Jose Garcıa-Barrado, Marıa, Consuelo Sancho, Carmen Iglesias-Osma, and Julio Moratinos (2001). "Effects of verapamil and elgodipine on isoprenaline-induced metabolic responses in rabbits". In: *European Journal of Pharmacology* 415, pp. 105–115.

Jost, Manda Clair, David M. Hillis, Ying Lu, John W. Kyle, Harry A. Fozzard, and Harold H. Zakon (2008). "Toxin-resistant sodium channels: Parallel adaptive evolution across a complete gene family". In: *Molecular Biology and Evolution* 25.6, pp. 1016–1024. ISSN: 07374038. DOI: 10.1093/molbev/msn025.

Kaji, H, M Okada, A Hamaue, M Mori, and M Nagai (2016). "Blockade of the neuropeptide Y Y2 receptor with the potent antagonist BIIE0246 regulates gene expression levels in the lipid metabolic pathways in human hepatoma cell line HepG2". In: *Integrative Molecular Medicine* 3.2, pp. 576–582. DOI: 10.15761/imm.1000207.

Kalil, Graziela Z. and William G. Haynes (2012). "Sympathetic nervous system in obesity-related hypertension: Mechanisms and clinical implications". In: *Hypertension Research* 35.1, pp. 4–16. ISSN: 09169636. DOI: 10.1038/hr.2011.173.

Kanatani, Akio, Akane Ishihara, Hisashi Iwaasa, Kayo Nakamura, Osamu Okamoto, Masayasu Hidaka, Junko Ito, Takahiro Fukuroda, Douglas J. MacNeil, Lex H.T. Van Der Ploeg, Yasuyuki Ishii, Takayoshi Okabe, Takehiro Fukami, and Masaki Ihara (May 2000). "L-152,804: Orally active and selective neuropeptide Y Y5 receptor antago-

nist". In: *Biochemical and Biophysical Research Communications* 272.1, pp. 169–173. ISSN: 0006291X. DOI: 10.1006/bbrc.2000.2696.

Kario, Kazuomi, Shin Ichi Ando, Hidenori Kido, Jin Nariyama, Shin Takiuchi, Tetsuo Yagi, Toshiki Shimizu, Kazuo Eguchi, Minoru Ohno, Osamu Kinoshita, and Takahisa Yamada (Feb. 2013). "The Effects of the L/N-Type Calcium Channel Blocker (Cilnidipine) on Sympathetic Hyperactive Morning Hypertension: Results From ACHIEVE-ONE". In: *Journal of Clinical Hypertension* 15.2, pp. 133–142. ISSN: 15246175. DOI: 10.1111/jch.12042.

Karmakar, Mausita, Michael A. Katsnelson, George R. Dubyak, and Eric Pearlman (Feb. 2016). "Neutrophil P2X7 receptors mediate NLRP3 inflammasome-dependent IL-1β secretion in response to ATP". In: *Nature Communications* 7. ISSN: 20411723. DOI: 10.1038/ncomms10555.

Katz, B and R Miledi (1967). "A study of synaptic transmission in the absence of nerve impulses". In: *Journal of Physiology* 192, pp. 407–436.

Kawai, Tatsuo, Michael V. Autieri, and Rosario Scalia (Mar. 2021). "Adipose tissue inflammation and metabolic dysfunction in obesity". In: *American Journal of Physiology - Cell Physiology* 320.3, pp. C375–C391. ISSN: 15221563. DOI: 10.1152/ajpcell.00379.2020.

Kelly, K L, J T Deeney, and B E Corkey (Aug. 1989). "Cytosolic Free Calcium in Adipocytes". In: *Journal of Biological Chemistry* 264.22, pp. 12754–12757. ISSN: 00219258. DOI: 10.1016/s0021-9258(18)51549-0.

Kim, Joyce S, Sonya Meeker, Fei Ru, Minh Tran, Tanja S Zabka, David Hackos, and Bradley J Undem (2024). "Role of Na V 1.7 in postganglionic sympathetic nerve function in human and guinea-pig arteries". In: *The Journal of Physiology*, pp. 1–14. DOI: 10.1113/JP286538{\#}support-information-section.

Kim, Junhyoung, Sujung Lee, and William Ramos (May 2021). "Investigating the relationship between accessibility of green space and adult obesity rates: A secondary data analysis in the united states". In: *Journal of Preventive Medicine and Public Health* 54.3, pp. 208–217. ISSN: 19758375. DOI: 10.3961/JPMPH.20.625.

Kita, Toshiyuki and Naokatu Arakaki (2015). "Contribution of extracellular ATP on the cell-surface f1f0-ATP synthasemediated intracellular triacylglycerol accumulation".

In: *Biomedical Research (Japan)* 36.2, pp. 115–120. ISSN: 1880313X. DOI: 10.2220/biomedres.36.115.

Klein, Shannon G., Samhan M. Alsolami, Silvia Arossa, Gerardo Ramos-Mandujano, Anieka J. Parry, Alexandra Steckbauer, Carlos M. Duarte, and Mo Li (Dec. 2022). "In situ monitoring reveals cellular environmental instabilities in human pluripotent stem cell culture". In: *Communications Biology* 5.1. ISSN: 23993642. DOI: 10.1038/s42003-022-03065-w.

Konkar, Anish A, Ying Zhai, and James G Granneman (1999). "-Adrenergic Receptors Mediate 3-Adrenergic-Independent Effects of CGP 12177 in Brown Adipose Tissue". In: *The American Society for Pharmacology and Experimental Therapeutics* 57, pp. 252–258.

Kuo, Lydia E., Joanna B. Kitlinska, Jason U. Tilan, Lijun Li, Stephen B. Baker, Michael D. Johnson, Edward W. Lee, Mary Susan Burnett, Stanley T. Fricke, Richard Kvetnansky, Herbert Herzog, and Zofia Zukowska (July 2007). "Neuropeptide Y acts directly in the periphery on fat tissue and mediates stress-induced obesity and metabolic syndrome". In: *Nature Medicine* 13.7, pp. 803–811. ISSN: 10788956. DOI: 10.1038/nm1611.

Kwok, Kelvin H.M., Karen S.L. Lam, and Aimin Xu (2016). "Heterogeneity of white adipose tissue: Molecular basis and clinical implications". In: *Experimental and Molecular Medicine* 48.3. ISSN: 20926413. DOI: 10.1038/emm.2016.5.

Labelle, Martin, Yvan Boulanger, Alain Fournier, Serge St-pierre, Roland Savard, Y Boulanger, A Fournier, S St-pierre, and R Savard (1997). "Tissue-Specific Regulation of Fat Cell Lipolysis by NPY in 6-OHDA-Treated Rats". In: 18.6, pp. 801–808.

Lafontan, M., A. Bousquet-Melou, J. Galitzky, P. Barbe, C. Carpéné, D. Langin, M. Berlan, P. Valet, I. Castan, and A. Bouloumié (1995). "Adrenergic receptors and fat cells: differential recruitment by physiological amines and homologous regulation." In: *Obesity research* 3. ISSN: 10717323. DOI: 10.1002/j.1550-8528.1995.tb00220.x.

Lafontan, Max (2012). "Historical perspectives in fat cell biology: the fat cell as a model for the investigation of hormonal and metabolic pathways". In: *Am J Physiol Cell Physiol* 302, pp. 327–359. DOI: 10.1152/ajpcell.00168.2011.-For.

Lafontan, Max, Cédric Moro, Coralie Sengenes, Jean Galitzky, François Crampes, and Michel Berlan (2005). "An unsuspected metabolic role for atrial natriuretic peptides: The control of lipolysis, lipid mobilization, and systemic nonesterified fatty acids levels in humans". In: *Arteriosclerosis, Thrombosis, and Vascular Biology* 25.10, pp. 2032–2042. ISSN: 10795642. DOI: 10.1161/01.ATV.0000183728.14712.d8.

Laitinen, Liisa (1987). *Griffonia simplicifolia lectins bind specifically to endothelial cells and some epithelial cells in mouse tissues*. Tech. rep., pp. 225–234.

Lambrecht, Günter, Thomas Friebe, Ulrike Grimm, Ursula Windscheif, Edwin Bungardt, Caren Hildebrandt, Hans G. Bäumert, Gerhard Spatz-Kümbel, and Ernst Mutschler (1992). "PPADS, a novel functionally selective antagonist of P2 purinoceptor-mediated responses". In: *European Journal of Pharmacology* 217.2-3, pp. 217–219. ISSN: 00142999. DOI: 10.1016/0014-2999(92)90877-7.

Laplante, Marc André, Laurent Monassier, Monique Freund, Pascal Bousquet, and Christian Gachet (2010). "The purinergic P2Y1 receptor supports leptin secretion in adipose tissue". In: *Endocrinology* 151.5, pp. 2060–2070. ISSN: 00137227. DOI: 10.1210/en.2009-1134.

Latremoliere, Alban, Long Cheng, Michelle DeLisle, Chen Wu, Sheena Chew, Elizabeth B. Hutchinson, Andrew Sheridan, Chloe Alexandre, Frederic Latremoliere, Shu Hsien Sheu, Sara Golidy, Takao Omura, Eric A. Huebner, Yanjie Fan, Mary C. Whitman, Elaine Nguyen, Crystal Hermawan, Carlo Pierpaoli, Max A. Tischfield, Clifford J. Woolf, and Elizabeth C. Engle (Aug. 2018). "Neuronal-Specific TUBB3 Is Not Required for Normal Neuronal Function but Is Essential for Timely Axon Regeneration". In: *Cell Reports* 24.7, pp. 1865–1879. ISSN: 22111247. DOI: 10.1016/j.celrep.2018.07.029.

Laurindo, Lucas Fornari, Sandra Maria Barbalho, Elen Landgraf Guiguer, Maricelma da Silva Soares de Souza, Gabriela Achete de Souza, Thiago Marques Fidalgo, Adriano Cressoni Araújo, Heron F.de Souza Gonzaga, Daniel de Bortoli Teixeira, Thais de Oliveira Silva Ullmann, Katia Portero Sloan, and Lance Alan Sloan (2022). "GLP-1a: Going Beyond Traditional Use". In: *International Journal of Molecular Sciences* 23.2. ISSN: 14220067. DOI: 10.3390/ijms23020739.

Lauschke, Volker M. and Carolina E. Hagberg (2023). "Next-generation human adipose tissue culture methods". In: *Current Opinion in Genetics and Development* 80, pp. 1–6. ISSN: 18790380. DOI: 10.1016/j.gde.2023.102057.

Lay, Abigail C, A Fern Barrington, Jenny A Hurcombe, Raina D Ramnath, Mark Graham, Philip A Lewis, Marieangela C Wilson, Kate J Heesom, Matthew J Butler, Rebecca M Perrett, Chris R Neal, Eleanor Herbert, Edward Mountjoy, Denize Atan, Viji Nair, Wenjun Ju, Robert G Nelson, Matthias Kretzler, Simon C Satchell, Craig A Mcardle, Gavin I Welsh, and Richard J M Coward (2020). "A role for NPY-NPY2R signaling in albuminuric kidney disease". In: *PNAS* 117.27, pp. 15862–15873. DOI: 10.1073/pnas.2004651117/-/DCSupplemental.

Layhadi, Janice A., Jeremy Turner, David Crossman, and Samuel J. Fountain (Feb. 2018). "ATP Evokes Ca2+ Responses and CXCL5 Secretion via P2X4 Receptor Activation in Human Monocyte-Derived Macrophages". In: *The Journal of Immunology* 200.3, pp. 1159–1168. ISSN: 0022-1767. DOI: 10.4049/jimmunol.1700965.

Lechner, Stefan G., Mario M. Dorostkar, Martina Mayer, Hannah Edelbauer, Halyna Pankevych, and Stefan Boehm (Dec. 2004). "Autoinhibition of transmitter release from PC12 cells and sympathetic neurons through a P2Y12 receptor-mediated inhibition of voltage-gated Ca2+ channels". In: *European Journal of Neuroscience* 20.11, pp. 2917–2928. ISSN: 0953816X. DOI: 10.1111/j.1460-9568.2004.03760.x.

Ledoux, Séverine, Isabelle Queguiner, Simon Msika, Sophie Calderari, Pierre Rufat, Jean Marie Gasc, Pierre Corvol, and Etienne Larger (2008). "Angiogenesis associated with visceral and subcutaneous adipose tissue in severe human obesity". In: *Diabetes* 57.12, pp. 3247–3257. ISSN: 1939327X. DOI: 10.2337/db07-1812.

Lee, Hyun, Dong-jae Jun, Byung-chang Suh, Bo-hwa Choi, Jong-hee Lee, Myoungsool Do, Byung-sun Suh, Hyunjung Ha, and Kyong-tai Kim (2005). "Dual Roles of P2 Purinergic Receptors in Insulin-stimulated Leptin Production and Lipolysis in Differentiated Rat White Adipocytes". In: *Journal of Biological Chemistry* 280.31, pp. 28556–28563. ISSN: 0021-9258. DOI: 10.1074/jbc.M411253200.

Lee, Jaekwang., Jin Young. Bae, Justin J. Lee, and Yong Chul Bae (Apr. 2018). "Electrophysiological evidence for functional astrocytic P2X3 receptors in the mouse trigeminal caudal nucleus". In: *Experimental Neurobiology* 27.2, pp. 88–93. ISSN: 20938144. DOI: 10.5607/en.2018.27.2.88.

Lemaire, A, M Vanorlé, M Horckmans, L di Pietrantonio, S Clouet, B Robaye, JM Boeynaems, and D Communi (2017). "Mouse P2Y4 Nucleotide Receptor Is a Negative Regulator of Cardiac Adipose-Derived Stem Cell Differentiation and Cardiac Fat Formation". In: *Stem Cells and Development* 26.5, pp. 363–373.

Lévesque, S. A., É G. Lavoie, J. Lecka, F. Bigonnesse, and J. Sévigny (Sept. 2007). "Specificity of the ecto-ATPase inhibitor ARL 67156 on human and mouse ectonucleotidases". In: *British Journal of Pharmacology* 152.1, pp. 141–150. ISSN: 00071188. DOI: 10.1038/sj.bjp.0707361.

Levi, Giulio, Vittorio Gallo, and Maurizio Raiteri (1980). "A reevaluation of veratridine as a tool for studying the depolarisation-induced release of neurotransmitters from nerve endings". In: *Neurochemical Research* 5.3, pp. 282–295.

Li, Qian and Kirsty L. Spalding (2022). *The regulation of adipocyte growth in white adipose tissue*. DOI: 10.3389/fcell.2022.1003219.

Li, Yongguo, Zhen Li, Devi Anggraini Ngandiri, Mireia Llerins Perez, Alexander Wolf, and Yuanyuan Wang (2022). "The Molecular Brakes of Adipose Tissue Lipolysis". In: *Frontiers in Physiology* 13. ISSN: 1664042X. DOI: 10.3389/fphys.2022.826314.

Lim, Hwee Ying, Sheau Yng Lim, Chek Kun Tan, Chung Hwee Thiam, Chi Ching Goh, Daniel Carbajo, Samantha Hui Shang Chew, Peter See, Svetoslav Chakarov, Xiao Nong Wang, Li Hui Lim, Louise A. Johnson, Josephine Lum, Chui Yee Fong, Ariff Bongso, Arijit Biswas, Chern Goh, Maximilien Evrard, Kim Pin Yeo, Ranu Basu, Jun Kit Wang, Yingrou Tan, Rohit Jain, Shweta Tikoo, Cleo Choong, Wolfgang Weninger, Michael Poidinger, Richard E. Stanley, Matthew Collin, Nguan Soon Tan, Lai Guan Ng, David G. Jackson, Florent Ginhoux, and Véronique Angeli (2018). "Hyaluronan Receptor LYVE-1-Expressing Macrophages Maintain Arterial Tone through Hyaluronan-Mediated Regulation of Smooth Muscle Cell Collagen". In: *Immunity* 49.2, pp. 326–341. ISSN: 10974180. DOI: 10.1016/j.immuni.2018.06.008.

Lim, Seona, Jinbong Park, and Jae Young Um (2019). "Ginsenoside Rb1 induces beta 3 adrenergic receptor–dependent lipolysis and thermogenesis in 3T3-L1 adipocytes and db/db mice". In: *Frontiers in Pharmacology* 10. ISSN: 16639812. DOI: 10.3389/fphar.2019.01154.

Lin, J., T. Takano, G. Arcuino, X. Wang, F. Hu, Z. Darzynkiewicz, M. Nunes, S. Goldman, and M. Nedergaard (2008). "Dev. Biol." In: *Trends Cell Biol.* 302.1, pp. 356–366. ISSN: 15378276.

Liu, Bo Xun, Ming Qiu, Peng Yu Zong, Xu Guan Chen, Kun Zhao, Yong Li, Peng Li, Wei Sun, and Xiang Qing Kong (2019). "Distribution, morphological characterization, and resiniferatoxin-susceptibility of sensory neurons that innervate rat perirenal adipose tissue". In: *Frontiers in Neuroanatomy* 13.March, pp. 1–13. ISSN: 16625129. DOI: 10.3389/fnana.2019.00029.

Liu, D M, C Katnik, M Stafford, and D J Adams (2000). "P2Y purinoceptor activation mobilizes intracellular Ca2+ and induces a membrane current in rat intracardiac neurones". In: *Journal of Physiology* 526.2, pp. 287–298.

Liu, Tian, Akiko Kamiyoshi, Takayuki Sakurai, Yuka Ichikawa-Shindo, Hisaka Kawate, Lei Yang, Megumu Tanaka, Xian Xian, Akira Imai, Liuyu Zhai, Kazutaka Hirabayashi, Kun Dai, Keiya Tanimura, Teng Liu, Nanqi Cui, Kyoko Igarashi, Akihiro Yamauchi, and Takayuki Shindo (May 2017). "Endogenous calcitonin gene-related peptide regulates lipid metabolism and energy homeostasis in male mice". In: *Endocrinology* 158.5, pp. 1194–1206. ISSN: 19457170. DOI: 10.1210/en.2016-1510.

Loh, Kim, Herbert Herzog, and Yan Chuan Shi (Mar. 2015). "Regulation of energy homeostasis by the NPY system". In: *Trends in Endocrinology and Metabolism* 26.3, pp. 125–135. ISSN: 18793061. DOI: 10.1016/j.tem.2015.01.003.

Long, Min, Jiyin Zhou, Dandan Li, Lu Zheng, Zihui Xu, and Shiwen Zhou (May 2015). "Long-term over-expression of Neuropeptide Y in hypothalamic paraventricular nucleus contributes to adipose tissue insulin resistance partly via the Y5 receptor". In: *PLoS ONE* 10.5. ISSN: 19326203. DOI: 10.1371/journal.pone.0126714.

Lonnqvist, Fredrik, Hans Wahrenberg, Lena Hellstrom, Signy Reynisdottir, and Peter Amer (1992). "Lipolytic Catecholamine Resistance Due to Decreased B2-Adrenoceptor Expression in Fat Cells". In: *The American Society for Clinical Investigation* 90, pp. 2175–2186.

Louis, Simon N S, Graham P Jackman, Tracy L Nero, Dimitri Iakovidis, and William J Louis (2000). *Role of β-Adrenergic Receptor Subtypes in Lipolysis*. Tech. rep., pp. 565–577.

Lu, Xin, Xingyuan Yang, and Jun Liu (2010). "Differential control of ATGL-mediated lipid droplet degradation by CGI-58 and G0S2". In: *Cell Cycle* 9.14, pp. 2791–2797. ISSN: 15514005. DOI: 10.4161/cc.9.14.12181.

Lundberg, Jan M, Anders Rudehill, Alf Sollevi, and Bertil Hamberger (1989). *Evidence for co-transmitter role of neuropeptide Y in the pig spleen*. Tech. rep., pp. 675–687.

Luo, Liping and Meilian Liu (2016). "Adipose tissue in control of metabolism". In: *Journal of Endocrinology* 231.3, pp. 77–99. ISSN: 14796805. DOI: 10.1530/JOE-16-0211.

Luong, Quyen, Jun Huang, and Kevin Y. Lee (2019). "Deciphering white adipose tissue heterogeneity". In: *Biology* 8.2. ISSN: 20797737. DOI: 10.3390/biology8020023.

MacDonald, Tara L., Rebecca MacPherson, Laura Castellani, Daniel Cervone, Eoin Anderson, David C. Wright, and David J. Dyck (Apr. 2017). "Estradiol does not directly regulate adipose lipolysis". In: *Adipocyte* 6.2, pp. 76–86. ISSN: 2162397X. DOI: 10.1080/21623945.2017.1287638.

Malfacini, Davide and Alexander Pfeifer (2023). "GPCR in Adipose Tissue Function—Focus on Lipolysis". In: *Biomedicines* 11.2. ISSN: 22279059. DOI: 10.3390/biomedicines11020588.

Manczak, Maria, Peizhong Mao, Kazuhiro Nakamura, Christopher Bebbington, Byung Park, and P. Hemachandra Reddy (2009). "Neutralization of granulocyte macrophage colony-stimulating factor decreases amyloid beta 1-42 and suppresses microglial activity in a transgenic mouse model of Alzheimer's disease". In: *Human Molecular Genetics* 18.20, pp. 3876–3893. ISSN: 09646906. DOI: 10.1093/hmg/ddp331.

Manousiouthakis, Eleana, Monica Mendez, Madeline C. Garner, Prisca Exertier, and Takako Makita (May 2014). "Venous endothelin guides sympathetic innervation of the developing mouse heart". In: *Nature Communications* 5. ISSN: 20411723. DOI: 10.1038/ncomms4918.

Manzini, Stefano (1992). "Bronchodilatation by tachykinins and capsaicin in the mouse main bronchus". In: *British Journal of Pharmacology* 105.4, pp. 968–972. ISSN: 14765381. DOI: 10.1111/j.1476-5381.1992.tb09086.x.

Martinez-Sanchez, Noelia, Owen Sweeney, Davi Sidarta-Oliveira, Alexandre Caron, Sarah A. Stanley, and Ana I. Domingos (2022). "The sympathetic nervous system in the 21st century: Neuroimmune interactions in metabolic homeostasis and obesity". In: *Neuron* 110.21, pp. 3597–3626. ISSN: 10974199. DOI: 10.1016/j.neuron.2022.10.017.

Matsushita, Yumi, Miki Manabe, Naoki Kitamura, and Izumi Shibuya (Jan. 2018). "Adrenergic receptors inhibit TRPV1 activity in the dorsal root ganglion neurons of rats". In: *PLoS ONE* 13.1. ISSN: 19326203. DOI: 10.1371/journal.pone.0191032.

Maus, Mate, Mario Cuk, Bindi Patel, Jayson Lian, Mireille Ouimet, Ulrike Kaufmann, Jun Yang, Rita Horvath, Hue Tran Hornig-Do, Zofia M. Chrzanowska-Lightowlers, Kathryn J. Moore, Ana Maria Cuervo, and Stefan Feske (Mar. 2017). "Store-Operated Ca2+ Entry Controls Induction of Lipolysis and the Transcriptional Reprogramming to Lipid Metabolism". In: *Cell Metabolism* 25.3, pp. 698–712. ISSN: 19327420. DOI: 10.1016/j.cmet.2016.12.021.

McDermott, Lucy A., Greg A. Weir, Andreas C. Themistocleous, Andrew R. Segerdahl, Iulia Blesneac, Georgios Baskozos, Alex J. Clark, Val Millar, Liam J. Peck, Daniel Ebner, Irene Tracey, Jordi Serra, and David L. Bennett (Mar. 2019). "Defining the Functional Role of Na V 1.7 in Human Nociception". In: *Neuron* 101.5, pp. 905–919. ISSN: 10974199. DOI: 10.1016/j.neuron.2019.01.047.

Merlin, Jon, Masaaki Sato, Cameron Nowell, Mohsen Pakzad, Richard Fahey, Jie Gao, Nodi Dehvari, Roger J. Summers, Tore Bengtsson, Bronwyn A. Evans, and Dana S. Hutchinson (Jan. 2018). "The PPARγ agonist rosiglitazone promotes the induction of brite adipocytes, increasing β-adrenoceptor-mediated mitochondrial function and glucose uptake". In: *Cellular Signalling* 42, pp. 54–66. ISSN: 18733913. DOI: 10.1016/j.cellsig.2017.09.023.

Michel, Martin C., Peter Ochodnicky, and Roger J. Summers (Aug. 2010). *Tissue functions mediated by β 3-adrenoceptors - Findings and challenges*. DOI: 10.1007/s00210-010-0529-2.

Miegueu, Pierre, David H. St-Pierre, Marc Lapointe, Pegah Poursharifi, Hui Ling Lu, Abhishek Gupta, and Katherine Cianflone (Feb. 2013). "Substance P decreases fat storage and increases adipocytokine production in 3T3-L1 adipocytes". In: *American Journal of Physiology - Gastrointestinal and Liver Physiology* 304.4. ISSN: 01931857. DOI: 10.1152/ajpgi.00162.2012.

Mills, S (2000). "Beta-adrenergic receptor subtypes mediating lipolysis in porcine adipocytes. Studies with BRL-37344, a putative B3-adrenergic agonist". In: *Comparative Biochemistry and Physiology* 126, pp. 11–20.

Mishra, Amrita and Girdhari Lal (2021). "Neurokinin receptors and their implications in various autoimmune diseases". In: *Current Research in Immunology* 2, pp. 66–78. ISSN: 25902555. DOI: 10.1016/j.crimmu.2021.06.001.

Mishra, Gargi and Kristy L. Townsend (2023). "The metabolic and functional roles of sensory nerves in adipose tissues". In: *Nature Metabolism* 5.9, pp. 1461–1474. ISSN: 25225812. DOI: 10.1038/s42255-023-00868-x.

Mishra, Gargi and Kristy L. Townsend (2024). "Sensory nerve and neuropeptide diversity in adipose tissues". In: *Molecules and Cells* 47.2, pp. 1–14. ISSN: 02191032. DOI: 10.1016/j.mocell.2024.100030.

Misra, Sudhakar, Karnam S. Murthy, Huiping Zhou, and John R. Grider (Dec. 2004). "Coexpression of Y1, Y2, and Y4 receptors in smooth muscle coupled to distinct signaling pathways". In: *Journal of Pharmacology and Experimental Therapeutics* 311.3, pp. 1154–1162. ISSN: 00223565. DOI: 10.1124/jpet.104.071415.

Mizuno, Katsushige, Yasunari Kanda, Yasutomi Kuroki, Masahiro Nishio, and Yasuhiro Watanabe (2002). "Stimulation of β3-adrenoceptors causes phosphorylation of p38 mitogen-activated protein kinase via a stimulatory G protein-dependent pathway in 3T3-L1 adipocytes". In: *British Journal of Pharmacology* 135.4, pp. 951–960. ISSN: 00071188. DOI: 10.1038/sj.bjp.0704537.

Moerenhout, M., B. Himpens, and J. Vereecke (2001). "Intercellular communication upon mechanical stimulation of CPAE-endothelial cells is mediated by nucleotides". In: *Cell Calcium* 29.2, pp. 125–136. ISSN: 01434160. DOI: 10.1054/ceca.2000.0165.

Mohammed, Zainab A., Ciara Doran, David Grundy, and Mohammed A. Nassar (Mar. 2017). "Veratridine produces distinct calcium response profiles in mouse Dorsal Root Ganglia neurons". In: *Scientific Reports* 7. ISSN: 20452322. DOI: 10.1038/srep45221.

Molloy, Caitlyn T., Jennifer S. Andonian, Harrison M. Seltzer, Megan C. Procario, Michael E. Watson, and Jason B. Weinberg (2017). "Contributions of CD8 T cells to the pathogenesis of mouse adenovirus type 1 respiratory infection". In: *Virology* 507.March, pp. 64–74. ISSN: 10960341. DOI: 10.1016/j.virol.2017.04.005.

Moore, Shannon J. and Geoffrey G. Murphy (Sept. 2020). "The role of L-type calcium channels in neuronal excitability and aging". In: *Neurobiology of Learning and Memory* 173. ISSN: 10959564. DOI: 10.1016/j.nlm.2020.107230.

Mota, Roberto I., Samuel E. Morgan, and Edward M. Bahnson (Mar. 2020). *Diabetic Vasculopathy: Macro and Microvascular Injury*. DOI: 10.1007/s40139-020-00205-x.

Motagally, Mohamed A, Shadia Neshat, and Alan E Lomax (2009). "Inhibition of sympathetic N-type voltage-gated Ca 2 current underlies the reduction in norepinephrine release during colitis". In: *Am J Physiol Gastrointest Liver Physiol* 296, pp. 1077–1084. DOI: 10.1152/ajpgi.00006.2009.-Inflammatory.

Muangsanit, Papon, Rebecca J. Shipley, and James B. Phillips (2018). "Vascularization Strategies for Peripheral Nerve Tissue Engineering". In: *Anatomical Record* 301.10, pp. 1657–1667. ISSN: 19328494. DOI: 10.1002/ar.23919.

Mueller, Alan L, Michael R Palmer, Barry J Hoffer, and Thomas V Dunwiddie (1982). *Hippocampal Noradrenergic Responses in vivo and in vitro Characterization of Alpha and Beta Components*. Tech. rep., pp. 259–266.

Mullins, Garrett R., Lifu Wang, Vidisha Raje, Samantha G. Sherwood, Rebecca C. Grande, Salome Boroda, James M. Eaton, Sara Blancquaert, Pierre P. Roger, Norbert Leitinger, and Thurl E. Harris (Dec. 2014). "Catecholamine-induced lipolysis causes mTOR complex dissociation and inhibits glucose uptake in adipocytes". In: *Proceedings of the National Academy of Sciences of the United States of America* 111.49, pp. 17450–17455. ISSN: 10916490. DOI: 10.1073/pnas.1410530111.

Musovic, Saliha, Ali M Komai, Marina Kalds Said, Man Mohan Shrestha, Yanling Wu, Ingrid Wernstedt Asterholm, and Charlotta S Olofsson (2022a). "Molecular and Cellular Endocrinology Noradrenaline and ATP regulate adiponectin exocytosis in white adipocytes : Disturbed adrenergic and purinergic signalling in obese and insulin-resistant mice". In: *Molecular and Cellular Endocrinology* 549.February, p. 111619. ISSN: 0303-7207. DOI: 10.1016/j.mce.2022.111619.

Musovic, Saliha, Ali M. Komai, Marina Kalds Said, Man Mohan Shrestha, Yanling Wu, Ingrid Wernstedt Asterholm, and Charlotta S. Olofsson (June 2022b). "Noradrenaline and ATP regulate adiponectin exocytosis in white adipocytes: Disturbed adrenergic

and purinergic signalling in obese and insulin-resistant mice". In: *Molecular and Cellular Endocrinology* 549. ISSN: 18728057. DOI: 10.1016/j.mce.2022.111619.

Nakagawa, Yoshimi, Aoi Satoh, Hitomi Tezuka, Song iee Han, Kenta Takei, Hitoshi Iwasaki, Shigeru Yatoh, Naoya Yahagi, Hiroaki Suzuki, Yasumasa Iwasaki, Hirohito Sone, Takashi Matsuzaka, Nobuhiro Yamada, and Hitoshi Shimano (2016). "CREB3L3 controls fatty acid oxidation and ketogenesis in synergy with PPARα". In: *Scientific Reports* 6.1. ISSN: 20452322. DOI: 10.1038/srep39182.

Nap, Alexander, Marie Jeanne Mathy, Jippe C. Balt, Martin Pfaffendorf, and Pieter A. Van Zwieten (June 2004). "The evaluation of the N-type channel blocking properties of cilnidipine and other voltage-dependent calcium antagonists". In: *Fundamental and Clinical Pharmacology* 18.3, pp. 309–319. ISSN: 07673981. DOI: 10.1111/j.1472-8206.2004.00236.x.

Nastasi, Nicoletta, Gennaro Bruno, Claudio Favre, and Maura Calvani (June 2022). "Role of β3-Adrenergic Receptor in Bone Marrow Transplant as Therapeutical Support in Cancer". In: *Frontiers in Oncology* 12. ISSN: 2234943X. DOI: 10.3389/fonc.2022.889634.

National Institute for Health and Care Excellence, https://cks.nice.org.uk/topics/ obesity/background-information/causes-risk-factors/, accessed 19/07/2024. (July 2024).

Negri, Irene, Esteban Diaz Villamil, Lucas De Roeck, Didier Communi, and Michael Horckmans (Jan. 2020). "P2Y2 Nucleotide Receptor Is a Regulator of the Formation of Cardiac Adipose Tissue and Its Fat-Associated Lymphoid Clusters". In: *Stem Cells and Development* 29.2, pp. 100–109. ISSN: 15578534. DOI: 10.1089/scd.2019.0200.

Nielsen, Thomas Svava, Niels Jessen, Jens Otto L. Jørgensen, Niels Møller, and Sten Lund (2014). "Dissecting adipose tissue lipolysis: Molecular regulation and implications for metabolic disease". In: *Journal of Molecular Endocrinology* 52.3, pp. 199–222. ISSN: 14796813. DOI: 10.1530/JME-13-0277.

Nishida, Motohiro, Yoji Sato, Aya Uemura, Yusuke Narita, Hidetoshi Tozaki-Saitoh, Michio Nakaya, Tomomi Ide, Kazuhiro Suzuki, Kazuhide Inoue, Taku Nagao, and Hitoshi Kurose (Dec. 2008). "P2Y6 receptor-Gα12/13 signalling in cardiomyocytes triggers pressure overload-induced cardiac fibrosis". In: *EMBO Journal* 27.23, pp. 3104–3115. ISSN: 02614189. DOI: 10.1038/emboj.2008.237.

Norenburg, W, I Gobel, A Meyer, S. L. Cox, K. Starke, and A. U. Trendelenburg (2001). "Stimulation of mouse cultured sympathetic neurons by uracil but not adenine nucleotides". In: *Neuroscience* 103.1, pp. 227–236.

Ohyama, Kana, Yoshihito Nogusa, Kosaku Shinoda, Katsuya Suzuki, Makoto Bannai, and Shingo Kajimura (May 2016). "A synergistic antiobesity effect by a combination of capsinoids and cold temperature through promoting beige adipocyte biogenesis". In: *Diabetes* 65.5, pp. 1410–1423. ISSN: 1939327X. DOI: 10.2337/db15-0662.

Ouchi, Noriyuki, Jennifer L. Parker, Jesse J. Lugus, and Kenneth Walsh (2011). "Adipokines in inflammation and metabolic disease". In: *Nature Reviews Immunology* 11.2, pp. 85–97. ISSN: 14741733. DOI: 10.1038/nri2921.

Palty, Raz, William F. Silverman, Michal Hershfinkel, Teresa Caporale, Stefano L. Sensi, Julia Parnis, Christiane Nolte, Daniel Fishman, Varda Shoshan-Barmatz, Sharon Herrmann, Daniel Khananshvili, and Israel Sekler (2010). "NCLX is an essential component of mitochondrial Na+/Ca 2+ exchange". In: *Proceedings of the National Academy of Sciences of the United States of America* 107.1, pp. 436–441. ISSN: 00278424. DOI: 10.1073/pnas.0908099107.

Pang, Zhiping P and Thomas C Südhof (2010). "Cell Biology of Ca 2+-Triggered Exocytosis". In: *Current Opinions in Cell Biology* 22.4, pp. 496–505.

Park, Chan Yoon and Sung Nim Han (2021). "The role of vitamin D in adipose tissue biology: Adipocyte differentiation, energy metabolism, and inflammation". In: *Journal of Lipid and Atherosclerosis* 10.2, pp. 130–144. ISSN: 22882561. DOI: 10.12997/jla.2021.10.2.130.

Park, Jin Ah, Anne L. Crews, William R. Lampe, Shijing Fang, Joungjoa Park, and Kenneth B. Adler (2007). "Protein kinase Cδ regulates airway mucin secretion via phosphorylation of MARCKS protein". In: *American Journal of Pathology* 171.6, pp. 1822–1830. ISSN: 00029440. DOI: 10.2353/ajpath.2007.070318.

Park, Joohee, Coralyne Proux, William Ehanno, Léa Réthoré, Emilie Vessières, Jennifer Bourreau, Julie Favre, Gilles Kauffenstein, César Mattei, Hélène Tricoire-Leignel, Daniel Henrion, Claire Legendre, and Christian Legros (Mar. 2023). "Tetrodotoxin Decreases the Contractility of Mesenteric Arteries, Revealing the Contribution of Voltage-Gated Na+ Channels in Vascular Tone Regulation". In: *Marine Drugs* 21.3. ISSN: 16603397. DOI: 10.3390/md21030196.

Parnis, Julia, Vedrana Montana, Ignacio Delgado-Martinez, Vitali Matyash, Vladimir Parpura, Helmut Kettenmann, Israel Sekler, and Christiane Nolte (Apr. 2013). "Mitochondrial exchanger NCLX plays a major role in the intracellular Ca2+ signaling, gliotransmission, and proliferation of astrocytes". In: *Journal of Neuroscience* 33.17, pp. 7206–7219. ISSN: 02706474. DOI: 10.1523/JNEUROSCI.5721-12.2013.

Pasznik, Pawel, Ewelina Rutkowska, Szymon Niewieczerzal, Judyta Cielecka-Piontek, and Dorota Latek (Jan. 2019). "Potential off-target effects of beta-blockers on gut hormone receptors: In silico study including GUT-DOCK-A web service for small-molecule docking". In: *PLoS ONE* 14.1. ISSN: 19326203. DOI: 10.1371/journal.pone.0210705.

Pati, Sukanya, Wadeed Irfan, Ahmad Jameel, Shahid Ahmed, and Rabia K. Shahid (Jan. 2023). *Obesity and Cancer: A Current Overview of Epidemiology, Pathogenesis, Outcomes, and Management*. DOI: 10.3390/cancers15020485.

Paz, Nathaniel G dela, Benoît Melchior, John A Frangos, and N G dela Paz (2017). "Shear stress induces G q/11 activation independently of G protein-coupled receptor activation in endothelial cells". In: *Am J Physiol Cell Physiol* 312, pp. 428–437. DOI: 10.1152/ajpcell.00148.2016.-Mechanochemical.

Pedragosa-Badia, Xavier, Jan Stichel, and Annette G. Beck-Sickinger (2013). "Neuropeptide y receptors: How to get subtype selectivity". In: *Frontiers in Endocrinology* 4.FEB. ISSN: 16642392. DOI: 10.3389/fendo.2013.00005.

Perdikari, Aliki, Tessa Cacciottolo, Elana Henning, Edson Mendes De Oliveira, Julia M. Keogh, and I. Sadaf Farooqi (2022). "Visualization of sympathetic neural innervation in human white adipose tissue". In: *Open Biology* 12.3. ISSN: 20462441. DOI: 10.1098/rsob.210345.

Pérez-Medina, Carlos, Niral Patel, Mathew Robson, Adam Badar, Mark F. Lythgoe, and Erik Årstad (Dec. 2012). "Evaluation of a 125I-labelled benzazepinone derived voltage-gated sodium channel blocker for imaging with SPECT". In: *Organic and Biomolecular Chemistry* 10.47, pp. 9474–9480. ISSN: 14770520. DOI: 10.1039/c2ob26695d.

Perrone, M. and A Scilimati (2010). "Beta-3 Adrenoceptor Agonists and (Antagonists as) Inverse Agonists:History, Perspective,Constitutive Activity, and Stereospecific Binding". In: *Methods in Enzymology* 484, pp. 197–230.

Perrone, Maria Grazia, Ernesto Santandrea, Laura Bleve, Paola Vitale, Nicola Antonio Colabufo, Ralf Jockers, Ferdinando Maria Milazzo, Anna Floriana Sciarroni, and Antonio Scilimati (Mar. 2008). "Stereospecific synthesis and bio-activity of novel β3-adrenoceptor agonists and inverse agonists". In: *Bioorganic and Medicinal Chemistry* 16.5, pp. 2473–2488. ISSN: 09680896. DOI: 10.1016/j.bmc.2007.11.060.

Petersen, M C and G I Shulman (2018). "Mechanisms of Insulin Action and Insulin Resistance". In: *Physiol Rev* 98, pp. 2133–2223. DOI: 10.1152/physrev.

Pfeifer, Alexander, Mickel Mikhael, and Birte Niemann (2024). "Inosine: novel activator of brown adipose tissue and energy homeostasis". In: *Trends in Cell Biology* 34.1, pp. 72–82. ISSN: 18793088. DOI: 10.1016/j.tcb.2023.04.007.

Pirzgalska, Roksana M., Elsa Seixas, Jason S. Seidman, Verena M. Link, Noelia Martínez Sánchez, Inês Mahú, Raquel Mendes, Vitka Gres, Nadiya Kubasova, Imogen Morris, Bernardo A. Arús, Chelsea M. Larabee, Miguel Vasques, Francisco Tortosa, Ana L. Sousa, Sathyavathy Anandan, Erin Tranfield, Maureen K. Hahn, Matteo Iannacone, Nathanael J. Spann, Christopher K. Glass, and Ana I. Domingos (Nov. 2017). "Sympathetic neuron-associated macrophages contribute to obesity by importing and metabolizing norepinephrine". In: *Nature Medicine* 23.11, pp. 1309–1318. ISSN: 1546170X. DOI: 10.1038/nm.4422.

Platel, J.-C, S Boisseau, A Dupuis, J Brocard, A Poupard, M Savasta, M Villaz, and M Albrieux (2005). "Na channel-mediated Ca 2 entry leads to glutamate secretion in mouse neocortical preplate". In: *PNAS* 102.52, pp. 19174–19179.

Possik, Elite, Anfal Al-Mass, Marie Line Peyot, Rasheed Ahmad, Fahd Al-Mulla, S. R.Murthy Madiraju, and Marc Prentki (2021). "New Mammalian Glycerol-3-Phosphate Phosphatase: Role in β-Cell, Liver and Adipocyte Metabolism". In: *Frontiers in Endocrinology* 12, pp. 1–9. ISSN: 16642392. DOI: 10.3389/fendo.2021.706607.

Preite, Nailliw Z., Bruna P.P. Do Nascimento, Cynthia R. Muller, Anna Laura V. Américo, Talita S. Higa, Fabiana S. Evangelista, Carmen L. Lancellotti, Felipe dos Santos Henriques, Miguel Luiz Batista, Antonio C. Bianco, and Miriam O. Ribeiro (2016). "Disruption of beta3 adrenergic receptor increases susceptibility to DIO in mouse". In: *Journal of Endocrinology* 231.3, pp. 259–269. ISSN: 14796805. DOI: 10.1530/JOE-16-0199.

Preitner, Frederic, Patrick Muzzin, Jean-Pierre Revelli, Josiane Seydoux, Jean Galitzky, Michel Berlan, Max Lafontan, and Jean-Paul Giacobino (1998). "Metabolic response to various b-adrenoceptor agonists in b3-adrenoceptor knockout mice: Evidence for a new b-adrenergic receptor in brown adipose tissue". In: *British Journal of Pharmacology* 124, pp. 1684–1688.

Pruneau, D. and J A. Angus (1990). "omega-Conotoxin GVIA is a potent inhibitor of sympathetic neurogenic responses in rat small mesenteric arteries". In: *British Journal of Pharmacology* 100, pp. 180–184.

Qi, Lin, Erin K. Knapton, Xu Zhang, Tongwen Zhang, Chen Gu, and Yi Zhao (Dec. 2017). "Pre-culture Sudan Black B treatment suppresses autofluorescence signals emitted from polymer tissue scaffolds". In: *Scientific Reports* 7.1. ISSN: 20452322. DOI: 10.1038/s41598-017-08723-2.

Qiao, Liping, Brice Kinney, Jerome Schaack, and Jianhua Shao (May 2011). "Adiponectin inhibits lipolysis in mouse adipocytes". In: *Diabetes* 60.5, pp. 1519–1527. ISSN: 00121797. DOI: 10.2337/db10-1017.

Queiroz, Glória, Carlos Talaia, and Jorge Gonçalves (Nov. 2003). "ATP Modulates Noradrenaline Release by Activation of Inhibitory P2Y Receptors and Facilitatory P2X Receptors in the Rat Vas Deferens". In: *Journal of Pharmacology and Experimental Therapeutics* 307.2, pp. 809–815. ISSN: 00223565. DOI: 10.1124/jpet.103.054809.

Ralevic, Vera and Geoffrey Burnstock (1998). "Receptors for Purines and Pyrimidines". In: *Pharmacological Reviews* 50.3, pp. 413–492.

Razzoli, Maria, Andrea Frontini, Allison Gurney, Eleonora Mondini, Cankut Cubuk, Liora S Katz, Cheryl Cero, Patrick J Bolan, Joaquin Dopazo, Antonio Vidal-puig, Saverio Cinti, and Alessandro Bartolomucci (2016). "Stress-induced activation of brown adipose tissue prevents obesity in conditions of low adaptive thermogenesis". In: *Molecular Metabolism* 5.1, pp. 19–33. ISSN: 2212-8778. DOI: 10.1016/j.molmet.2015.10.005.

Reggio, Sophie, Vanessa Pellegrinelli, Karine Clément, and Joan Tordjman (2013). "Fibrosis as a Cause or a Consequence of White Adipose Tissue Inflammation in Obesity". In: *Current Obesity Reports* 2.1, pp. 1–9. ISSN: 21624968. DOI: 10.1007/s13679-012-0037-4.

Revelli, Jean Pierre, Frédéric Preitner, Sonia Samec, Pedro Muniesa, Françoise Kuehne, Olivier Boss, Jean Dominique Vassalli, Abdul Dulloo, Josiane Seydoux, Jean Paul Giacobino, Joachim Huarte, and Christiane Ody (1997). "Targeted gene disruption reveals a leptin-independent role for the mouse β3-adrenoceptor in the regulation of body composition". In: *Journal of Clinical Investigation* 100.5, pp. 1098–1106. ISSN: 00219738. DOI: 10.1172/JCI119620.

Reynisdottir, S, H Wahrenberg, K Carlstriim, S Riissner, and P Arner (1994). *Catecholamine resistance in fat cells of women with upper-body obesity due to decreased expression of beta2-adrenoceptors*. Tech. rep., pp. 428–435.

Robidoux, Jacques, Naresh Kumar, Kiefer W. Daniel, Fatiha Moukdar, Michel Cyr, Alexander V. Medvedev, and Sheila Collins (Dec. 2006). "Maximal β3-adrenergic regulation of lipolysis involves Src and epidermal growth factor receptor-dependent ERK1/2 activation". In: *Journal of Biological Chemistry* 281.49, pp. 37794–37802. ISSN: 00219258. DOI: 10.1074/jbc.M605572200.

Robson, Simon C., Jean Sévigny, and Herbert Zimmermann (May 2006). "The E-NTPDase family of ectonucleotidases: Structure function relationships and pathophysiological significance". In: *Purinergic Signalling* 2.2, pp. 409–430. ISSN: 15739538. DOI: 10.1007/s11302-006-9003-5.

Roca-Lapirot, Olivier, Houda Radwani, Franck Aby, Frédéric Nagy, Marc Landry, and Pascal Fossat (2018). "Calcium signalling through L-type calcium channels: role in pathophysiology of spinal nociceptive transmission". In: *British Journal of Pharmacology* 175, pp. 2362–2374. DOI: 10.1111/bph.v175.12/issuetoc.

Rosenbaum M, Malbon CC, Hirsch J, and Leibel RL. (1993). "Lack of beta 3-adrenergic effect on lipolysis in human subcutaneous adipose tissue". In: *The Journal of clinical endocrinology and metabolism* 77.2, pp. 352–355.

Rowland, Leslie A., Adilson Guilherme, Felipe Henriques, Chloe DiMarzio, Sean Munroe, Nicole Wetoska, Mark Kelly, Keith Reddig, Gregory Hendricks, Meixia Pan, Xianlin Han, Olga R. Ilkayeva, Christopher B. Newgard, and Michael P. Czech (Dec. 2023). "De novo lipogenesis fuels adipocyte autophagosome and lysosome membrane dynamics". In: *Nature Communications* 14.1. ISSN: 20411723. DOI: 10.1038/s41467-023-37016-8.

Roy, Debasish, Julia M. Myers, and Andrea Tedeschi (Sept. 2022). "Protocol for assessing ex vivo lipolysis of murine adipose tissue". In: *STAR Protocols* 3.3. ISSN: 26661667. DOI: 10.1016/j.xpro.2022.101518.

Ruiz, A, E Alberdi, and C Matute (2014). "CGP37157, an inhibitor of the mitochondrial Na+/Ca2+ exchanger, protects neurons from excitotoxicity by blocking voltage-gated Ca2+ channels". In: *Cell Death and Disease* 5.4. ISSN: 20414889. DOI: 10.1038/cddis.2014.134.

Ruiz, Manuel and Richard Kraus (2015). "Voltage-Gated Sodium Channels: Structure, Function, Pharmacology, and Clinical Indications". In: *Journal of Medicinal Chemistry* 58.18, pp. 7093–7118. ISSN: 15204804. DOI: 10.1021/jm501981g.

Rungta, Ravi L., Hyun B. Choi, John R. Tyson, Aqsa Malik, Lasse Dissing-Olesen, Paulo J.C. Lin, Stuart M. Cain, Pieter R. Cullis, Terrance P. Snutch, and Brian A. Macvicar (Apr. 2015). "The cellular mechanisms of neuronal swelling underlying cytotoxic edema". In: *Cell* 161.3, pp. 610–621. ISSN: 10974172. DOI: 10.1016/j.cell.2015.03.029.

Ryu, Vitaly, Alan G. Watts, Bingzhong Xue, and Timothy J. Bartness (2017). "Bidirectional crosstalk between the sensory and sympathetic motor systems innervating brown and white adipose tissue in male Siberian hamsters". In: *American Journal of Physiology - Regulatory Integrative and Comparative Physiology* 312.3, R324–R337. ISSN: 15221490. DOI: 10.1152/ajpregu.00456.2015.

Ryuid, Vitaly and Christoph Buettner (Feb. 2019). "Fat cells gobbling up norepinephrine?" In: *PLoS Biology* 17.2. ISSN: 15457885. DOI: 10.1371/journal.pbio.3000138.

Saffari, Tiam M., Meiwand Bedar, Caroline A. Hundepool, Allen T. Bishop, and Alexander Y. Shin (2020). "The role of vascularization in nerve regeneration of nerve graft". In: *Neural Regeneration Research* 15.9, pp. 1573–1579. ISSN: 18767958. DOI: 10.4103/1673-5374.276327.

Sakai, Tatsuo and Yasue Hosoyamada (2013). "Are the precapillary sphincters and metarterioles universal components of the microcirculation? An historical review". In: *Journal of Physiological Sciences* 63.5, pp. 319–331. ISSN: 18806546. DOI: 10.1007/s12576-013-0274-7.

Sakr, Nawar, Olga Glazova, Liudmila Shevkova, Nikita Onyanov, Samira Kaziakhmedova, Alena Shilova, Maria V. Vorontsova, and Pavel Volchkov (Feb. 2023). "Character-

izing and Quenching Autofluorescence in Fixed Mouse Adrenal Cortex Tissue". In: *International Journal of Molecular Sciences* 24.4. ISSN: 14220067. DOI: 10.3390/ijms24043432.

Saladin, Kenneth S (2021). *Anatomy & physiology : the unity of form and function*. 9th ed. McGraw-Hill Education. ISBN: 1260256006.

Sandhu, Bynvant, Maria C. Perez-Matos, Stephanie Tran, Garima Singhal, Ismail Syed, Linda Feldbrügge, Shuji Mitsuhashi, Julie Pelletier, Jinhe Huang, Yusuf Yalcin, Eva Csizmadia, Shilpa Tiwari-Heckler, Keiichi Enjyoji, Jean Sévigny, Eleftheria Maratos-Flier, Simon C Robson, and Z Gordon Jiang (2021). "Global deletion of NTPDase3 protects against diet-induced obesity by increasing basal energy metabolism". In: *Metabolism: Clinical and Experimental* 118, p. 154731. ISSN: 15328600. DOI: 10.1016/j.metabol.2021.154731.

Santos-Carvalho, A., F. Elvas, A. R. Álvaro, A. F. Ambrósio, and C. Cavadas (May 2013). "Neuropeptide y receptors activation protects rat retinal neural cells against necrotic and apoptotic cell death induced by glutamate". In: *Cell Death and Disease* 4.5. ISSN: 20414889. DOI: 10.1038/cddis.2013.160.

Sato, Junichiro, Noriko Makita, and Taroh Iiri (2016). *Inverse agonism: the classic concept of GPCRs revisited*. Tech. rep. 6, pp. 507–514.

Sato, Masaaki, Dana S. Hutchinson, Bronwyn A. Evans, and Roger J. Summers (Nov. 2008). "The β3-adrenoceptor agonist 4-[[(hexylamino)carbonyl]amino] -N-[4-[2-[[(2S)-2-hydroxy-3-(4-hydroxyphenoxy)propyl]amino]ethyl]-phenyl] -benzenesulfonamide (L755507) and antagonist (S)-N-[4-[2-[[3-[3- (acetamidomethyl)phenoxy]-2-hydroxypropyl]amino]-ethyl]phenyl] benzenesulfonamide (L748337) activate different signaling pathways in Chinese hamster ovary-K1 cells [...]" In: *Molecular Pharmacology* 74.5, pp. 1417–1428. ISSN: 0026895X. DOI: 10.1124/mol.108.046979.

Saxton, Sophie N., Sarah B. Withers, Jakob Nyvad, Aleksandra Mazur, Vladimir Matchkov, Anthony M. Heagerty, and Christian Aalkjær (Dec. 2019). "Perivascular Adipose Tissue Contributes to the Modulation of Vascular Tone in vivo". In: *Journal of Vascular Research* 56.6, pp. 320–332. ISSN: 14230135. DOI: 10.1159/000502689.

Schäkel, Laura, Constanze C. Schmies, Riham M. Idris, Xihuan Luo, Sang Yong Lee, Vittoria Lopez, Salahuddin Mirza, The Hung Vu, Julie Pelletier, Jean Sévigny, Vigneshwaran Namasivayam, and Christa E. Müller (Sept. 2020). "Nucleotide Analog

ARL67156 as a Lead Structure for the Development of CD39 and Dual CD39/CD73 Ectonucleotidase Inhibitors". In: *Frontiers in Pharmacology* 11. ISSN: 16639812. DOI: 10.3389/fphar.2020.01294.

Schena, Giorgia and Michael J. Caplan (2019). "Everything you always wanted to know about β3-ar * (* But were afraid to ask)". In: *Cells* 8.4, pp. 1–24. ISSN: 20734409. DOI: 10.3390/cells8040357.

Schödel, Johannes, Ina Weise, Reinhard Klinger, and Martin Schmidt (2004). "Stimulation of lipogenesis in rat adipocytes by ATP, a ligand for P2-receptors". In: *Biochemical and Biophysical Research Communications* 321.4, pp. 767–773. ISSN: 0006291X. DOI: 10.1016/j.bbrc.2004.06.179.

Schweiger, Martina, Renate Schreiber, Guenter Haemmerle, Achim Lass, Christian Fledelius, Poul Jacobsen, Hans Tornqvist, Rudolf Zechner, and Robert Zimmermann (2006). "Adipose triglyceride lipase and hormone-sensitive lipase are the major enzymes in adipose tissue triacylglycerol catabolism". In: *Journal of Biological Chemistry* 281.52, pp. 40236–40241. ISSN: 00219258. DOI: 10.1074/jbc.M608048200.

Sengene, C, A Bouloumie, H Hauner, M Berlan, R Busse, M Lafontan, and J Galitzky (2003). "Involvement of a cGMP-dependent Pathway in the Natriuretic Peptide-mediated Hormone-sensitive Lipase Phosphorylation in Human Adipocytes". In: *The Journal of Biological Chemistry* 278.49, pp. 48617–48626.

Serone, Adrian P and James A Angus (1999). *Role of N-type calcium channels in autonomic neurotransmission in guinea-pig isolated left atria*. Tech. rep. Victoria: University of Melbourne, pp. 927–934.

Sharma, Arya M, Tobias Pischon, Sandra Hardt, Iris Kunz, and Friedrich C Luft (2001). "Adrenergic Receptor Blockers and Weight Gain A Systematic Analysis Hypothesis". In: *Hypertension* 37, pp. 250–254.

Sheng, Yulan and Li Zhu (2018). *The crosstalk between autonomic nervous system and blood vessels*. Tech. rep. 1, pp. 17–28.

Shi, Haifei and Timothy J. Bartness (2005). "White adipose tissue sensory nerve denervation mimics lipectomy-induced compensatory increases in adiposity". In: *American Journal of Physiology - Regulatory Integrative and Comparative Physiology* 289.2 58-2, pp. 514–520. ISSN: 03636119. DOI: 10.1152/ajpregu.00036.2005.

Shi, Zhen, Wei Wei Chen, Xiao Qing Xiong, Ying Han, Ye Bo Zhou, Feng Zhang, Xing Ya Gao, and Guo Qing Zhu (2012). "Sympathetic activation by chemical stimulation of white adipose tissues in rats". In: *Journal of Applied Physiology* 112.6, pp. 1008–1014. ISSN: 87507587. DOI: 10.1152/japplphysiol.01164.2011.

Shrirao, Anil B., Rene S. Schloss, Zachary Fritz, Mayur V. Shrirao, Robert Rosen, and Martin L. Yarmush (2021). "Autofluorescence of blood and its application in biomedical and clinical research". In: *Biotechnology and Bioengineering* 118.12, pp. 4550–4576. ISSN: 10970290. DOI: 10.1002/bit.27933.

Silva, Ana P., Joana Lourenco, Sara Xapelli, Raquel Ferreira, Heidi Kristiansen, David P. D. Woldbye, Catarina R. Oliveira, and Joao O. Malva (Mar. 2007). "Protein kinase C activity blocks neuropeptide Y-mediated inhibition of glutamate release and contributes to excitability of the hippocampus in status epilepticus". In: *The FASEB Journal* 21.3, pp. 671–681. ISSN: 0892-6638. DOI: 10.1096/fj.06-6163com.

Simmonds, M., A. Llewellyn, C. G. Owen, and N. Woolacott (Feb. 2016). "Predicting adult obesity from childhood obesity: A systematic review and meta-analysis". In: *Obesity Reviews* 17.2, pp. 95–107. ISSN: 1467789X. DOI: 10.1111/obr.12334.

Singer, Kanakadurga, David L. Morris, Kelsie E. Oatmen, Tianyi Wang, Jennifer DelProposto, Taleen Mergian, Kae Won Cho, and Carey N. Lumeng (Mar. 2013). "Neuropeptide Y Is Produced by Adipose Tissue Macrophages and Regulates Obesity-Induced Inflammation". In: *PLoS ONE* 8.3. ISSN: 19326203. DOI: 10.1371/journal.pone.0057929.

Sinitsky, Maxim Yu, Vera G. Matveeva, Maxim A. Asanov, and Anastasia V. Ponasenko (2018). "Modifications in routine protocol of RNA isolation can improve quality of RNA purified from adipocytes". In: *Analytical Biochemistry* 543, pp. 128–131. ISSN: 10960309. DOI: 10.1016/j.ab.2017.12.020.

Sipe, L. M., C. Yang, J. Ephrem, E. Garren, J. Hirsh, and C. D. Deppmann (Apr. 2017). "Differential sympathetic outflow to adipose depots is required for visceral fat loss in response to calorie restriction". In: *Nutrition and Diabetes* 7.4. ISSN: 20444052. DOI: 10.1038/nutd.2017.13.

Sivamani, RK, CE Pullar, CG Manabat-Hidalgo, DM Rocke, RC Carlsen, DG Greenhalgh, and RR. Isseroff (Mar. 2009). "Stress-Mediated Increases in Systemic and Local

Epinephrine Impair Skin Wound Healing: Potential New Indication for Beta Blockers". In: *PLoS ONE* 12.4. ISSN: 19326203. DOI: 10.1371/journal.

Soeder, K J, S K Snedden, W Cao, G J D Rocca, K W Daniel, L M Luttrell, and S Collins (1999). "The B3 adrenergic receptor activates mitogen-activated protein kinase in adipocytes". In: *The Journal of Biological Chemistry* 274.17, pp. 12017–12022.

Soma, Shin, Haruhiro Kuwashima, Chiaki Matsumura, and Tomohiko Kimura (2006). "Inhibition by SEA0400, a selective inhibitor of Na+/Ca 2+ exchanger, of Na+-dependent Ca2+ uptake and catecholamine release in bovine adrenal chromaffin cells". In: *Journal of Pharmacological Sciences* 102.1, pp. 88–95. ISSN: 13478648. DOI: 10.1254/jphs.FPJ06006X.

Song, Mun Gyu, Hye Jin Lee, Bo Yeong Jin, Ruth Gutierrez-Aguilar, Kyung Ho Shin, Sang Hyun Choi, Sung Hee Um, and Dong Hoon Kim (2016). "Depot-specific differences in angiogenic capacity of adipose tissue in differential susceptibility to diet-induced obesity". In: *Molecular Metabolism* 5.11, pp. 1113–1120. ISSN: 22128778. DOI: 10.1016/j.molmet.2016.09.001.

Song, Wenxin, Qi Luo, Yuping Zhang, Linkang Zhou, Ye Liu, Zhilong Ma, Jianan Guo, Yuedong Huang, Lili Cheng, Ziyi Meng, Zicheng Li, Bin Zhang, Siqi Li, Sook Wah Yee, Hao Fan, Peng Li, Kathleen M. Giacomini, and Ligong Chen (2019). "Organic cation transporter 3 (Oct3) is a distinct catecholamines clearance route in adipocytes mediating the beiging of white adipose tissue". In: *PLoS Biology* 17.1. ISSN: 15457885. DOI: 10.1371/journal.pbio.2006571.

Spalding, Kirsty L., Erik Arner, Pål O. Westermark, Samuel Bernard, Bruce A. Buchholz, Olaf Bergmann, Lennart Blomqvist, Johan Hoffstedt, Erik Näslund, Tom Britton, Hernan Concha, Moustapha Hassan, Mikael Rydén, Jonas Frisén, and Peter Arner (2008). "Dynamics of fat cell turnover in humans". In: *Nature* 453.7196, pp. 783–787. ISSN: 14764687. DOI: 10.1038/nature06902.

Sperlágh, Beáta, Ferenc Erdélyi, Gábor Szabó, and E. Sylvester Vizi (2000). "Local regulation of [3H]-noradrenaline release from the isolated guinea-pig right atrium by P2X-receptors located on axon terminals". In: *British Journal of Pharmacology* 131.8, pp. 1775–1783. ISSN: 00071188. DOI: 10.1038/sj.bjp.0703757.

Sperlágh, Beáta, Attila Heinrich, and Cecilia Csölle (2007). *P2 receptor-mediated modulation of neurotransmitter release - An update*. DOI: 10.1007/s11302-007-9080-0.

Srivastava, Swayam Prakash, Han Zhou, Ocean Setia, Alan Dardik, Carlos Fernandez-Hernando, and Julie Goodwin (2021). "Podocyte glucocorticoid receptors are essential for glomerular endothelial cell homeostasis in diabetes mellitus". In: *Journal of the American Heart Association* 10.15. ISSN: 20479980. DOI: 10.1161/JAHA.120.019437.

Stacey, Peter, Anne Mai Wassermann, Laura Kammonen, Emma Impey, Anna Wilbrey, and Darren Cawkill (July 2018). "Plate-Based Phenotypic Screening for Pain Using Human iPSC-Derived Sensory Neurons". In: *SLAS Discovery* 23.6, pp. 585–596. ISSN: 24725560. DOI: 10.1177/2472555218764678.

Stanley, Glenn B, Stavroula Kyrkouli E, Lampert Sharon, and Sarah Leibowitz (1986). *Neuropeptide Y Chronically Injected Into the Hypothalamus: A Powerful Neurochemical Inducer of Hyperphagia and Obesity*. Tech. rep., pp. 1189–1192.

Steinman, Joe, Margaret M. Koletar, Bojana Stefanovic, and John G. Sled (2017). "3D morphological analysis of the mouse cerebral vasculature: Comparison of in vivo and ex vivo methods". In: *PLoS ONE* 12.10, pp. 1–17. ISSN: 19326203. DOI: 10.1371/journal.pone.0186676.

Stevens, Marijke, Steve Peigneur, and Jan Tytgat (2011). "Neurotoxins and their binding areas on voltage-gated sodium channels". In: *Frontiers in Pharmacology* 2.71, pp. 1–13. ISSN: 16639812. DOI: 10.3389/fphar.2011.00071.

Straznicky, N E, P J Nestel, and M D Esler (2009). *Autonomic Nervous System: Metabolic Function*. Tech. rep. Melbourne: Baker Heart Research Institute, pp. 951–959.

Stylianopoulos, Triantafyllos, Ming Zher Poh, Numpon Insin, Moungi G. Bawendi, Dai Fukumura, Lance L. Munn, and Rakesh K. Jain (Sept. 2010). "Diffusion of particles in the extracellular matrix: The effect of repulsive electrostatic interactions". In: *Biophysical Journal* 99.5, pp. 1342–1349. ISSN: 15420086. DOI: 10.1016/j.bpj.2010.06.016.

Südhof, Thomas C. (2012). "Calcium control of neurotransmitter release". In: *Cold Spring Harbor Perspectives in Biology* 4.1. ISSN: 19430264. DOI: 10.1101/cshperspect.a011353.

Sun, Chao, Li Wang, Jun Yan, and Shumin Liu (Feb. 2012). "Calcium ameliorates obesity induced by high-fat diet and its potential correlation with p38 MAPK pathway". In:

Molecular Biology Reports 39.2, pp. 1755–1763. ISSN: 03014851. DOI: 10.1007/s11033-011-0916-x.

Suppiramaniam, V, E A Abdel-Rahman, M A Buabeid, and K Parameshwaran (2010). "Nervous System and Behavioural Toxicology 3.09 Ion Channels". In: 11, pp. 155–181.

Surwit, Richard S, Shiying Wang, Ann E Petro, Daniel Sanchis, Serge Raimbault, Daniel Ricquier, and Sheila Collins (1998). *Diet-induced changes in uncoupling proteins in obesity-prone and obesity-resistant strains of mice (UCP2UCP3gene expressionwhite adipose tissuebrown adipose tissue)*. Tech. rep., pp. 4061–4065.

Susulic, Vedrana S, Robert C Frederich, Joel Lawitts, Effie Tozzo, Barbara B Kahn, Mary-Ellen Harper, Jean Himms-Hagen, Jeffrey S Flier, and Bradford B Lowell (1995). "Targeted Disruption of the 3-Adrenergic Receptor Gene*". In: *The Journal of Biological Chemistry* 270.49, pp. 29483–29492.

Tanaka, Yoshio, Yumi Mochizuki, Hikaru Tanaka, and Koki Shigenobu (1999). "Significant role of neuronal non-N-type calcium channels in the sympathetic neurogenic contraction of rat mesenteric artery". In: *British Journal of Pharmacology* 128, pp. 1602–1608.

Tang, Hao Neng, Chen Yi Tang, Xiao Fei Man, Shu Wen Tan, Yue Guo, Jun Tang, Ci La Zhou, and Hou De Zhou (2017). "Plasticity of adipose tissue in response to fasting and refeeding in male mice". In: *Nutrition and Metabolism* 14.1. ISSN: 17437075. DOI: 10.1186/s12986-016-0159-x.

Thomas, Gail D (2011). "Neural control of the circulation". In: *Adv Physiol Educ* 35, pp. 28–32. DOI: 10.1152/advan.00114.2010.-The.

Thomas, Gail D and Steven S Segal (2004). "Skeletal and Cardiac Muscle Blood Flow Neural control of muscle blood flow during exercise". In: *Journal of Applied Physiology* 97, pp. 731–738. DOI: 10.1152/japplphysiol.00076.

Thompson, Airlia C.S., Martha Nuñez, Ryan Davidson, Teresa Horm, Karina Schnittker, Madeline V. Hart, Allen M. Suarez, and Tsu Shuen Tsao (Dec. 2012). "Mitigation of isolation-associated adipocyte interleukin-6 secretion following rapid dissociation of adipose tissue". In: *Journal of Lipid Research* 53.12, pp. 2797–2805. ISSN: 00222275. DOI: 10.1194/jlr.D031286.

Tian, Tian, Markus Heine, Ioannis Evangelakos, Michelle Y Jaeckstein, Nicola Schaltenberg, Tobias Stähler, Friedrich Koch-Nolte, Manju Kumari, and Joerg Heeren (2020). "The P2X7 ion channel is dispensable for energy and metabolic homeostasis of white and brown adipose tissues". In: *Purinergic Signalling* 16.4, pp. 529–542. ISSN: 15739546. DOI: 10.1007/s11302-020-09738-7.

Tozzi, Marco, Jacob B Hansen, and Ivana Novak (2020). "Pannexin-1 mediated ATP release in adipocytes is sensitive to glucose and insulin and modulates lipolysis and macrophage migration". In: *Acta Physiologica* 228.2, pp. 1–18. ISSN: 17481716. DOI: 10.1111/apha.13360.

Tozzi, Marco and Ivana Novak (2017). "Purinergic receptors in adipose tissue as potential targets in metabolic disorders". In: *Frontiers in Pharmacology* 8, pp. 1–8. ISSN: 16639812. DOI: 10.3389/fphar.2017.00878.

Trapero, Carla and Mireia Martín-Satué (2020). "Purinergic signaling in endometriosis-associated pain". In: *International Journal of Molecular Sciences* 21.22, pp. 1–28. ISSN: 14220067. DOI: 10.3390/ijms21228512.

Trayhurn, Paul (2013). "Hypoxia and Adipose Tissue Function and Dysfunction in Obesity". In: *Physiol Rev* 93, pp. 1–21. DOI: 10.1152/physrev.00017.2012.-The.

Treble, D. H. and J. Mayer (1963). *Glycerolkinase Activity in White Adipose Tissue of Obese-hyperglycæmic Mice*. Tech. rep., pp. 363–364.

Tsai, Minglun, Akihiro Asakawa, Haruka Amitani, and Akio Inui (2012). "Stimulation of leptin secretion by insulin". In: *Indian Journal of Endocrinology and Metabolism* 16.9, p. 543. ISSN: 2230-8210. DOI: 10.4103/2230-8210.105570.

Turovsky, Egor A, Elena G Varlamova, and Maria V Turovskaya (2021). "Activation of Cx43 Hemichannels Induces the Generation of Ca 2+ Oscillations in White Adipocytes and Stimulates Lipolysis". In: *International Journal of Molecular Sciences Article* 22, pp. 1–28. DOI: 10.3390/ijms.

Turtzo, L Christine, Ruth Marx, and M Daniel Lane (2001). "Cross-talk between sympathetic neurons and adipocytes in coculture". In: *PNAS* 98.22, pp. 12385–12390.

Uebele, Victor N., Cindy E. Nuss, Vincent P. Santarelli, Susan L. Garson, James C. Barrow, Shaun R. Stauffer, Kenneth S. Koblan, John J. Renger, Sara Aton, Julie Seibt, Michelle Dumoulin, Sushil K. Jha, Tammi Coleman, and Marcos G. Frank (Feb. 2009). "T-type calcium channels regulate cortical plasticity in-vivo NR-D-08-

7049". In: *NeuroReport* 20.3, pp. 257–262. ISSN: 09594965. DOI: 10.1097/WNR.0b013e3283200111.

Ulbricht, Werner (2005). "Sodium Channel Inactivation: Molecular Determinants and Modulation". In: *Physiological Reviews* 85, pp. 1271–1301. DOI: 10.1152/physrev.00024.2004.-Voltage-gated.

Uneyama, Hisayuki, Hirohisa Uchida, Tomoyuki Konda, and Ryota Yoshimoto (1999). "Cilnidipine: Preclinical profile and clinical evaluation". In: *Cardiovascular Drug Reviews* 17.4, pp. 341–357. ISSN: 08975957. DOI: 10.1111/j.1527-3466.1999.tb00024.x.

Ussar, Siegfried, Kevin Y Lee, Simon N Dankel, Jeremie Boucher, Max Felix Haering, Andre Kleinridders, Thomas Thomou, Ruidan Xue, Yazmin Macotela, Aaron M. Cypess, Yu Hua Tseng, Gunnar Mellgren, and C Ronald Kahn (2014). "ASC-1, PAT2, and P2RX5 are cell surface markers for white, beige, and brown adipocytes". In: *Science Translational Medicine* 6.247. ISSN: 19466242. DOI: 10.1126/scitranslmed.3008490.

Valentine, Joseph M., Maryam Ahmadian, Omer Keinan, Mohammad Abu-Odeh, Peng Zhao, Xin Zhou, Mark P. Keller, Hui Gao, Ruth T. Yu, Christopher Liddle, Michael Downes, Jin Zhang, Aldons J. Lusis, Alan D. Attie, Ronald M. Evans, Mikael Rydén, and Alan R. Saltiel (2022). "β3-Adrenergic receptor downregulation leads to adipocyte catecholamine resistance in obesity". In: *Journal of Clinical Investigation* 132.2. ISSN: 15588238. DOI: 10.1172/JCI153357.

Valet, Philippe, Danica Grujic, Jennifer Wade, Moriko Ito, M. Cristina Zingarettii, Veronika Soloveva, Susan R. Ross, Reed A. Graves, Saverio Cinti, Max Lafontan, and Bradford B. Lowell (Nov. 2000). "Expression of human α2-adrenergic receptors in adipose tissue of β-adrenergic receptor-deficient mice promotes diet-induced obesity". In: *Journal of Biological Chemistry* 275.44, pp. 34797–34802. ISSN: 00219258. DOI: 10.1074/jbc.M005210200.

Vedel, Line, Hans Bräuner-Osborne, and Jesper Mosolff Mathiesen (Aug. 2015). "A cAMP biosensor-based high-throughput screening assay for identification of Gs-coupled GPCR ligands and phosphodiesterase inhibitors". In: *Journal of Biomolecular Screening* 20.7, pp. 849–857. ISSN: 1552454X. DOI: 10.1177/1087057115580019.

Vetter, Irina, Christine A. Mozar, Thomas Durek, Joshua S. Wingerd, Paul F. Alewood, MacDonald J. Christie, and Richard J. Lewis (2012). "Characterisation of Na v types endogenously expressed in human SH-SY5Y neuroblastoma cells". In: *Biochemical Pharmacology* 83.11, pp. 1562–1571. ISSN: 00062952. DOI: 10.1016/j.bcp.2012.02.022.

Vrecl, Milka, Rasmus Jorgensen, Azra Pogačnik, and Anders Heding (June 2004). "Development of a BRET2 screening assay using β-arrestin 2 mutants". In: *Journal of Biomolecular Screening* 9.4, pp. 322–333. ISSN: 10870571. DOI: 10.1177/1087057104263212.

Vrydag, Wim and Martin C. Michel (2007). "Tools to study β3-adrenoceptors". In: *Naunyn-Schmiedeberg's Archives of Pharmacology* 374.5, pp. 385–398. ISSN: 00281298. DOI: 10.1007/s00210-006-0127-5.

Wada, A, Y Uezono, M Arita, K Tsuji, N Yanagihara, H Kobayashi, and F Izumi (1992). "[22] Neosurugatoxin: A Probe for Neuronal Nicotinic Receptors in Adrenal Medulla, Brain, and Ganglia". In: *Methods in Neurosciences* 8, pp. 311–322.

Walker, Christopher S., Alex C. Conner, David R. Poyner, and Debbie L. Hay (Oct. 2010). "Regulation of signal transduction by calcitonin gene-related peptide receptors". In: *Trends in Pharmacological Sciences* 31.10, pp. 476–483. ISSN: 01656147. DOI: 10.1016/j.tips.2010.06.006.

Walker, Christopher S., Debbie L. Hay, Sandra M. Fitzpatrick, Garth J.S. Cooper, and Kerry M. Loomes (2014). "α-Calcitonin gene related peptide (α-CGRP) mediated lipid mobilization in 3T3-L1 adipocytes". In: *Peptides* 58, pp. 14–19. ISSN: 18735169. DOI: 10.1016/j.peptides.2014.05.011.

Wang, Dao W., Akshitkumar M. Mistry, Kristopher M. Kahlig, Jennifer A. Kearney, Jizhou Xiang, and Alfred L. George (2010). "Propranolol blocks cardiac and neuronal voltage-gated sodium channels". In: *Frontiers in Pharmacology* 1.144, pp. 1–12. ISSN: 16639812. DOI: 10.3389/fphar.2010.00144.

Wang, Jun, Shao Wu Ou, and Yun Jie Wang (Nov. 2017). "Distribution and function of voltage-gated sodium channels in the nervous system". In: *Channels* 11.6, pp. 534–554. ISSN: 19336969. DOI: 10.1080/19336950.2017.1380758.

Wang, Tong, Yan Zang, Wenhua Ling, Barbara E. Corkey, and Wen Guo (2003). "Metabolic partitioning of endogenous fatty acid in adipocytes". In: *Obesity Research* 11.7, pp. 880–887. ISSN: 10717323. DOI: 10.1038/oby.2003.121.

Wang, Yu, Verina H. Leung, Yunxiao Zhang, Victoria S. Nudell, Meaghan Loud, M. Rocio Servin-Vences, Dong Yang, Kristina Wang, Maria Dolores Moya-Garzon, Veronica L. Li, Jonathan Z. Long, Ardem Patapoutian, and Li Ye (2022). "The role of somatosensory innervation of adipose tissues". In: *Nature* 609.7927, pp. 569–574. ISSN: 14764687. DOI: 10.1038/s41586-022-05137-7.

Waterman, Sally A. (1997). "Role of N-, P- and Q-type voltage-gated calcium channels in transmitter release from sympathetic neurones in the mouse isolated vas deferens". In: *British Journal of Pharmacology* 120.3, pp. 393–398. ISSN: 00071188. DOI: 10.1038/sj.bjp.0700948.

Weiss, Benjamin and Rcger P Maicicelt (1965). *SYMPATHETIC NERVOUS CONTROL OF ADIPOSE TISSUE LIPOLYSIS*. Tech. rep., pp. 393–403.

Westcott, Erika B. and Steven S. Segal (2013). "Perivascular Innervation: A Multiplicity of Roles in Vasomotor Control and Myoendothelial Signaling". In: *Microcirculation* 20.3, pp. 217–238. ISSN: 10739688. DOI: 10.1111/micc.12035.

Westenbroek, Ruth E, Johannes W Hell, Conception Warner, Stefan J Dubel, Terry P Snutch, and William A Catterall (1992). *Biochemical Properties and Subcellular Distribution of an N-type Calcium Channel al Subunit*. Tech. rep.

Westfall, T D, I C Kennedy &, and P Sneddon (1996). *Enhancement of sympathetic purinergic neurotransmission in the guinea-pig isolated vas deferens by the novel ecto-ATPase inhibitor ARL 67156*. Tech. rep.

Whorlow, S L, J A Angus, and C E Wright (1996). "Selectivity of omega-conotoxin GVIA for n-type calcium channels in rat isolated small mesenteric arteries". In: *Clinical and Experimental Pharmacology Physiology* 23.1, pp. 16–21.

Wieser, P B., M A. Zeiger, and John N Fain (1977). "EFFECTS OF DIMETHYLSULFOXIDE ON CYCLIC AMP ACCUMULATION, LIPOLYSIS AND GLUCOSE METABOLISM OF FAT CELLS*". In: *Biochemical Pharmacology* 26, pp. 775–778.

Wilding, John P.H., Rachel L. Batterham, Melanie Davies, Luc F. Van Gaal, Kristian Kandler, Katerina Konakli, Ildiko Lingvay, Barbara M. McGowan, Tugce Kalayci Oral, Julio Rosenstock, Thomas A. Wadden, Sean Wharton, Koutaro Yokote, and Robert

F. Kushner (Aug. 2022). "Weight regain and cardiometabolic effects after withdrawal of semaglutide: The STEP 1 trial extension". In: *Diabetes, Obesity and Metabolism* 24.8, pp. 1553–1564. ISSN: 14631326. DOI: 10.1111/dom.14725.

Willows, Jake W., Magdalena Blaszkiewicz, Amy Lamore, Samuel Borer, Amanda L. Dubois, Emma Garner, William P. Breeding, Karissa B. Tilbury, Andre Khalil, and Kristy L. Townsend (2021). "Visualization and analysis of whole depot adipose tissue neural innervation". In: *iScience* 24.10, p. 103127. ISSN: 25890042. DOI: 10.1016/j.isci.2021.103127.

Willows, Jake W., Gilian Gunsch, Emma Paradie, Magdalena Blaszkiewicz, Jeffrey R. Tonniges, Maria F. Pino, Steven R. Smith, Lauren M. Sparks, and Kristy L. Townsend (Mar. 2023). "Schwann cells contribute to demyelinating diabetic neuropathy and nerve terminal structures in white adipose tissue". In: *iScience* 26.3. ISSN: 25890042. DOI: 10.1016/j.isci.2023.106189.

Windscheif, Ursula, Otmar Pfaff, Airat U. Ziganshin, Charles H.V. Hoyle, Hans G. Baumert, Ernst Mutschler, Geoffrey Burastock, and Gunter Lambrecht (1995). "Inhibitory action of PPADS on relaxant responses to adenine nucleotides or electrical field stimulation in guinea-pig taenia coli and rat duodenum". In: *British Journal of Pharmacology* 115.8, pp. 1509–1517. ISSN: 14765381. DOI: 10.1111/j.1476-5381.1995.tb16644.x.

Wingler, Laura M. and Robert J. Lefkowitz (2020). "Conformational Basis of G Protein-Coupled Receptor Signaling Versatility". In: *Trends in Cell Biology* 30.9, pp. 736–747. ISSN: 18793088. DOI: 10.1016/j.tcb.2020.06.002.

Wittrisch, Stefanie, Nora Klöting, Karin Mörl, Rima Chakaroun, Matthias Blüher, and Annette G. Beck-Sickinger (Jan. 2020). "NPY1R-targeted peptide-mediated delivery of a dual PPARα/γ agonist to adipocytes enhances adipogenesis and prevents diabetes progression". In: *Molecular Metabolism* 31, pp. 163–180. ISSN: 22128778. DOI: 10.1016/j.molmet.2019.11.009.

Wolf, Katharine, Haidi Hu, Toshihiko Isaji, and Alan Dardik (2019). "Molecular identity of arteries, veins, and lymphatics". In: *Journal of Vascular Surgery* 69.1, pp. 253–262. ISSN: 10976809. DOI: 10.1016/j.jvs.2018.06.195.

Wolfe, Robert R, Samuel Klein, Fabio Carraro, Jean-Michel Weber, and Jean-Michel Weber Role (1990). "Role of triglyceride-fatty acid cycle in controlling fat metabolism in

humans during and after exercise". In: *American Physiological Society* 258, pp. 382–389.

Wood, Sarah J. and Clarke R. Slater (2001). "Safety factor at the neuromuscular junction". In: *Progress in Neurobiology* 64.4, pp. 393–429. ISSN: 03010082. DOI: 10.1016/S0301-0082(00)00055-1.

Wootten, Denise, Arthur Christopoulos, Maria Marti-Solano, M. Madan Babu, and Patrick M. Sexton (2018). "Mechanisms of signalling and biased agonism in G protein-coupled receptors". In: *Nature Reviews Molecular Cell Biology* 19.10, pp. 638–653. ISSN: 14710080. DOI: 10.1038/s41580-018-0049-3.

World Health Organization, https:// www.who.int/health-topics/#O, accessed 22/07/2024. (2024).

World Obesity Fedoration (2023). *World Obesity Atlas 2023, https://data.worldobesity.org/publications/?cat=19, accessed 22/07/2024.* Tech. rep.

Xu, Jianfeng, Hidetaka Morinaga, Dayoung Oh, Pingping Li, Ai Chen, Saswata Talukdar, Eduardo Lazarowski, Jerrold M. Olefsky, and Jane J. Kim (Aug. 2012). "GPR105 Ablation Prevents Inflammation and Improves Insulin Sensitivity in Mice with Diet-Induced Obesity". In: *The Journal of Immunology* 189.4, pp. 1992–1999. ISSN: 0022-1767. DOI: 10.4049/jimmunol.1103207.

Xu, Y F and W D Atchison (1996). "Effects of omega-agatoxin-IVA and omega-conotoxin-MVIIC on perineurial Ca++ and Ca(++)-activated K+ currents of mouse motor nerve terminals". In: *Journal of Pharmacology and Experimental Therapeutics* 279.3, pp. 1229–1236.

Xue, B., A. G. Greenberg, F. B. Kraemer, and M. B. Zemel (2001). "Mechanism of intracellular calcium ([Ca2+]i) inhibition of lipolysis in human adipocytes." In: *The FASEB journal : official publication of the Federation of American Societies for Experimental Biology* 15.13, pp. 2527–2529. ISSN: 15306860. DOI: 10.1096/fj.01-0278fje.

Yang, Chieh Hsin, Danise Ann-Onda, Xuzhu Lin, Stacey Fynch, Shaktypreya Nadarajah, Evan G. Pappas, Xin Liu, John W. Scott, Jonathan S. Oakhill, Sandra Galic, Yanchuan Shi, Alba Moreno-Asso, Cassandra Smith, Thomas Loudovaris, Itamar Levinger, Decio L. Eizirik, D. Ross Laybutt, Herbert Herzog, Helen E. Thomas, and Kim Loh (Jan. 2022). "Neuropeptide Y1 receptor antagonism protects β-cells and

improves glycemic control in type 2 diabetes". In: *Molecular Metabolism* 55. ISSN: 22128778. DOI: 10.1016/j.molmet.2021.101413.

Yang, Kaiping, Haiyan Guan, Edith Arany, David J. Hill, and Xiang Cao (July 2008). " Neuropeptide Y is produced in visceral adipose tissue and promotes proliferation of adipocyte precursor cells via the Y1 receptor ". In: *The FASEB Journal* 22.7, pp. 2452–2464. ISSN: 0892-6638. DOI: 10.1096/fj.07-100735.

Yang, Rong, Tuo Wei, Hannah Goldberg, Weiping Wang, Kathleen Cullion, and Daniel S. Kohane (2017). "Getting Drugs Across Biological Barriers". In: *Advanced Materials* 29.37, pp. 1–54. ISSN: 15214095. DOI: 10.1002/adma.201606596.

Yang, Xingyuan, Xiaodong Zhang, Bradlee L. Heckmann, Xin Lu, and Jun Liu (Nov. 2011). "Relative contribution of adipose triglyceride lipase and hormone-sensitive lipase to tumor necrosis factor-α (TNF-α)-induced lipolysis in adipocytes". In: *Journal of Biological Chemistry* 286.47, pp. 40477–40485. ISSN: 00219258. DOI: 10.1074/jbc.M111.257923.

Youngstrom, Timothy G and Timothy J Bartness (1995). "Catecholaminergic innervation of white adipose tissue in Siberian hamsters". In: *Am. J. Physiol* 268, pp. 744–751.

Youngstrom, Timothy G and Timothy J Bartness (1998). "White adipose tissue sympathetic nervous system denervation increases fat pad mass and fat cell number". In: *The American Physiological Society*, pp. 1488–1493.

Zanetti, L A (1993). "Sotalol: a new class III antiarrhythmic agent". In: *Clinical Pharmacy* 12.12, pp. 883–891.

Zatterale, Federica, Michele Longo, Jamal Naderi, Gregory Alexander Raciti, Antonella Desiderio, Claudia Miele, and Francesco Beguinot (Jan. 2020). *Chronic Adipose Tissue Inflammation Linking Obesity to Insulin Resistance and Type 2 Diabetes*. DOI: 10.3389/fphys.2019.01607.

Zemel, Michael (2004). "Role of calcium and dairy products in energy partitioning and weight management". In: *American Journal for Clinical Nutrition* 79, pp. 907–912.

Zeng, Wenwen, Roksana M. Pirzgalska, Mafalda M.A. Pereira, Nadiya Kubasova, Andreia Barateiro, Elsa Seixas, Yi Hsueh Lu, Albina Kozlova, Henning Voss, Gabriel G. Martins, Jeffrey M. Friedman, and Ana I. Domingos (2015). "Sympathetic Neuro-adipose Connections Mediate Leptin-Driven Lipolysis". In: *Cell* 163.1, pp. 84–94. ISSN: 10974172. DOI: 10.1016/j.cell.2015.08.055.

Zhai, Jin and Ruchun Ma (May 1991). "Effect of nifedipine on neurons of guinea pig celiac ganglion". In: *Brain Research* 550.1, pp. 108–114. ISSN: 00068993. DOI: 10.1016/0006-8993(91)90411-N.

Zhai, Mingzhu, Dazhi Yang, Weihong Yi, and Wuping Sun (2020). "Involvement of calcium channels in the regulation of adipogenesis". In: *Adipocyte* 9.1, pp. 132–141. ISSN: 2162397X. DOI: 10.1080/21623945.2020.1738792.

Zhang, C and Z Zhou (2002). "Ca(2+)-independent but voltage-dependent secretion in mammalian dorsal root ganglion neurons". In: *Nature Neuroscience* 5.5, pp. 425–430.

Zhang, Jin, Qiang He, Qiu Y. Liu, Wei Guo, Xue M. Deng, Wei W. Zhang, Xiao X. Hu, and Ning Li (Nov. 2007). "Differential gene expression profile in pig adipose tissue treated with/ without clenbuterol". In: *BMC Genomics* 8. ISSN: 14712164. DOI: 10.1186/1471-2164-8-433.

Zhang, Pengcheng, Daniels Konja, and Yu Wang (2020). "Adipose tissue secretory profile and cardiometabolic risk in obesity". In: *Endocrine and Metabolic Science* 1.3-4. ISSN: 26663961. DOI: 10.1016/j.endmts.2020.100061.

Zhang, Wei, Mark A Cline, and Elizabeth R Gilbert (2014). "Hypothalamus-adipose tissue crosstalk: Neuropeptide y and the regulation of energy metabolism". In: *Nutrition and Metabolism* 11.1, pp. 1–12. ISSN: 17437075. DOI: 10.1186/1743-7075-11-27.

Zhang, Wen jun, Hong liang Luo, and Zheng ming Zhu (2020). "The role of P2X4 receptors in chronic pain: A potential pharmacological target". In: *Biomedicine and Pharmacotherapy* 129, pp. 110446–110447. ISSN: 19506007. DOI: 10.1016/j.biopha.2020.110447.

Zhang, Xiao., Rui yun Bi, Peng Zhang, and Ye hua Gan (2018). "Veratridine modifies the gating of human voltage-gated sodium channel Nav1.7". In: *Acta Pharmacologica Sinica* 39.11, pp. 1716–1724. ISSN: 17457254. DOI: 10.1038/s41401-018-0065-z.

Zhao, Jin, Barbara Cannon, and Jan Nedergaard (Dec. 1997). "α1-Adrenergic stimulation potentiates the thermogenic action of β3- adrenoreceptor-generated cAMP in brown fat cells". In: *Journal of Biological Chemistry* 272.52, pp. 32847–32856. ISSN: 00219258. DOI: 10.1074/jbc.272.52.32847.

Zhao, Wanming, Xingyu Wang, Kai Hui Sun, and Lan Zhou (2018). "A-Smooth Muscle Actin Is Not a Marker of Fibrogenic Cell Activity in Skeletal Muscle Fibrosis". In: *PLoS ONE* 13.1, pp. 1–16. ISSN: 19326203. DOI: 10.1371/journal.pone.0191031.

Zheng, Junbo, Yongbo Huang, Diana Islam, Xiao Yan Wen, Sulong Wu, Catherine Streutker, Alice Luo, Manshu Li, Julie Khang, Bing Han, Nanshan Zhong, Yimin Li, Kaijiang Yu, and Haibo Zhang (Sept. 2018). "Dual effects of human neutrophil peptides in a mouse model of pneumonia and ventilator-induced lung injury". In: *Respiratory Research* 19.1. ISSN: 1465993X. DOI: 10.1186/s12931-018-0869-x.

Zhong, Yu, Philip M Dunn, and Geoffrey Burnstock (2000). "Guinea-pig sympathetic neurons express varying proportions of two distinct P2X receptors". In: *Journal of Physiology* 523.2, pp. 391–402.

Zhu, Feipeng, Lina Liu, Jie Li, Bing Liu, Qinglong Wang, Ruiying Jiao, Yongxin Xu, Lun Wang, Suhua Sun, Xiaoxuan Sun, Muhammad Younus, Changhe Wang, Tomas Hokfelt, Bo Zhang, Howard Gu, Zhi Qing David Xu, and Zhuan Zhou (Aug. 2022). "Cocaine increases quantal norepinephrine secretion through NET-dependent PKC activation in locus coeruleus neurons". In: *Cell Reports* 40.7. ISSN: 22111247. DOI: 10.1016/j.celrep.2022.111199.

Zou, Shan, Roderick Chisholm, Joseph S. Tauskela, Geoff A. Mealing, Linda J. Johnston, and Catherine E. Morris (Aug. 2013). "Force Spectroscopy Measurements Show That Cortical Neurons Exposed to Excitotoxic Agonists Stiffen before Showing Evidence of Bleb Damage". In: *PLoS ONE* 8.8. ISSN: 19326203. DOI: 10.1371/journal.pone.0073499.

Chapter 7

Appendix

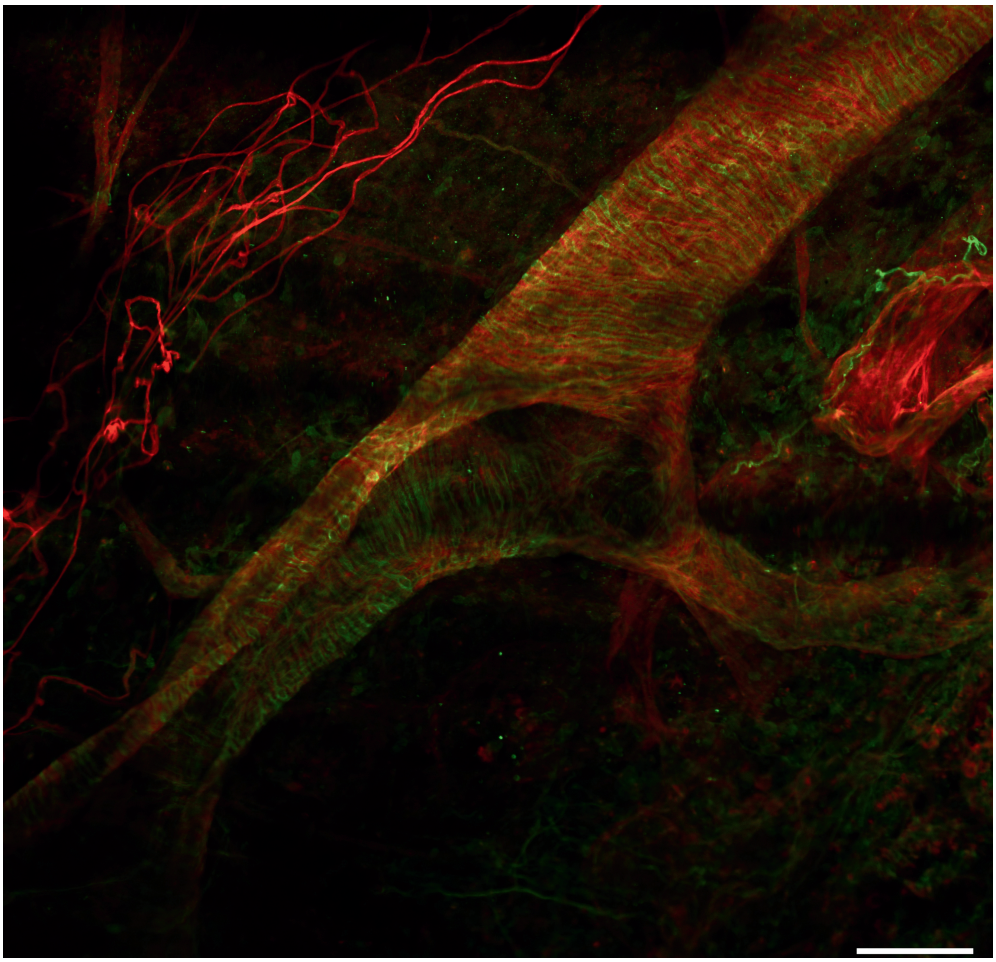

Figure 7.1: Lymph vasculature. Confocal image illustrating an example of lymph vasculature captured in optimisation experiments, using a trial of Pecam-1 antibodies (Alexa 647) additional to IB4 (Alexa 647) and β3-tubulin (Alexa 488), whereby the distinctive striped pattern is evident. Scale bar represents 100 μm.

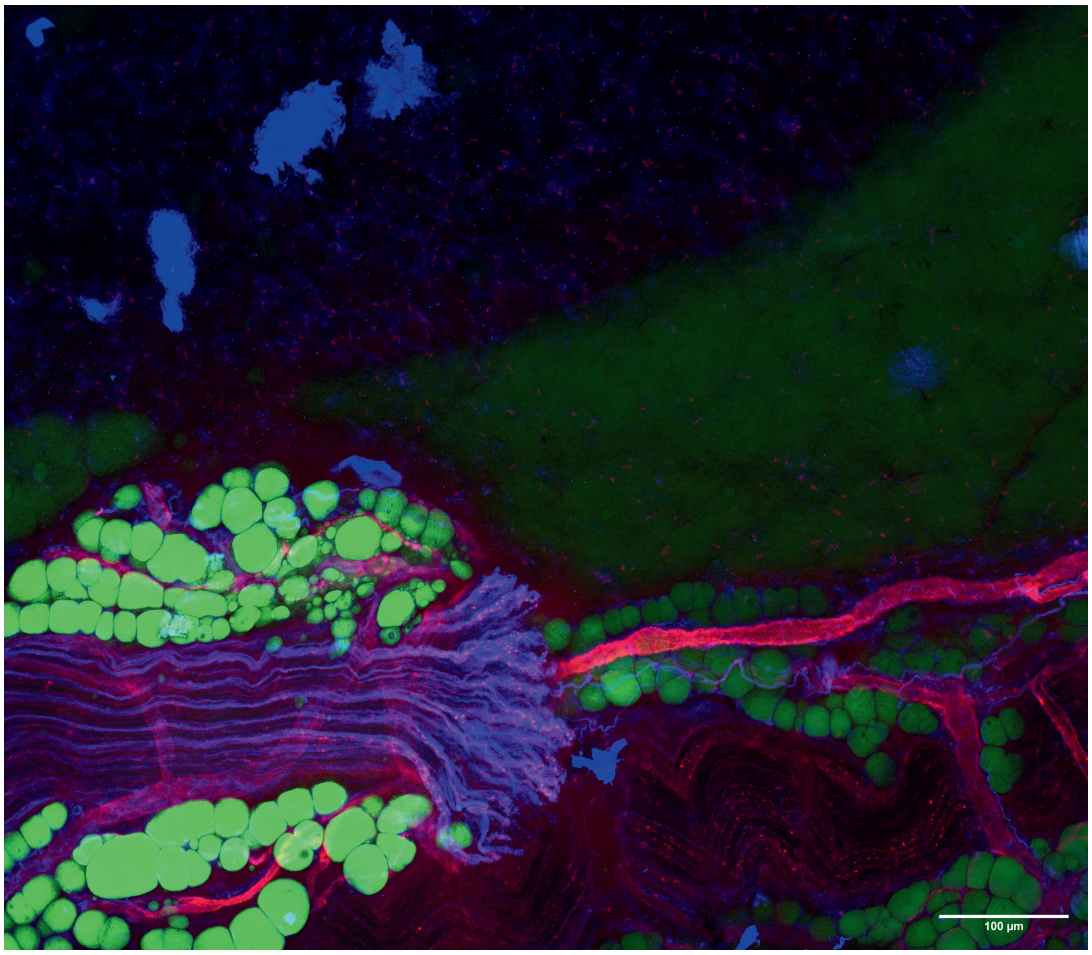

Figure 7.2: Severed nerve bundle among adipocytes and vasculature. Confocal image illustrating interaction between a severed nerve bundle (Alexa 405), among BODIPY-stained adipocytes (green channel) and IB4-stained vasculature (Alexa 647). Scale bar represents 100 μm.

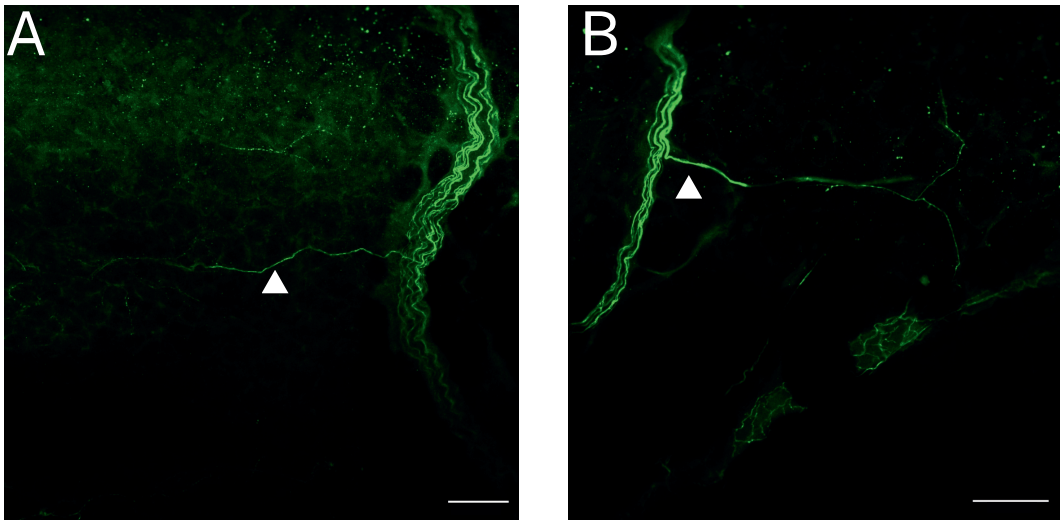

Figure 7.3: Nerve bundle branching. Confocal image from optimisation experiments illustrating TH-stained nerve bundles (Alexa 488) appearing to branch away from the main bundle structure (white arrowheads). Scale bar represents 100 μm.

Table 7.1: Standard deviation values for data presented in this thesis VC vehicle control, ISO isoprenaline, NE, norepinephrine, VTD veratridine, CtX conotoxin.

Figure #	Group	SD value
4.1A	Basal 1 hour	0.49
	Basal 2 hour	0.76
	Basal 3 hour	0.75
	Basal 4 hour	0.79
4.1C	VC	3.04
	ISO 10 μM	5.11
	NE 10 μM	11.33
4.2B	VC 1 hour	2.58
	VC 2 hour	2.39
	VC 3 hour	2.55
	NE 1 hour	4.18
	NE 2 hour	3.5
	NE 3 hour	3.28
4.3A	VC	4.07

Continuation of Table 7.1

Figure #	Group	SD value
	VTD 10 μM	5.99
	VTD 50 μM	7.01
	VTD 100 μM	3.81
4.3B	VC	2.36
	NE 2μM	2.98
	VTD 100 μM	2.93
4.3C	VC 1 hour	1.06
	VC 2 hour	3.17
	VC 3 hour	4.38
	VTD 1 hour	3.15
	VTD 2 hour	3.86
	VTD 3 hour	6.15
4.3D	1% DMSO	3.35
	Control	2.78
4.4A	VC	2.29
	VTD + TTX (1 μM)	3.8
	VTD	6.68
4.4B	VC	2.21
	TTX 1μM	2.67
4.4C	NE	61.64
	VTD	5.7
	VC	5.64
4.5A	VC	3.79
	VC + propranolol 10 μM	0.85
	VTD	1.28
	VTD + propranolol 10 μM	5.19
4.5B	VC	2.55
Veratridine	VC + propranolol 10 μM	2.73

Continuation of Table 7.1

Figure #	Group	SD value
Tetrodotoxin	NE	1.45
Propranolol	NE + propranolol 10 μM	4.91
4.5C	VC	1.33
	VC + sotalol 10 μM	1.32
	VC + sotalol 100 μM	1.64
	VTD	6
	VTD + sotalol 10 μM	4.87
	VTD + sotalol 100 μM	5.14
4.6A i	VC	2.76
	VC + CGP20712 (1μM)	2.77
	VC + CGP20712 (10μM)	3.9
	VTD	6.4
	VTD + CGP20712 (1μM)	6.34
	VTD + CGP20712 (10μM)	5.21
4.6A ii	VC	2.08
	VC + ICI118551 (1 μM)	1.48
	VC + ICI118551 (10 μM)	2.36
	VTD	6.46
	VTD + ICI118551 (1 μM)	1.57
	VTD + ICI118551 (10 μM)	1.89
4.6A iii	VC	1.19
	VC + L748337 (1μM)	6.25
	VC + L748337 (10μM)	3.02
	VTD	7.82
	VTD + L748337 (1μM)	3.76
	VTD + L748337 (10μM)	4.11
4.6B i	VC	0.94
	VC + CGP20712 (1μM)	1.55
	VC + CGP20712 (10μM)	1.65

Continuation of Table 7.1

Figure #	Group	SD value
	NE	4.36
	NE + CGP20712 (1μM)	9.14
	NE + CGP20712 (10μM)	4.37
4.6B ii	VC	1.83
	VC + ICI118551 (1 μM)	2.24
	VC + ICI118551 (10 μM)	0.85
	NE	10.13
	NE + ICI118551 (1 μM)	8.99
	NE + ICI118551 (10 μM)	9.54
4.6B iii	VC	2.58
	VC + L748337 (1μM)	8.3
	VC + L748337 (10μM)	6.39
	NE	11.31
	NE + L748337 (1μM)	9.38
	NE + L748337 (10μM)	8.22
4.6C i	NE	30.63
	NE + CGP20712 (1 μM)	41.72
	CGP20712 (1 μM)	0.94
4.6C ii	NE	42.01
	NE + ICI118551 (1 μM)	48.84
	ICI118551 (1 μM)	1.48
4.6C iii	NE	87.87
	NE + L748337 (1 μM)	78.62
	L748337 (1 μM)	53.61
4.7	VC	2.55
	VC + propranolol (10 μM)	2.73
	L748337 (10 μM)	7.98
	L748337 (10 μM) + propranolol (10 μM)	6.94

Continuation of Table 7.1

Figure #	Group	SD value
4.8A	VC	4.37
	VC + SR59230A (1μM)	1.54
	VC + SR59230A (10μM)	2.39
	VTD	7.21
	VTD + SR59230A (1μM)	6.21
	VTD + SR59230A (10μM)	2.13
4.8B	VC	2.17
	VC + SR59230A (1μM)	2.2
	VC + SR59230A (10μM)	3.24
	NE	0.77
	NE + SR59230A (1μM)	5.24
	NE + SR59230A (10μM)	1.36
4.8C	NE	10.27
	NE + SR59230A (1μM)	12.05
	SR59230A (1μM)	22.37
4.9A	VC	7.93
	VC + CtX GVIA (1μM)	3.19
	VC + CtX GVIA (10μM)	3.37
	VTD	5.05
	VTD + CtX GVIA (1μM)	4.15
	VTD + CtX GVIA (10μM)	3.44
4.9B	VC	1.14
	VC + CtX MVIIC (1μM)	5.07
	VC + CtX MVIIC (10μM)	1.71
	VTD	1.85
	VTD + CtX MVIIC (1μM)	6.48
	VTD + CtX MVIIC (10μM)	6.06
4.9C	VC	1.3
	VC + clindipine (1μM)	0.24

Continuation of Table 7.1

Figure #	Group	SD value
	VC + clindipine (10μM)	4.43
	VTD	0.59
	VTD + clindipine (1μM)	1.08
	VTD + clindipine (10μM)	1.86
4.9D	VC	1.67
	VC + nifedipine (10μM)	0.61
	VC + nifedipine (100μM)	3.92
	VTD	3.57
	VTD + nifedipine (10μM)	1.75
	VTD + nifedipine (10μM)	4.01
4.10A	VC	4.07
	VC + CGP37157 (10μM)	4.53
	VC + CGP37157 (20μM)	4.52
	VTD	6.58
	VTD + CGP37157 (10μM)	3.09
	VTD + CGP37157 (20μM)	4.21
4.10B	VC	9.1
	VC + KB-R7943 (1μM)	8.04
	VC + KB-R7943 (10μM)	5.71
	VTD	1.55
	VTD + KB-R7943 (1μM)	3.31
	VTD + KB-R7943 (10μM)	7.05
4.11	VC	0.74
	VC + yohimbine (1μm)	7.37
	VC + yohimbine (10μm)	0.67
	VTD	5.01
	VTD + yohimbine (1μm)	1.94
	VTD + yohimbine (10μm)	4.31
4.12	VC	5.77

Continuation of Table 7.1

Figure #	Group	SD value
	VC + A317491 (10 μM)	5.18
	VTD	7.27
	VTD + A317491 (10 μM)	7.68
4.13A	VC	1.29
	VC + BIBN 4096 (100 nM)	1.09
	VC + BIBN 4096 (1 μM)	1.01
	VTD	2.32
	VTD + BIBN 4096 (100 nM)	3.44
	VTD + BIBN 4096 (1 μM)	3.1
4.13B	VC	1.61
	VC + CP-96345 (100 nM)	3.37
	VC + CP-96345 (1 μM)	2.47
	VTD	3.74
	VTD + CP-96345 (100 nM)	4.23
	VTD + CP-96345 (1 μM)	4.06
4.14A	VC	2.89
	VC + BIBO 3304 (1 μM)	4.17
	VTD	5.17
	VTD + BIBO 3304 (1 μM)	5.13
4.14B	VC	2.89
	VC + BIIE 0246 (1 μM)	1.35
	VTD	5.17
	VTD + BIIE 0246 (1 μM)	5.13
4.14C	VC	4.18
	VC + L-152804 (1 μM)	4.99
	VC + L-152804 (10 μM)	2.95
	VTD	2.88
	VTD + L-152804 (1 μM)	2.68

Continuation of Table 7.1

Figure #	Group	SD value
	VTD + L-152804 (10 μM)	4.31
4.15A	VC	2.8
	VC + suramin (100 μm)	2.11
	VTD	5.64
	VTD + suramin (100 μm)	4.81
4.15B	VC	2.56
	VC + PPADS (100 μm)	3.85
	VTD	5.17
	VTD + PPADS (100 μm)	5.00
4.15C	VC	1.00
	VTD + PPADS (100 μm)	1.35
	NE	5.25
	NE + PPADS (100 μm)	3.53
4.18A	VC	4.22
	VC + PSB-12062 (10 μM)	3.56
	VTD	3.62
	VTD + PSB-12062 (10 μM)	7.69
4.18B	VC	4.22
	VC + MRS 2578 (10 μM)	2.36
	VTD	3.62
	VTD + MRS 2578 (10 μM)	5.87
4.19A	VC	2.44
	VC + ATP (100μM)	2.53
	VC + ADP (100μM)	2.6
	VC + UTP (100 μM)	1.34
	VC + UDP (100 μM)	1.88
4.19B	VC	2.44
	NE + ATP (100μM)	6.92

Continuation of Table 7.1

Figure #	Group	SD value
	NE + ADP (100μM)	6
	NE + UTP (100 μM)	7.32
	NE + UDP (100 μM)	2.98
	NE	6.84
4.19C	VC	1.38
	VC + ATP (1mM)	1.7
	VC + ADP (1mM)	2.57
	VC + UTP (1mM)	1.23
	VC + UDP (1mM)	3.37
4.19D	VC	1.38
	NE + ATP (1mM)	5.14
	NE + ADP (1mM)	0.92
	NE + UTP (1mM)	5.44
	NE + UDP (1mM)	9.47
	NE	6.58
4.20A	VC	3.26
	ATP (100 μM) + ARL67156 (100 μM)	1.75
	ATP (100 μM)	2.25
	ADP (100 μM) + ARL67156 (100 μM)	4.71
	ADP (100 μM)	1.59
	UTP (100 μM) + ARL67156 (100 μM)	1.08
	UTP (100 μM)	1.36
	UDP (100UM) + ARL67156 (100 μM)	1.29
	UDP (100 μM)	2.89
4.20B	VC	3.26
	VC + ARL67156 (100 μM)	1.58
	NE	13.43
	NE + ARL67156 (100 μM)	8.69
4.21	VC	1.68

Continuation of Table 7.1

Figure #	Group	SD value
	VC + apyrase (10U/mL)	1.39
	NE	8.58
	NE + apyrase (10U/mL)	2.76